

Investigating pathomechanisms underlying malformations of human cortical development

Dissertation

zur

Erlangung des Doktorgrades (Dr. rer. nat.)
der Mathematisch-Naturwissenschaftlichen Fakultät
der Rheinischen Friedrich-Wilhelms Universität Bonn

vorgelegt von

Ammar Alexander Jabali

aus Oldenburg

Bonn, 2023

Angefertigt mit Genehmigung der Mathematisch-Naturwissenschaftlichen
Fakultät der Rheinischen Friedrich-Wilhelms-Universität Bonn

Erstgutachter: Professor Doktor Philipp Koch
Zweitgutachter: Professor Doktor Michael Pankratz

Fachgruppenfremdes Mitglied: Professor Doktor Günther Weindl

Vorsitzender der Prüfungskommission: Professor Doktor Hubert Schorle

Tag der Promotion: 08.05.23

Erscheinungsjahr: 2023

Table of Contents

Table of Contents	I
Abstract	III
Zusammenfassung	V
1. Introduction	7
1.1 Human cortex development	7
1.2 Malformation of human cortical development	13
1.3 Cerebral organoids as tool to unravel mechanisms underlying MCD and neuropsychiatric disorders	18
Thesis aims	23
2. Publications	25
2.1 Generation of Standardized and Reproducible Forebrain-type Cerebral Organoids from Human Induced Pluripotent Stem Cells	25
2.2 An Organoid-based Model of Cortical Development Identifies Non-Cell-Autonomous Defects in Wnt Signaling Contributing to Miller-Dieker Syndrom	28
2.3 Mutations in the Heterotopia Gene Eml1/EML1 Severely Disrupt the Formation of Primary Cilia.	31
2.4 Human cerebral organoids reveal progenitor pathology in EML1-linked cortical malformation	33
3. Summary	36
4. References	42
5. Contributions	54
6. Appendix	55
6.1 Publication I	55
6.2 Publication II	64
6.3 Publication III	75
6.4 Publication IV	92

7. Eidesstattliche Erklärung	110
8. Danksagung	111

Abstract

During human development the brain has to form a complex neuronal network requiring a well-orchestrated sequence of neurogenesis, neuronal migration and correct positioning within cortical layers followed by synaptogenesis. Malformations associated with cortical development (MCD) can be the result of interferences with one or several elements of this sequence and subsequently lead to different manifestations of MCD with severe consequences including epilepsy, cognitive impairment and intellectual deficiency. In order to investigate the resulting cortical disorganization various mouse models have been used to approximate pathological human corticogenesis. Numerous aspects of MCD can be recapitulated in mouse models making it possible to draw conclusions regarding underlying pathomechanisms. These models are limited in regard of human specific aspects of brain development though.

The advent of human induced pluripotent stem cells (hiPSCs) and three-dimensional (3D) organoid cell culture enables scientists to circumvent the limitations of mouse models and to address human specific features of MCD in a spatio-temporal context. The capability of self-organization in combination with the patterning into forebrain organoids makes it a suitable *in vitro* system to study early corticogenesis and linked developmental disorders in a human context.

In addition, using single-cell RNA sequencing (scRNA seq.) technologies it becomes possible to resolve the cytoarchitecture of organoids in order to look at the cell composition on single cell based resolution. Information based on single cell transcriptomic data allows us to deconstruct the 3D model into different cell types and identify aspects of pathological mechanisms adding up to findings acquired by the repertoire of molecular biology methods.

The beginning of this compendium describes the protocol we developed for the generation of standardized and reproducible forebrain-type organoids from hiPSC, constituting the prerequisite for the investigation of two distinct forms of MCD found in humans. One of these two studies deals with the characterization and underlying pathomechanism of a form of lissencephaly induced by the heterozygous loss of the genes *PAFAH1B1* and *YWHAE*, called Miller-Dieker syndrome (MDS). Using iPSC-derived organoids from Miller-Dieker-syndrome patients a disturbance of the cortical niche was identified, which leads to alterations in N-cadherin/ b-catenin signaling consequently leading to a non-cell autonomous radial glia cell expansion defect. Moreover, with this study we demonstrate a proof of concept regarding the use of our organoid protocol for disease modeling *in vitro*.

The subsequent part of this compendium is a study in which the role of the Echinoderm Microtubule-Associated Protein-like 1 (*Eml1/EML1*) gene in subcortical heterotopia formation is investigated in an *in vivo* context. With the help of a Heterotopic Cortex (HeCo) mutant mouse model and human patient fibroblasts as well as hiPSC derived cortical progenitors, heterotopia formation driver as well as a potentially underlying primary cilia and Golgi apparatus phenotype were identified.

As mentioned before, mouse model can reflect certain aspects of human cortical development but it remains challenging to recapitulate human specific features of neurodevelopmental disorders. The last part of this compendium focuses on the formation of subcortical heterotopia in human patients, characterized by the presence of abnormally positioned neurons, alongside megalencephaly and polymicrogyria induced by mutations in the aforementioned gene *EML1*. Investigation of iPSC-derived cerebral organoids from *EML1*-patients and *EML1*-KO lines showed so far unrecognized abundance of perturbed progenitor cells with increased basal radial glia cell and extracellular matrix (ECM) gene expression profiles in the heterotopic area. This cell population additionally displayed a massive aberrant YAP1 mediated expansion.

Congruencies of major phenotypic findings in hiPSC-derived organoids and the HeCo mouse model reinforces not only the idea that forebrain-type organoids reflect *in vivo* results, but it also emphasizes the synergistic and complementary potential of our *in vitro* model by bridging an evolutionary gap.

Taken together, the studies presented in this compendium deliver greater insight into human MCD mechanisms and support the idea that organoid-based systems serve as promising models to study early human cortical development and associated disorders.

Zusammenfassung

Die menschliche Gehirnentwicklung zeichnet sich durch den Aufbau eines komplexen neuronalen Netzwerks aus welcher auf der präzisen Abfolge aus Neurogenese, neuronaler Migration sowie dem korrekten Eingliedern der Neurone in die verschiedenen Großhirnrinden-Laminae gestützt ist. Abschließend werden die eingegliederten Nervenzellen durch den Prozess der Synaptogenese miteinander verschaltet. Missbildungen während der Kortikogenese können das Resultat von Störungen einer, oder mehrerer Elemente dieses Ablaufs sein und infolgedessen zu verschiedenen Ausprägungen von Fehlbildungen führen welche mit Epilepsie, kognitiven Beeinträchtigungen sowie Einschränkungen intellektueller Fähigkeiten einhergehen können. Um die Entstehung der resultierenden kortikalen Missbildungen untersuchen zu können, gibt es verschiedene etablierte Mausmodelle. Zahlreiche Aspekte kortikaler Missbildungen konnten dadurch in diesen Modellen dargestellt werden was ermöglichte Schlussfolgerungen hinsichtlich zugrundeliegender Pathomechanismen zu machen.

Während diese Modelle bestimmte Aspekte der humanen kortikalen Entwicklung abbilden können, sind dennoch Limitierungen hinsichtlich human spezifischer Aspekte zu verzeichnen. Mit humanen induzierten pluripotenten Stammzellen (iPSZ) und darauf basierender 3D Organoid Zellkulturen stehen uns Methoden zur Verfügung die es ermöglichen diese Limitationen zu umgehen und human spezifische Merkmale kortikaler Missbildungen in einem zeitlich und räumlichen Kontext zu untersuchen. Die Methodik des Einzelzell-RNA Sequenzierens ermöglicht es zusätzlich den Zytoarchitektur Aspekt dreidimensionaler Organoid aufzulösen und die Zell-Zusammensetzung kortikaler Bereiche genauer zu untersuchen. Einzelzell-Transkriptom Daten ermöglichen es Rückschlüsse auf die verschiedenen Zelltypen und Zusammensetzungs-Verhältnisse innerhalb des 3D Modells zu machen und darauf basierend etwaige Pathomechanismen zu identifizieren, welche Erkenntnisse, die durch das bisherige Repertoire molekularbiologischer Methoden gewonnen worden sind, ergänzen. Der erste Teil dieses Kompendiums umfasst die Entwicklung eines Protokolls um standardisierte und reproduzierbare Vorderhirn Organoid auf Basis von humanen iPSZ zu generieren. Dieses humane *in vitro* Modell bildet die Grundlage für weiterführende Untersuchungen zweier verschiedener Formen humaner kortikaler Missbildungen. Eine dieser beiden Studien behandelt die Charakterisierung einer Form der Lissenzephalie, genannt Miller-Dieker Syndrom, hervorgerufen durch den heterozygoten Verlust der Gene *PAFAH1B1* und *YWHAE*. Unter Verwendung von Organoiden generiert von Miller-Dieker-Syndrom Patienten-iPSZs war es möglich eine

Störung der kortikalen Nische zu identifizieren, welche den N-cadherin/ b-catenin Signalweg beeinflusst und schließlich einen Glia Zell Expansions-Defekt zur Folge hat. Darüber hinaus demonstrieren wir mit dieser Studie einen Machbarkeitsnachweis hinsichtlich der Verwendung unseres Organoid-Protokolls für die Modellierung von Erkrankungen *in vitro*. Der darauf folgende Teil dieses Kompendiums behandelt eine Studie in welcher die Rolle des *Echinoderm Microtubule-Associated Protein-like 1 (Eml1/EML1)* Gens in der Entstehung subkortikaler Heterotopien in einem *in vivo* Kontext untersucht worden ist. Mithilfe des heterotopic cortex (HeCo) Mausmodells, humaner Fibroblasten sowie kortikaler Vorläuferzellen, differenziert von humanen iPSZ, wurden Mechanismen der Heterotopie Entstehung, sowie zugrundeliegende primäre Cilien und Golgi-Apparat Phänotypen identifiziert. Während Mausmodelle bestimmte Aspekte der menschlichen kortikalen Entwicklung widerspiegeln können, bleibt es eine Herausforderung, human spezifische Merkmale neurologischer Entwicklungsstörungen zu rekapitulieren.

Die letzte Studie behandelt die Entstehung einer subkortikalen Heterotopie in Menschen, charakterisiert durch abnormal lokalisierte Neurone, induziert durch Mutationen, oder den Mangel des zuvor erwähnten Gens *EML1*. Untersuchungen von *EML1*-Patienten-, sowie *EML1*-KO-iPSZ basierten Organoiden zeigte ein bisher unidentifiziertes Aufkommen von abnormalen Vorläuferzellen mit aberrant erhöhter basal Radial Glia- sowie extrazellulären Matrix (EZM) Genexpression in der entstehenden Heterotopie. Diese Zellpopulation zeichnete sich weiterhin durch abnormale, massive, YAP1-getriebene Expansion aus.

Übereinstimmungen phänotypischer Befunde in humanen iPSZ-abgeleiteten Organoiden und dem HeCo-Mausmodell bekräftigen nicht nur die Idee, dass Vorderhirn Organoide *in vivo* Ergebnisse widerspiegeln, sondern betonen auch das synergistische und ergänzende Potenzial unseres *in vitro* Modells durch die Überbrückung des evolutionären Unterschiedes zwischen Mensch und Maus. Zusammengefasst liefern die in diesem Kompendium vorgestellten Studien neue Erkenntnisse hinsichtlich MCD im Menschen und unterstützen die Idee, dass Organoid-basierte Systeme als vielversprechende Modelle für die Erforschung früher Entwicklungsstörungen der humanen Großhirnrinde dienen können.

1. Introduction

1.1 Human cortex development

Based on a well-orchestrated sequence of progenitor cell proliferation, neurogenesis, neuronal migration, neuritogenesis as well as synaptogenesis, a complex neuronal network is formed during human cortical development. The process of corticogenesis including the correct positioning within cortical layers ensures aspects ranging from basic physiological to higher cognitive function in humans throughout life. Physiologically, the cerebral cortex encompasses the entorhinal cortex (paleocortex), the hippocampus (archicortex) as well as the neocortex (Bear et al. 2016). Comprising 90% of the cerebral cortex, the neocortex is not only the phylogenetically most recently evolved brain region in humans but also the major part accounting for approximately 80% of the total human brain volume (Azevedo et al. 2009).

Around the third week after conception, the human nervous system begins to develop (Stiles and Jernigan 2010). Induced by signals secreted by the Spemann's organizer, also called primitive node in mammals, the nervous system's further development is initiated from a region within the developing embryo called the neural plate (Bystron et al. 2006; Sadler 2005). A high proliferative capacity of neuroepithelial stem cells (NES) in this region leads to the thickening of the neural plate, which simultaneously to massive cell movements, eventually leads to the folding, invagination and formation of the neural tube (Keller et al. 2000; Keller et al. 1992; Nikolopoulou et al. 2017; Sausedo et al. 1997; Smith and Schoenwolf 1989). During development, the neural tube gives rise to the different parts the mature brain is composed of: the most rostral part of the neural tube is giving rise to the prosencephalon (forebrain) later subdividing into telencephalon and diencephalon, while more caudally mesencephalon (midbrain) and subsequently rhombencephalon (hindbrain) are formed (Stiles and Jernigan 2010).

The aforementioned cerebral cortex evolves from the dorsal region of the forebrain while the ventral region gives rise to the basal ganglia (Dennis et al. 2016; Mukhtar and Taylor 2018; Stiles and Jernigan 2010). In both of these proliferative areas specific progenitors are the founding cell type leading to the further development of this regions in the growing brain (Fig. 1) (Buchsbaum and Cappello 2019; Dennis et al. 2016).

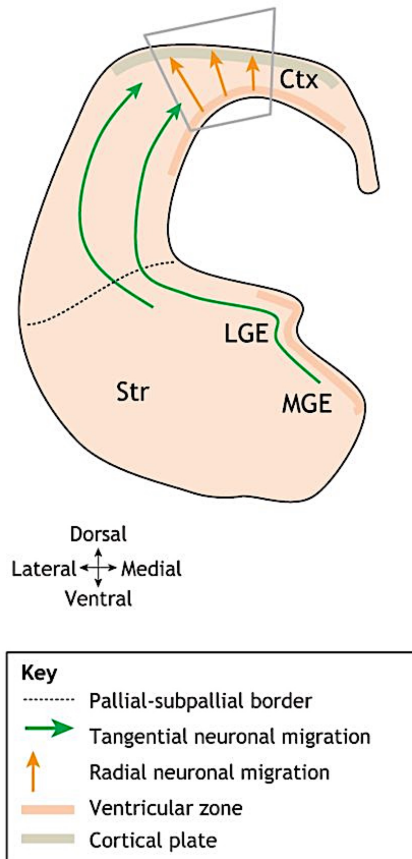


Figure 1: Cell proliferation and migration during corticogenesis.

In the ventricular zone of the dorsal telencephalon neural progenitors give rise to excitatory neurons, which migrate radially to the basal membrane. In a second proliferative ventricular zone, progenitors give rise to inhibitory interneurons, which migrate tangentially from the lateral and medial ganglionic eminences into the developing cortical plate. Adapted from Buchsbaum and Cappello, 2019.

Ctx: cerebral cortex; CP: cortical plate; GE: ganglionic eminence; IZ: intermediate zone; LGE: lateral ganglionic eminence; MGE: medial ganglionic eminence; Str: striatum

In the dorsal part of the forebrain, the NES cells undergo rapid symmetric cell divisions generating two NES daughter cells thereby massively increasing the progenitor pool (Huttner and Kosodo 2005; Rakic 1995), which leads to the radial and lateral expansion of the cortical structure (Florio and Huttner 2014). This procedure takes place adjacent to the dorsal ventricular system, thus this area of expansion is termed ventricular zone (VZ) (Lodato and Arlotta 2015; Molyneaux et al. 2007). Between gestational week 5 and 6 the neuroepithelium becomes multilayered and a fraction of NES cells start to down-regulate some of their characteristic epithelial features like tight-junctions thereby transitioning into a cell type referred to as apical radial glia cells (aRG cells) (Beattie and Hippenmeyer 2017; Götz and Huttner 2005). Over time the cell population of aRG cells will replace NES cells being the dominant neocortical progenitor cell inhabiting the VZ. The apical part of bipolar aRG cells is connected to the ventricular surface (VS) with an organelle termed primary cilium within the apical endfeet protruding into the ventricle thereby sensing signaling molecules within the cerebrospinal fluid (Kriegstein and Alvarez-Buylla 2009). The primary cilium is thought to have crucial influence on cortical neurogenesis, aRG cell polarity and overall cilium-mediated signaling at the VS (Hasenpusch-Theil and Theil 2021). As part of their

apicobasal polarity these cells are spanning a second process to the basal lamina creating the radial scaffold fundamental for the migration of early born neurons (Taverna et al. 2014).

In relation to the VS, aRG cells can divide in three possible modes of cell division based on the angle of the spindle apparatus; symmetric, asymmetric or oblique (Matsuzaki and Shitamukai 2015). This mode of cell division is determinant regarding the cell fate of the progeny. While symmetrical cell divisions are reported to give rise to two daughter aRG cells during early corticogenesis thereby increasing the pool of progenitors, asymmetric divisions, including oblique division modes, will leave one self renewing cell in addition to a differentiating early born neuron or intermediate progenitor (IP) (Matsuzaki and Shitamukai 2015). At later stages during cortex formation, specifically during peak neurogenesis by the middle of the second trimester, asymmetric cell divisions are reported to give rise to basal radial glia cells (bRG cells) (LaMonica et al. 2013). During this cell division a daughter cell is generated that inherits the basal process without the apical endfoot and will delaminate (Delaunay et al. 2017; Shitamukai et al. 2011), while the remaining cell maintains its apical anchoring at the ventricular surface and becomes a truncated radial glia cell (Nowakowski et al. 2016).

Besides IPs, bRG cells and glutamatergic neurons, aRG cells also give rise to astrocyte and oligodendrocyte progenitors in addition to forming the radial scaffold spanning from apical to basal during early corticogenesis (Florio and Huttner 2014; Paridaen and Huttner 2014).

The transiently expanding cell population of IPs is located in a part of the developing neocortex called subventricular zone (SVZ), adjacent to the VZ (Pontious et al. 2008). By asymmetric division, aRG cells and IPs can fulfill their neurogenic potential and differentiate into immature cortical neurons which subsequently migrate along the scaffold formed by radial glia cells into the early, deep layers of the developing cortex thereby forming the preplate (PP) (Gilmore and Herrup 1997). As the number of incoming early born neurons grows the PP will split into the marginal zone (MZ) and the subplate (SP), which will then grow in size due to following waves of neurons derived from aRG cells or IPs (Kwan et al. 2012). Later arriving neurons will contribute to the formation of the cortical plate (CP).

The abundance of IPs and the highly proliferative bRG cells leads to the subdivision of the SVZ into the inner (iSVZ) and outer SVZ (oSVZ), with IPs populating the iSVZ and bRG cells mainly being located in the oSVZ (Hansen et al. 2010; Lewitus et al. 2013). The oSVZ is congruently described as one feature contributing significantly to the massive expansion and complexification regarding the primate cerebral cortex (Dehay

et al. 2015; Lewitus et al. 2013). Partially responsible for the increased expansion and folding of the neocortex is the high proliferative capacity of bRG cells. These cells residing in the oSVZ of the developing cortex can be seen as a cell type very specific to humans, primates and most of the gyrencephalic species (Dehay et al. 2015; Lui et al. 2011). In contrast to aRG cells, bRG cells have been described as a unipolar glia cell attached to the basal side of the developing cortex. This idea of a strictly uniform appearance has been challenged describing the morphology as diverse, ranging from monopolar connected to the apical or basal side to bipolar connections to both boundaries of the growing cortex (Betizeau et al. 2013; Kalebic et al. 2019; Pilz et al. 2013). In addition to aRG cells and IPs, this cell type contributes to the generation of both deeper and upper layer neurons during peak neurogenesis in humans (Pollen et al. 2015). Moreover, it has been demonstrated that bRG cells give rise to astrocytes and oligodendrocytes once most of the deeper and upper layer neurons have been generated (Rash et al. 2019).

During the second trimester between gestational week 15 and 18 the physical scaffold formed by aRG cells, which newly generated neurons use to migrate along into their final position, undergoes significant changes. The onset of bRG cell generation marks the establishment of a discontinuous scaffolding system; the newly generated bRG cell inherit the process spanning to the basal side of the developing cortex while the remaining truncated aRG cell keeps the apical connection and only develops a shortened glial scaffold not reaching the pial surface. From this point on in corticogenesis the newly generated bRG cells build up the scaffolding path into the CP (Fig.2). This leads to the consequence that during late neurogenesis, only neurons born in the oSVZ will reach the upper layers of the growing cortex (Nowakowski et al. 2016).

Based on the continuous generation of cortical neurons by these neurogenic cell types, the mature human cortex will be built of 6 layers of neurons starting from the earliest born deep layer neurons (layer VI) to the upper layer neurons in layer I while eventually resolving MZ and SP (Germain et al. 2010; Gilmore and Herrup 1997). In an „inside-out“ process layer VI neurons originate first followed by layer V neurons which traverse alongside the glial scaffold above layer VI; the next wave of neurons will migrate above the respective subsequent layer until layer I arrives in its destination as the earliest born in the upper most layer (Fig.2) (Angevine and Sidman 1961).

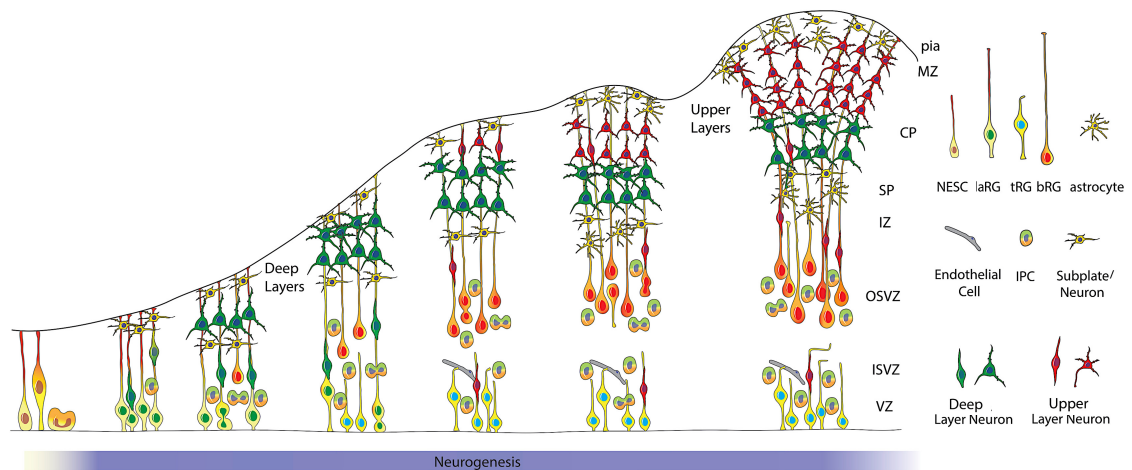


Figure 2: Overview of human corticogenesis.

During early corticogenesis apical radial glia build the scaffold contacting the basal side of the cortex. Newborn neurons migrate radially along these glial fibers. The subsequent layering of neurons follows an inside-out fashion: deep layer are established first, while later born neurons forming the upper layers migrating along basal radial glia fibers. Adapted from Nowakowski et al., 2016.

VZ: Ventricular Zone; NESCs: neuroepithelial stem cells; iSVZ: inner subventricular zone; oSVZ: outer subventricular zone; IZ: intermediate zone; SP: subplate; CP: cortical plate; MZ: marginal zone; IPC: intermediate progenitor cell; aRG: apical radial glia; tRG: truncated radial glia; bRG: basal radial glia

Besides excitatory, glutamatergic projection neurons the mature mammalian cortex is populated by GABAergic inhibitory interneurons providing the balance of inhibitory and excitatory inputs in this neuronal network. These GABAergic interneurons arise from a region ventral to the cerebral cortex called subpallium, which comprises the lateral, medial and caudal ganglionic eminences (Wonders and Anderson 2006). The interneurons generated in these regions follow a tangential migratory stream into the area of the developing cerebral cortex subsequently switching to a final phase of migration in which they move radially into their position within the appropriate cortical layer (Huang et al. 2007). Within these migratory routes the interneurons are guided by chemo-attractants and repulsive cues from the respective ganglionic eminences. In a final step, these cells establish synapses with the resident cortical projection neurons to fully integrate into the neuronal network. As far more neurons and thereof synapses are created during initial corticogenesis, the number of neurons is reduced via programmed cell death during refinement of interconnectivity (Buss et al. 2006; Oppenheim 1991). A feature that distinguishes the human brain from most of the other mammalian brains is an architectural feature of the neocortex. Gyrfication can be described as the process in which the outer surface of the cortex is forming the folds leading to an increase of brain surface (Fig.3) (Garcia et al. 2018; Rakic 2009), taking place during the last period of cortical development (Kroenke and Bayly 2018).

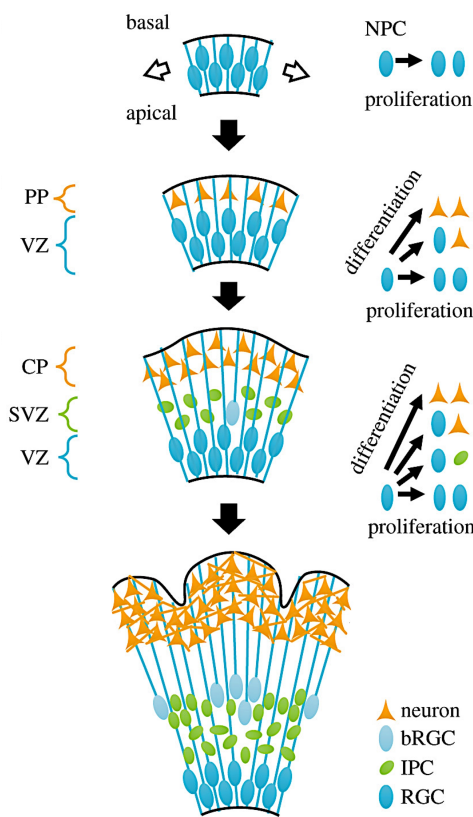


Figure 3: Overview of the development of a gyrencephalic brain.

During early corticogenesis neural progenitor cells expand radially and tangentially followed by the generation of the first differentiating neurons migrating into the preplate. Subsequently, radial glia cells give rise to intermediate progenitors and basal radial glia cells, which in turn contribute to the next waves of neurons migrating into the cortical plate. Different signaling cascades and mechanical parameters contribute to the folding of the outermost grey matter during the last period of cortical development resulting in convolutions.

Adapted from Garcia et al., 2016.

VZ: Ventricular Zone; PP: preplate; CP: cortical plate; SVZ: subventricular zone; NPC: neural progenitor cell; bRGC: basal radial glia cell; IPC: intermediate progenitor cell; RGC: radial glia cell

Due to the fact that this fundamental process during human brain development is not fully understood yet, several studies are trying to shed light on the generation of gyri (the folding of cortical tissue) and sulci (the depression of grooves between two gyri). According to recent studies one of the parameters contributing to the convolution of the cortex is the influence of extracellular matrix as described in a study from 2018 (Long et al. 2018). Three identified extracellular matrix components namely collagen I, lumican and hyaluronan and proteoglycan link protein 1 (HAPLN1) caused local changes of tissue stiffness and cortical plate folding when applied to fetal human neocortex. Furthermore, the study indicates that these processes are mediated via hyaluronic acid receptor CD168 and downstream ERK signaling. It can be assumed that this represents processes in humans mediated by the ECM-rich meningeal membranes which follow neuronal layer I along the border of the cortical surface. As already mentioned afore the abundance of bRG cells is commonly described as one of the key parameters for evolutionary neocortex expansion and gyrification (Borrell and Götz 2014; Liu et al. 2017; Matsumoto et al. 2020; Rash et al. 2019). The observation that the degree of cortical folding correlates significantly with the abundance of bRG cells and thereby the proliferation in the oSVZ additionally underscores the role of

these cells regarding the evolution of gyrencephalic brains (Pilz et al. 2013; Reillo et al. 2011). Due to their high mitotic capacity, cortical areas with an abundance of bRG cells display greater proliferation in the oSVZ, a tangential dispersion of radially migrating neurons and thus, the highest level of surface area expansion and gyrification (Borrell and Götz 2014). Complementary to the tangential expansion based on high proliferation in the iSVZ and oSVZ, a recent publication is highlighting the role of another cell type of the central nervous system in a second step within cortical folding. This study reports that during this second phase in gyri formation, spatially restricted FGF-signaling feedback loops mediate local astrocyte expansion resulting in a more pronounced vertical expansion of cortical folds contributing to the formation of convolutions (Shinmyo et al. 2022). An additional physical parameter has been highlighted in another study from 2018 in which researcher demonstrate the influence of spatial confinement contributing to the convolution of the cortex. Researches used an *in vitro* method to mimic compressive forces during the expansion of neuroectodermal tissue (Karzbrun et al. 2018). Thereby, this study identified mechanical forces in the form of cytoskeletal contraction at the *in vitro* model's core and simultaneous cell-cycle dependent nuclear expansion at the outer part of the 3D model.

Taken together, these are some of the hypotheses shedding light onto this complex brain feature of gyrencephalic species. This well orchestrated process is yet another sequence of events during brain development in which disturbances can lead to drastic changes regarding the physiology of the human brain. The following part of this compendium is giving an overview of malformations of human cortical development including malformations that occur due to affected cortical folding.

1.2 Malformation of human cortical development

Malformations associated with human cortical development (MCD) can be the result of interferences with one or several elements of the sequence of steps during corticogenesis. Depending on the extent of the malformation, the classification can be uni- or bilateral, symmetric or asymmetric and can occur as comorbidity as part of a complex syndrome. Changes in progenitor cell proliferation, abnormal neuronal migration, excess of bRG cells, premature delamination of neural progenitors or abnormal neuron positioning can be causes for MCD in humans and mammals (Cappello et al. 2013; Guo et al. 2015; Hong et al. 2000; Johnson et al. 2018; Shimada et al. 2019). Clinical consequences caused by MCD can range from developmental delay, motor- and intellectual disabilities, epilepsy, to a spectrum of neuropsychiatric

symptoms (Guerrini and Dobyns 2014). Macroscopic anatomical manifestations regarding disrupted cortical development include microcephaly (smaller brain size), megalencephaly (larger brain size), lissencephaly (loss or disruption of lamination and/or gyrfication), heterotopia (abnormally positioned neurons) and polymicrogyria (numerous small cortical convolutions) (Fig. 4).

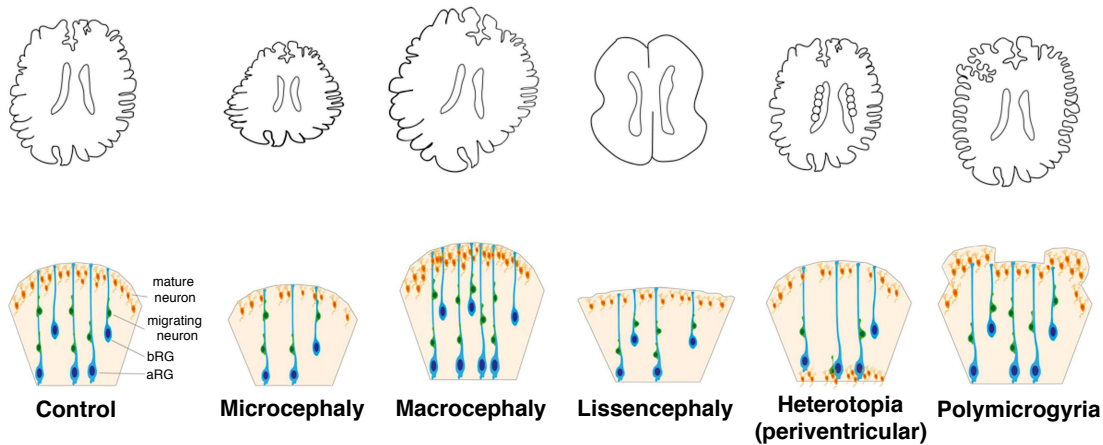


Figure 4: Malformations of human cortical development.

Upper row: Schematic depiction of a healthy brain and brains affected by different cortical malformations: microcephaly, macrocephaly, lissencephaly, periventricular heterotopia and polymicrogyria. Lower row: Schematic depiction of phenotypical features and the pathomechanism underlying each form of cortical malformation. Adapted from Ossola and Kalebic, 2021.

VZ: ventricular zone; SVZ: subventricular zone; CP: cortical plate; aRG: apical radial glia; bRG: basal radial glia

These different forms of MCD can coexist in complex forms (Guerrini and Dobyns 2014; Klingler et al. 2021; Ossola and Kalebic 2021). The causes for MCD can be diverse as different cellular features or processes can be disturbed. Causes for the onset of MCD can be mutations in adherens junction proteins like α/β -catenin, N-cadherin or cell-cell contact proteins like DCHS1 or FAT4 (Cappello et al. 2013; Kadowaki et al. 2007; Lien et al. 2006). As a consequence, aRG cell polarity and cell divisions as well as neuronal migration are impaired. Mutations or loss of the aforementioned adherens junction protein N-cadherin can lead to impaired cortical development as well. Conditional knockout has been demonstrated to lead to the breakdown of cortical organization with postmitotic and proliferating cells scattered across the cortex (Kadowaki et al. 2007), while other studies demonstrate that inactivation lead to increased progenitor proliferation and eventually to malformation resembling a subcortical band heterotopia (SBH) (Gil-Sanz et al. 2014). Disturbances of adherens junctions can influence apical-basal orientation of progenitor cells and the correct establishment of architectural cortical features, but these are not the only determinants for polarity during corticogenesis. aRG cells contain a specialized polarity

complex consisting of PAR3, PAR6 and aPKC, which not only establishes cell polarity but also influences progenitor proliferation, delamination and differentiation (Bultje et al. 2009; Costa et al. 2008). It has been shown that loss of PAR3 promotes an abnormal switch in aRG cell division mode leading to an initial increase of mitotic progenitors and delaminated, mispositioned progenitors outside the VZ. As a consequence the enlargement of the affected brain can be observed. In addition to that the ectopic progenitors undergo massive neurogenesis, which results in heterotopia formation (Liu et al. 2018).

Another determinant for polarity and attachment to the VS is the primary cilium (Zaidi et al. 2022). The complex of impairments, summarized under the term “ciliopathies” sheds light on abnormal primary cilia structure or ciliogenesis leading to abnormal cortex development. Genes like *WDR62*, *KIF2A*, *BBS1*, *BBS7*, *BBS10* and *TMEM216* are reported to have impact on primary cilia and centrosome growth and integrity and thereby cause cortical malformation as a consequence if mutated or perturbed (Guo et al. 2015; Zhang et al. 2019). Consequences of impaired primary cilia can range from abnormal progenitor cell cycle progression and decreased proliferation, disturbed sensing of signaling input via the cerebrospinal fluid (CSF) in the ventricles to disruption of the polarized RG scaffold and distinct phases of neuronal migration (Guo et al. 2015; Liu et al. 2021). The organization and regulation of the spindle apparatus can be a parameter for the initiation of MCD as well, the development of microcephaly in particular. Genes such as *MCPH1* or *ASPM* are reported to be critical for correct corticogenesis or as potential MCD drivers (Bond et al. 2002; Jackson et al. 2002; Zhong et al. 2006). Spindle organization and orientation as well as centrosome maturation can be critical regarding potential influences on cortex development. Centrosomes and centrioles harbor spindle-regulating properties and play a crucial role in progenitor proliferation and the correct distribution of chromosomes during cell division; abnormal chromosomal numbers leading to apoptosis or abnormal spindle assembly or orientation can be the consequence (Marthiens and Basto 2020). The latter case has a profound influence on the division mode and further development of a cell. While symmetric divisions increase the progenitor pool, asymmetric and oblique cell divisions lead to the generation of one progenitor cell while the second progeny delaminates from the VZ surface and transitions into a neuron or bRG cell (LaMonica et al. 2013; Matsuzaki and Shitamukai 2015). A premature shift from symmetric to asymmetric depletes the progenitor pool thereby leading to reduced brain size, the hallmark feature of microcephaly. In the case of mutations in the gene *CENPJ* for example, the progressive loss of centrioles has been observed causing increased detachment of aRG cells. While these progenitors still proliferate, a mitotic delay

initiates programmed cell death eventually decreasing the progenitor pool leading to microcephaly (Insolera et al. 2014).

The capability to undergo massive self-renewal within the VZ area is a crucial feature of progenitor cells. Premature differentiation as well as alterations regarding cell cycle progression and length can disturb the balance between progenitor expansion and neurogenesis. Excessive proliferation or accelerated cell cycle can lead to megalencephaly while decreased proliferation, increase in apoptosis, prolonged cell cycle and premature neurogenesis can lead to microcephaly with or without lissencephaly (Gabriel et al. 2016; Mirzaa et al. 2014; Wilson et al. 2012; Zhang et al. 2019). Another crucial prerequisite for correct corticogenesis is the integrity of the cellular cytoskeleton. The significant involvement in different cellular processes like cell division, migration and neuritogenesis is a potential explanation for the frequent contribution of genes associated with cytoskeleton dynamics to MCD. Mutations in tubulin genes for example are reported to lead to various different forms of malformation including microcephaly, lissencephaly, neuronal heterotopia or polymicrogyria (Fallet-Bianco et al. 2014). Genes involved in assembling and stabilizing microtubules like *DCX* or *EML1* have been reported to cause subcortical heterotopia (des Portes et al. 1998; Kielar et al. 2014), while mutations or deletion of *PAFAH1B1*, responsible for microtubule dynamics and regulation of dynein, have been identified as the most common cause for lissencephaly in humans (Kato and Dobyns 2003). The impact of *PAFAH1B1* perturbations leads to a plethora of defects ranging from defects in proliferation due to spindle apparatus misorientation, microtubule cytoskeleton instability and WNT pathway deregulation over premature neurogenesis to increased cell death and disturbed neuronal migration (Bershteyn et al. 2017; Feng and Walsh 2004; Yingling et al. 2008). Processes within a cell like intracellular trafficking can be affected by truncation of cytoskeletal components, which in turn can have major impact on correct corticogenesis (Passemar et al. 2019). Microcephaly and periventricular heterotopia have been diagnosed in patients with mutations in the gene *ARFGEF2*, of which the protein BIG2 is required for correct vesicle and membrane trafficking of the Golgi apparatus network. As a consequence, a study indicates that progenitor proliferation as well as neuronal migration during human neocortical development are affected and responsible for the diagnosed microcephaly and the formation of periventricular heterotopia in those patients (Sheen et al. 2004). But not only assembly and integrity of cytoskeletal components is of importance as posttranslational as well as posttranscriptional deregulation of cytoskeletal-related proteins display a potential cause for MCD. An example is the abnormal splicing of *Flna*, a protein that crosslinks actin filaments and attaches these to cell membrane

proteins. Irregularities throughout the splicing process are reported to lead to the formation of periventricular heterotopia (Zhang et al. 2016). A central key for the correct cortical architecture is the undisturbed procedure of radial migration along a glial scaffold into the correct laminar destination performed by postmitotic neurons. Certainly one of the major drivers for malformations of the cortex displays any impairment of neuronal migration leading either to disruption of lamination, failed preplate splitting, or ectopically located neurons. Neuronal migration along the radial scaffold relies on the extension of a leading process, somal translocation and locomotion (Nadarajah and Parnavelas 2002), emphasizing once again the importance of intact cytoskeletal dynamics; mutations impairing actin or microtubule integrity, assembly and disassembly account for a fraction of cortical malformation as migration of neurons can be severely perturbed (Copp and Harding 1999). As mentioned afore, preplate splitting into the transient marginal zone and the subplate can be regarded as impaired neuronal migration (Olson 2014). Mutations in the genes *RELN* or *POMGNT2* are well characterized and studies indicate that mutations in the gene or absence of the proteins are causative not only for abnormal neuronal migration but also for impaired preplate splitting (Hong et al. 2000; Nakagawa et al. 2015). Mutations in genes not belonging to the aforementioned categories can lead to severe forms of MCD as well. Among those, transcription factors like *PAX6*, *EOMES*, *FOXP1* and *YAP1* are reported to be malformation driver (Baala et al. 2007; Davis et al. 2008; Najas et al. 2020; Pringsheim et al. 2019; Saito et al. 2018) as well as genes involved in epigenetic modifications like histone modifications or in general chromatin remodeling (Heyn et al. 2019; Ostrowski et al. 2019). Until this point the vast majority of cortical malformation has been investigated using animal models in order to approximate human cortical development. The following part emphasizes the potential of human PSC-derived 3D cultures recapitulating certain aspects of human brain development thereby presenting an additional tool to decipher human specific aspects of MCD. MCD based on genetic mutations or environmental influences can be investigated in different *in vivo* models, most frequently done so in rodent models. In the past, this has lead to detailed insights into pathomechanisms in regard of different aspects of impaired corticogenesis and mammalian brain development in general. But the more light got shed on the genes involved, the more evident it got that genes were affected by mutations, which functions evolutionary progressed in humans compared to other experimental models emphasizing an incomplete picture gained by developmental brain research solely based on animal models. Several differences regarding brain development and cellular brain composition of mice, the most frequently used animal model, and humans can make it difficult to draw conclusions applying for human brain development and

pathomechanisms underlying MCD. Significant differences in gene expression programs, the far lesser brain to body ratio and the absence of gyrification in mouse brains are some examples underscoring this (Taverna et al. 2014). Three major evolutionary aspects lead to the substantial differences between human and mice brains: The increased proliferative capacity of NES as the founder cells in the neural tube (Florio and Huttner 2014), a species specific program causing aRG cells to continue expanding during neurogenesis (Otani et al. 2016) and an increased abundance of highly proliferative bRG cells in the oSVZ of humans contributing massively to the expansion of the neocortex (Hansen et al. 2010). In addition to that, more evidence suggests that human specific genes or variants of genes played a crucial role during the evolution of the human brain. These variants of genes have been shown to be involved in the expansion of the progenitor pool resident in the VZ like *NOTCH2NL* (Fiddes et al. 2018), or the progenitor pool primarily located in the oSVZ as for the case of *ARHGAP11B* (Fischer et al. 2022; Florio et al. 2015), or *TKTL1* (Pinson et al. 2022). This further supports the idea to develop appropriate human *in vitro* models.

1.3 Cerebral organoids as tool to unravel mechanisms underlying MCD and neuropsychiatric disorders

The advent of human iPSC cell culture and the generation of cerebral organoids enabled researcher to develop and investigate such human *in vitro* models. Pioneering work of Shinya Yamanaka and his colleagues in 2006 and 2007 made it possible to generate iPSCs from mouse and human fibroblasts using defined factors (Takahashi et al. 2007; Takahashi and Yamanaka 2006). This reprogramming method from a differentiated cell type into a self-renewing pluripotent cell initiated a myriad of work in diverse areas of biological research, especially in those cases in which the use of embryonic stem cells in research was limited or prohibited. These publications also demonstrated the derivation of ectoderm, mesoderm and endoderm in teratoma after transplantation of iPSCs into immune suppressed mice thereby indicating the potential to differentiate the reprogrammed iPSC into cells of the three germ layers. A feature of teratoma formation is the uncontrolled differentiation, and in many cases, the self-organization into compartmentalized somatic tissues from all three germ layers in those tumors (Li et al. 2021; Przyborski 2005). Based on these observations and trailblazing work of Yoshiki Sasai and his colleagues the transition of protocols from uncontrolled differentiation and self-organization of pluripotent stem cells to gradually controlled differentiation and

subsequent self-organization into organ-like structures took place (Eiraku et al. 2008; Kadoshima et al. 2013; Sasai 2013a; 2013b). In his work he summarized the fundamental processes during *in vitro* organogenesis in 3D stem cell culture as 1) self-assembly, the spatiotemporal positioning and control of cells to each other, 2) self-patterning, the acquisition of region-specific cell fates forming a heterogeneous group of spatially patterned cells and 3) self-driven morphogenesis, which he describes as the spontaneous formation of tissue-like structures based on tissue intrinsic mechanisms (Sasai 2013a). Over time protocols of 3D cell culture or so-called organoids were developed covering organs of every germ layer (Tang et al. 2022).

The resemblance of organoids to human organs is based on three implications: 1) The organoid has to consist of different organ-specific cell types, which 2) as single cell or as a tissue is capable of recapitulating some organ-specific functions. These organ-specific cell types have to be 3) grouped together in a spatial manner resembling the actual organ. The first protocols to generate cerebral organoids became public and gained attention in 2008 and 2013 with the publications by the groups of Yoshiki Sasai and Jürgen Knoblich (Eiraku et al. 2008; Lancaster et al. 2013). In both cases pluripotent stem cells were the founding cell type, which emphasizes the general capacity of pluripotent stem cells to self-organize into an *in vitro* reminiscence of the respective organ. This 3D cell culture model makes it possible to recapitulate early human corticogenesis as it displays cyto-architectural hallmarks like VZ-like areas growing around a VZ surface lining as well as the generation of early born neurons organized in a CP-like structures. In addition, cerebral organoids contain almost all of the relevant progenitor cell populations contributing to the growth and development of structures reminiscent of an early human cortex. Some of these first protocols have been developed for the generation of whole brain organoids, which display multiple brain-like regions within one organoid (Lancaster et al. 2013), while other organoid protocols mainly displayed the development of cortical structures including VZ, SVZ as well as CP-like regions (Eiraku et al. 2008). Based on the success of her pioneering work in the field of brain organoid research, Madeleine Lancaster and her colleagues then proceeded to further develop the established protocols thereby contributing significantly to the research in this field (Giandomenico et al. 2019; Lancaster et al. 2017; Pellegrini et al. 2020).

Modulating specific pathways using small molecules or morphogens lead to protocols specifically designed for the generation of dorsal or ventral forebrain-like, midbrain-like, hypothalamus-like and cerebellum-like organoids (Huang et al. 2021; Kadoshima et al. 2013; Muguruma et al. 2015; Qian et al. 2016). In addition to a similarity in cytoarchitecture, the organoids generated display high congruency with human primary

brain tissue regarding transcriptomic profiles and gene regulatory changes (Kanton et al. 2019; Quadrato et al. 2017; Velasco et al. 2019). Another prerequisite to be fulfilled for brain organoids is the functionality of cells or parts of the tissue formed. Recent studies suggest that brain organoids do have the capability to generate complex neuronal networks as well as neural oscillations and epileptiform changes (Samarasinghe et al. 2021; Trujillo et al. 2019; Zafeiriou et al. 2020). The spatial and temporal recapitulation of human brain, especially cortex development, combined with the aforementioned transcriptomic and functional qualities of brain organoids qualifies this method as a suitable *in vitro* model for developmental research as well as disease modeling.

Brain organoids have been used to study different MCD occurring in humans ranging from micro- and megalencephaly as well as lissencephaly and different forms of heterotopias gaining deeper insight into underlying pathomechanisms (Bershteyn et al. 2017; Karzbrun et al. 2018; Klaus et al. 2019; Lancaster et al. 2013; Li et al. 2017). In one of the first publications using brain organoids to model a MCD, Lancaster and colleagues demonstrated the recapitulation of microcephaly hallmarks like decreased size and premature neuronal differentiation using patient-derived fibroblasts (Lancaster et al. 2013). In a study from 2017, Li and colleagues investigate the pathological increase in brain size via PTEN deletion in iPSCs in order to confirm existing genetic evidence from human patients suffering from megalencephaly. Not only did they demonstrate increased brain organoid growth due to enhanced progenitor proliferation and surface folding upon PTEN deletion, but also used the model to demonstrate the deleterious effect of ZIKA virus infection on organoid growth (Li et al. 2017). In two studies different parameters contributing to the development of a smooth, lissencephalic brain were identified (Bershteyn et al. 2017; Karzbrun et al. 2018). Using cells derived from patients suffering from lissencephaly, Bershteyn and colleagues were able to identify increased apoptosis and asymmetric cell divisions in aRG cells residing in the VZ decreasing the progenitor pool as well as a prolonged mitosis in bRG cells leading to an overall decrease in size and an increase in deep layer neurons (Bershteyn et al. 2017). The reduction of LIS1 protein lead to the decrease in folding in an organoid on-a-chip model and enabled Karzbrun and colleagues to connect this phenotype to changes in nuclear motion in aRG cells as well as aberrant ECM and cytoskeleton related gene expression (Karzbrun et al. 2018). Of note is the study from Klaus et al. 2019 as an example of a follow-up study investigating the consequences of perturbations in the aforementioned genes *DCHS1* or *FAT4* in context of the formation of periventricular heterotopia in humans (Klaus et al. 2019). Mutations or knockdown of these genes lead to changes in progenitor morphology and defective neuronal

migration in a subset of neurons in iPSC derived cortical organoids thereby validating and exceeding the results generated in a mouse model (Cappello et al. 2013).

In addition to MCD based on genetic alterations, the organoid model has been successfully tested in the context of environmental factors causing developmental disorders leading to cortical malformations. Here, some of the most prominent examples have been studies outlining the causation between ZIKA and other viral infections and significant decrease of cerebral organoid size indicating microcephaly (Krenn et al. 2021; Qian et al. 2016). With more advanced protocols facilitating the functionality of organoids it is possible to model developmental disorders of the brain, which do not primarily manifest as MCD. Neuropsychiatric disorders and epileptiform events can become evident in iPSC-derived organoids on different levels. On a cellular level, synaptic abnormalities as well as impaired glial function have been recapitulated modeling Rett syndrome, schizophrenia or autism spectrum disorder (ASD) (Notaras et al. 2022; Samarasinghe et al. 2021; Zhang et al. 2020). In addition to that, organoids have been used to investigate abnormalities on neural circuit level and gene expression level detectable as imbalance of excitatory and inhibitory activity and overall impaired electrophysiology or abnormal gene expression profile (Amiri et al. 2018; Kathuria et al. 2020; Samarasinghe et al. 2021; Sawada et al. 2020).

Although this model system enables researcher to decipher human specific pathomechanisms underlying MCD and neuropsychiatric disorders it is important to consider that the organoid system has limitations. Most protocols for generating brain organoids are challenged by batch-to-batch heterogeneity. The usage of multiple iPSC lines including patient-derived cells as well as genome edited cells and their respective isogenic controls increases reproducibility across different lines thereby demonstrating robustness when it comes to reliability of the results in the experimental context. Furthermore, the correct starting cell number for iPSC aggregation at the beginning of the organoid generation in combination with the use of small molecules to guide the forming neuroectodermal structure into the brain area needed can improve protocols significantly as shown in part I of this compendium. Although protocols continuously improved over time, especially in regard of functionality, brain organoids are still restricted to recapitulate early developmental stages (Kanton et al. 2019; Quadrato et al. 2017; Velasco et al. 2019). On a structural level, some features of human brain development still need to be mimicked in this 3D in vitro model. The separation of the SVZ into a distinct iSVZ and a proportionally increased oSVZ resembling the second trimester of a developing cortex as well as a distinct 6-layer CP architecture is only replicated to a restricted extend (Qian et al. 2020; Watanabe et al. 2017). A developmental hallmark of a human cortex is gyrification (Rash et al. 2019). The

appearance of convolutions *in vitro* have been reported in studies either genetically modulating the founder iPSCs (Li et al. 2017) or by modulating the mechanical input the growing organoid is exposed to (Karzbrun et al. 2018). However, this “*in vitro* gyrification” mainly affects the germinal zones rather than the CP-like structures thereby not completely reflecting the human situation. Based on recent studies it can be assumed that certain ECM-mediated pathways need to be modified in order to achieve a *bona fide* gyrification of cortical structures *in vitro* (Long et al. 2018). Concomitant with the early developmental stages recapitulated it can be observed that in most of the protocols, glia cells like astrocytes and oligodendrocytes, are underrepresented therefore not contributing to synaptogenesis, myelination and in general normal physiological homeostasis (Quadrato et al. 2017). Improved protocols demonstrate that increasing glial content in brain organoids drastically improves functionality in terms of progressive neuronal network maturation, network burst development and long-term potentiation (Zafeiriou et al. 2020). Another parameter influencing further development and comprehensiveness as a model for the developing brain is the lack of cell types originating from germ layers other than the neuroectoderm. Cells of the vasculature as well as cells building up the CNS-specific immune system are two examples of extensive research in order to advance brain organoid protocols (Ahn et al. 2021; Cakir et al. 2019; Fagerlund et al. 2021; Xu et al. 2021).

Thesis aims

Disturbances of every step of the complex choreography of brain development and specifically corticogenesis can lead to various forms of MCD with severe consequences for human patients. First, we set out to develop a reliable protocol for the generation of forebrain-type cerebral organoids. We then applied this protocol to elucidate the underlying pathomechanisms leading to the formation of MCD using state of the art techniques and to highlight the use of human iPSC-derived cerebral organoids as an additional model to rodent models for early brain development and associated disorders.

This compendium of published scientific works outlines the development of an organoid-based platform and based on that the investigation of two different MCD: a form of lissencephaly induced by the heterozygous deletion of the genes *PAFAH1B1* and *YWHAE* known to be involved in Miller-Dieker syndrome as well as a form of SBH linked to mutations or deficiency regarding the *EML1* gene. Including a mouse model for *Eml1*-driven heterotopia formation, it is demonstrated how different model systems can be used to decipher mechanisms underlying pathological brain development.

In order to investigate the impact of mutations or perturbed gene expression in general on human cortex development *in vitro* we developed a model for iPSC based brain development in 3D. This protocol has been published in 2018 describing the step-by-step generation and quality control of standardized and reproducible forebrain-type cerebral organoids (Kreff et al. 2018). Previously, we demonstrated the benefit of this model in a study investigating the consequences of a heterozygous loss of the genes *PAFAH1B1* and *YWHAE* on human cortical development and identified a disturbance of the cortical niche leading to alterations in N-cadherin/ β -catenin signaling resulting in a non-cell autonomous radial glia cell expansion defect (Iefremova et al. 2017). In the study of Uzquiano et al. 2019, a mouse model harboring a deleterious insertion in the *Eml1* gene as well as human control and patient fibroblasts and iPSC-derived cortical progenitor cells were used to identify disrupted primary cilia formation, altered Golgi apparatus and as a consequence thereof a perturbed primary cilia-Golgi axis (Uzquiano et al. 2019). Recently we have used our model system in order to elucidate the consequence of *EML1* deficiency during human cortical development (Jabali et al. 2022). The organoid model enabled us to recapitulate primary cilia and spindle apparatus defects in a human model for *EML1* deficiency. In combination with the observation of the formation of ectopic rosette-like structures it suggests premature delamination of apical progenitor cells from the ventricular surface. Besides the demonstration of heterotopic neurons forming nodules or bands below the CP-like

structure, we were able to show that deregulated YAP1 signaling contributes to the massive expansion of ectopic proliferating cells and the formation of ectopic rosette-like structures. Our data highlight the recapitulation of human MCD *in vitro* supported and complemented by data gained in a mouse model and provide new mechanistic insight into the human disease pathology. This suggests that organoid-based systems serve as promising models to study early human cortical development and associated disorders.

2. Publications

Preface

This dissertation has been prepared cumulative. The data obtained in the presented work has been described in detail in four publications, which are listed in the appendix section.

2.1 Publication I

Generation of Standardized and Reproducible Forebrain-type Cerebral Organoids from Human Induced Pluripotent Stem Cells.

Kreff O, Jabali A, Iefremova V, Koch P, Ladewig J. J Vis Exp 2018 Jan 23;(131): 56768. DOI: 10.3791/56768

The human cortex displays a complex structure and is highly expanded compared to other mammalian species. Additionally, the increased mitotic capacity and expansion of the progenitors in the ventricular zone (VZ) as well as the increased abundance of bRG cells in the oSZV differ from any other species. This explains the restricted possibilities to study human cerebral cortex development, as availability of model systems approximating the human brain development as well as access to primary tissue is limited. The advent of iPSC culture and the capacity of these cells to self-organize into 3D structures displaying multiple organ-specific cell types and specific functions of the organ makes it possible to mimic early stages of human brain development *in vitro*.

The protocol we developed for the homogenous and reproducible generation of forebrain-type cerebral organoids combines the ability of PSCs to self-organize into 3D structures with the use of small molecules in order to guide the forming structure into anterior neuroectodermal fate and the support of matrix embedding to facilitate the formation of continuous neuroepithelium. The first part of the published protocol describes the proper culture of human iPSCs in order ensure the ideal outcome when embryoid bodies (EB) are formed. The stage when iPSC cultures reach 70-90% confluence indicates the moment when the cells can be used for the generation of these iPSC aggregates. The aggregate shares similarities with the developmental stage during early gastrulation eventually leading to the differentiation into cell derivatives of the three germ layers if no extrinsic patterning or guiding medium

conditions are applied (Lanza 2009). After an initial growth phase in medium supporting pluripotency, we induced the formation of anterior neuroectoderm. In order to restrict the development of this EB into the (neuro-) ectodermal lineage, we exposed the EBs to a cocktail of small molecules to pattern the growing aggregate towards an anterior telencephalic regional identity using dual inhibition of SMAD signaling (Chambers et al. 2009) and inhibition of WNT signaling in order to prevent posteriorization (Kadoshima et al. 2013). Compared to protocols for generation of organoids based on self-assembly without extrinsic stimuli (Lancaster and Knoblich 2014), our standardized protocol was designed using guided differentiation in order to give rise to forebrain-specific organoids from human iPSCs with a lower intra- and inter batch variability. After 4 to 5 days of neural induction, smooth, translucent neuroectodermal tissue can be observed indicating the ideal time point for the embedding of the EB into basement membrane extract (BME), which acts as a matrix scaffold and supports the formation of neuroepithelium and growth of neural rosette-like structures. The embedded EBs gradually develop into forebrain-type cerebral organoids throughout the next weeks (Lancaster and Knoblich 2014). After another day of stationary cultivation, ultra-low attachment cell-culture dishes containing organoids are transferred onto an orbital shaker. The cultivation under agitation with low shear stress allows the optimal nutrient support, which will preserve the growing 3D structure more efficiently. Simultaneously to the cultivation under agitation, the medium is adapted to a neural differentiation medium, which is composed of compounds supporting the optimal growing conditions of neuroepithelial structures and components reducing oxidative stress. For extended culture beyond 50 days we adapted the medium, supplementing it with Brain-derived neurotrophic factor (BDNF) and Glia cell line-derived neurotrophic factor (GDNF). Enabling further increase of complexity in our 3D model the medium is supplemented with additional BME as it has been shown to significantly contribute to the organization of the CP-like region and the formation of a basement membrane (Lancaster et al. 2017).

Moreover, we provide guidelines for fixation, preparation for cryosectioning and general quality control steps to ensure the generation of standardized forebrain-type cerebral organoids. Immunocytochemical as well as reverse-transcription polymerase chain reaction (RT-PCR) analyses demonstrate the reproducible generation of organoids with dorsal cortical identity around day 20. The organoids generated express genes like *FOXP1* and *EMX1* whereas midbrain (*FOXA2* and *PAX5*) and hindbrain (*HOXB2*, *HOXA4*, *HOXB4*, *HOXB6*) genes are absent. This is supported by immunocytochemical characterization using antibodies against epitopes of proteins typically expressed in developing neuroepithelial structures like SOX2, PAX6 and

EMX1. My task was to develop a standardized protocol for organoid generation in such a way that it displays a high degree of reproducibility in close collaboration with Olivia Krefft and Vira Iefremova guided by Philipp Koch and Julia Ladewig. I have performed the theoretical design and practical validation of the generated organoids via RT-PCR and immunocytochemical characterization in this publication. In order to maximize the comprehension and enable other researchers to reproduce our protocol efficiently, this study has been published alongside a visualized step-by-step experimental procedure featuring Olivia Krefft and me as experimenters as well as Olivia Krefft, Julia Ladewig and me as commentators and can be watched on the journals platform online.

Summing up, the protocol presented here describes a method, which allows the generation of standardized forebrain-type cerebral organoids as an *in vitro* model for human cerebral cortex development. The potential of this methodology is further highlighted by part II and IV of this compendium, in which this tool has been applied to investigate MCD occurring in patients in order to elucidate human specific aspects of the respective underlying pathomechanism.

2.2 Publication II

An Organoid-Based Model of Cortical Development Identifies Non-Cell-Autonomous Defects in Wnt Signaling Contributing to Miller-Dieker Syndrome

Iefremova V, Manikakis G, Krefft O, **Jabali A**, Weynans K, Wilkens R, Marsoner F, Brändl B, Müller F-J, Koch P, Ladewig J. Cell Rep. 2017 Apr 4; 19(1): 50-95.

DOI: 10.1016/j.celrep.2017.03.047

An outstanding feature of the human brain, distinct from most mammals, is the increased expansion of cortex surface facilitated by the formation of convolutions in the form of gyri and sulci. This evolved feature of gyrencephalic species is assumed to be one of the reasons contributing to the extraordinary cognitive abilities of humans. Loss or disruption of the lamination or gyrification of the cortex are considered to be malformations of cortical development and are often accompanied by neuronal disorganization. The loss of convolution is called lissencephaly and can be caused by the impairment of different steps within the sequence of corticogenesis (Fry et al. 2014). In this study we identified a new aspect contributing to the pathomechanism of a form of lissencephaly induced by the heterozygous loss of the genes *PAFAH1B1* and *YWHAE* due to a deletion on chromosome 17p13.3 (Dobyns et al. 1993). This aberration results in a disease that can be referred to as Miller-Dieker syndrome (MDS). Patients diagnosed with this syndrome suffer from cognitive impairment, growth restriction and intractable epilepsy while the syndrome is furthermore associated with lissencephaly and reduced brain size (Dobyns et al. 1991; Dobyns et al. 1993; Nagamani et al. 2009). So far, insights into the pathogenesis of lissencephaly associated with loss or perturbation of LIS1 (the respective protein to the gene *PAFAH1B1*) have been largely derived from post-mortem brain tissue of patients or mouse models like the *Pafah1b1* mutant mice line (Hirotsune et al. 1998; Sheen et al. 2006; Smith et al. 2000). Taken together, most of these previous studies concluded that LIS1-mediated lissencephaly, including MDS, is due to defects in neuronal migration (Kato and Dobyns 2003; Sheen et al. 2006). On a molecular level, NDEL1 together with the proteins LIS1 and YWHAE are part of an intracellular multi-protein complex, which is reported to be essential for centrosomal protein localization, microtubule dynamics and the regulation of cytoplasmic dynein (Faulkner et al. 2000; Moon et al. 2014; Tanaka et al. 2004). Moreover, LIS1 is required for the correct orientation of the spindle apparatus in mitotic neuroepithelial progenitors undergoing symmetric cell division (Yingling et al. 2008). Although, as aforementioned, mouse

models have been widely used to study the cellular function of the LIS1/NDEL1/YWHAE multi-protein complex, they are not fully recapitulating the severity of the lissencephaly as seen in human patients induced by the deficiency in *PAFAH1B1* and *YWHAE*. Analyzing forebrain-type cerebral organoids (introduced in part II of this compendium) derived from two MDS patients and control iPSC lines, we were able to recapitulate the reduced expansion rate of MDS brains as well as an reduction in length of the VS and the diameter and area of individual VZs *in vitro*. Reintroduction of *PAFAH1B1* or *YWHAE* into the respective MDS patient lines lead to a partial rescue of these parameters in organoids derived from these lines. As LIS1 is involved in microtubule organization and spindle apparatus orientation via dynein, we investigated possible impacts on acetylated-tubulin integrity in the VZ and orientation of the mitotic spindle of dividing cells at the VS. Thereby we were able to identify severe disturbances in the microtubule network of aRG cell in the VZ of MDS derived organoids as well as alterations of plane of cell division shifting from symmetric divisions towards asymmetric division modes. This significant switch of plane of cell divisions favoring asymmetric cell divisions causes a decrease in radial glia cell amplification in the ventricular zone and can be correlated with premature neurogenesis and a significant reduction in size of the MDS patient organoids. This is in line with the identification of an increase in neurogenesis and the abundance of mitotically restricted IPs. Furthermore, we were able to demonstrate a disruption of the VZ niche architecture in organoids derived from MDS patients. As a consequence, changes of the N-Cadherin/b-Catenin signaling axis can be observed. Several different experiments pointed out that impairments in the cell adhesion molecule N-Cadherin within the VZ niche directly influences a downstream signaling cascade via AKT and the phosphorylation of b-Catenin, which results in a decrease in canonical WNT signaling. Thereby we identified a non-cell autonomous expansion defect in MDS derived organoids and cortical cultures that affects radial glia cells. Noticeably, from experiments in mice it is known that the signaling cascade via N-Cadherin, AKT and b-Catenin within the VZ niche facilitates self-renewal while inhibiting differentiation of cortical aRG cells (Zhang et al. 2013; Zhang et al. 2010). Based on these findings we tested whether activation of the canonical WNT signaling cascade will restore some of the phenotypic alterations found in MDS derived organoids. Therefore, we pharmacologically activated the canonical WNT signaling in MDS derived organoids and analyzed features, which are perturbed upon loss of *PAFAH1B1* and *YWHAE*. Indeed, the expansion defect as well as plane of cell division alterations were rescued upon WNT activation. Taken together, this study highlights the role of LIS1 and YWHAE in maintaining the cortical niche architecture and the potential of our iPSC-

based organoid system to decipher the impact of loss of single genes on early human cortical development. Immunocytochemical and gene expression analyses of control organoids as well as the investigation of the canonical WNT pathway in control and patient derived 2D cortical progenitors have been performed by me.

2.3 Publication III

Mutations in the Heterotopia Gene *Eml1/EML1* Severely Disrupt the Formation of Primary Cilia.

Uzquiano A, Cifuentes-Diaz C, **Jabali A**, Romero D, Houllier A, Dingli F, Maillard C, Boland A, Deleuze J F, Loew D, Mancini G M.S., Bahi-Buisson N, Ladewig J, Francis F. Cell Rep. 2019 Aug 6; 28(6): 1596-1611.e10. DOI: 10.1016/j.celrep.2019.06.096

Corticogenesis can be summarized as a sequence of processes necessary for the formation of the cerebral cortex during the development of the CNS (Budday et al. 2015). Impairments of aRG cells during corticogenesis can result in cortical malformations during mammalian brain development. These malformations include SBH, which is characterized by misplaced neurons below the actual cortex. In other cases of SBH genes like *PAFAH1B1*, *DCX* and *TUBA1A* have been found to be mutated and highlight the involvement of the microtubule cytoskeleton in this manifestation of MCD (Jaglin and Chelly 2009). The pathogenesis regarding the formation of SBH remained little understood as the respective mouse models rarely display the typical formation of ectopically located neurons in the form of a band (Corbo et al. 2002; Hirotsune et al. 1998; Keays et al. 2007). Mutations in *Eml1/EML1* on the other hand consistently lead to SBH formation in mice and humans, which enabled colleagues and us to investigate the mechanisms underlying the formation of heterotopias *in vivo* in mice and *in vitro* using cells of human origin. It has been demonstrated that *Eml1/EML1* is involved in organization and assembly of the microtubule cytoskeleton, thereby affecting spindle apparatus assembly and orientation as well as ciliogenesis (Bizzotto et al. 2017; Jijumon et al. 2022; Kielar et al. 2014; Markus et al. 2021; Yin et al. 2021). These impairments are proposed to have a detrimental influence on neurodevelopmental processes and we set out to investigate additional cellular or molecular perturbations and their contribution to the formation of SBH.

In this study collaborators and we used the HeCo mouse model as well as human control and *EML1*-patient fibroblasts (Kielar et al. 2014) and iPSC-derived cortical progenitor cells in order to investigate the underlying pathomechanism of *Eml1/EML1*-driven malformations of brain development. As reported previously in Kielar et al. 2014, the HeCo mouse line bears an insertion of a 5.5-kilobasepair retrotransposon eventually leading to perturbed *Eml1* transcripts and the overall absence of wildtype *Eml1* transcripts in HeCo brains. This in turn impairs protein conformation and proper

function of Eml1. The impairment of Eml1 leads to ectopic proliferating cells in the developing cortical wall, perturbed aRG cells cell behavior presumably due to the aforementioned aberrant primary cilia and abnormalities regarding the spindle apparatus (Bizzotto et al. 2017; Kielar et al. 2014). In addition to this mouse model we had access to fibroblasts from two human patients diagnosed with different mutations in *EML1* initially mentioned in 2014 (Kielar et al. 2014). As mentioned afore, Magnetic resonance imaging (MRI) of these patients revealed several manifestations of MCD (alongside the previously mentioned SBH) discussed in more detail in publication IV of this compendium. The mutations in *EML1* identified in the human cells either lead to the abort of transcription or affected the proteins capacity to associate and bind microtubule, thus significantly impairing the proteins function (Jijumon et al. 2022).

The identification of abnormally positioned aRG cells in mutant mice led to the question regarding the function and the involvement in biological processes of Eml1/EML1 in aRG cell and the pathomechanism underlying the premature delamination and mitotic behavior outside the VZ in aberrant basal positions. Using the HeCo mouse model as well as human fibroblast and iPSC-derived cortical progenitors we confirmed a role of Eml1/EML1 in the formation of primary cilia leading to less, shorter and aberrantly positioned cilia. In order to elucidate other potential cellular roles of EML1, pull-down experiments were performed using the full-length protein with the aim to identify potential, previously unreported, interaction partners. Mass spectrometry analyses revealed a significant number of ciliary-related interaction partner, like RPGRIP1L, alongside cell-cell adhesion, actin and microtubule associated proteins as well as proteins falling into the category of Golgi-derived protein transport. Based on the significance of cargo trafficking and Golgi-mediated protein transport for proper primary cilia formation (Bernabé-Rubio and Alonso 2017), our colleagues focused on the Golgi apparatus and related protein trafficking. *In utero* electroporation of plasmids expressing Golgi apparatus targeting fluorescent proteins and electron microscopic analyses demonstrated disruption of the rodent and human Golgi structures. Tracing experiments furthermore revealed perturbations of the anterograde trafficking from Golgi structures in Eml1/EML1 deficient cells. Based on the novel role of Eml1/EML1 in Golgi apparatus integrity and related protein trafficking, it can be concluded that the disrupted Golgi-primary cilia axis impacts aRG cell dynamics in pathological conditions thereby contributing to the heterotopia formation.

The generation of the human iPSC lines from patient fibroblasts as well as the generation and culture of thereof derived cortical progenitors and the generation of control cortical progenitors for this study have been performed by me.

2.4 Publication IV

Human cerebral organoids reveal progenitor pathology in *EML1*-linked cortical malformation

Jabali A, Hoffrichter A, Uzquiano A, Marsoner F, Wilkens R, Siekmann M, Bohl B, Rossetti A C, Horschitz S, Koch P, Francis F, Ladewig J. *EMBO Rep.* 2022 Mar 15:e54027. DOI: 10.15252/embr.202154027

The human cerebral cortex is a complex structure consisting of layers and folds and errors within the sequence of steps leading to the formation of the cortex can result in cortical disorganization with severe consequences including epilepsy and intellectual disability. The third publication of this compendium described the consequences of impairment in the *Eml1/EML1* gene using the HeCo mouse model to gain insight into *Eml1*-linked cortical malformation *in vivo*, while this study recapitulates and extends our findings using the human iPSC-based organoid model introduced in part one of this compendium in order to gain more insight into human specific aspects of *EML1*-linked cortical malformation. In addition to our 2D cortical progenitor cell culture model, we used cerebral organoids derived from patients and genome edited iPSCs to investigate pathophysiological changes associated with SBH, megalencephaly and polymicrogyria. The *EML1*-deficient fibroblasts we reprogrammed into iPSCs haven been donated by patients diagnosed with different mutations in the gene *EML1* (Kielar et al. 2014). The same patient lines have been used in the context of experiments within the third publication in the form of iPSC derived 2D cortical progenitors (Uzquiano et al. 2019). MRI of these patients revealed the presence of a SBH and lead to the diagnosis of megalencephaly and polymicrogyria as well as hydrocephaly in one of the two patients (Kielar et al. 2014; Oegema et al. 2019; Shaheen et al. 2017). In one patient a compound heterozygous mutation in *EML1* could be diagnosed; one allele harbored a mutation terminating the transcription while the other allele resulted in a protein with decreased capacity to associate and bind microtubule. The *EML1* sequence of the other patient harbored a homozygous mutation presumably perturbing the binding affinity to microtubule. In both patients the missense mutations are located in the Hydrophobic Echinoderm-Like Protein (HELP) domain, which is assumed to contribute significantly to the microtubule-binding properties of *EML1* and its paralogs (Richards et al. 2014; Tegha-Dunghu et al. 2008). A recent study indeed demonstrated the effect of the disease-related mutations in *EML1* on microtubule binding *in vitro* (Jijumon et al. 2022). From experiments in mice and human fibroblasts and cortical progenitors it is

already known that perturbations of *Eml1*/*EML1* affect the spindle apparatus orientation and length, the cell shape of mitotic cells, primary cilia as well as the Golgi apparatus (Bizzotto et al. 2017; Kielar et al. 2014; Uzquiano et al. 2019). As consequences, premature delamination of mitotic cortical progenitors, a disorganized RGC scaffold and the formation of a heterotopia can be found in mouse and rat cortices (Collins et al. 2019; Grosenbaugh et al. 2020; Kielar et al. 2014; Markus et al. 2021). Moreover, researchers were able to connect *Eml1* impairment with retinal photoreceptor migration and survival and the overall disruption of the retinal lamination (Collin et al. 2020; Poria et al. 2022). In this study we demonstrate that *EML1*-deficient organoids display ectopic neural rosettes at the basal side of the ventricular zone and clusters of heterotopic neurons below an early formation of a normotopic CP-like region. This phenotype additionally could be observed in organoids derived from two different heterozygous *EML1*-KO (*EML1*-heKO) iPSC lines generated via a CRISPR-Cas9 system. Furthermore, we were able to replicate perturbed aRG cell behavior, including significant changes in the plane of cell division of *EML1*-deficient cells and reduced length as well as perturbed structures of their primary cilia as seen in mouse and rat models of *Eml1*-deficiency. To gain further insight into the hypothesis that *EML1*-deficient aRG cells delaminate prematurely from the VS, we generated organoids consistent of healthy control cells and a small fraction of *EML1*-heKO labeled with EGFP. Analyzing these hybrid organoids, we were able to show a significant increase of EGFP positive *EML1*-heKO cells at the basal side of the VZ compared to hybrid organoids generated from control iPSCs and control-EGFP cells. Thereby we could conclude that *EML1*-deficiency causes a cell intrinsic mechanism leading to the accumulation of ectopic progenitors. Analysis of single-cell RNA sequencing data from control and *EML1*-deficient organoids showed a significant up-regulation of bRG cell markers and human-specific extracellular matrix components in the ectopic cell population. In order to identify parameters contributing to the massive expansion of ectopic cells and the underlying mechanism we looked into the Hippo signaling pathway recently reported to cause premature progenitor delamination, ectopic rosette formation, heterotopia formation as well as megalencephaly in mice and chicken (Cappello et al. 2013; Liu et al. 2018; Najas et al. 2020; O'Neill et al. 2018; Saito et al. 2018). The occurrence of ectopically proliferating progenitors could be linked to a significant increase in YAP1 (downstream effector of the Hippo signaling pathway) translocations into the nucleus in delaminated RG cells. We further demonstrated that this YAP1-driven expansion as well as the formation of ectopic rosettes could be partially restored by pharmacological modulation of Hippo signaling, thereby further supporting the idea that deregulation of this pathway contributes to heterotopia

formation in humans. Our data highlights a progenitor origin of *EML1*-linked MCD and provide new mechanistic insight into the formation of subcortical heterotopia in a human context. As stated in the “Author contribution” section of the publication presented here, my task was, kindly guided by Julia Ladewig, to design the experiments, investigate, curate and analyze the data supported by colleagues and collaborators listed as co-authors.

3. Summary

The development of the mammalian cortex comprises a sequence of steps including the expansion of RG cells, generation of neurons followed by neuronal migration and their organization into a laminated structure typically consisting of 6 layers of neurons in a mature brain (Casingal et al. 2022; Rakic 2009). Disturbances of any of these steps involved in corticogenesis can lead to cortical malformation with severe consequences for the individual affected. These can include epilepsy, intellectual disabilities and a variety of neuropsychiatric manifestations (Klingler et al. 2021).

In order to get deeper insight into mammalian cortical development and associated MCD, the different studies put together in this compendium exhibit a range of model systems utilized. These include a mouse model, iPSC-derived cortical progenitors and thereof differentiated neurons as well as iPSC-derived cerebral organoids. This enabled us to investigate underlying pathomechanisms of different MCD *in vivo*, on a human cellular level of homogeneous 2D cell cultures and in a 3D contextualized model for fetal brain development. To underscore the significance of our human cerebral organoid model, one part of this compendium is describing in-depth the generation and quality assessment of this *in vitro* model in addition to a scientific video depicting the methodology in detail (Kreff et al. 2018). We were able to demonstrate the standardized generation of forebrain-type cerebral organoids recapitulating early stages of human brain development from iPSCs emphasizing the high reproducibility across batches. In order to address future questions and to adapt this *in vitro* model, further steps additional to the existing protocol are planned with the aim to develop our organoid platform into a more complex system. Research on neuropsychiatric diseases as well as on epileptiform activity relies on an organoid model faithfully recapitulating electrophysiological activity and circuit formation (Foliaki et al. 2021; Samarasinghe et al. 2021; Trujillo et al. 2019). To achieve this we will enable organoids to grow older and mature simultaneously by slicing them on a regular basis, which increases nutrient support to the core of the organoid thereby avoiding the formation of necrotic centers (Giandomenico et al. 2019; Qian et al. 2020). Regarding the investigation of neural circuits and crosstalk between different brain regions and associated disturbances, it will be necessary to develop the fusion of area-specific brain organoids, so-called assembloids, as demonstrated in recent work from the group of Sergiu Pasca (Marton and Paşca 2020; Miura et al. 2020). In cases of specific research questions we will adapt and modify our protocol in order to facilitate cellular diversity by promoting gliogenesis (oligodendrogenesis in particular) thereby further supporting neuronal

activity and synchronicity (Zafeiriou et al. 2020) and in specific cases accelerate the maturation of neurons using a cocktail of small molecules (Ciceri et al. 2022; Hergenreder et al. 2022). Based on the idea to increase the cellular complexity of the organoid cell culture and thereby the proximity to the *in vivo* situation it can be discussed to add specific cell types to the 3D structure separately. Microglia, a major component of the CNS-specific part of the immune system, can be efficiently derived from iPSC cultures in high number (Abud et al. 2017; Haenseler et al. 2017; Hasselmann and Blurton-Jones 2020; Muffat et al. 2016) and studies demonstrated increased neuronal maturation, functionality and decreased DNA damage in RGCs after integration into brain organoids (Popova et al. 2021; Sabate-Soler et al. 2022). A vascular-like system is another component missing in most of the organoid systems and recent research indicates the beneficial influence of vascularization on brain organoids making it a more complete and significant model (Cakir et al. 2019; Yu 2021).

Iefremova *et al.* validates this significance of brain organoids in the context of investigations of the pathomechanism underlying MDS associated lissencephaly (Iefremova et al. 2017). Access to fibroblasts from two patients suffering from MDS made it possible to reprogram the cells into iPSCs. Thereof we generated cortical progenitors, neurons and cerebral organoids and compared different parameters like growth, onset of neurogenesis, cytoarchitectural aspects as well as signaling pathways between patient and control cells and organoids. Thereby, we identified altered microtubule networks and premature neurogenesis of patient cells in 2D and 3D, which leads to reduced expansion of patient organoids. Furthermore, analysis of the patient ventricular surfaces enabled us to demonstrate disruption of the VZ area niche architecture, which eventually led to the conclusion that this impairment is causative for alterations of the N-cadherin/ β -catenin signaling axis. Modulation of this axis rescued phenotypic alterations in patient-derived organoids supporting the findings of this study. The study highlights that our organotypic 3D cell-culture model contributes to an advanced understanding of the mechanism causing lissencephaly and severe reduction in total brain size as observed in MDS patients (Sheen et al. 2006). The relevance of organoid research in this context is supported by a study published simultaneously (Bershteyn et al. 2017) reporting additionally a phenotype in bRG cell mitosis, a cell type abundant in oSVZs of species with convoluted brains like primates and human. The involvement of the highly proliferative bRG cells in the pathophysiology of Miller-Dieker syndrome suggests a link between this cell type and the development of the observed lissencephaly. This is reinforced by a recent study, indicating that Lis1 dysfunction impairs bRG cell production and positioning in mice

telencephalon (Penisson et al. 2022). To achieve this, the researchers increased number of bRG-like cells in mouse embryonic brains by *in utero* electroporation of the hominid-specific gene *TBC1D3*. After confirming that the number of bRG-like cells in basal location increased in wildtype brains upon expression of *TBC1D3*, the same approach was used in the context of heterozygous *Lis1* mutant mice. These recent results confirm our findings that heterozygous *Lis1* depletion alters mitotic spindle orientation at the VS as well as adhesion proteins like N-cadherin, and demonstrate that this can lead to an increase in abventricular mitoses in *Lis1*-deficient mice. In addition to that, our most recent findings confirm alterations regarding cytoarchitecture, neurogenesis, microtubule stability and niche-dependent WNT-signaling in our organoid model derived from different *LIS1*-deficient human iPSC lines. Furthermore, we demonstrate that, depending on the locus of alteration in the gene, heterozygous mutations within *PAFAH1B1* lead to different phenotype severities in patient iPSC-derived organoids reflecting the lissencephaly severity in humans (Rossetti et al. 2022). Another pathological change that can occur during brain development, which we investigated across two independent publications, can be termed *Eml1/EML1*-linked cortical malformation. Caused by impairment or deficiency of the protein EML1, this malformation comprises several different forms of MCD in humans (Oegema et al. 2019; Shaheen et al. 2017). MRI of patients suffering from *EML1*-linked cortical malformation demonstrates increased brain size (megalencephaly), polymicrogyria (numerous small cortical convolutions) as well as a massive accumulation of neurons below the actual cortex (subcortical band heterotopia) of which the latter can be found in mouse and rat models of *Eml1* deficiency as well (Collins et al. 2019; Grosenbaugh et al. 2020; Kielar et al. 2014). In the third study investigating the consequences of *Eml1/EML1* mutations, collaborators and we used the HeCo mouse model and human patient fibroblasts as well as patient iPSC-derived cortical progenitors to investigate consequences of *Eml1/EML1* deficiency for corticogenesis (Uzquiano et al. 2019). The identification of abnormally positioned aRG cells above the VZ in HeCo mice led to the question regarding the function of *Eml1/EML1* in aRG cells and its role in maintaining these cells at the ventricular surface and in the VZ. The function of *Eml1/EML1* in microtubule cytoskeleton assembly and organization suggested investigation of organelles dependent on dynamic microtubule assembly and disassembly as well as microtubule stability. Primary cilia, a microtubule-based cellular organelle, well known to harbor critical function during brain development (Park et al. 2019), were identified to be affected by *Eml1/EML1*-impairment. We demonstrated a perturbed formation of mice and human primary cilia leading to less, shorter and mispositioned cilia in mutant mice and patient derived cortical progenitors. In addition, we identified RPGRIP1L as a

ciliary interaction partner of *Eml1/EML1*, critical for proper primary cilia formation as well. Another organelle affected upon mutations in *Eml1/EML1* was the Golgi apparatus, an organelle responsible for post-translational modification and vesicular transport of proteins synthesized in the endoplasmic reticulum. Data from the HeCo mouse model, patient fibroblasts and patient iPSC-derived cortical progenitors demonstrated a significantly reduced number of Golgi-elements, an altered distribution within aRG cell extensions as well as an overall disruption of the Golgi apparatus and its anterograde transport. It can be hypothesized that this disruption leads to abnormal adhesion molecule transport to the endfeet of aRG cell and impaired membrane attachment, which consequently contributes to premature delamination from the VS. This delamination can be seen as causative for the formation of heterotopia seen in mice cortices deficient for *Eml1*.

In order to decipher the human-specific features of *EML1*-linked MCD we focused on human iPSC-derived cortical progenitors and cerebral organoids from *EML1*-patients and *EML1*-KO lines while comparing them to control lines (Jabali et al. 2022). Using our cerebral organoid model (Kreff et al. 2018) we were able to recapitulate the formation of SBH-like phenotypes displaying β -III-tubulin neurons misplaced in between the VZ area and an ectopic cell population. Interestingly, this ectopic cell population in part organizes into rosette-like structures exhibiting an accumulation of N-cadherin in their centers above the VZ areas in all *EML1*-deficient organoids. Moreover, we confirmed the primary cilia phenotype in *EML1*-deficient cortical progenitors as well as the altered plane of cell division at the ventricular surface as observed in the HeCo model (Kielar et al. 2014). Using an *EML1*-KO iPSC line tagged by EGFP mixed with control cells, we could demonstrate that these cells delaminate prematurely from the VZ surface even if residing in a healthy control environment. This observation points towards a cell autonomous phenomenon. In order to get a detailed insight into the cell composition and specifically the ectopic cell population we performed single-cell RNA sequencing on *EML1*-KO and control organoids. Thereby we could get more detailed insight into the ectopic cell population composed of perturbed progenitor cells, which is most likely not reflecting a cell type during normal brain development. These cells display aberrant expression of ECM and bRG cell marker genes and could be identified in organoid slices using antibodies against COL1A2 and MEIS2. Morphological analysis of the cells forming the ectopic rosettes confirmed a rather perturbed morphology in contrast to a RG-like elongated organization with an apical or basal process found in control organoids. To further shed light on the unproportional expansion of this ectopic, perturbed progenitor population, we focused on cell proliferation outside the VZ areas. Increased proliferation at the

basal side of the VZ areas in all *EML1*-deficient organoids raised the question regarding the underlying mechanism resulting in increased mitotic behavior of the ectopic cells. Recent scientific work investigating premature cortical progenitor delamination, ectopic rosette formation, megalencephaly and the formation of periventricular neuronal heterotopia link these pathological features to a deregulation of the Hippo signaling pathway (Cappello et al. 2013; Liu et al. 2018; Najas et al. 2020; O'Neill et al. 2018; Saito et al. 2018; Samarasinghe et al. 2021). When investigating YAP1, a major downstream effector of the Hippo pathway, we could identify increased nuclear YAP1 in the cortical progenitors positioned distally to the VZ surface within the VZ areas as well as increased nuclear signal in mitotically active, ectopic cells outside the VZ areas. Pharmacological modulation of the function of YAP1 resulted in a significant decrease in mitotic cells at the basal side of VZ areas as well as a significant decrease in the formation of ectopic rosette-like structures. These findings lead to the conclusion that deregulation of YAP1-mediated signaling is a strong influence regarding the proliferative behavior of delaminated, ectopic progenitors eventually leading to the massive amount of mislocated cells above the VZ area. Using our *in vitro* model, we were able to demonstrate for the first time in a human context that *EML1*-deficiency leads to the formation of ectopic neural rosettes and the formation of an early heterotopia driven by YAP1 mediated expansion of delaminated progenitors. Additional experiments could focus on the mechanism behind the deregulation of the Hippo signaling pathway. One hypothesis to follow up could be the suggested potential increase in mechanical stress in VZs of *Emi1/EML1*-deficient mice or organoids due to longer metaphase spindles and flatter mitotic cells occupying more space at the VS (Bizzotto et al. 2017). On the one hand the mechanical stress could encourage the delamination of progenitors at the VS and on the other hand it could potentially contribute to the translocation of YAP1 into the nucleus of these cells. Studies investigating mechanical input on cells identified YAP1 as a mechanosensitive transcription factor, which is activated upon stiffening or increased tension of surrounding tissue (Cai et al. 2021; Scott et al. 2021; Shao et al. 2020). Changes in cellular cytoskeletal properties, cell-cell contact and changes in ECM environment influencing rigidity and stiffness of cellular microenvironment upon *EML1*-impairment could further explain the increase in YAP1 translocation promoting mitotic behavior of delaminated cells, pointing towards a potential connection between aberrant ECM gene expression in *EML1*-KO organoids and an increase in YAP1 activity (Halder et al. 2012; Hao et al. 2014; Zhao et al. 2007). Future experiments will also show whether in later stages of organoid development and/or additional modification of the organoid protocol

(Karzbrun et al. 2018) human specific pathophysiological features like megalencephaly and polymicrogyria-like cortices (Kielar et al. 2014) can be detected.

A noteworthy aspect of the presented studies III and IV is the recapitulation of certain phenotypic features reported in mice and our organoid model. This underlines the reliability of this system on the one hand but also highlights the potential of brain organoids to add to the full picture whenever previously gained insight regarding neurodevelopmental disorders need to be completed in regard of human specific aspects. This can open the door in light of drug discovery and screening on human iPSC derived organoids whenever animal models show their limitations (Bailey and Balls 2019; Wang et al. 2021).

Taken together, we could show that we can get deeper insight into the pathomechanisms of neurodevelopmental disorders like MCD utilizing mouse models and human iPSC-derived cerebral organoids. In addition, we could demonstrate that we can not only reproduce findings discovered by investigating mouse models but also have the capability to exceed previous research in a human-specific context by utilizing our human 3D model for early corticogenesis. This suggests that organoid-based systems serve as promising models to study early human cortical development and associated disorders.

4. References

- Abud EM, Ramirez RN, Martinez ES, Healy LM, Nguyen CHH, Newman SA, Yeromin AV, Scarfone VM, Marsh SE, Fimbres C et al. 2017. Ipsc-derived human microglia-like cells to study neurological diseases. *Neuron*. 94(2):278-293.e279.
- Ahn Y, An JH, Yang HJ, Lee DG, Kim J, Koh H, Park YH, Song BS, Sim BW, Lee HJ et al. 2021. Human blood vessel organoids penetrate human cerebral organoids and form a vessel-like system. *Cells*. 10(8).
- Amiri A, Coppola G, Scuderi S, Wu F, Roychowdhury T, Liu F, Pochareddy S, Shin Y, Safi A, Song L et al. 2018. Transcriptome and epigenome landscape of human cortical development modeled in organoids. *Science*. 362(6420).
- Angevine JB, Sidman RL. 1961. Autoradiographic study of cell migration during histogenesis of cerebral cortex in the mouse. *Nature*. 192:766-768.
- Azevedo FA, Carvalho LR, Grinberg LT, Farfel JM, Ferretti RE, Leite RE, Jacob Filho W, Lent R, Herculano-Houzel S. 2009. Equal numbers of neuronal and nonneuronal cells make the human brain an isometrically scaled-up primate brain. *J Comp Neurol*. 513(5):532-541.
- Baala L, Briault S, Etchevers HC, Laumonier F, Natiq A, Amiel J, Boddaert N, Picard C, Sbiti A, Asermouh A et al. 2007. Homozygous silencing of t-box transcription factor *eomes* leads to microcephaly with polymicrogyria and corpus callosum agenesis. *Nat Genet*. 39(4):454-456.
- Bailey J, Balls M. 2019. Recent efforts to elucidate the scientific validity of animal-based drug tests by the pharmaceutical industry, pro-testing lobby groups, and animal welfare organisations. *BMC Med Ethics*. 20(1):16.
- Beattie R, Hippenmeyer S. 2017. Mechanisms of radial glia progenitor cell lineage progression. *FEBS Lett*. 591(24):3993-4008.
- Bernabé-Rubio M, Alonso MA. 2017. Routes and machinery of primary cilium biogenesis. *Cell Mol Life Sci*. 74(22):4077-4095.
- Bershteyn M, Nowakowski TJ, Pollen AA, Di Lullo E, Nene A, Wynshaw-Boris A, Kriegstein AR. 2017. Human ipsc-derived cerebral organoids model cellular features of lissencephaly and reveal prolonged mitosis of outer radial glia. *Cell Stem Cell*. 20(4):435-449.e434.
- Betizeau M, Cortay V, Patti D, Pfister S, Gautier E, Bellemin-Ménard A, Afanassieff M, Huissoud C, Douglas RJ, Kennedy H et al. 2013. Precursor diversity and complexity of lineage relationships in the outer subventricular zone of the primate. *Neuron*. 80(2):442-457.
- Bizzotto S, Uzquiano A, Dingli F, Ershov D, Houllier A, Arras G, Richards M, Loew D, Minc N, Croquelois A et al. 2017. *Eml1* loss impairs apical progenitor spindle length and soma shape in the developing cerebral cortex. *Sci Rep*. 7(1):17308.
- Bond J, Roberts E, Mochida GH, Hampshire DJ, Scott S, Askham JM, Springell K, Mahadevan M, Crow YJ, Markham AF et al. 2002. *Aspm* is a major determinant of cerebral cortical size. *Nat Genet*. 32(2):316-320.
- Borrell V, Götz M. 2014. Role of radial glial cells in cerebral cortex folding. *Curr Opin Neurobiol*. 27:39-46.
- Buchsbaum IY, Cappello S. 2019. Neuronal migration in the cns during development and disease: Insights from. *Development*. 146(1).
- Budday S, Steinmann P, Kuhl E. 2015. Physical biology of human brain development. *Front Cell Neurosci*. 9:257.
- Bultje RS, Castaneda-Castellanos DR, Jan LY, Jan YN, Kriegstein AR, Shi SH. 2009. Mammalian *par3* regulates progenitor cell asymmetric division via notch signaling in the developing neocortex. *Neuron*. 63(2):189-202.
- Buss RR, Sun W, Oppenheim RW. 2006. Adaptive roles of programmed cell death during nervous system development. *Annu Rev Neurosci*. 29:1-35.

- Bystron I, Rakic P, Molnár Z, Blakemore C. 2006. The first neurons of the human cerebral cortex. *Nat Neurosci.* 9(7):880-886.
- Cai X, Wang KC, Meng Z. 2021. Mechanoregulation of yap and taz in cellular homeostasis and disease progression. *Front Cell Dev Biol.* 9:673599.
- Cakir B, Xiang Y, Tanaka Y, Kural MH, Parent M, Kang YJ, Chapeton K, Patterson B, Yuan Y, He CS et al. 2019. Engineering of human brain organoids with a functional vascular-like system. *Nat Methods.* 16(11):1169-1175.
- Cappello S, Gray MJ, Badouel C, Lange S, Einsiedler M, Srouf M, Chitayat D, Hamdan FF, Jenkins ZA, Morgan T et al. 2013. Mutations in genes encoding the cadherin receptor-ligand pair *dchs1* and *fat4* disrupt cerebral cortical development. *Nat Genet.* 45(11):1300-1308.
- Casingal CR, Descant KD, Anton ES. 2022. Coordinating cerebral cortical construction and connectivity: Unifying influence of radial progenitors. *Neuron.* 110(7):1100-1115.
- Chambers SM, Fasano CA, Papapetrou EP, Tomishima M, Sadelain M, Studer L. 2009. Highly efficient neural conversion of human es and ips cells by dual inhibition of smad signaling. *Nat Biotechnol.* 27(3):275-280.
- Ciceri G, Cho H, Kshirsagar M, Baggiolini A, Aromolaran AA, Walsh RM, Goldstein PA, Koche RP, Leslie CS, Studer L. 2022. An epigenetic barrier sets the timing of human neuronal maturation. *bioRxiv.*
- Collin GB, Won J, Krebs MP, Hicks WJ, Charette JR, Naggert JK, Nishina PM. 2020. Disruption in murine *eml1* perturbs retinal lamination during early development. *Sci Rep.* 10(1):5647.
- Collins SC, Uzquiano A, Selloum M, Wendling O, Gaborit M, Osipenko M, Birling MC, Yalcin B, Francis F. 2019. The neuroanatomy of *eml1* knockout mice, a model of subcortical heterotopia. *J Anat.* 235(3):637-650.
- Copp AJ, Harding BN. 1999. Neuronal migration disorders in humans and in mouse models--an overview. *Epilepsy Res.* 36(2-3):133-141.
- Corbo JC, Deuel TA, Long JM, LaPorte P, Tsai E, Wynshaw-Boris A, Walsh CA. 2002. Doublecortin is required in mice for lamination of the hippocampus but not the neocortex. *J Neurosci.* 22(17):7548-7557.
- Costa MR, Wen G, Lepier A, Schroeder T, Götz M. 2008. Par-complex proteins promote proliferative progenitor divisions in the developing mouse cerebral cortex. *Development.* 135(1):11-22.
- Davis LK, Meyer KJ, Rudd DS, Librant AL, Epping EA, Sheffield VC, Wassink TH. 2008. *Pax6* 3' deletion results in aniridia, autism and mental retardation. *Hum Genet.* 123(4):371-378.
- Dehay C, Kennedy H, Kosik KS. 2015. The outer subventricular zone and primate-specific cortical complexification. *Neuron.* 85(4):683-694.
- Delaunay D, Kawaguchi A, Dehay C, Matsuzaki F. 2017. Division modes and physical asymmetry in cerebral cortex progenitors. *Curr Opin Neurobiol.* 42:75-83.
- Dennis D, Picketts D, Slack RS, Schuurmans C. 2016. Forebrain neurogenesis: From embryo to adult. *Trends Dev Biol.* 9(1):77-90.
- des Portes V, Francis F, Pinard JM, Desguerre I, Moutard ML, Snoeck I, Meiners LC, Capron F, Cusmai R, Ricci S et al. 1998. Doublecortin is the major gene causing x-linked subcortical laminar heterotopia (sclh). *Hum Mol Genet.* 7(7):1063-1070.
- Dobyns WB, Curry CJ, Hoyme HE, Turlington L, Ledbetter DH. 1991. Clinical and molecular diagnosis of miller-dieker syndrome. *Am J Hum Genet.* 48(3):584-594.
- Dobyns WB, Reiner O, Carrozzo R, Ledbetter DH. 1993. Lissencephaly. A human brain malformation associated with deletion of the *lis1* gene located at chromosome 17p13. *JAMA.* 270(23):2838-2842.

- Eiraku M, Watanabe K, Matsuo-Takasaki M, Kawada M, Yonemura S, Matsumura M, Wataya T, Nishiyama A, Muguruma K, Sasai Y. 2008. Self-organized formation of polarized cortical tissues from escs and its active manipulation by extrinsic signals. *Cell Stem Cell*. 3(5):519-532.
- Fagerlund I, Dougalis A, Shakirzyanova A, Gómez-Budia M, Pelkonen A, Konttinen H, Ohtonen S, Fazaludeen MF, Koskivi M, Kuusisto J et al. 2021. Microglia-like cells promote neuronal functions in cerebral organoids. *Cells*. 11(1).
- Fallet-Bianco C, Laquerrière A, Poirier K, Razavi F, Guimiot F, Dias P, Loeuillet L, Lascelles K, Beldjord C, Carion N et al. 2014. Mutations in tubulin genes are frequent causes of various foetal malformations of cortical development including microlissencephaly. *Acta Neuropathol Commun*. 2:69.
- Faulkner NE, Dujardin DL, Tai CY, Vaughan KT, O'Connell CB, Wang Y, Vallee RB. 2000. A role for the lissencephaly gene *lis1* in mitosis and cytoplasmic dynein function. *Nat Cell Biol*. 2(11):784-791.
- Feng Y, Walsh CA. 2004. Mitotic spindle regulation by *nde1* controls cerebral cortical size. *Neuron*. 44(2):279-293.
- Fiddes IT, Lodewijk GA, Mooring M, Bosworth CM, Ewing AD, Mantalas GL, Novak AM, van den Bout A, Bishara A, Rosenkrantz JL et al. 2018. Human-specific *notch2nl* genes affect notch signaling and cortical neurogenesis. *Cell*. 173(6):1356-1369.e1322.
- Fischer J, Fernández Ortuño E, Marsoner F, Artioli A, Peters J, Namba T, Eugster Oegema C, Huttner WB, Ladewig J, Heide M. 2022. Human-specific *arhgap11b* ensures human-like basal progenitor levels in hominid cerebral organoids. *EMBO Rep*. 23(11):e54728.
- Florio M, Albert M, Taverna E, Namba T, Brandl H, Lewitus E, Haffner C, Sykes A, Wong FK, Peters J et al. 2015. Human-specific gene *arhgap11b* promotes basal progenitor amplification and neocortex expansion. *Science*. 347(6229):1465-1470.
- Florio M, Huttner WB. 2014. Neural progenitors, neurogenesis and the evolution of the neocortex. *Development*. 141(11):2182-2194.
- Foliaki ST, Schwarz B, Groveman BR, Walters RO, Ferreira NC, Orrù CD, Smith A, Wood A, Schmit OM, Freitag P et al. 2021. Neuronal excitatory-to-inhibitory balance is altered in cerebral organoid models of genetic neurological diseases. *Mol Brain*. 14(1):156.
- Fry AE, Cushion TD, Pilz DT. 2014. The genetics of lissencephaly. *Am J Med Genet C Semin Med Genet*. 166C(2):198-210.
- Gabriel E, Wason A, Ramani A, Gooi LM, Keller P, Pozniakovsky A, Poser I, Noack F, Telugu NS, Calegari F et al. 2016. *Cpap* promotes timely cilium disassembly to maintain neural progenitor pool. *EMBO J*. 35(8):803-819.
- Garcia KE, Kroenke CD, Bayly PV. 2018. Mechanics of cortical folding: Stress, growth and stability. *Philos Trans R Soc Lond B Biol Sci*. 373(1759).
- Germain N, Banda E, Grabel L. 2010. Embryonic stem cell neurogenesis and neural specification. *J Cell Biochem*. 111(3):535-542.
- Giandomenico SL, Mierau SB, Gibbons GM, Wenger LMD, Masullo L, Sit T, Sutcliffe M, Boulanger J, Tripodi M, Derivery E et al. 2019. Cerebral organoids at the air-liquid interface generate diverse nerve tracts with functional output. *Nat Neurosci*. 22(4):669-679.
- Gil-Sanz C, Landeira B, Ramos C, Costa MR, Müller U. 2014. Proliferative defects and formation of a double cortex in mice lacking *mltt4* and *cdh2* in the dorsal telencephalon. *J Neurosci*. 34(32):10475-10487.
- Gilmore EC, Herrup K. 1997. Cortical development: Layers of complexity. *Curr Biol*. 7(4):R231-234.

- Grosenbaugh DK, Joshi S, Fitzgerald MP, Lee KS, Wagley PK, Koepfel AF, Turner SD, McConnell MJ, Goodkin HP. 2020. A deletion in *eml1* leads to bilateral subcortical heterotopia in the tish rat. *Neurobiol Dis.* 140:104836.
- Guerrini R, Dobyns WB. 2014. Malformations of cortical development: Clinical features and genetic causes. *Lancet Neurol.* 13(7):710-726.
- Guo J, Higginbotham H, Li J, Nichols J, Hirt J, Ghukasyan V, Anton ES. 2015. Developmental disruptions underlying brain abnormalities in ciliopathies. *Nat Commun.* 6:7857.
- Götz M, Huttner WB. 2005. The cell biology of neurogenesis. *Nat Rev Mol Cell Biol.* 6(10):777-788.
- Haenseler W, Sansom SN, Buchrieser J, Newey SE, Moore CS, Nicholls FJ, Chintawar S, Schnell C, Antel JP, Allen ND et al. 2017. A highly efficient human pluripotent stem cell microglia model displays a neuronal-co-culture-specific expression profile and inflammatory response. *Stem Cell Reports.* 8(6):1727-1742.
- Halder G, Dupont S, Piccolo S. 2012. Transduction of mechanical and cytoskeletal cues by *yap* and *taz*. *Nat Rev Mol Cell Biol.* 13(9):591-600.
- Hansen DV, Lui JH, Parker PR, Kriegstein AR. 2010. Neurogenic radial glia in the outer subventricular zone of human neocortex. *Nature.* 464(7288):554-561.
- Hao J, Zhang Y, Wang Y, Ye R, Qiu J, Zhao Z, Li J. 2014. Role of extracellular matrix and *yap/taz* in cell fate determination. *Cell Signal.* 26(2):186-191.
- Hasenpusch-Theil K, Theil T. 2021. The multifaceted roles of primary cilia in the development of the cerebral cortex. *Front Cell Dev Biol.* 9:630161.
- Hasselmann J, Blurton-Jones M. 2020. Human ipsc-derived microglia: A growing toolset to study the brain's innate immune cells. *Glia.* 68(4):721-739.
- Hergenreder E, Zorina Y, Zhao Z, Munguba H, Calder EL, Baggiolini A, Minotti AP, Walsh RM, Liston C, Levitz J et al. 2022. Combined small molecule treatment accelerates timing of maturation in human pluripotent stem cell-derived neurons. *bioRxiv.*
- Heyn P, Logan CV, Fluteau A, Challis RC, Auchynnikava T, Martin CA, Marsh JA, Tagliani F, Kilanowski F, Parry DA et al. 2019. Gain-of-function *dnmt3a* mutations cause microcephalic dwarfism and hypermethylation of polycomb-regulated regions. *Nat Genet.* 51(1):96-105.
- Hirotsune S, Fleck MW, Gambello MJ, Bix GJ, Chen A, Clark GD, Ledbetter DH, McBain CJ, Wynshaw-Boris A. 1998. Graded reduction of *pafah1b1* (*lis1*) activity results in neuronal migration defects and early embryonic lethality. *Nat Genet.* 19(4):333-339.
- Hong SE, Shugart YY, Huang DT, Shahwan SA, Grant PE, Hourihane JO, Martin ND, Walsh CA. 2000. Autosomal recessive lissencephaly with cerebellar hypoplasia is associated with human *reln* mutations. *Nat Genet.* 26(1):93-96.
- Huang WK, Wong SZH, Pather SR, Nguyen PTT, Zhang F, Zhang DY, Zhang Z, Lu L, Fang W, Chen L et al. 2021. Generation of hypothalamic arcuate organoids from human induced pluripotent stem cells. *Cell Stem Cell.* 28(9):1657-1670.e1610.
- Huang ZJ, Di Cristo G, Ango F. 2007. Development of gaba innervation in the cerebral and cerebellar cortices. *Nat Rev Neurosci.* 8(9):673-686.
- Huttner WB, Kosodo Y. 2005. Symmetric versus asymmetric cell division during neurogenesis in the developing vertebrate central nervous system. *Curr Opin Cell Biol.* 17(6):648-657.
- Iefremova V, Manikakis G, Krefft O, Jabali A, Weynans K, Wilkens R, Marsoner F, Brändl B, Müller FJ, Koch P et al. 2017. An organoid-based model of cortical development identifies non-cell-autonomous defects in *wnt* signaling contributing to miller-dieker syndrome. *Cell Rep.* 19(1):50-59.
- Insolera R, Bazzi H, Shao W, Anderson KV, Shi SH. 2014. Cortical neurogenesis in the absence of centrioles. *Nat Neurosci.* 17(11):1528-1535.

- Jabali A, Hoffrichter A, Uzquiano A, Marsoner F, Wilkens R, Siekmann M, Bohl B, Rossetti AC, Horschitz S, Koch P et al. 2022. Human cerebral organoids reveal progenitor pathology in *eml1*-linked cortical malformation. *EMBO Rep.*e54027.
- Jackson AP, Eastwood H, Bell SM, Adu J, Toomes C, Carr IM, Roberts E, Hampshire DJ, Crow YJ, Mighell AJ et al. 2002. Identification of microcephalin, a protein implicated in determining the size of the human brain. *Am J Hum Genet.* 71(1):136-142.
- Jaglin XH, Chelly J. 2009. Tubulin-related cortical dysgeneses: Microtubule dysfunction underlying neuronal migration defects. *Trends Genet.* 25(12):555-566.
- Jijumon AS, Bodakuntla S, Genova M, Bangerla M, Sackett V, Besse L, Maksut F, Henriot V, Magiera MM, Sirajuddin M et al. 2022. Lysate-based pipeline to characterize microtubule-associated proteins uncovers unique microtubule behaviours. *Nat Cell Biol.* 24(2):253-267.
- Johnson MB, Sun X, Kodani A, Borges-Monroy R, Girskis KM, Ryu SC, Wang PP, Patel K, Gonzalez DM, Woo YM et al. 2018. *Aspm* knockout ferret reveals an evolutionary mechanism governing cerebral cortical size. *Nature.* 556(7701):370-375.
- Kadoshima T, Sakaguchi H, Nakano T, Soen M, Ando S, Eiraku M, Sasai Y. 2013. Self-organization of axial polarity, inside-out layer pattern, and species-specific progenitor dynamics in human es cell-derived neocortex. *Proc Natl Acad Sci U S A.* 110(50):20284-20289.
- Kadowaki M, Nakamura S, Machon O, Krauss S, Radice GL, Takeichi M. 2007. N-cadherin mediates cortical organization in the mouse brain. *Dev Biol.* 304(1):22-33.
- Kalebic N, Gilardi C, Stepien B, Wilsch-Bräuninger M, Long KR, Namba T, Florio M, Langen B, Lombardot B, Shevchenko A et al. 2019. Neocortical expansion due to increased proliferation of basal progenitors is linked to changes in their morphology. *Cell Stem Cell.* 24(4):535-550.e539.
- Kanton S, Boyle MJ, He Z, Santel M, Weigert A, Sanchís-Calleja F, Guijarro P, Sidow L, Fleck JS, Han D et al. 2019. Organoid single-cell genomic atlas uncovers human-specific features of brain development. *Nature.* 574(7778):418-422.
- Karzbrun E, Kshirsagar A, Cohen SR, Hanna JH, Reiner O. 2018. Human brain organoids on a chip reveal the physics of folding. *Nat Phys.* 14(5):515-522.
- Kathuria A, Lopez-Lengowski K, Jagtap SS, McPhie D, Perlis RH, Cohen BM, Karmacharya R. 2020. Transcriptomic landscape and functional characterization of induced pluripotent stem cell-derived cerebral organoids in schizophrenia. *JAMA Psychiatry.* 77(7):745-754.
- Kato M, Dobyns WB. 2003. Lissencephaly and the molecular basis of neuronal migration. *Hum Mol Genet.* 12 Spec No 1:R89-96.
- Keays DA, Tian G, Poirier K, Huang GJ, Siebold C, Cleak J, Oliver PL, Fray M, Harvey RJ, Molnár Z et al. 2007. Mutations in alpha-tubulin cause abnormal neuronal migration in mice and lissencephaly in humans. *Cell.* 128(1):45-57.
- Keller R, Davidson L, Edlund A, Elul T, Ezin M, Shook D, Skoglund P. 2000. Mechanisms of convergence and extension by cell intercalation. *Philos Trans R Soc Lond B Biol Sci.* 355(1399):897-922.
- Keller R, Shih J, Sater AK, Moreno C. 1992. Planar induction of convergence and extension of the neural plate by the organizer of *xenopus*. *Dev Dyn.* 193(3):218-234.
- Kielar M, Tuy FP, Bizzotto S, Lebrand C, de Juan Romero C, Poirier K, Oegema R, Mancini GM, Bahi-Buisson N, Olaso R et al. 2014. Mutations in *eml1* lead to ectopic progenitors and neuronal heterotopia in mouse and human. *Nat Neurosci.* 17(7):923-933.
- Klaus J, Kanton S, Kyrousi C, Ayo-Martin AC, Di Giaimo R, Riesenberger S, O'Neill AC, Camp JG, Tocco C, Santel M et al. 2019. Altered neuronal migratory

- trajectories in human cerebral organoids derived from individuals with neuronal heterotopia. *Nat Med.* 25(4):561-568.
- Klingler E, Francis F, Jabaudon D, Cappello S. 2021. Mapping the molecular and cellular complexity of cortical malformations. *Science.* 371(6527).
- Kreff O, Jabali A, Iefremova V, Koch P, Ladewig J. 2018. Generation of standardized and reproducible forebrain-type cerebral organoids from human induced pluripotent stem cells. *J Vis Exp.* (131).
- Krenn V, Bosone C, Burkard TR, Spanier J, Kalinke U, Calistri A, Salata C, Rilo Christoff R, Pestana Garcez P, Mirazimi A et al. 2021. Organoid modeling of zika and herpes simplex virus 1 infections reveals virus-specific responses leading to microcephaly. *Cell Stem Cell.* 28(8):1362-1379.e1367.
- Kriegstein A, Alvarez-Buylla A. 2009. The glial nature of embryonic and adult neural stem cells. *Annu Rev Neurosci.* 32:149-184.
- Kroenke CD, Bayly PV. 2018. How forces fold the cerebral cortex. *J Neurosci.* 38(4):767-775.
- Kwan KY, Sestan N, Anton ES. 2012. Transcriptional co-regulation of neuronal migration and laminar identity in the neocortex. *Development.* 139(9):1535-1546.
- LaMonica BE, Lui JH, Hansen DV, Kriegstein AR. 2013. Mitotic spindle orientation predicts outer radial glial cell generation in human neocortex. *Nat Commun.* 4:1665.
- Lancaster MA, Corsini NS, Wolfinger S, Gustafson EH, Phillips AW, Burkard TR, Otani T, Livesey FJ, Knoblich JA. 2017. Guided self-organization and cortical plate formation in human brain organoids. *Nat Biotechnol.* 35(7):659-666.
- Lancaster MA, Knoblich JA. 2014. Generation of cerebral organoids from human pluripotent stem cells. *Nat Protoc.* 9(10):2329-2340.
- Lancaster MA, Renner M, Martin CA, Wenzel D, Bicknell LS, Hurles ME, Homfray T, Penninger JM, Jackson AP, Knoblich JA. 2013. Cerebral organoids model human brain development and microcephaly. *Nature.* 501(7467):373-379.
- Lanza RP. 2009. *Essentials of stem cell biology.* Amsterdam ; Boston: Elsevier/Academic Press.
- Lewitus E, Kelava I, Huttner WB. 2013. Conical expansion of the outer subventricular zone and the role of neocortical folding in evolution and development. *Front Hum Neurosci.* 7:424.
- Li H, Gao L, Du J, Ma T, Ye Z, Li Z. 2021. To better generate organoids, what can we learn from teratomas? *Front Cell Dev Biol.* 9:700482.
- Li Y, Muffat J, Omer A, Bosch I, Lancaster MA, Sur M, Gehrke L, Knoblich JA, Jaenisch R. 2017. Induction of expansion and folding in human cerebral organoids. *Cell Stem Cell.* 20(3):385-396.e383.
- Lien WH, Klezovitch O, Fernandez TE, Delrow J, Vasioukhin V. 2006. Alpha-catenin controls cerebral cortical size by regulating the hedgehog signaling pathway. *Science.* 311(5767):1609-1612.
- Liu J, Liu W, Yang L, Wu Q, Zhang H, Fang A, Li L, Xu X, Sun L, Zhang J et al. 2017. The primate-specific gene *tmem14b* marks outer radial glia cells and promotes cortical expansion and folding. *Cell Stem Cell.* 21(5):635-649.e638.
- Liu S, Trupiano MX, Simon J, Guo J, Anton ES. 2021. The essential role of primary cilia in cerebral cortical development and disorders. *Curr Top Dev Biol.* 142:99-146.
- Liu WA, Chen S, Li Z, Lee CH, Mirzaa G, Dobyns WB, Ross ME, Zhang J, Shi SH. 2018. *Pard3* dysfunction in conjunction with dynamic hippo signaling drives cortical enlargement with massive heterotopia. *Genes Dev.* 32(11-12):763-780.
- Lodato S, Arlotta P. 2015. Generating neuronal diversity in the mammalian cerebral cortex. *Annu Rev Cell Dev Biol.* 31:699-720.
- Long KR, Newland B, Florio M, Kalebic N, Langen B, Kolterer A, Wimberger P, Huttner WB. 2018. Extracellular matrix components *hapln1*, *lumican*, and *collagen i*

- cause hyaluronic acid-dependent folding of the developing human neocortex. *Neuron*. 99(4):702-719.e706.
- Lui JH, Hansen DV, Kriegstein AR. 2011. Development and evolution of the human neocortex. *Cell*. 146(1):18-36.
- Markus F, Kannengießer A, Näder P, Atigbire P, Scholten A, Vössing C, Bültmann E, Korenke GC, Owczarek-Lipska M, Neidhardt J. 2021. A novel missense variant in the *eml1* gene associated with bilateral ribbon-like subcortical heterotopia leads to ciliary defects. *J Hum Genet*. 66(12):1159-1167.
- Marthiens V, Basto R. 2020. Centrosomes: The good and the bad for brain development. *Biol Cell*. 112(6):153-172.
- Marton RM, Paşca SP. 2020. Organoid and assembloid technologies for investigating cellular crosstalk in human brain development and disease. *Trends Cell Biol*. 30(2):133-143.
- Matsumoto N, Tanaka S, Horiike T, Shinmyo Y, Kawasaki H. 2020. A discrete subtype of neural progenitor crucial for cortical folding in the gyrencephalic mammalian brain. *Elife*. 9.
- Matsuzaki F, Shitamukai A. 2015. Cell division modes and cleavage planes of neural progenitors during mammalian cortical development. *Cold Spring Harb Perspect Biol*. 7(9):a015719.
- Mirzaa G, Parry DA, Fry AE, Giamanco KA, Schwartzentruber J, Vanstone M, Logan CV, Roberts N, Johnson CA, Singh S et al. 2014. De novo *ccnd2* mutations leading to stabilization of cyclin d2 cause megalencephaly-polymicrogyria-polydactyly-hydrocephalus syndrome. *Nat Genet*. 46(5):510-515.
- Miura Y, Li MY, Birey F, Ikeda K, Revah O, Thete MV, Park JY, Puno A, Lee SH, Porteus MH et al. 2020. Generation of human striatal organoids and cortico-striatal assembloids from human pluripotent stem cells. *Nat Biotechnol*. 38(12):1421-1430.
- Molyneaux BJ, Arlotta P, Menezes JR, Macklis JD. 2007. Neuronal subtype specification in the cerebral cortex. *Nat Rev Neurosci*. 8(6):427-437.
- Moon HM, Youn YH, Pemble H, Yingling J, Wittmann T, Wynshaw-Boris A. 2014. *Lis1* controls mitosis and mitotic spindle organization via the *lis1-ndel1-dynein* complex. *Hum Mol Genet*. 23(2):449-466.
- Muffat J, Li Y, Yuan B, Mitalipova M, Omer A, Corcoran S, Bakiasi G, Tsai LH, Aubourg P, Ransohoff RM et al. 2016. Efficient derivation of microglia-like cells from human pluripotent stem cells. *Nat Med*. 22(11):1358-1367.
- Muguruma K, Nishiyama A, Kawakami H, Hashimoto K, Sasai Y. 2015. Self-organization of polarized cerebellar tissue in 3d culture of human pluripotent stem cells. *Cell Rep*. 10(4):537-550.
- Mukhtar T, Taylor V. 2018. Untangling cortical complexity during development. *J Exp Neurosci*. 12:1179069518759332.
- Nadarajah B, Parnavelas JG. 2002. Modes of neuronal migration in the developing cerebral cortex. *Nat Rev Neurosci*. 3(6):423-432.
- Nagamani SC, Zhang F, Shchelochkov OA, Bi W, Ou Z, Scaglia F, Probst FJ, Shinawi M, Eng C, Hunter JV et al. 2009. Microdeletions including *ywhae* in the miller-dieker syndrome region on chromosome 17p13.3 result in facial dysmorphisms, growth restriction, and cognitive impairment. *J Med Genet*. 46(12):825-833.
- Najas S, Pijuan I, Esteve-Codina A, Usieto S, Martinez JD, Zwijsen A, Arbonés ML, Martí E, Le Dréau G. 2020. A *smad1/5-yap* signalling module drives radial glia self-amplification and growth of the developing cerebral cortex. *Development*. 147(13).
- Nakagawa N, Yagi H, Kato K, Takematsu H, Oka S. 2015. Ectopic clustering of cajal-retzius and subplate cells is an initial pathological feature in *pomgnt2*-knockout mice, a model of dystroglycanopathy. *Sci Rep*. 5:11163.

- Nikolopoulou E, Galea GL, Rolo A, Greene ND, Copp AJ. 2017. Neural tube closure: Cellular, molecular and biomechanical mechanisms. *Development*. 144(4):552-566.
- Notaras M, Lodhi A, Dündar F, Collier P, Sayles NM, Tilgner H, Greening D, Colak D. 2022. Schizophrenia is defined by cell-specific neuropathology and multiple neurodevelopmental mechanisms in patient-derived cerebral organoids. *Mol Psychiatry*. 27(3):1416-1434.
- Nowakowski TJ, Pollen AA, Sandoval-Espinosa C, Kriegstein AR. 2016. Transformation of the radial glia scaffold demarcates two stages of human cerebral cortex development. *Neuron*. 91(6):1219-1227.
- O'Neill AC, Kyrousi C, Einsiedler M, Burtscher I, Drukker M, Markie DM, Kirk EP, Götz M, Robertson SP, Cappello S. 2018. Mob2 insufficiency disrupts neuronal migration in the developing cortex. *Front Cell Neurosci*. 12:57.
- Oegema R, McGillivray G, Leventer R, Le Moing AG, Bahi-Buisson N, Barnicoat A, Mandelstam S, Francis D, Francis F, Mancini GMS et al. 2019. Eml1-associated brain overgrowth syndrome with ribbon-like heterotopia. *Am J Med Genet C Semin Med Genet*. 181(4):627-637.
- Olson EC. 2014. Analysis of preplate splitting and early cortical development illuminates the biology of neurological disease. *Front Pediatr*. 2:121.
- Oppenheim RW. 1991. Cell death during development of the nervous system. *Annu Rev Neurosci*. 14:453-501.
- Ossola C, Kalebic N. 2021. Roots of the malformations of cortical development in the cell biology of neural progenitor cells. *Front Neurosci*. 15:817218.
- Ostrowski PJ, Zachariou A, Loveday C, Beleza-Meireles A, Bertoli M, Dean J, Douglas AGL, Ellis I, Foster A, Graham JM et al. 2019. The chd8 overgrowth syndrome: A detailed evaluation of an emerging overgrowth phenotype in 27 patients. *Am J Med Genet C Semin Med Genet*. 181(4):557-564.
- Otani T, Marchetto MC, Gage FH, Simons BD, Livesey FJ. 2016. 2d and 3d stem cell models of primate cortical development identify species-specific differences in progenitor behavior contributing to brain size. *Cell Stem Cell*. 18(4):467-480.
- Paridaen JT, Huttner WB. 2014. Neurogenesis during development of the vertebrate central nervous system. *EMBO Rep*. 15(4):351-364.
- Park SM, Jang HJ, Lee JH. 2019. Roles of primary cilia in the developing brain. *Front Cell Neurosci*. 13:218.
- Passemard S, Perez F, Gressens P, El Ghouzzi V. 2019. Endoplasmic reticulum and golgi stress in microcephaly. *Cell Stress*. 3(12):369-384.
- Pellegrini L, Bonfio C, Chadwick J, Begum F, Skehel M, Lancaster MA. 2020. Human CNS barrier-forming organoids with cerebrospinal fluid production. *Science*. 369(6500).
- Penisson M, Jin M, Wang S, Hirotsune S, Francis F, Belvindrah R. 2022. Lis1 mutation prevents basal radial glia-like cell production in the mouse. *Hum Mol Genet*. 31(6):942-957.
- Pilz GA, Shitamukai A, Reillo I, Pacary E, Schwausch J, Stahl R, Ninkovic J, Snippert HJ, Clevers H, Godinho L et al. 2013. Amplification of progenitors in the mammalian telencephalon includes a new radial glial cell type. *Nat Commun*. 4:2125.
- Pinson A, Xing L, Namba T, Kalebic N, Peters J, Oegema CE, Traikov S, Reppe K, Riesenberger S, Maricic T et al. 2022. Human tktl1 implies greater neurogenesis in frontal neocortex of modern humans than neanderthals. *Science*. 377(6611):eabl6422.
- Pollen AA, Nowakowski TJ, Chen J, Retallack H, Sandoval-Espinosa C, Nicholas CR, Shuga J, Liu SJ, Oldham MC, Diaz A et al. 2015. Molecular identity of human outer radial glia during cortical development. *Cell*. 163(1):55-67.

- Pontious A, Kowalczyk T, Englund C, Hevner RF. 2008. Role of intermediate progenitor cells in cerebral cortex development. *Dev Neurosci.* 30(1-3):24-32.
- Popova G, Soliman SS, Kim CN, Keefe MG, Hennick KM, Jain S, Li T, Tejera D, Shin D, Chhun BB et al. 2021. Human microglia states are conserved across experimental models and regulate neural stem cell responses in chimeric organoids. *Cell Stem Cell.* 28(12):2153-2166.e2156.
- Poria D, Sun C, Santeford A, Kielar M, Apte RS, Kisselev OG, Chen S, Kefalov VJ. 2022. Eml1 is essential for retinal photoreceptor migration and survival. *Sci Rep.* 12(1):2897.
- Pringsheim M, Mitter D, Schröder S, Warthemann R, Plümacher K, Kluger G, Baethmann M, Bast T, Braun S, Büttel HM et al. 2019. Structural brain anomalies in patients with foxg1 syndrome and in foxg1+/- mice. *Ann Clin Transl Neurol.* 6(4):655-668.
- Przyborski SA. 2005. Differentiation of human embryonic stem cells after transplantation in immune-deficient mice. *Stem Cells.* 23(9):1242-1250.
- Qian X, Nguyen HN, Song MM, Hadiono C, Ogden SC, Hammack C, Yao B, Hamersky GR, Jacob F, Zhong C et al. 2016. Brain-region-specific organoids using mini-bioreactors for modeling zikv exposure. *Cell.* 165(5):1238-1254.
- Qian X, Su Y, Adam CD, Deutschmann AU, Pather SR, Goldberg EM, Su K, Li S, Lu L, Jacob F et al. 2020. Sliced human cortical organoids for modeling distinct cortical layer formation. *Cell Stem Cell.* 26(5):766-781.e769.
- Quadrato G, Nguyen T, Macosko EZ, Sherwood JL, Min Yang S, Berger DR, Maria N, Scholvin J, Goldman M, Kinney JP et al. 2017. Cell diversity and network dynamics in photosensitive human brain organoids. *Nature.* 545(7652):48-53.
- Rakic P. 1995. A small step for the cell, a giant leap for mankind: A hypothesis of neocortical expansion during evolution. *Trends Neurosci.* 18(9):383-388.
- Rakic P. 2009. Evolution of the neocortex: A perspective from developmental biology. *Nat Rev Neurosci.* 10(10):724-735.
- Rash BG, Duque A, Morozov YM, Arellano JI, Micali N, Rakic P. 2019. Gliogenesis in the outer subventricular zone promotes enlargement and gyrification of the primate cerebrum. *Proc Natl Acad Sci U S A.* 116(14):7089-7094.
- Reillo I, de Juan Romero C, García-Cabezas M, Borrell V. 2011. A role for intermediate radial glia in the tangential expansion of the mammalian cerebral cortex. *Cereb Cortex.* 21(7):1674-1694.
- Richards MW, Law EW, Rennalls LP, Busacca S, O'Regan L, Fry AM, Fennell DA, Bayliss R. 2014. Crystal structure of eml1 reveals the basis for hsp90 dependence of oncogenic eml4-alk by disruption of an atypical β -propeller domain. *Proc Natl Acad Sci U S A.* 111(14):5195-5200.
- Rossetti AC, Fechtner O, Maillard C, Hoffrichter A, Zillich L, Poisel E, Jabali A, Marsoner F, Wilkens R, Francis F et al. 2022. Capturing the pathomechanisms of different disease severities in a human cerebral organoid model of lis1-lissencephaly. *bioRxiv.2022.2012.2019.520907.*
- Sabate-Soler S, Nickels SL, Saraiva C, Berger E, Dubonyte U, Barmpa K, Lan YJ, Kouno T, Jarazo J, Robertson G et al. 2022. Microglia integration into human midbrain organoids leads to increased neuronal maturation and functionality. *Glia.* 70(7):1267-1288.
- Sadler TW. 2005. Embryology of neural tube development. *Am J Med Genet C Semin Med Genet.* 135C(1):2-8.
- Saito K, Kawasoe R, Sasaki H, Kawaguchi A, Miyata T. 2018. Neural progenitor cells undergoing yap/tead-mediated enhanced self-renewal form heterotopias more easily in the diencephalon than in the telencephalon. *Neurochem Res.* 43(1):180-189.
- Samarasinghe RA, Miranda OA, Buth JE, Mitchell S, Ferando I, Watanabe M, Allison TF, Kurdian A, Fotion NN, Gandal MJ et al. 2021. Identification of neural

- oscillations and epileptiform changes in human brain organoids. *Nat Neurosci.* 24(10):1488-1500.
- Sasai Y. 2013a. Cytosystems dynamics in self-organization of tissue architecture. *Nature.* 493(7432):318-326.
- Sasai Y. 2013b. Next-generation regenerative medicine: Organogenesis from stem cells in 3d culture. *Cell Stem Cell.* 12(5):520-530.
- Sausedo RA, Smith JL, Schoenwolf GC. 1997. Role of nonrandomly oriented cell division in shaping and bending of the neural plate. *J Comp Neurol.* 381(4):473-488.
- Sawada T, Chater TE, Sasagawa Y, Yoshimura M, Fujimori-Tonou N, Tanaka K, Benjamin KJM, Paquola ACM, Erwin JA, Goda Y et al. 2020. Developmental excitation-inhibition imbalance underlying psychoses revealed by single-cell analyses of discordant twins-derived cerebral organoids. *Mol Psychiatry.* 25(11):2695-2711.
- Scott KE, Fraley SI, Rangamani P. 2021. A spatial model of yap/taz signaling reveals how stiffness, dimensionality, and shape contribute to emergent outcomes. *Proc Natl Acad Sci U S A.* 118(20).
- Shaheen R, Sebai MA, Patel N, Ewida N, Kurdi W, Altweijri I, Sogaty S, Almardawi E, Seidahmed MZ, Alnemri A et al. 2017. The genetic landscape of familial congenital hydrocephalus. *Ann Neurol.* 81(6):890-897.
- Shao W, Yang J, He M, Yu XY, Lee CH, Yang Z, Joyner AL, Anderson KV, Zhang J, Tsou MB et al. 2020. Centrosome anchoring regulates progenitor properties and cortical formation. *Nature.* 580(7801):106-112.
- Sheen VL, Ferland RJ, Neal J, Harney M, Hill RS, Banham A, Brown P, Chenn A, Corbo J, Hecht J et al. 2006. Neocortical neuronal arrangement in miller dieker syndrome. *Acta Neuropathol.* 111(5):489-496.
- Sheen VL, Ganesh VS, Topcu M, Sebire G, Bodell A, Hill RS, Grant PE, Shugart YY, Imitola J, Khoury SJ et al. 2004. Mutations in arfgef2 implicate vesicle trafficking in neural progenitor proliferation and migration in the human cerebral cortex. *Nat Genet.* 36(1):69-76.
- Shimada IS, Somatilaka BN, Hwang SH, Anderson AG, Shelton JM, Rajaram V, Konopka G, Mukhopadhyay S. 2019. Derepression of sonic hedgehog signaling upon gpr161 deletion unravels forebrain and ventricular abnormalities. *Dev Biol.* 450(1):47-62.
- Shinmyo Y, Saito K, Hamabe-Horiike T, Kameya N, Ando A, Kawasaki K, Duong TAD, Sakashita M, Roboon J, Hattori T et al. 2022. Localized astrogenesis regulates gyrification of the cerebral cortex. *Sci Adv.* 8(10):eabi5209.
- Shitamukai A, Konno D, Matsuzaki F. 2011. Oblique radial glial divisions in the developing mouse neocortex induce self-renewing progenitors outside the germinal zone that resemble primate outer subventricular zone progenitors. *J Neurosci.* 31(10):3683-3695.
- Smith DS, Niethammer M, Ayala R, Zhou Y, Gambello MJ, Wynshaw-Boris A, Tsai LH. 2000. Regulation of cytoplasmic dynein behaviour and microtubule organization by mammalian lis1. *Nat Cell Biol.* 2(11):767-775.
- Smith JL, Schoenwolf GC. 1989. Notochordal induction of cell wedging in the chick neural plate and its role in neural tube formation. *J Exp Zool.* 250(1):49-62.
- Stiles J, Jernigan TL. 2010. The basics of brain development. *Neuropsychol Rev.* 20(4):327-348.
- Takahashi K, Tanabe K, Ohnuki M, Narita M, Ichisaka T, Tomoda K, Yamanaka S. 2007. Induction of pluripotent stem cells from adult human fibroblasts by defined factors. *Cell.* 131(5):861-872.
- Takahashi K, Yamanaka S. 2006. Induction of pluripotent stem cells from mouse embryonic and adult fibroblast cultures by defined factors. *Cell.* 126(4):663-676.

- Tanaka T, Serneo FF, Higgins C, Gambello MJ, Wynshaw-Boris A, Gleeson JG. 2004. Lis1 and doublecortin function with dynein to mediate coupling of the nucleus to the centrosome in neuronal migration. *J Cell Biol.* 165(5):709-721.
- Tang XY, Wu S, Wang D, Chu C, Hong Y, Tao M, Hu H, Xu M, Guo X, Liu Y. 2022. Human organoids in basic research and clinical applications. *Signal Transduct Target Ther.* 7(1):168.
- Taverna E, Götz M, Huttner WB. 2014. The cell biology of neurogenesis: Toward an understanding of the development and evolution of the neocortex. *Annu Rev Cell Dev Biol.* 30:465-502.
- Tegha-Dunghu J, Neumann B, Reber S, Krause R, Erfle H, Walter T, Held M, Rogers P, Hupfeld K, Ruppert T et al. 2008. Eml3 is a nuclear microtubule-binding protein required for the correct alignment of chromosomes in metaphase. *J Cell Sci.* 121(Pt 10):1718-1726.
- Trujillo CA, Gao R, Negraes PD, Gu J, Buchanan J, Preissl S, Wang A, Wu W, Haddad GG, Chaim IA et al. 2019. Complex oscillatory waves emerging from cortical organoids model early human brain network development. *Cell Stem Cell.* 25(4):558-569.e557.
- Uzquiano A, Cifuentes-Diaz C, Jabali A, Romero DM, Houllier A, Dingli F, Maillard C, Boland A, Deleuze JF, Loew D et al. 2019. Mutations in the heterotopia gene *eml1/eml1* severely disrupt the formation of primary cilia. *Cell Rep.* 28(6):1596-1611.e1510.
- Velasco S, Kedaigle AJ, Simmons SK, Nash A, Rocha M, Quadrato G, Paulsen B, Nguyen L, Adiconis X, Regev A et al. 2019. Individual brain organoids reproducibly form cell diversity of the human cerebral cortex. *Nature.* 570(7762):523-527.
- Wang H, Brown PC, Chow ECY, Ewart L, Ferguson SS, Fitzpatrick S, Freedman BS, Guo GL, Hedrich W, Heyward S et al. 2021. 3d cell culture models: Drug pharmacokinetics, safety assessment, and regulatory consideration. *Clin Transl Sci.* 14(5):1659-1680.
- Watanabe M, Buth JE, Vishlaghi N, de la Torre-Ubieta L, Taxidis J, Khakh BS, Coppola G, Pearson CA, Yamauchi K, Gong D et al. 2017. Self-organized cerebral organoids with human-specific features predict effective drugs to combat zika virus infection. *Cell Rep.* 21(2):517-532.
- Wilson SL, Wilson JP, Wang C, Wang B, McConnell SK. 2012. Primary cilia and gli3 activity regulate cerebral cortical size. *Dev Neurobiol.* 72(9):1196-1212.
- Wonders CP, Anderson SA. 2006. The origin and specification of cortical interneurons. *Nat Rev Neurosci.* 7(9):687-696.
- Xu R, Boreland AJ, Li X, Erickson C, Jin M, Atkins C, Pang ZP, Daniels BP, Jiang P. 2021. Developing human pluripotent stem cell-based cerebral organoids with a controllable microglia ratio for modeling brain development and pathology. *Stem Cell Reports.* 16(8):1923-1937.
- Yin H, Zhang T, Wang H, Hu X, Hou X, Fang X, Yin Y, Li H, Shi L, Su YQ. 2021. Echinoderm microtubule associated protein like 1 is indispensable for oocyte spindle assembly and meiotic progression in mice. *Front Cell Dev Biol.* 9:687522.
- Yingling J, Youn YH, Darling D, Toyo-Oka K, Pramparo T, Hirotsune S, Wynshaw-Boris A. 2008. Neuroepithelial stem cell proliferation requires *lis1* for precise spindle orientation and symmetric division. *Cell.* 132(3):474-486.
- Yu J. 2021. Vascularized organoids: A more complete model. *Int J Stem Cells.* 14(2):127-137.
- Zafeiriou MP, Bao G, Hudson J, Halder R, Blenkle A, Schreiber MK, Fischer A, Schild D, Zimmermann WH. 2020. Developmental gaba polarity switch and neuronal plasticity in bioengineered neuronal organoids. *Nat Commun.* 11(1):3791.

- Zaidi D, Chinnappa K, Francis F. 2022. Primary cilia influence progenitor function during cortical development. *Cells*. 11(18).
- Zhang J, Shemezis JR, McQuinn ER, Wang J, Sverdlov M, Chenn A. 2013. Akt activation by n-cadherin regulates beta-catenin signaling and neuronal differentiation during cortical development. *Neural Dev*. 8:7.
- Zhang J, Woodhead GJ, Swaminathan SK, Noles SR, McQuinn ER, Pisarek AJ, Stocker AM, Mutch CA, Funatsu N, Chenn A. 2010. Cortical neural precursors inhibit their own differentiation via n-cadherin maintenance of beta-catenin signaling. *Dev Cell*. 18(3):472-479.
- Zhang W, Ma L, Yang M, Shao Q, Xu J, Lu Z, Zhao Z, Chen R, Chai Y, Chen JF. 2020. Cerebral organoid and mouse models reveal a rab39b-pi3k-mtor pathway-dependent dysregulation of cortical development leading to macrocephaly/autism phenotypes. *Genes Dev*. 34(7-8):580-597.
- Zhang W, Yang SL, Yang M, Herrlinger S, Shao Q, Collar JL, Fierro E, Shi Y, Liu A, Lu H et al. 2019. Modeling microcephaly with cerebral organoids reveals a wdr62-cep170-kif2a pathway promoting cilium disassembly in neural progenitors. *Nat Commun*. 10(1):2612.
- Zhang X, Chen MH, Wu X, Kodani A, Fan J, Doan R, Ozawa M, Ma J, Yoshida N, Reiter JF et al. 2016. Cell-type-specific alternative splicing governs cell fate in the developing cerebral cortex. *Cell*. 166(5):1147-1162.e1115.
- Zhao B, Wei X, Li W, Udan RS, Yang Q, Kim J, Xie J, Ikenoue T, Yu J, Li L et al. 2007. Inactivation of yap oncoprotein by the hippo pathway is involved in cell contact inhibition and tissue growth control. *Genes Dev*. 21(21):2747-2761.
- Zhong X, Pfeifer GP, Xu X. 2006. Microcephalin encodes a centrosomal protein. *Cell Cycle*. 5(4):457-458.

5. Contributions

Here I would like to appreciate the support of my colleagues and collaborators enabling me to present the body of work in this study.

Every individual contribution can be seen in the “Author contributions” section of every publication if not specifically mentioned otherwise.

6. Appendix

6.1 Publication I

Generation of Standardized and Reproducible Forebrain-type Cerebral Organoids from Human Induced Pluripotent Stem Cells.

Kreff O, **Jabali A**, Iefremova V, Koch P, Ladewig J. J Vis Exp 2018 Jan 23;(131): 56768. DOI: 10.3791/56768

Video Article

Generation of Standardized and Reproducible Forebrain-type Cerebral Organoids from Human Induced Pluripotent Stem Cells

Olivia Krefft¹, Ammar Jabali¹, Vira Iefremova¹, Philipp Koch^{1,2,3}, Julia Ladewig¹¹Institute of Reconstructive Neurobiology, University of Bonn²Central Institute of Mental Health, University of Heidelberg/Medical Faculty Mannheim³Hector Institute for Translational Brain Research (HITBR gGmbH)

* These authors contributed equally

Correspondence to: Julia Ladewig at jladewig@uni-bonn.deURL: <https://www.jove.com/video/56768>DOI: [doi:10.3791/56768](https://doi.org/10.3791/56768)

Keywords: Developmental Biology, Issue 131, Induced pluripotent stem cells, neurobiology, cerebral organoids, human cortical development, cortical malformations, disease modeling

Date Published: 1/23/2018

Citation: Krefft, O., Jabali, A., Iefremova, V., Koch, P., Ladewig, J. Generation of Standardized and Reproducible Forebrain-type Cerebral Organoids from Human Induced Pluripotent Stem Cells. *J. Vis. Exp.* (131), e56768, doi:10.3791/56768 (2018).

Abstract

The human cortex is highly expanded and exhibits a complex structure with specific functional areas, providing higher brain function, such as cognition. Efforts to study human cerebral cortex development have been limited by the availability of model systems. Translating results from rodent studies to the human system is restricted by species differences and studies on human primary tissues are hampered by a lack of tissue availability as well as ethical concerns. Recent development in human pluripotent stem cell (PSC) technology include the generation of three-dimensional (3D) self-organizing organotypic culture systems, which mimic to a certain extent human-specific brain development *in vitro*. Currently, various protocols are available for the generation of either whole brain or brain-region specific organoids. The method for the generation of homogeneous and reproducible forebrain-type organoids from induced PSC (iPSC), which we previously established and describe here, combines the intrinsic ability of PSC to self-organize with guided differentiation towards the anterior neuroectodermal lineage and matrix embedding to support the formation of a continuous neuroepithelium. More specifically, this protocol involves: (1) the generation of iPSC aggregates, including the conversion of iPSC colonies to a confluent monolayer culture; (2) the induction of anterior neuroectoderm; (3) the embedding of neuroectodermal aggregates in a matrix scaffold; (4) the generation of forebrain-type organoids from neuroectodermal aggregates; and (5) the fixation and validation of forebrain-type organoids. As such, this protocol provides an easily applicable system for the generation of standardized and reproducible iPSC-derived cortical tissue structures *in vitro*.

Video Link

The video component of this article can be found at <https://www.jove.com/video/56768/>

Introduction

The human brain is clearly one of the most complex organs and is responsible for all human intellectual abilities. Thus, a deeper understanding of human-specific brain development is a critical prerequisite for the understanding of human cognitive abilities. Traditionally, transgenic animals served as model organisms to study brain development. These models provided fundamental insight into the principles of brain development. We now know that a common feature of brain development in all mammals is a precise choreography of progenitor proliferation, neurogenesis, and neuronal migration. There are, however, significant structural differences between the brains of model organisms, such as rodents and humans, especially in the neocortex. The primary mechanisms that have been proposed to contribute to primate cortical evolution are an increased proliferation of stem and progenitor cells as well as the generation of outer radial glia cells (oRGs), which are only very rarely found in rodents^{1,2,3}.

Methods to model human cerebral cortex development include the generation of PSC-derived telencephalic progenitor cells and cerebral cortex projection neurons as monolayer cultures. These standardized differentiation protocols replay certain aspects of human cortical development such as the stereotypical temporal order of cortical neurogenesis⁴. They, however, fall short when it comes to the recapitulation of developmental processes of organogenesis such as spatial patterning and morphogenesis. More recent developments in stem cell biology led to the establishment of 3D organoid cultures from PSCs, which are revolutionizing the research of *in vitro* human organogenesis. Utilizing the capacity of PSCs to self-organize into organotypic structures, various organoids, which reflect key structural and functional properties of organs including those of kidney, gut, the eye, and the brain have been established⁵. Such organoids contain multiple organ-specific cellular subtypes, which group together and spatially organize very similar to the developing organs *in vivo*^{5,6}. In addition, cell composition, lineage relationship, and gene network studies using single-cell RNA sequencing revealed that human cerebral organoids faithfully recapitulate major aspects of human fetal neocortex development such as gene expression programs^{7,8}. One major drawback, which prevented their broad application so far, was, however, the large batch-to-batch variations and organoid-to-organoid heterogeneity⁹.

Here, we provide a detailed protocol for a simple and standardized forebrain-type organoid culture system. The key feature of this system is that it efficiently and reproducibly generates PSC-derived organoids of almost exclusive dorsal telencephalic identity. The protocol is based on the methods used in our recent *Cell Reports* paper¹⁰. It combines the self-organization capacity of iPSCs with selective induction of cortical neuroepithelium and can robustly generate homogeneous cultures of early dorsal telencephalic tissue within 3 weeks. The protocol builds on the previously reported SMAD signaling and Wnt inhibition strategy that guides the differentiation of PSC towards the anterior neuroectodermal lineage^{11,12} in combination with matrix embedding, which promotes the formation of large and continuous neuroepithelial structures¹³. We have successfully used the described method on various iPSC lines, with several clones per individual. We showed that this system is suitable for downstream applications in which reproducibility and homogeneity are of major importance such as disease modeling. When applying the protocol to iPSCs derived from patients suffering from a severe cortical malformation, we were able to recapitulate pathological hallmarks of the disease *in vitro* and to identify new molecular mechanisms leading to the phenotypic changes¹⁰. We suggest that the described organoid protocol can be utilized to close the gap between reductionist PSC-derived cortical monolayer cultures and *in vivo* studies, and that it represents a reliable and stable cell-based model system to simulate early human cortical development in health and disease outside the human body.

Protocol

1. Generation of iPSC Aggregates

1. Generation of single-cell monolayer cultures from iPSC colonies
 1. Prepare a basement membrane extract (BME) coated 6-well plate. Thaw BME on ice at 4 °C for 2-3 h, dilute it with cold Dulbecco's Modified Eagle Medium F12 (DMEM-F12; 1:50 dilution), cover the plate with 1 mL/well of the diluted BME solution, and store the plate overnight at 4 °C.
 2. Aspirate the medium and wash intact iPSC colonies of at least 2 wells of a 6-well plate with 0.5 mM EDTA in phosphate buffered saline (PBS) twice before incubating colonies with 0.5 mM ethylenediaminetetraacetic acid (EDTA) in PBS for 4 min at room temperature (RT). Aspirate EDTA solution and gently detach the colonies by washing them off the bottom of the dish with 5 mL of DMEM-F12 medium. Collect them in a 15-mL tube and pellet them by centrifugation (4 min at 1,200 x g at RT).
Note: iPSCs reprogrammed from commercially available fibroblasts has been successfully used¹⁰.
 3. Aspirate the supernatant and incubate the iPSC colonies with 500 µL of cell-dissociation reagent for 6 min at 37 °C.
 4. Pipet the cell suspension several times gently up and down with a 1 mL pipette to break remaining cell clusters into single cells.
 5. Add 4 mL of DMEM-F12 to the cell suspension to dilute the cell-dissociation reagent.
 6. Spin the cells down at 1,200 x g for 4 min at RT.
 7. Resuspend the cells in 2 mL of iPSC medium supplemented with 5 µM Y-27632 and seed cells into one well of a BME coated 6-well plate.
Note: Use the iPSC medium specified in the **Table of Materials** for a single-cell monolayer iPSC cultures.
 8. On the next day, replace the medium with fresh iPSC medium lacking Y-27632. From this point, continue to culture the cells, changing the medium every day until iPSCs are 100% confluent. Depending on the cell line and the confluency of the starting wells, this will take between 2-4 days.
 9. Once confluent, passage the iPSCs. Aspirate medium and apply 500 µL of cell-dissociation reagent on the cells.
 10. Incubate the cells for 5-10 min at 37 °C. Gently rock the plate to detach the cells.
 11. Wash the cells from the well using 2 mL of DMEM-F12 and collect them in a 15-mL tube. Add DMEM-F12 for a total volume of 5 mL.
 12. Spin down the cells at 1,200 x g for 4 min at RT and aspirate the supernatant.
 13. Seed the cells in iPSC medium supplemented with 5 µM Y-27632 in a 1:2 to 1:4 ratio on a BME coated 6-well plate (2 mL/well of medium).
 14. Continue to culture the cells for 2-5 days and change iPSC medium lacking Y-27632 every day. Once confluent, passage iPSCs (steps 1.1.4-1.1.8).
Note: Culture the iPSCs for at least 2 passages as a monolayer in the iPSC medium specified in the **Table of Materials** before using them for the generation of iPSC aggregates to allow the cells to adapt to the culture conditions.
2. Use monolayer iPSC cultures when they are 70-90% confluent for the generation of iPSC aggregates.
Note: iPSC adapted to the culture conditions as single cells are less prone to stress that leads to cell death during the dissociation and aggregation procedure. Monolayer iPSC cultures need to display typical pluripotent morphology with no evidence of differentiation. Test the cultures on a regular basis for mycoplasma contamination. Work only with mycoplasma-free iPSC cultures.
 1. Aspirate the culture medium from one well of a 6-well plate and apply 500 µL of cell-dissociation reagent on the cells.
 2. Incubate the cells for 5-10 min at 37 °C. Gently rock the plate to detach the cells.
 3. Wash cells from the well using 2 mL of DMEM-F12 and collect them in a 15-mL tube. Add DMEM-F12 for a total volume of 10 mL.
 4. For cell counting, take 25 µL from the cell suspension and mix it with 25 µL of trypan blue to mark dead cells. Count the living cells using a counting chamber.
 5. Collect enough cells (4,500 cells per iPSC aggregate) from the cell suspension in a 15 mL tube.
 6. Spin down the cells at 1,200 x g for 4 min at RT and aspirate the supernatant.
 7. Resuspend the cells in an appropriate volume of iPSC medium supplemented with 50 µM Y-27632 to obtain 4,500 live cells per 150 µL.
Note: Using a high concentration of Y-27632 (50 µM) is critical for the survival of the iPSCs.
 8. Plate 150 µL in each well of a low-attachment 96-well U-bottom plate and place it in the incubator at 37 °C and 5% CO₂.
Note: When generating iPSC aggregates, consider that at least 6 organoids are needed for quality control at day 20 (see Section 5).

2. Induction of Anterior Neuroectoderm

1. Closely monitor morphology changes of the iPSC aggregates every day under the tissue culture microscope using a 4X or 10X power lens. Observe at day 1, cell aggregates with clear borders. Continue to culture iPSC aggregates in the incubator at 37 °C and 5% CO₂.

- Note:** A certain number of dead cells/well is normal and will not affect organoid generation.
2. Feed the iPSC aggregates starting from day 2 and continuing with every other day by gently aspirating approximately 2/3 of the medium without disturbing the cell aggregates at the bottom. Add an additional 100 μ L of iPSC medium lacking Y-27632.
Note: Within 4-6 days the cell aggregates will be 350-450 μ m in diameter and exhibit smooth edges.
 3. At this stage, pool the cell aggregates with a cut 100 μ L pipette tip into a low-attachment 6 cm dish (maximum of 20 aggregates/dish) in cortical induction medium containing DMEM-F12 with N2 supplement (1:200), B27 supplement (1:100), glucose (0.2 mg/mL), cyclic adenosine monophosphate (cAMP; 0.15 μ g/mL), 0.5% non-essential amino acids (NEAA), 1% L-alanyl-L-glutamine, heparin (10 μ g/mL), and the compounds LDN-193189 (180 nM), A83-01 (500 nM), and inhibitor of Wnt response-1 (IWR-1) (10 μ g/mL). Feed the cell aggregates by changing the cortical induction medium 3 days after transferring them to the 6-cm dish.
 4. Closely monitor morphological changes during cortical induction under the tissue culture microscope using a 4X power lens.
Note: After 4-5 days in cortical induction medium, edges of the cell aggregates should begin to brighten at the surface, indicating neuroectodermal differentiation. At this stage, radial organization of a pseudostratified epithelium emerges. Proceed to Section 3 to embed the cell aggregates in a BME matrix.

3. Embedding of Neuroectodermal Aggregates in a Matrix Scaffold

1. Thaw BME on ice at 4 $^{\circ}$ C for 2-3 h. Aliquot undiluted BME in sufficient amounts.
2. Prepare a plastic paraffin film sheet for the embedding procedure. Cut the plastic paraffin film using sterile scissors in 4 cm x 4 cm large pieces, put a piece of the plastic paraffin film over an empty 100 μ L tip tray for 100 μ L tips, and press with a gloved finger so that small dimples in the plastic paraffin film sheet are created (1 dimple/cell aggregate needed). Clean the plastic paraffin film with 70% ethanol and irradiate it with UV light (power: 15 watts, wavelength: 435 nm) under the closed sterile bench for 30 min.
3. Transfer each cell aggregate to one dimple of the plastic paraffin film sheet using a 100 μ L cut tip with 1.5-2 mm opening in diameter. In the case that two cell aggregates are fused, do not separate them but transfer them together to one dimple.
4. Gently aspirate the medium surrounding the cell aggregates using an uncut 100 μ L pipette tip.
Note: Be careful not to suck the cell aggregates into the tip, as this will damage the aggregates.
5. Add 40 μ L of undiluted BME to each cell aggregate.
6. Position each cell aggregate in the middle of the BME drop using an uncut 100 μ L pipette tip.
Note: Be very careful not to harm the developing neuroepithelium with the pipette tip.
7. Carefully transfer the plastic paraffin film sheet using sterile forceps into a 10 cm Petri dish (or another sufficient cell culture dish) and place the dish in the incubator for 15-20 min to allow the BME to solidify.
8. Meanwhile, prepare a low-attachment 6 cm dish containing 5 mL of cortical induction medium.
9. After the polymerization of BME, remove the droplets containing the cell aggregates from the plastic paraffin film sheet. Turn the plastic paraffin film over using sterile forceps and gently squeeze the cell aggregates into the slightly tilted (about 30 $^{\circ}$) low-attachment 6 cm dish until the droplets fall off the plastic paraffin film sheet. Transfer a maximum of 16 cell aggregates into one 6 cm dish.
10. Continue to incubate the cell aggregates at 37 $^{\circ}$ C.

4. Generation of Forebrain-type Organoids from Neuroectodermal Aggregates

1. One day after embedding in a BME matrix, place organoid culture dishes on a rocking cell culture shaker with a tilting angle of 5 $^{\circ}$ and 14 rpm, installed in a cell culture incubator.
2. Monitor organoids every day. Homogeneous neuroepithelial loop-like structures gradually develop after embedding in BME matrix.
3. When neuroepithelial loop structures are visible, change the medium to organoid differentiation medium containing DMEM-F12 with N2 supplement (1:200), B27 supplement (1:100), glucose (0.2 mg/mL), cAMP (0.15 μ g/mL), 0.5% NEAA, 1% L-alanyl-L-glutamine, insulin (2.5 μ g/mL).
4. Replace organoid differentiation medium every 3-4 days until the desired differentiation time point is reached. Then fix organoids (see Section 5).
Note: Occasionally, the tissue may exhibit buds of optically translucent tissue without loop structures. Although this is not ideal, this is not affecting the development of cortical structures. The organoids can be cultured in organoid differentiation medium for up to 40 days. For extended culture periods (40-100 days) the organoid differentiation medium can be supplemented with 1:50 BME to increase tissue complexity and with BDNF and GDNF to allow neuronal survival and maturation^{14,15}.

5. Fixation and Validation of Forebrain-type Organoids

1. For the validation, collect 6 organoids at day 20. Use 3 organoids for mRNA isolation and PCR analyses. Transfer the additional 3 organoids to a 24-well plate containing PBS using a cut 1 mL pipette tip with an opening of 3-3.5 mm for fixation and sequential immunocytochemical analyses.
2. Wash the organoids twice by carefully aspirating the PBS and replacing it with fresh PBS using a 5-mL pipette. Fix the organoids for 15 min in cold 4% paraformaldehyde (PFA) (pH 7.4).
Caution: Beware that PFA is a known human carcinogen. All work must be done in a chemical fume hood wearing nitrile gloves. It is recommended to wear safety glasses. Formaldehyde can cause irreversible damage to the cornea.
3. Aspirate the PFA carefully and wash three times using room temperature PBS for 10 min.
4. Replace the PBS with a 30% sucrose solution (wt/vol, PBS-based) and store the samples at 4 $^{\circ}$ C to allow organoids to dehydrate. Organoids can be stored for up to 7 days until further processing.
5. One day after fixation, pre-stain the dehydrated organoids by adding trypan blue at approximately 1:50 for 10 min to allow the visualization of the organoids during the cryosectioning procedure.
6. Prepare the embedding medium containing 10% sucrose, 7.5% gelatin wt/vol in PBS, and warm it to 75 $^{\circ}$ C until it is liquid.
7. Replace 30% sucrose solution with embedding medium and transfer the 24-well plate onto a heating plate (60 $^{\circ}$ C) for 15 min to equilibrate the organoids.

8. Cover the bottom of the embedding molds with a layer of embedding media and place them on ice to polymerize.
9. Transfer the organoids from the 24-well plate to the embedding molds containing the polymerized embedding medium, add additional embedding medium on top so that the organoids are covered, and place the mold quickly in a 100% ethanol/dry ice freezing bath (temperature should be between -30 to -50 °C) for at least 1 min to shock-freeze.
10. Place the mold with forceps on dry ice temporarily and either store them at -80 °C or directly proceed with cryosectioning.
11. Cryosection organoids at 20 μm thickness and collect the sections on microscope slides, keeping track of the order of sections on the slides (sequential uptake). Allow sections to dry on slides for several hours, before storing them at -80 °C or directly performing immunocytochemical staining.

Representative Results

The standardized forebrain-type organoid protocol described here typically generates highly homogenous organoid cultures of almost exclusively dorsal cortical identity from human iPSCs within 20 days of cultivation (protocol outlined in **Figure 1A**). It is recommended to perform several quality control steps during the time course of the protocol, defined here as: 'go' (continue the differentiation process) and 'no-go' (suboptimal cultures, it is recommended to terminate the batch) (**Figure 1**). It is also advisable to document each quality control step well by taking images and notes.

The first critical step in generating forebrain-type organoids is to start with high-quality iPSC cultures. It is important that iPSCs do not contain larger fractions of differentiated cells. Only use iPSC cultures that present as a homogeneous monolayer of undifferentiated cells at the starting population (**Figures 1B, C**). In addition, it is crucial to start with the given cell number for iPSC aggregation. The first detailed inspection of the iPSC aggregates should be performed on day 2. At this stage, the aggregates should have formed compact cell buds with smooth edges ('go') whereas irregular appearing aggregates or aggregates with cavities should be discarded ('no-go') (**Figures 1D, E**). The next quality control step should be performed at day 10 of the protocol. At this time point, the cell aggregates should show smooth and optically translucent tissue on the outer surface representing induction of neuroectoderm ('go') whereas the absence of such tissue indicates suboptimal neural induction ('no-go') (**Figures 1F, G**). Only those aggregates that exhibit a translucent surface (**Figure 1F**) should be embedded into BME matrix. Once embedded, the cortical organoids will develop continuous neuroepithelial loop-like structures, which will expand quickly. Analyze the efficiency of the cortical induction at day 15 and day 20 by investigating whether the organoids have developed polarized neural ectoderm as demonstrated in **Figure 1H, J** ('go'). In the case that organoids have not developed such neuroepithelial buds ('no-go' as illustrated in **Figure 1I, K**), critically revise the performed quality control steps for troubleshooting. When tightly following the protocol, highly standardized organoid batches will be generated (**Figures 2A, B**), which will show ≥ 90% homogeneity in polarized neural ectoderm formation within and across batches (**Figure 2C**). A common mistake leading to variable efficiency of polarized neural ectoderm formation is to increase the starting cell number for iPSC aggregation, or to start with low-quality iPSC cultures such as mycoplasma contaminated cultures or cultures that contain differentiated cells.

A detailed validation of the dorsal telencephalic identity of the generated organoids should be performed at day 20. To that end, 3 organoids should be fixed and used for immunofluorescence analyses. Stratified neuroepithelial loops (**Figure 3A**) express the neural stem cell marker Sox2 (**Figure 3B, D**), the forebrain markers Pax6 and Otx2 (**Figures 3C, E**), and the dorsal cortical marker Emx1 (**Figure 3F**). These cortical loops are further characterized by an apical localization of N-cadherin and ZO-1 (**Figures 3G, H**), ventricular zone radial glia cell (vRGC)-derived microtubule, which spans from the apical to the basal side of the structures (**Figure 3I**), and apical located dividing cells that stain positive for phosphorylated vimentin (p-Vimentin, **Figure 3J**). Cell death might be present inside the organoid structures. Central apoptosis is normal and does not affect the development of cortical tissue. Additionally, 3 organoids should be used to assess the homogeneity of the protocol by gene expression analyses. Forebrain-type organoids show expression of the dorsal forebrain markers (FoxG1, Otx2, Emx1), while expression of the midbrain (FoxA2, Pax5) and the hindbrain (HoxB2, HoxA4, HoxB4, HoxB6) markers is not detectable (**Figure 3K**).

Batches of quality-controlled organoids can be used for various applications like the analyses of the division plane of apical radial glial cells. To that end, we suggest performing double staining using antibodies against p-Vimentin and Tpx2 (**Figure 3J**). P-Vimentin is phosphorylated by CDK1 during mitosis and is located in the nucleus, thus marking all nuclei in the mitotic phase¹⁶. Tpx2 is a microtubule associated protein that can visualize the mitotic spindle and the apical processes during interkinetic nuclear migration^{17,18}. Using these markers, three aspects of vRGC division can in principle be analyzed: (I) whether cell division takes place at the apical side, (II) whether the division plane is aligned vertical (indicating symmetric cell division), horizontal, or oblique (indicating asymmetric cell division) to the apical surface, and (III) whether microtubule organizing centers are formed normally.

Organoids can be also further differentiated into more complex organized and stratified cortical tissue structures. Cortical structures within day 35 ± 2 organoids are composed of a ventricular zone (VZ)-, an inner and outer subventricular zone (SVZ), as well as a cortical plate (CP)-like area. Within the VZ and the inner and outer SVZ, vRGCs, intermediate progenitors (IPs), and cells reminiscent of oRGCs can be identified. In addition, the initial formation of a layered cortex can be observed in the CP-like area with deep cortical neurons expressing Tbr1 and Ctip2 inside and upper cortical neurons expressing Satb2, as well as Reelin-expressing cells in the outer regions¹⁰.

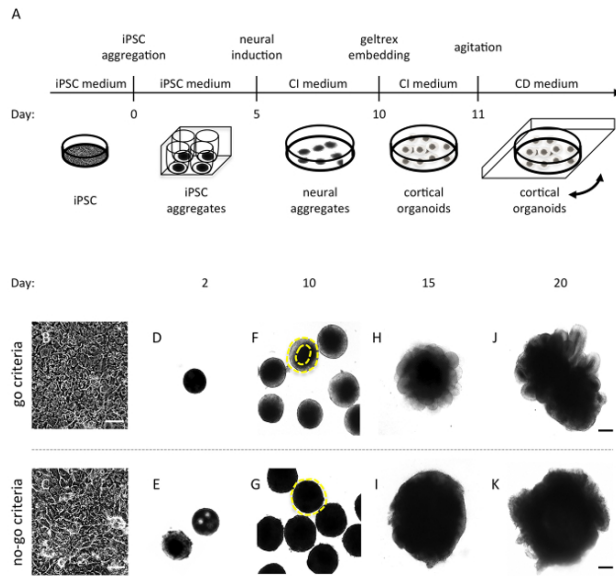


Figure 1: Schematic overview of the organoid protocol and illustration of 'go' and 'no-go' criteria. (A) Schematic overview of the protocol. CI medium: cortical induction medium; CD: cortical differentiation medium. (B-C) Image of an optimal 90% confluent iPSC monolayer culture (B) and a non-suitable iPSC culture exhibiting differentiation (C). (D-E) An iPSC aggregate optimal in size, cell density, and surface appearance (D) and two 'no-go' cell aggregates exhibiting either cell spares cavities (E, upper aggregate) or irregular edges (E, lower aggregate) two days following cell aggregation. (F-G) Cell aggregates exhibiting translucencies and smooth edges (F) and cell aggregates lacking optical clearing (G). The yellow line is visualizing the area of interest. (H-K) An optimal organoid with continuous neuroepithelial loops (H, J) and an organoid that failed to develop radially organized neuroectoderm (I, K) imaged at day 15 and day 20, respectively. Scale bars, B-C 500 μ m; D-K 200 μ m. [Please click here to view a larger version of this figure.](#)

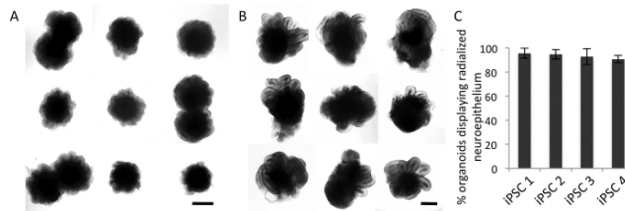


Figure 2: Homogeneity and reproducibility of the forebrain-type organoid protocol. (A-B) Representative bright-field images of organoids from one batch at day 15 (A) and day 26 (B). (C) Quantitative analyses of organoids at day 20. Organoids which display at the outer surface a neuroepithelium, recognizable in bright-field as optically clear superficial tissue with a clear border and evidence of radial cellular architecture were quantified (n = 3 per iPSC line with at least 16 organoids per experiment). Scale bars, A-B: 500 μ m. Error bars \pm SD. [Please click here to view a larger version of this figure.](#)

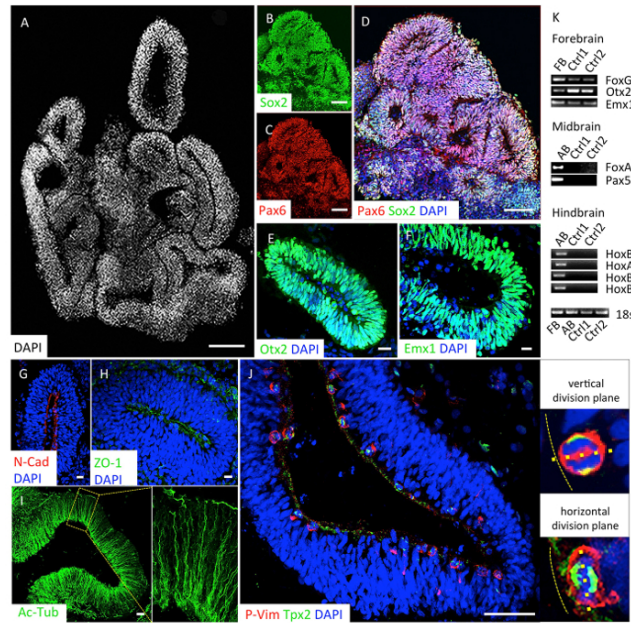


Figure 3: Validation of forebrain-type organoids at day 20. (A-J) Immunocytochemical characterization of organoids. Organoids organize in multiple neuroepithelial loops (A, counterstained with DAPI). Stratified organized cells within the neuroepithelial loops express the neural stem cell marker Sox2 (B, D), the forebrain markers Pax6 (C, D) and Otx2 (E), as well as the dorsal forebrain marker Emx1 (F). Cortical loop structures exhibited a fine adherent junction belt at the most apical side with the accumulation of N-cadherin (G) and zona occludens protein 1 (ZO-1; H). Ventricular RGCs' microtubule networks (stained by acetylated α -tubulin, Ac-Tub) extend from the apical to the basal side of the loop structures (I). Proliferating cells expressing p-vimentin (p-Vim) are located at the apical surface. Mitotic spindles are stained by Tpx2. Representative higher magnification image of a vertical and a horizontal division plane are shown on the right (J). (K) RT-PCR analysis for the region-specific transcription factors at day 20 of two independent sets of organoids derived from 2 different iPSC lines. FB: fetal brain control; AB: adult brain control. Scale bars, A-D 200 μ m; E-I 10 μ m. [Please click here to view a larger version of this figure.](#)

Epitope	Dilution
Sox2	1 - 300
Pax6	1 - 500
Otx2	1 - 500
Emx1	1 - 50
N-cadherin	1 - 500
ZO-1	1 - 100
P-Vimentin	1 - 1000
Tpx2	1 - 500
Acetylated α -tubulin	1 - 500
Alexa488 anti ms	1 - 1000
Alexa488 anti rb	1 - 1000
Alexa555 anti ms	1 - 1000
Alexa555 anti rb	1 - 1000

Table 1: Antibodies for quality control of organoids at day 20.

Primer	Sequence
Otx2 forward	tcagggttctctgtgat
Otx2 reverse	agggtcagagcaattgacca
FoxG1 forward	cctcccatttctgtacgttt
FoxG1 reverse	ctggcggtcttagagat
Emx1 forward	agacgcagggaagggtgg
Emx1 reverse	caggcaggcagctctcc
FoxA2 forward	ccaccaccaacccccacaaaatg
FoxA2 reverse	tgcaacaccgtctcccaaatg
Pax5 forward	aggatgccgctgtggaglac
Pax5 reverse	tggaggagtgaatcagcttg
HoxB2 forward	ttagccgtcgcttagagg
HoxB2 reverse	cggatagctggagacaggag
HoxA4 forward	ttcagcaaatgcctctct
HoxA4 reverse	tagccagctccacagtct
HoxB4 forward	acaccgcctacaacatgagg
HoxB4 reverse	gcacgaaagatgaggagag
HoxB6 forward	gaactgaggagcggactcac
HoxB6 reverse	ctgggatcaggaggtctca
18s forward	ttcctggaccggcgcaag
18s reverse	gccgatcgcggctcg

Table 2: Primer and primer sequences for gene expression profile.

Discussion

Brain organoids represent a powerful tool for studying human brain development *in vitro* as they provide the relevant species background and the complex 3D arrangement of cells in a tissue context. With that, they bridge the gap between non-human animal models and reductionist human two-dimensional monolayer cell culture techniques. Their applications are, however, hampered by a lack of reproducibility⁹. We have developed a forebrain-type organoid protocol, which overcomes the large sample-to-sample variability by combining the self-organizing capacity of iPSC with their amenability to patterning factors. Specifically, iPSCs were aggregated to promote self-organization and subsequently inhibit TGF- β /SMAD signaling to promote dorsal cortex differentiation by exposing the cultures to a BMP (LDN-193189) and a TGF- β type I receptor inhibitor (A83-01). Additionally, a compound inhibiting the Wnt pathway (IWR) to prevent posteriorization was applied. In contrast to 'intrinsic' cerebral organoid protocols¹⁹, which are based on self-assembly without external control giving rise to rather heterogeneous brain organoids and exhibiting large batch variations (measured by the efficiencies of polarized neural ectoderm formation¹⁵), the protocol described here reproducibly generates homogeneous forebrain-specific organoids from human iPSCs.

These forebrain-type organoids can be used for a variety of applications such as neurodevelopmental studies, evolutionary studies including gene function studies, disease modeling and, potentially, drug testing and therapeutic purposes. The protocol is, however, most suitable to examine early aspects of human cortical development. We have for example used the forebrain-type organoids to examine human-specific aspects of vRGC behavior. More specifically, pathophysiological changes associated with a severe form of lissencephaly, a human cortical malformation characterized by a near absence of cortical folding, was addressed. Only certain aspects of this disease can be modeled in mice as the mouse brain is naturally lissencephalic. When applying the organoid system to lissencephaly patient-derived iPSCs, we could reliably recapitulate human-specific aspects of the disease and identify underlying mechanisms. More specifically, we could demonstrate that patient-derived organoids show a significant reduction in size caused by a switch from symmetric to asymmetric cell division of vRGCs. This switch was associated with alterations in the organization of vRGCs' microtubule network, a disruption of the architecture of the VZ niche and altered expression of cell adhesion molecules, leading to an impaired activation of the N-cadherin/ β -catenin signaling axis¹⁰. Of note: β -catenin-dependent regulation of vRGC division modes was suggested to be human-specific as overexpression of β -catenin in mice leads to tangential cortex expansion and subsequently cortical folding²⁰. Thus, our data highlight that the forebrain-type organoid system represents a promising tool to study in a quantifiable manner the human-specific aspects of early cortical development *in vitro*.

A major challenge for the future is to maintain the homogeneity of the organoids across extended time periods in order to achieve more mature neuronal phenotypes. This might be realized by one or more of the following: culturing the organoids in a bioreactor system¹⁴, applying floating scaffolds¹⁵, supplementing the differentiation medium with neural growth, or neuronal survival factors. Finally, a controlled increase in brain complexity might be achieved by fusing the forebrain-type organoids with cerebral organoids of different regional identity^{21,22}.

Taken together, the forebrain-type organoid protocol presented here offers an easily applicable and reliable tool for the generation of early cortical structures *in vitro*. The protocol gives rise to highly homogeneous early cortical tissue across multiple iPSC lines and can be utilized

to reliably generate individual-specific cortical tissue. Thus, the system is particularly suitable for applications that require a high degree of homogeneity and reproducibility such as disease modeling.

Disclosures

The authors have nothing to disclose.

Acknowledgements

The work was supported by the Ministry of Innovation Science and Research of North Rhine-Westphalia (Junior Research Group) and by the ERA-NET NEURON, JTC 2015 Neurodevelopmental Disorders, STEM-MCD.

References

- Otani, T., Marchetto, M. C., Gage, F. H., Simons, B. D., Livesey, F. J. 2D and 3D Stem Cell Models of Primate Cortical Development Identify Species-Specific Differences in Progenitor Behavior Contributing to Brain Size. *Cell Stem Cell*. **18** (4), 467-480 (2016).
- Fietz, S. A. *et al.* OSVZ progenitors of human and ferret neocortex are epithelial-like and expand by integrin signaling. *Nat Neurosci*. **13** (6), 690-699 (2010).
- Hansen, D. V., Lui, J. H., Parker, P. R., Kriegstein, A. R. Neurogenic radial glia in the outer subventricular zone of human neocortex. *Nature*. **464** (7288), 554-561 (2010).
- Shi, Y., Kirwan, P., Smith, J., Robinson, H. P., Livesey, F. J. Human cerebral cortex development from pluripotent stem cells to functional excitatory synapses. *Nat Neurosci*. **15** (3), 477-486, S471 (2012).
- Lancaster, M. A., Knoblich, J. A. Organogenesis in a dish: modeling development and disease using organoid technologies. *Science*. **345** (6194), 1247-1255 (2014).
- Eiraku, M., Sasai, Y. Self-formation of layered neural structures in three-dimensional culture of ES cells. *Curr Opin Neurobiol*. **22** (5), 768-777 (2012).
- Camp, J. G. *et al.* Human cerebral organoids recapitulate gene expression programs of fetal neocortex development. *Proc Natl Acad Sci U S A*. **112** (51), 15672-15677 (2015).
- Quadrato, G. *et al.* Cell diversity and network dynamics in photosensitive human brain organoids. *Nature*. **545** (7652), 48-53 (2017).
- Kelava, I., Lancaster, M. A. Stem Cell Models of Human Brain Development. *Cell Stem Cell*. **18** (6), 736-748 (2016).
- Iefremova, V. *et al.* An Organoid-Based Model of Cortical Development Identifies Non-Cell-Autonomous Defects in Wnt Signaling Contributing to Miller-Dieker Syndrome. *Cell Rep*. **19** (1), 50-59 (2017).
- Chambers, S. M. *et al.* Highly efficient neural conversion of human ES and iPS cells by dual inhibition of SMAD signaling. *Nat Biotechnol*. **27** (3), 275-280 (2009).
- Kadoshima, T. *et al.* Self-organization of axial polarity, inside-out layer pattern, and species-specific progenitor dynamics in human ES cell-derived neocortex. *Proc Natl Acad Sci U S A*. **110** (50), 20284-20289 (2013).
- Lancaster, M. A. *et al.* Cerebral organoids model human brain development and microcephaly. *Nature*. **501** (7467), 373-379 (2013).
- Qian, X. *et al.* Brain-Region-Specific Organoids Using Mini-bioreactors for Modeling ZIKV Exposure. *Cell*. **165** (5), 1238-1254 (2016).
- Lancaster, M. A. *et al.* Guided self-organization and cortical plate formation in human brain organoids. *Nat Biotechnol*. (2017).
- Yamaguchi, T. *et al.* Phosphorylation by Cdk1 induces Plk1-mediated vimentin phosphorylation during mitosis. *J Cell Biol*. **171** (3), 431-436 (2005).
- Heidebrecht, H. J. *et al.* p100: a novel proliferation-associated nuclear protein specifically restricted to cell cycle phases S, G2, and M. *Blood*. **90** (1), 226-233 (1997).
- Kosodo, Y. *et al.* Regulation of interkinetic nuclear migration by cell cycle-coupled active and passive mechanisms in the developing brain. *EMBO J*. **30** (9), 1690-1704 (2011).
- Lancaster, M. A., Knoblich, J. A. Generation of cerebral organoids from human pluripotent stem cells. *Nat Protoc*. **9** (10), 2329-2340 (2014).
- Chenn, A., Walsh, C. A. Regulation of cerebral cortical size by control of cell cycle exit in neural precursors. *Science*. **297** (5580), 365-369 (2002).
- Bagley, J. A., Reumann, D., Bian, S., Levi-Strauss, J., Knoblich, J. A. Fused cerebral organoids model interactions between brain regions. *Nat Methods*. (2017).
- Birey, F. *et al.* Assembly of functionally integrated human forebrain spheroids. *Nature*. **545** (7652), 54-59 (2017).

6.2 Publication II

An Organoid-Based Model of Cortical Development Identifies Non-Cell-Autonomous Defects in Wnt Signaling Contributing to Miller-Dieker Syndrome

Iefremova V, Manikakis G, Krefft O, **Jabali A**, Weynans K, Wilkens R, Marsoner F, Brändl B, Müller F-J, Koch P, Ladewig J. Cell Rep. 2017 Apr 4; 19(1): 50-95. DOI: 10.1016/j.celrep.2017.03.047

An Organoid-Based Model of Cortical Development Identifies Non-Cell-Autonomous Defects in Wnt Signaling Contributing to Miller-Dieker Syndrome

Vira Iefremova,^{1,3} George Manikakis,^{1,3} Olivia Krefft,¹ Ammar Jabali,¹ Kevin Weynans,¹ Ruven Wilkens,¹ Fabio Marsoner,¹ Björn Brändl,² Franz-Josef Müller,² Philipp Koch,^{1,4,*} and Julia Ladewig^{1,4,*}

¹Institute of Reconstructive Neurobiology, University of Bonn, Bonn 53127, Germany

²Department of Psychiatry and Psychotherapy, University Hospital Schleswig Holstein, Kiel 24105, Germany

³Co-first author

⁴Lead Contact

*Correspondence: philipp.koch@uni-bonn.de (P.K.), jladewig@uni-bonn.de (J.L.)

<http://dx.doi.org/10.1016/j.celrep.2017.03.047>

SUMMARY

Miller-Dieker syndrome (MDS) is caused by a heterozygous deletion of chromosome 17p13.3 involving the genes *LIS1* and *YWHAE* (coding for 14.3.3 ϵ) and leads to malformations during cortical development. Here, we used patient-specific forebrain-type organoids to investigate pathological changes associated with MDS. Patient-derived organoids are significantly reduced in size, a change accompanied by a switch from symmetric to asymmetric cell division of ventricular zone radial glia cells (vRGCs). Alterations in microtubule network organization in vRGCs and a disruption of cortical niche architecture, including altered expression of cell adhesion molecules, are also observed. These phenotypic changes lead to a non-cell-autonomous disturbance of the N-cadherin/ β -catenin signaling axis. Reinstalling active β -catenin signaling rescues division modes and ameliorates growth defects. Our data define the role of *LIS1* and 14.3.3 ϵ in maintaining the cortical niche and highlight the utility of organoid-based systems for modeling complex cell-cell interactions in vitro.

INTRODUCTION

The evolutionary increase in the size of the human cerebral cortex is thought to be responsible for the extraordinary cognitive abilities of humans. This evolution was achieved by increased expansion of the surface area accompanied by the formation of gyri and sulci. Lissencephaly represents a malformation of cortical development (MCD) connected with neuronal disorganization and absent or abnormal gyrification (Francis et al., 2006). Heterozygous deletions or mutations of *LIS1* constitute the most common cause of lissencephaly in humans (Kato and Dobyns, 2003). The *LIS1* protein is a component of an intracellular multiprotein complex including NDEL1 and 14.3.3 ϵ , which is essential

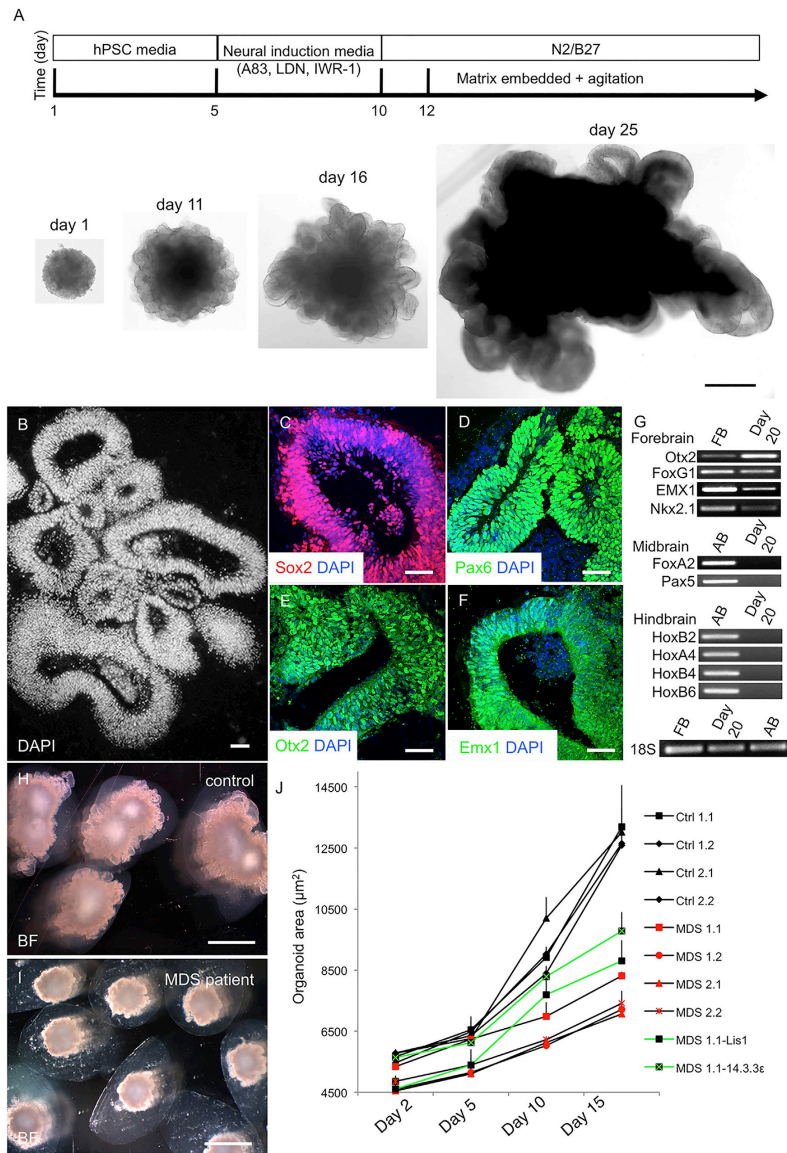
for the regulation of cytoplasmic dynein, centrosomal protein localization, and microtubule dynamics (Wynshaw-Boris, 2007). Traditionally, *LIS1*-associated lissencephalies were considered as isolated neuronal migration defects (Moon and Wynshaw-Boris, 2013). More recent data, however, highlight a role of the *LIS1*/NDEL1/14.3.3 ϵ complex in the proliferation of radial glia cells (RGCs) (Bi et al., 2009; Tsai et al., 2005; Yingling et al., 2008). In Miller-Dieker syndrome (MDS), two components of the *LIS1*/NDEL1/14.3.3 ϵ complex (*LIS1* and 14.3.3 ϵ) are affected resulting in increased structural alterations of the cortical architecture compared to isolated lissencephaly. Although mouse models have confirmed a role of the *LIS1*/NDEL1/14.3.3 ϵ complex in several cellular processes, they failed to recapitulate the severity of the human phenotype (Toyooka et al., 2003; Yingling et al., 2008). Recent progress in modeling human brain development in vitro uses the capacity of pluripotent stem cells (PSCs) to self-organize into organoids. Brain organoids contain different neural and neuronal subtypes, which spatially organize similarly to the developing human brain and faithfully recapitulate developmental gene expression patterns (Camp et al., 2015; Kadoshima et al., 2013; Lancaster et al., 2013; Mariani et al., 2015; Qian et al., 2016).

In this study, we used a standardized forebrain organoid protocol to model changes associated with MDS in vitro. We observed a reduced expansion rate of MDS organoids associated with an unexpected switch of the division mode of ventricular radial glia cells (vRGCs, or also called apical radial glia) from symmetric to asymmetric cell division. Furthermore, we identified a unrecognized mechanism of how a deficiency of the *LIS1*/NDEL1/14.3.3 ϵ complex converges into an impairment of ventricular zone niche signaling and cell-fate control via the N-cadherin/ β -catenin signaling axis in a non-cell-autonomous fashion.

RESULTS

Generation of Standardized iPSC-Derived Forebrain-type Organoids

We generated induced pluripotent stem cells (iPSCs) from two patients with MDS and two age- and gender-matched controls



(legend on next page)

(two clones each; characterization of iPSCs is illustrated in Figures S1A–S1G and Table S1). The MDS patient-specific heterozygous deletion of chromosome 17p13.3 was confirmed by SNP genotyping and reduced expression of LIS1 and YWHAE by qRT-PCR (Figures S1G–S1I). As isogenic controls and to address the specific role of LIS1 and 14.3.3e in MDS, we generated LIS1 and 14.3.3e rescue cell lines by introducing a doxycycline-inducible LIS1 (MDS-LIS1) or YWHAE (MDS-14.3.3e) into the human AAVS1 locus of MDS iPSCs. Addition of doxycycline increased the expression of LIS1 or YWHAE back to expression levels comparable to control cultures (Figures S1J and S1K).

We next generated standardized organoids of forebrain identity by combining guided differentiation of iPSCs into anterior neuroectoderm using SMAD and Wnt inhibition (Kadoshima et al., 2013) with matrix embedding to promote continuous neuroepithelium formation (Lancaster et al., 2013). To increase oxygen exchange, cultures were maintained under agitating conditions (Lancaster et al., 2013; Qian et al., 2016) (protocol outlined in Figure 1A). Control iPSC-derived organoids consistently increased in size over time while forming large neuroepithelial loops (Figures 1A and S2A–S2C). Immunocytochemical analysis revealed that at day 20 ± 2 organoids consist of stratified neuroepithelial loops expressing the neural progenitor marker Sox2 and the forebrain markers Pax6, Otx2, and Emx1, indicating a dorsal telencephalic identity (Figures 1B–1F). Few loops stained positive for the ventral forebrain progenitor-associated transcription factor Nkx2.1 (Figure S2D). Dividing cells expressing phosphorylated vimentin (p-vimentin) locate at the apical surface of the cortical loops (Figure S2E). RT-PCR investigating typical forebrain, midbrain, and hindbrain markers confirmed homogeneous forebrain identity of the organoids (Figures 1G and S2F). At later time points (day 35 ± 2 days), loops developed into a more complex organized and stratified cortical tissue with densely packed Sox2-positive cortical progenitors preferentially locating on the inside/apical surface of the organoids and separating from βIII-tubulin-positive neurons at the outside/basal surface of the structures, reminiscent of a ventricular zone (VZ) and an initial cortical plate (CP), respectively (Figure S2G). Tbr2-positive intermediate progenitors (IPs) were located in a subventricular zone (SVZ)-like transition zone between the VZ- and the CP-like structure (Figure S2H). Sox2-positive progenitors were also observed in the SVZ-like area potentially representing outer radial glia (oRG or also called basal radial glia; Figure S2I). Within the CP-like area, initial cortical layering could be observed (Figures S2J–S2L).

Premature Neurogenesis Leads to Reduced Expansion of MDS Patient-Specific Organoids

The forebrain organoid protocol was then applied to MDS patient-derived iPSCs. Similar to control organoids, MDS organoids consistently produced Sox2-positive stratified loops expressing forebrain-specific transcription factors such as Otx2, Pax6, FoxG1, and Emx1, while typical mid- and hindbrain markers were undetectable (Figures S2F and S2M–S2Q). However, in contrast to control organoids, MDS-derived organoids were significantly smaller in size and showed significantly reduced expansion rates (Figures 1H–1J and S2R–S2S; Table S2). Re-expression of LIS1 or 14.3.3e resulted in a partial rescue of these expansion deficits (Figure 1J; Table S2). We further assessed the architecture of the neuroepithelial loops by determining the length of the apical and basal membrane, the diameter of the loops as well as the size of the ventricle-like area, the total loop area, and the loop tissue area in patient- and control-derived organoids. Here, we observed a significant reduction in all parameters in MDS-derived organoids compared to controls with re-expression of LIS1 or 14.3.3e leading to a partial rescue toward the wild-type situation (Figures 2A–2D and S3). This phenotype is in line with autopsy examinations of MDS patients' brains showing severe reduction in total brain size (Sheen et al., 2006).

The reduced brain size of MDS patients as well as the changes we observed in our model might arise from impairments in several developmental processes. We first investigated apoptotic cell death in neuroepithelial progenitors as a potential underlying mechanism of the reduced size and expansion rates of MDS organoids by quantifying cleaved (active) caspase-3 at several time points. This analysis revealed that apoptotic cell death is rare at all time points investigated and that there is no significant difference in the number of apoptotic neuroepithelial progenitors when comparing patients with controls (Figures S4A and S4B). Another potential mechanism postulated is that a disruption of the LIS1/NDEL1/14.3.3e complex results in a reduction and weakening of astral microtubules and decreased plus-end stability of cortical microtubules leading to alterations of the microtubule array. As a consequence, precise control of vRGCs' mitotic spindle orientation and plane of cleavage is disturbed resulting in a randomized spindle orientation with an increase in oblique cleavage planes (Yingling et al., 2008). Indeed, we observed severe alterations in the organization of MDS vRGCs' microtubule networks. Whereas in control organoids, the vRGC microtubule network (stained by acetylated α -tubulin) extends the entire distance from the apical to the basal side, MDS vRGCs' microtubules appear truncated and show a significant reduction of extensions toward the basal membrane (Figures 2E–2G, S4C, and S4D). In MDS-LIS1 and MDS-14.3.3e rescue organoids, microtubule networks still seemed to be altered but showed a more pronounced expansion of acetylated α -tubulin toward the basal surface (Figures 2G, S4O, and S4P).

Figure 1. Reduced Size and Expansion Rates of MDS Patient-Derived Forebrain-type Organoids

(A) Schematic overview of the organoid protocol and representative images. Scale bar, 500 μ m.
 (B–F) Immunocytochemical characterization of organoids at day 20 ± 2. Organoids organize in multiple neuroepithelial loops (B). Neuroepithelial cells express Sox2 (C), Pax6 (D), Otx2 (E), and Emx1 (F). Scale bars, 50 μ m.
 (G) RT-PCR analysis for region-specific transcription factors at day 20. FB, fetal brain control; AB, adult brain control.
 (H and I) Representative bright-field images of control- (H) and MDS patient- (I) derived organoids at day 25. Scale bars, 2.5 mm.
 (J) Expansion rates of control- (n = 30 for each clone), MDS- (n = 30 for each clone), MDS-LIS1- (n = 20), and MDS-14.3.3e- (n = 20) derived organoids. Depicted is the organoid area in μ m² at days 2, 5, 10, and 15. Error bars, \pm SD.

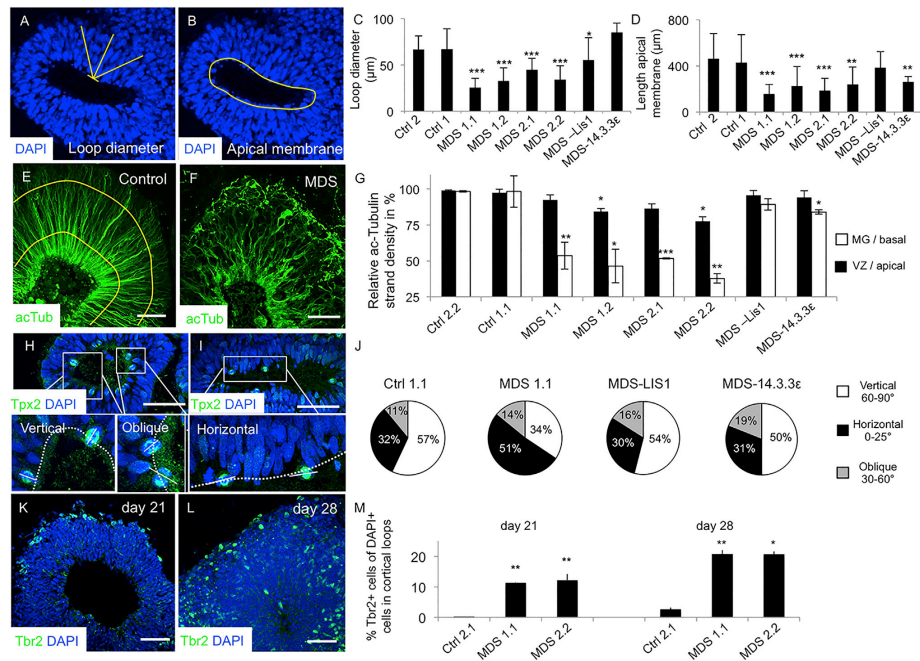


Figure 2. Altered Microtubule Networks and Increased Neurogenesis in MDS-Derived Organoids

(A and B) Schematic illustration of how loop diameter (A) and length of apical membrane (B) were quantified.

(C and D) Quantification of the loop diameter (C) and length of apical membrane (D) in control (Ctrl2 n = 42; Ctrl1 n = 24), patient (MDS1.1 n = 29; MDS1.2 n = 27; MDS2.1 n = 29; MDS2.2 n = 10), and the genetic rescue organoids (MDS-LIS1 n = 14; MDS14.3.3e n = 12). Error bars, \pm SD. * $p < 0.05$, ** $p < 0.01$, *** $p < 0.001$.

(E and F) Immunostaining for acetylated α -tubulin (acTub) in control- (E) and MDS- (F) derived organoids. Scale bars, 50 μ m.

(G) Quantification of the ac-tubulin strand density at the apical (VZ) and the basal (MG) side in control (Ctrl2.2 n = 5; Ctrl2.1 n = 8), patient (MDS1.1 n = 13; MDS1.2 n = 5; MDS2.1 n = 5; MDS2.2 n = 10), and rescue organoids (MDS-LIS1 n = 9; MDS-14.3.3e n = 10). A schematic illustration of the area of measurement (33 percentile VZ/apical, 66 percentile MG/basal) is shown in (E). Error bars, \pm SD. * $p \leq 0.05$; ** $p \leq 0.01$, *** $p \leq 0.001$.

(H and I) Representative images of vertical and oblique (H) as well as horizontal (I) division planes in mitotic vRGs. Mitotic spindles are stained by Tpx2. Scale bars, 50 μ m.

(J) Quantification of the division planes of vRGs in control (n = 91), MDS (n = 105), MDS-LIS1 (n = 63), and MDS-14.3.3e (n = 118) organoids at day 20.

(K and L) Representative images of MDS-derived organoids stained with Tbr2 at day 21 (K) and day 28 (L). Scale bars, 50 μ m.

(M) Quantification of Tbr2⁺ intermediate progenitors (IP) in control- and MDS-derived organoids (at day 21: n > 2,000 cells from a total of n = 6 loops per condition, day 28: n > 1,200 cells from a total of n = 6 loops per condition). Error bars, \pm SD. * $p < 0.05$, ** $p < 0.01$.

We thus wondered whether we could also observe an increase in oblique spindle orientation in dividing MDS vRGs by labeling the spindle of mitotic cells with Tpx2 and relating the orientation relative to the VZ-like surface (Figures 2H and 2I). Surprisingly, we found a prominent and significant switch of the spindle orientation from vertical, symmetric toward horizontal, asymmetric cleavage planes (Ctrl1.1: vertical: 57.14%, horizontal: 31.87%, oblique: 11.0%, n = 91; MDS1.1: vertical: 34.29%, horizontal: 51.43%, oblique: 14.23%, n = 105; Figure 2J; Tables S3 and S5), while the number of oblique cleavage planes was not significantly affected. In line with this observation, we found a strong

increase in the number of Tbr2⁺ IPs (day 21: Ctrl2.1: <1%; MDS1.1: 11.35% \pm 0.15%; MDS2.2: 12.2% \pm 1.98%; day 28: Ctrl2.1: 2.64% \pm 0.60%; MDS1.1: 20.79% \pm 1.22%; MDS2.2: 20.65% \pm 0.95%; Figures 2K–2M). Re-expression of LIS1 or 14.3.3e in MDS cells resulted in a partial restoration of the switch in vRGs' cleavage plane orientation (MDS-LIS1: vertical: 54.84%, horizontal: 29.84%, oblique: 15.32%, n = 63; MDS-14.3.3e: vertical: 50.0%, horizontal: 31.51%, oblique: 19.49%, n = 118; Figure 2J; Table S3) and a significant decrease in the number of Tbr2-positive IPs (Figure S4Q; day 28: MDS-LIS1: 11.7% \pm 1.28%, MDS-14.3.3e: 5.36% \pm 0.98%). These results

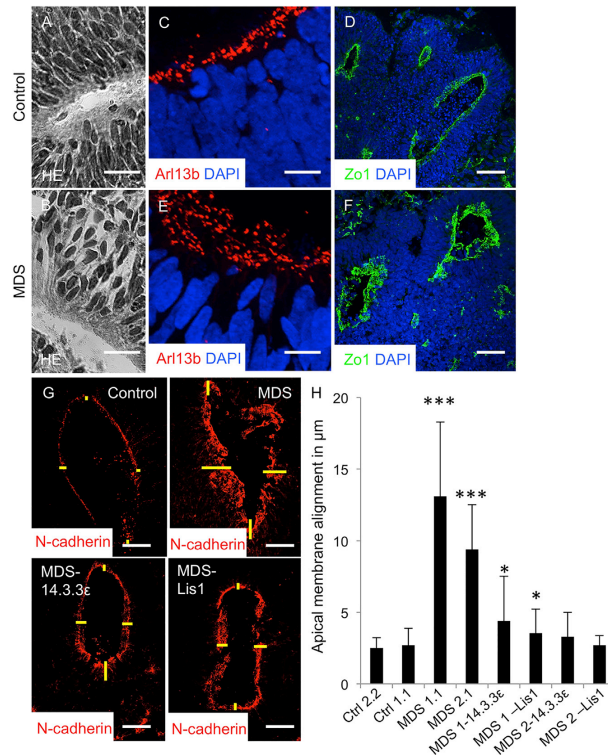


Figure 3. Disruption of the VZ Niche Architecture in MDS-Derived Organoids

(A and B) H&E staining of the VZ-like area in control- (A) and in MDS- (B) derived organoids. Scale bars, 30 μm . (C–F) Immunostainings for Arl13b and Zo1 in control- (C and D) and MDS- (E and F) derived organoids. Scale bars, in (C) and (E), 10 μm , and in (D) and (F), 50 μm . (G) Immunostaining for N-cadherin in control, MDS, MDS-LIS1 rescue, and MDS-14.3.3e rescue organoids. Scale bar, 50 μm . (H) Quantification of the apical membrane alignment in control (Ctrl2.2 n = 16; Ctrl1.1 n = 6), MDS (MDS1.1 n = 23; MDS2.1 n = 15), MDS-LIS1 rescue (MDS1-LIS1 n = 18; MDS2-LIS1 n = 16), and MDS-14.3.3e rescue (MDS1-14.3.3e n = 14; MDS2-14.3.3e n = 15) organoids. A schematic illustration of the area of measurement (yellow lines at 90°, 180°, 270°, and 360°) is shown in (G). Error bars, \pm SD. *p \leq 0.05; **p \leq 0.01, ***p \leq 0.001.

sults in disorganization of vRGCs' lateral cell-cell contacts and irregular expression of apical adhesion molecules (Pawlisz et al., 2008; Pramparo et al., 2011).

We thus investigated the organization of the apical ventricular surface in more detail. Indeed, we observed severe alterations in the organization of the ventricular niche in MDS organoids. Whereas vRGCs in control cultures arranged well-organized, stacked, and densely packed perpendicular to the ventricular surface, in MDS organoids vRGC organization was less tight with haphazard positioned cells retracted from the apical membrane (Figures 3A and 3B). This was associated with an indistinct apical lining of cilia along the VZ-like surface in MDS organoids (Figures 3C, 3E, S4E, and S4H). In addition,

we found severe alteration in the organization of cell adhesion molecules of the VZ niche. Whereas control organoids exhibited a fine adherent junction belt at the most apical side with accumulation of N-cadherin and zonula occludens protein 1 (Zo1), this organization was significantly altered in MDS-derived cultures without a compact apical distribution (Figures 3D, 3F–3H, S4F, S4G, S4I, and S4J). In MDS-LIS1 and MDS-14.3.3e rescue organoids, the organization of the cells within the VZ niche, expression of cell adhesion molecules, and apical membrane alignment was rescued to a stage more similar to control organoids (Figures 3G, 3H, and S4R–S4U). The observed changes in the organization of the VZ niche are also in line with histological data from MDS patients' autopsy brains showing disruption of the neuroepithelium along the VZ surface (Sheen et al., 2006).

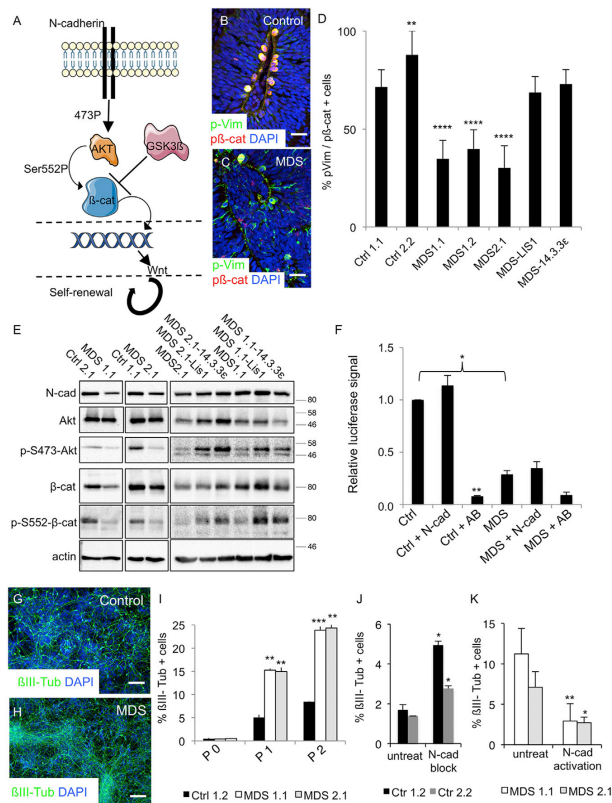
Disruption of the Cortical Niche in MDS-Derived Organoids Results in Alterations of the N-Cadherin/ β -Catenin Signaling Axis

The explicit switch in spindle orientation from vertical to horizontal division rather than a randomized increase of oblique cleavage planes suggests that in addition to cell-autonomous defects caused by alterations of the microtubule network other signaling pathways might contribute to the observed phenotype. In this context, adherens junctions have been described to control vRGCs' self-renewal (Marthiens et al., 2010; Stocker and Chenn, 2009), and data from transgenic mouse models have demonstrated that a disruption of the LIS1/NDEL1/14.3.3e complex re-

sults in disorganization of vRGCs' lateral cell-cell contacts and irregular expression of apical adhesion molecules (Pawlisz et al., 2008; Pramparo et al., 2011). We thus investigated the organization of the apical ventricular surface in more detail. Indeed, we observed severe alterations in the organization of the ventricular niche in MDS organoids. Whereas vRGCs in control cultures arranged well-organized, stacked, and densely packed perpendicular to the ventricular surface, in MDS organoids vRGC organization was less tight with haphazard positioned cells retracted from the apical membrane (Figures 3A and 3B). This was associated with an indistinct apical lining of cilia along the VZ-like surface in MDS organoids (Figures 3C, 3E, S4E, and S4H). In addition,

we found severe alteration in the organization of cell adhesion molecules of the VZ niche. Whereas control organoids exhibited a fine adherent junction belt at the most apical side with accumulation of N-cadherin and zonula occludens protein 1 (Zo1), this organization was significantly altered in MDS-derived cultures without a compact apical distribution (Figures 3D, 3F–3H, S4F, S4G, S4I, and S4J). In MDS-LIS1 and MDS-14.3.3e rescue organoids, the organization of the cells within the VZ niche, expression of cell adhesion molecules, and apical membrane alignment was rescued to a stage more similar to control organoids (Figures 3G, 3H, and S4R–S4U). The observed changes in the organization of the VZ niche are also in line with histological data from MDS patients' autopsy brains showing disruption of the neuroepithelium along the VZ surface (Sheen et al., 2006).

We next wondered how the alterations in the organization of the ventricular niche and distribution of adhesion molecules are connected to the reduced organoid size and premature



(MDS1.1: 34.79% ± 9.41% n = 9; MDS1.2: 39.84% ± 9.76% n = 15; MDS2: 30.21% ± 11.33% n = 9; Figures 4C and 4D). Re-expression of LIS1 or 14.3.3e resulted in a more widespread co-localization of p-Ser522-β-catenin-positive dividing vRGCs at the apical surface (MDS-LIS1: 68.62% ± 8.15% n = 11; MDS-14.3.3e: 71.93% ± 7.41% n = 11; Figure 4D). These data indicate that vRGCs in MDS organoids indeed show an impaired activation of β-catenin and that this might be due to alterations in the N-cadherin/β-catenin signaling axis.

differentiation phenotype and how the explicit and non-random switch of vRGC division planes might be explained mechanistically. Data from mouse models indicate that active Wnt/β-catenin signaling controls vRGC proliferation (Chenn and Walsh, 2002; Zechner et al., 2003) and that the adhesion molecule N-cadherin is involved in controlling Wnt activity by regulating AKT phosphorylation, which, in turn, phosphorylates β-catenin at serine 552 (p-Ser552-β-catenin) resulting in its stabilization and activation (Zhang et al., 2010, 2013). We thus investigated the phosphorylation state of β-catenin at Ser552 in dividing vRGCs. In control organoids, we observed widespread co-localization of p-Ser552-β-catenin in dividing p-vimentin-positive vRGCs (Ctrl1.1: 71.5% ± 8.78% n = 10; Ctrl2.2: 87.87% ± 12.27% n = 15; Figures 4B and 4D). In contrast, cortical loops from patient-derived organoids exhibited a significantly reduced expression of p-Ser552-β-catenin in p-vimentin-positive vRGCs

To investigate the interaction between N-cadherin and β-catenin in more detail and to decipher how these two proteins are connected functionally, we became interested in addressing Wnt activity in MDS and control vRGCs and whether manipulation of N-cadherin results in changes of the Wnt activation state. As these experiments are challenging in a 3D organoid system, we wondered whether certain aspects of the observed phenotypes are reflected in high-density 2D cultures consisting of essentially pure vRGCs organized as neural rosettes (Shi et al.,

2012). Indeed, we found that patient-derived rosettes exhibit reduced levels of the proteins involved in the intracellular cascades connecting niche signaling to β -catenin signaling (reduced levels of N-cadherin, phosphorylated AKT at Ser 473, β -catenin phosphorylated at Ser 552 as well as total β -catenin; Figure 4E). These alterations could be attributed to LIS1 and 14.3.3 ϵ as re-expression of LIS1 or 14.3.3 ϵ resulted in expression and phosphorylation levels of the proteins more similar to the wild-type situation (Figure 4E).

To further analyze Wnt signaling and the effect of N-cadherin on Wnt activity, we generated Wnt reporter cell lines expressing the pSuper8XTOPFlash luciferase reporter. Indeed, MDS-derived neural rosettes exhibit reduced levels of Wnt reporter activity compared to cells derived from healthy controls (Figure 4F). Interestingly and in line with the proposed mode of interaction, Wnt reporter activity directly depended on N-cadherin function as blocking N-cadherin activity with a N-cadherin blocking antibody resulted in a strong and highly significant decrease in Wnt reporter activity, whereas activating N-cadherin by exposure of the cultures to recombinant N-cadherin protein induced activation of the Wnt reporter (Figure 4F).

We next asked whether manipulation of N-cadherin would directly influence the proliferation and differentiation properties of our cultures. To that end, cortical rosettes were cultured in the absence of any growth factors, and differentiation into neurons was investigated by immunocytochemistry every 5 days. Interestingly, MDS-derived cultures showed a significant increase in the number of neurons over time when compared to cultures derived from healthy controls, indicating that the reduction of Wnt activity leads to premature neurogenesis also in 2D (Figures 4G–4I). Importantly, blocking N-cadherin in control cultures significantly induced differentiation of the cells (Figure 4J), whereas activating N-cadherin in MDS-derived cortical progenitors rescued early neurogenesis (Figure 4K). These data demonstrate that there is indeed a direct link between active N-cadherin signaling and the Wnt pathway. In addition, these data also suggest that this pathway is disrupted in MDS leading to an imbalance of proliferation and differentiation in patient-derived cortical progenitors and that manipulation of N-cadherin results in changes of this balance.

Phenotypic Alterations in MDS-Derived Organoids Can Be Rescued by Wnt Activation

Based on these results, we tested whether pharmacological activation of β -catenin by inhibition of GSK3 β affects the phenotypic alterations observed in MDS patient-derived organoids. Indeed, exposure of the cultures to the GSK3 β inhibitor CHIR99021 resulted in much more clear and homogeneous generation of cortical loops compared to the non-treated cultures (Figures 5A and 5B) and a marked rescue of the co-expression of p-Ser552- β -catenin in p-vimentin-positive dividing vRGCs (Figure 5C). When investigating the plane of cell division, we observed that exposure to CHIR99021 resulted in a switch of vertical and horizontal division planes in MDS organoids leading to division modes comparable to the healthy control situation (Figures 5D and 5E; Tables S3–S5). This was also reflected when quantifying the parameters at the level of the cortical loops where we observed a significant increase of all parameters

following exposure to the GSK3 β inhibitor (depicted are the relative change of all parameters compared to the untreated situation, the loop diameter, and length of the apical membrane; Figures 5E–5G and S5D–S5G). The phenotypic rescue was specific to MDS organoids as neither the plane of cell division nor the individual loop parameters were significantly affected by the exposure to CHIR99021 in control-derived organoids (Figures 5D–5G and S5; Tables S4 and S5). Importantly, the aberrant organization of ventricular niche and expression of cell adhesion molecules was not affected by β -catenin activation, suggesting that these alterations are upstream of β -catenin function (Figures S4K–S4N).

DISCUSSION

The most prominent histopathological hallmark of LIS1-associated lissencephalies is the disorganization of the cerebral cortex presenting with abnormally positioned neurons (Francis et al., 2006). This compelled researchers to concentrate on the role of LIS1 in neuronal migration. Indeed, the evolutionary conserved LIS1/NDEL1/14.3.3 ϵ protein complex has a well-documented function in regulating centrosomal protein localization and microtubule dynamics, both critically involved in nuclear movement and neuronal migration (Moon and Wynshaw-Boris, 2013). An additional and largely neglected phenotype of the disease is that most patients with lissencephaly are either microcephalic or have a borderline low brain size (Allanson et al., 1998). This points toward an additional role of LIS1 in neural progenitor proliferation. And indeed, data from rodents suggest that the LIS1/NDEL1/14.3.3 ϵ complex plays an important cell-autonomous role in controlling cell division by regulating the plane of the mitotic spindle during mitosis resulting in a random distribution of division planes of dividing neural progenitors (Moon et al., 2014; Pawlisz et al., 2008; Yingling et al., 2008). When we investigated cellular and molecular changes caused by a disruption of the LIS1/NDEL1/14.3.3 ϵ complex in our organotypic human in vitro model of cortical development, we were able to reproduce the “small-brain” phenotype and changes in the planes of cell division of dividing ventricular RGCs. In our hands, however, division planes appeared not random but presented with a systematic switch from vertical to horizontal division planes, compelling us to consider more global changes in cell signaling pathways participating in the observed phenotype.

Here, we describe a so-far unrecognized mechanism of how a deficiency of the LIS1/NDEL1/14.3.3 ϵ complex converges into an impairment of brain ventricular niche signaling and cell-fate control. We propose that alterations in the microtubule network of vRGCs lead to a disruption of the architecture of the ventricular niche, which, in turn, results in a non-cell-autonomous disturbance of the N-cadherin/ β -catenin/Wnt signaling axis. In line with this hypothesis, we demonstrate an irregular lining and distribution of N-cadherin at the apical surface and provide experimental evidence that N-cadherin is functionally connected to β -catenin/Wnt-signaling and the balance between proliferation and differentiation in vRGCs. Most importantly, external activation of the Wnt pathway results in a phenotypic rescue of the observed expansion defects

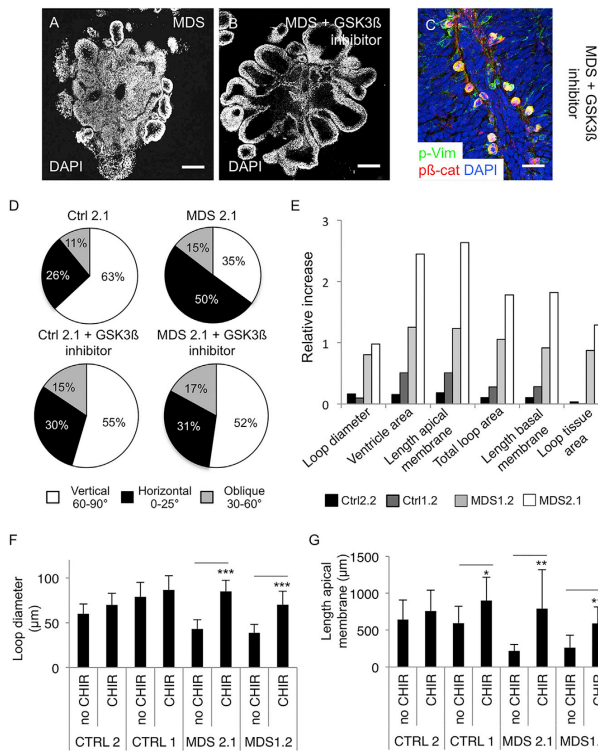


Figure 5. Activation of β -Catenin/Wnt Signaling Rescues Phenotypic Alterations in MDS-Derived Organoids

(A and B) Representative images of MDS organoids under standard culture conditions (A) and following exposure to the GSK3 β inhibitor CHIR99021 for 10 days (B, depicted are nuclei stained by DAPI). Scale bars, 200 μ m.

(C) P-Vimentin (p-Vim) and p-Ser552- β -catenin (p β -cat) immunostaining in MDS-derived organoids treated with the GSK3 β inhibitor CHIR99021. Scale bar, 25 μ m.

(D) Quantification of vertical, horizontal, and oblique division planes of dividing vRGCs in control- and patient-derived organoids in the absence and presence of the GSK3 inhibitor at day 20. Ctrl 1.2 (n = 127), MDS2.1 (n = 115), Ctrl 1.2 + Chir (n = 78), and MDS 2.1 + Chir (n = 88).

(E) Relative change of multiple parameters assessed in cortical neuroepithelial loops of control and patient organoids. Shown is the relative increase in the presence of the GSK3 inhibitor compared to the non-treated control.

(F and G) Quantification of the loop diameter (F) and length of apical membrane (G) in control- and patient-derived organoids in the absence (Ctrl2 n = 10; Ctrl1 n = 9; MDS2.1 n = 8; MDS1.2 n = 8) and the presence of the GSK3 inhibitor (Ctrl2 n = 8; Ctrl1 n = 9; MDS2.1 n = 8; MDS1.2 n = 10). Error bars \pm SD. *p < 0.05, **p < 0.01, ***p < 0.001.

caused by a dysfunction of single genes in a complex tissue environment.

EXPERIMENTAL PROCEDURES

Generation of Human iPSCs

Skin fibroblasts were obtained from the Coriell Biorepository (Ctrl1, 2-year-old female, catalog ID GM00969; Ctrl2, 5-month-old male donor, catalog ID GM08680; MDS1, 1-year-old female, catalog ID GM06097; MDS2, male fetus, 18th fetal week, catalog ID GM09208). MDS2 fibroblasts were reprogrammed using retrovirus approach as previously described (Koch et al., 2011). Ctrl1, Ctrl2, and MDS1 fibroblasts were reprogrammed by non-integrative delivery of OCT4, SOX2, KLF4, and c-MYC using Sendai virus (SeV) vectors (Ban et al., 2011). Detailed information on the maintenance of iPSCs, SNP analyses for karyotyping, and germ layer differentiation is provided in the Supplemental Experimental Procedures.

Generation of LIS1 and 14.3.3e Rescue Lines

Lis1 and 14.3.3e rescue lines were generated by integrating LIS1 or YWHAE into the human AAVS1 locus using plasmids containing the guide RNA (gRNA_AAVS1-T2, Addgene, catalog no. 41818), the Cas9 (hCas9_D10A, addgene, catalog no. 41816), and either the PB-TetON-AAVS1-LIS1 or PB-TetON-AAVS1-YWHAE vector. Detailed information on cloning and generation of LIS1 and 14-3-3e rescue cell lines is provided in the Supplemental Experimental Procedures.

Generation of Brain Organoids

On day 1 of organoid culture, iPSC were dissociated into single cells using TrypLE Express and plated in an ultra-low-binding 96-well plate (6,000–9,000 cells/well, Amsbio, lipidure-coat plate A-U96) in PluriPro (PP) medium (Cell Guidance Systems) supplemented with 50 μ M ROCK inhibitor Y-27632

specifically in patient-derived organoids. Our observations are in line with another recent study using a similar organoid-based system to investigate changes associated with Miller-Dieker lissencephaly. Without addressing the mechanistic details, they also realized the switch in vRGCs' division planes and an increase in neurogenesis (Bershteyn et al., 2017). Importantly, human brains comprise an additional expanding progenitor population named oRG cells or basal radial glia located in the outer SVZ (Fietz et al., 2010; Hansen et al., 2010) and Bershteyn and colleagues identified changes in cell division (cytokinesis delay) also in this population. The fact that vRGCs in human exhibit a prolonged and more extensive expansion capacity compared to rodents and that rodents exhibit only very few oRGs might in part also explain the decreased phenotypic severity of a disrupted LIS1/NDEL1/14.3.3e complex in mice (Toyo-oka et al., 2003; Yingling et al., 2008). Taken together, our study highlights the potential of organotypic cell-culture models to contribute to an advanced understanding of developmental mechanisms and disease-related changes

(Cell Guidance Systems). Medium was exchanged every other day. At day 5, embryoid bodies (EBs) were transferred to low-adhesion 6-cm plates (Labo-med) in neural induction media containing DMEM/F12 and Neurobasal (both Gibco and mixed in a 1:1 ratio), N2 supplement (Gibco, 1:200), B27 supplement (Gibco, 1:100), glucose (0.2 mg/mL), 0.5% non-essential amino acids (NEAA, Gibco), heparin (10 µg/mL, Sigma-Aldrich), 1% GlutaMax (Gibco), and the small molecules LDN-193189 (180 nM, Miltenyi Biotec), A83-01 (500 nM, Stemgent), and IWR-1 (10 µg/mL, Enzo Life Sciences). Five days later, small molecules were removed from the medium, and organoids were embedded into Geltrex (GT, Gibco) matrix at day 12 as previously described (Lancaster and Knoblich, 2014). Organoids were further cultured under continuous agitation using a cell-culture shaker with medium changes every 3–4 days until analyzed. When indicated, the GSK3β inhibitor CHIR99021 (1 µM, Miltenyi Biotec) was added to the culture medium. Quantitative assessments were performed on organoids where forebrain identity of neural tube structures was beforehand validated by immunostainings for Sox2, Pax6, Otx2, and Emx1. Detailed information is provided in the [Supplemental Experimental Procedures](#).

Generation of iPSC-Derived Cortical Rosettes

Differentiation of iPSC-derived cortical rosettes was performed as described by Shi et al. with slight adaptations (Shi et al., 2012). Detailed information is provided in the [Supplemental Experimental Procedures](#).

Generation of Wnt Reporter Lines and Luciferase Assay

Control- (Ctrl1.2) and patient- (MDS1.2) derived iPSCs were lentivirally transduced with a reporter construct expressing luciferase under the control of the Wnt responsive T-cell factor (TCF) promoter element (pSuperTOPflash; Addgene Plasmid #24308). Detailed information on the generation of the reporter lines and the luciferase assay is provided in the [Supplemental Experimental Procedures](#).

Histology and Immunofluorescence

Cells were fixed in 4% paraformaldehyde (PFA) for 10 min at room temperature and blocked in blocking solution (10% fetal calf serum [FCS] in PBS). For more detailed information, see [Supplemental Experimental Procedures](#).

Organoids were fixed in 4% PFA for 20 min at room temperature and allowed to sink in 30% sucrose at 4°C overnight before being embedded in 10%/7.5% gelatin/sucrose and cryosectioned at 20–30 µm. Cryosections were stained with H&E or used for immunostaining. For more detailed information, see [Supplemental Experimental Procedures](#).

Immunoblot

Cortical rosettes were harvested for immunoblot analysis 3–4 days following replating. Detailed information is provided in the [Supplemental Experimental Procedures](#).

RT-PCR Analysis

RT-PCR was performed in triplicates using biological duplicates. For detailed information, see [Supplemental Experimental Procedures](#).

Statistical Analyses

Quantitative data were generated at least in biological triplicates. No statistical methods were used to pre-determine sample sizes, but our sample sizes are similar to those generally employed in the field. All data were collected and processed randomly. Means and SD were computed. All results presented as bar graphs show mean ± SD. Two-sided one-way ANOVA test using Prism 6 software, two-proportion z-test, or Kruskal-Wallis test followed by Bonferroni-corrected pairwise comparisons using a Mann-Whitney U test was performed to determine whether a significant difference exists between groups.

SUPPLEMENTAL INFORMATION

Supplemental Information includes Supplemental Experimental Procedures, five figures, and five tables and can be found with this article online at <http://dx.doi.org/10.1016/j.celrep.2017.03.047>.

AUTHOR CONTRIBUTIONS

Conceptualization, P.K. and J.L.; Methodology, V.I., G.M., O.K., A.J., K.W., B.B., F.-J.M., and J.L.; Validation, V.I., G.M.; O.K., A.J., K.W., F.M., and R.W.; Formal Analysis, V.I., G.M., O.K., A.J., K.W., F.M., and J.L.; Investigation, V.I., G.M., O.K., A.J., K.W., F.M., R.W., and J.L.; Resources, B.B. and F.-J.M.; Writing – Original Draft, J.L.; Writing – Reviewing & Editing, P.K. and J.L.; Visualization, J.L.; Supervision, P.K. and J.L.; Project Administration, J.L.; Funding Acquisition, J.L.

ACKNOWLEDGMENTS

We thank D. Kühne for technical support and Linheng Li, Mark Hembree, and John Perry (Stowers Institute) for kindly providing the anti-p-Ser552-β-catenin antibody. The work was supported by the Ministry of Innovation Science and Research of North Rhine-Westphalia (Junior Research Group, to J.L.), by the University of Bonn BONFOR Program (to J.L.), the ERA-NET NEURON, JTC 2015 Neurodevelopmental Disorders, STEM-MCD (to J.L.), and the German Research Foundation (grant MU 3231/3-1 to F.-J.M.).

Received: July 11, 2016

Revised: January 25, 2017

Accepted: March 13, 2017

Published: April 4, 2017

REFERENCES

- Allanson, J.E., Ledbetter, D.H., and Dobyns, W.B. (1998). Classical lissencephaly syndromes: does the face reflect the brain? *J. Med. Genet.* 35, 920–923.
- Ban, H., Nishishita, N., Fusaki, N., Tabata, T., Saeki, K., Shikamura, M., Takada, N., Inoue, M., Hasegawa, M., Kawamata, S., and Nishikawa, S. (2011). Efficient generation of transgene-free human induced pluripotent stem cells (iPSCs) by temperature-sensitive Sendai virus vectors. *Proc. Natl. Acad. Sci. USA* 108, 14234–14239.
- Bershteyn, M., Nowakowski, T.J., Pollen, A.A., Di Lullo, E., Nene, A., Wynshaw-Boris, A., and Kriegstein, A.R. (2017). Human iPSC-derived cerebral organoids model cellular features of lissencephaly and reveal prolonged mitosis of outer radial glia. *Cell Stem Cell*, Published online January 9, 2017. <http://dx.doi.org/10.1016/j.stem.2016.12.007>.
- Bi, W., Sapir, T., Shchelochkov, O.A., Zhang, F., Withers, M.A., Hunter, J.V., Levy, T., Shinder, V., Peiffer, D.A., Gunderson, K.L., et al. (2009). Increased LIS1 expression affects human and mouse brain development. *Nat. Genet.* 41, 168–177.
- Camp, J.G., Badsha, F., Florio, M., Kanton, S., Gerber, T., Wilsch-Bräuninger, M., Lewitus, E., Sykes, A., Hevers, W., Lancaster, M., et al. (2015). Human cerebral organoids recapitulate gene expression programs of fetal neocortex development. *Proc. Natl. Acad. Sci. USA* 112, 15672–15677.
- Chenn, A., and Walsh, C.A. (2002). Regulation of cerebral cortical size by control of cell cycle exit in neural precursors. *Science* 297, 365–369.
- Fietz, S.A., Kelava, I., Vogt, J., Wilsch-Bräuninger, M., Stenzel, D., Fish, J.L., Corbeil, D., Riehn, A., Distler, W., Nitsch, R., and Huttner, W.B. (2010). OSVZ progenitors of human and ferret neocortex are epithelial-like and expand by integrin signaling. *Nat. Neurosci.* 13, 690–699.
- Francis, F., Meyer, G., Fallet-Bianco, C., Moreno, S., Kappeler, C., Socorro, A.C., Tuy, F.P., Beldjord, C., and Chelly, J. (2006). Human disorders of cortical development: from past to present. *Eur. J. Neurosci.* 23, 877–893.
- Hansen, D.V., Lui, J.H., Parker, P.R., and Kriegstein, A.R. (2010). Neurogenic radial glia in the outer subventricular zone of human neocortex. *Nature* 464, 554–561.
- Kadoshima, T., Sakaguchi, H., Nakano, T., Soen, M., Ando, S., Eiraku, M., and Sasai, Y. (2013). Self-organization of axial polarity, inside-out layer pattern, and species-specific progenitor dynamics in human ES cell-derived neocortex. *Proc. Natl. Acad. Sci. USA* 110, 20284–20289.
- Kato, M., and Dobyns, W.B. (2003). Lissencephaly and the molecular basis of neuronal migration. *Hum. Mol. Genet.* 12, R89–R96.

- Koch, P., Breuer, P., Peitz, M., Jungverdorben, J., Kesavan, J., Poppe, D., Doerr, J., Ladewig, J., Mertens, J., Tüting, T., et al. (2011). Excitation-induced ataxin-3 aggregation in neurons from patients with Machado-Joseph disease. *Nature* **480**, 543–546.
- Lancaster, M.A., and Knoblich, J.A. (2014). Generation of cerebral organoids from human pluripotent stem cells. *Nat. Protoc.* **9**, 2329–2340.
- Lancaster, M.A., Renner, M., Martin, C.A., Wenzel, D., Bicknell, L.S., Hurles, M.E., Homfray, T., Penninger, J.M., Jackson, A.P., and Knoblich, J.A. (2013). Cerebral organoids model human brain development and microcephaly. *Nature* **507**, 373–379.
- Mariani, J., Coppola, G., Zhang, P., Abyzov, A., Provini, L., Tomasini, L., Amenduni, M., Szekely, A., Palejev, D., Wilson, M., et al. (2015). FOXP1-dependent dysregulation of GABA/glutamate neuron differentiation in autism spectrum disorders. *Cell* **162**, 375–390.
- Marthiens, V., Kazanis, I., Moss, L., Long, K., and French-Constant, C. (2010). Adhesion molecules in the stem cell niche—more than just staying in shape? *J. Cell Sci.* **123**, 1613–1622.
- Moon, H.M., and Wynshaw-Boris, A. (2013). Cytoskeleton in action: Lissencephaly, a neuronal migration disorder. *Wiley Interdiscip. Rev. Dev. Biol.* **2**, 229–245.
- Moon, H.M., Youn, Y.H., Pemble, H., Yingling, J., Wittmann, T., and Wynshaw-Boris, A. (2014). LIS1 controls mitosis and mitotic spindle organization via the LIS1-NDEL1-dynein complex. *Hum. Mol. Genet.* **23**, 449–466.
- Pawlisz, A.S., Mutch, C., Wynshaw-Boris, A., Chenn, A., Walsh, C.A., and Feng, Y. (2008). Lis1-Nde1-dependent neuronal fate control determines cerebral cortical size and lamination. *Hum. Mol. Genet.* **17**, 2441–2455.
- Pramparo, T., Libiger, O., Jain, S., Li, H., Youn, Y.H., Hirotsune, S., Schork, N.J., and Wynshaw-Boris, A. (2011). Global developmental gene expression and pathway analysis of normal brain development and mouse models of human neuronal migration defects. *PLoS Genet.* **7**, e1001331.
- Qian, X., Nguyen, H.N., Song, M.M., Hadiono, C., Ogden, S.C., Hammack, C., Yao, B., Hamersky, G.R., Jacob, F., Zhong, C., et al. (2016). Brain-region-specific organoids using mini-bioreactors for modeling ZIKV exposure. *Cell* **165**, 1238–1254.
- Sheen, V.L., Ferland, R.J., Neal, J., Harney, M., Hill, R.S., Banham, A., Brown, P., Chenn, A., Corbo, J., Hecht, J., et al. (2006). Neocortical neuronal arrangement in Miller Dieker syndrome. *Acta Neuropathol.* **111**, 489–496.
- Shi, Y., Kirwan, P., Smith, J., Robinson, H.P., and Livesey, F.J. (2012). Human cerebral cortex development from pluripotent stem cells to functional excitatory synapses. *Nat. Neurosci.* **15**, 477–486.
- Stocker, A.M., and Chenn, A. (2009). Focal reduction of alphaE-catenin causes premature differentiation and reduction of beta-catenin signaling during cortical development. *Dev. Biol.* **328**, 66–77.
- Toyo-oka, K., Shionoya, A., Gambello, M.J., Cardoso, C., Leventer, R., Ward, H.L., Ayala, R., Tsai, L.H., Dobyns, W., Ledbetter, D., et al. (2003). 14-3-3epsilon is important for neuronal migration by binding to NUDEL: a molecular explanation for Miller-Dieker syndrome. *Nat. Genet.* **34**, 274–285.
- Tsai, J.W., Chen, Y., Kriegstein, A.R., and Vallee, R.B. (2005). LIS1 RNA interference blocks neural stem cell division, morphogenesis, and motility at multiple stages. *J. Cell Biol.* **170**, 935–945.
- Wynshaw-Boris, A. (2007). Lissencephaly and LIS1: Insights into the molecular mechanisms of neuronal migration and development. *Clin. Genet.* **72**, 296–304.
- Yingling, J., Youn, Y.H., Darling, D., Toyo-Oka, K., Pramparo, T., Hirotsune, S., and Wynshaw-Boris, A. (2008). Neuroepithelial stem cell proliferation requires LIS1 for precise spindle orientation and symmetric division. *Cell* **132**, 474–486.
- Zechner, D., Fujita, Y., Hülsken, J., Müller, T., Walther, I., Taketo, M.M., Crenshaw, E.B., 3rd, Birchmeier, W., and Birchmeier, C. (2003). beta-Catenin signals regulate cell growth and the balance between progenitor cell expansion and differentiation in the nervous system. *Dev. Biol.* **258**, 406–418.
- Zhang, J., Woodhead, G.J., Swaminathan, S.K., Noles, S.R., McQuinn, E.R., Pisarek, A.J., Stocker, A.M., Mutch, C.A., Funatsu, N., and Chenn, A. (2010). Cortical neural precursors inhibit their own differentiation via N-cadherin maintenance of beta-catenin signaling. *Dev. Cell* **18**, 472–479.
- Zhang, J., Shemezis, J.R., McQuinn, E.R., Wang, J., Sverdlöv, M., and Chenn, A. (2013). AKT activation by N-cadherin regulates beta-catenin signaling and neuronal differentiation during cortical development. *Neural Dev.* **8**, 7.

6.3 Publication III

Mutations in the Heterotopia Gene Eml1/EML1 Severly Disrupt the Formation of Primary Cilia.

Uzquiano A, Cifuentes-Diaz C, **Jabali A**, Romero D, Houllier A, Dingli F, Maillard C, Boland A, Deleuze J F, Loew D, Mancini G M.S., Bahi-Buisson N, Ladewig J, Francis F. Cell Rep. 2019 Aug 6; 28(6): 1596-1611.e10. DOI: 10.1016/j.celrep.2019.06.096

Mutations in the Heterotopia Gene *Eml1/EML1* Severely Disrupt the Formation of Primary Cilia

Ana Uzquiano,^{1,2,3} Carmen Cifuentes-Diaz,^{1,2,3} Ammar Jabali,^{4,5,6} Delfina M. Romero,^{1,2,3} Anne Houllier,^{1,2,3} Florent Dingli,⁷ Camille Maillard,^{8,9} Anne Boland,¹⁰ Jean-François Deleuze,¹⁰ Damaris Loew,⁷ Grazia M.S. Mancini,¹¹ Nadia Bahi-Buisson,^{8,9,12,13} Julia Ladewig,^{4,5,6} and Fiona Francis^{1,2,3,14,*}

¹INSERM U 1270, Paris, France

²Sorbonne University, UMR-S 1270, 75005 Paris, France

³Institut du Fer à Moulin, Paris, France

⁴Central Institute of Mental Health, Medical Faculty Mannheim, Heidelberg University, Mannheim, Germany

⁵HITBR Hector Institute for Translational Brain Research gGmbH, Mannheim, Germany

⁶German Cancer Research Center (DKFZ), Heidelberg, Germany

⁷Institut Curie, PSL Research University, Centre de Recherche, Laboratoire de Spectrométrie de Masse Protéomique, Paris, France

⁸Laboratory of Genetics and Development of the Cerebral Cortex, INSERM UMR1163 Imagine Institute, Paris, France

⁹Paris Descartes-Sorbonne Paris Cité University, Imagine Institute, Paris, France

¹⁰Centre National de Recherche en Génétique Humaine (CNRGH), Institut de Biologie François Jacob, CEA, Université Paris-Saclay, 91057 Evry, France

¹¹Department of Clinical Genetics, Erasmus MC University Medical Center, 3015CN Rotterdam, the Netherlands

¹²Pediatric Neurology APHP-Necker Enfants Malades University Hospital, Paris, France

¹³Centre de Référence, Déficiences Intellectuelles de Causes Rares, APHP-Necker Enfants Malades University Hospital, Paris, France

¹⁴Lead Contact

*Correspondence: fiona.francis@inserm.fr

<https://doi.org/10.1016/j.celrep.2019.06.096>

SUMMARY

Apical radial glia (aRGs) are predominant progenitors during corticogenesis. Perturbing their function leads to cortical malformations, including subcortical heterotopia (SH), characterized by the presence of neurons below the cortex. *EML1/Eml1* mutations lead to SH in patients, as well as to heterotopic cortex (*HeCo*) mutant mice. In *HeCo* mice, some aRGs are abnormally positioned away from the ventricular zone (VZ). Thus, unraveling *EML1/Eml1* function will clarify mechanisms maintaining aRGs in the VZ. We pinpoint an unknown *EML1/Eml1* function in primary cilium formation. In *HeCo* aRGs, cilia are shorter, less numerous, and often found aberrantly oriented within vesicles. Patient fibroblasts and human cortical progenitors show similar defects. *EML1* interacts with *RPGRIP1L*, a ciliary protein, and *RPGRIP1L* mutations were revealed in a heterotopia patient. We also identify Golgi apparatus abnormalities in *EML1/Eml1* mutant cells, potentially upstream of the cilia phenotype. We thus reveal primary cilia mechanisms impacting aRG dynamics in physiological and pathological conditions.

INTRODUCTION

The cerebral cortex is a highly organized structure whose development depends on different progenitor cell types. These give rise to post-mitotic neurons that migrate across the developing cortical wall to their final positions in the cortical plate. Apical

radial glia (aRGs) are the main progenitor type in early corticogenesis and are responsible for the production of other progenitors, hence regulating the final neuronal output (Uzquiano et al., 2018). aRGs are localized in the proliferative ventricular zone (VZ) and have a characteristic morphology, including a basal process extending to the pial surface and an apical process descending to the ventricular surface. The apical process of aRGs terminates by an endfoot characterized by the presence of a centrosome that during interphase acts as a basal body docking a primary cilium. These two structures are crucial for aRG polarity and function, and abnormal behavior of aRGs disrupts neocortical development, causing severe cortical malformations (Bizzotto and Francis, 2015). Primary cilium anomalies, as well as defects in pathways dependent on this organelle, are expected to severely impact neural progenitor behavior as well as other steps of corticogenesis (Ding et al., 2019; Foerster et al., 2017; Gabriel et al., 2016; Wang et al., 2016; Guo et al., 2015; Higginbotham et al., 2013; Li et al., 2011; Wilson et al., 2012).

We and others identified pathogenic mutations in *EML1* in a specific group of cortical malformations characterized by atypical subcortical heterotopia (SH), corpus callosum agenesis, and macrocrania (Kielar et al., 2014; Shaheen et al., 2017). *EML1* codes for a microtubule-associated protein. Remarkably, a retrotransposon insertion disrupting the mouse ortholog *Eml1* leads to a similar phenotype in the heterotopic cortex (*HeCo*) mouse mutant (Croquelois et al., 2009; Kielar et al., 2014). The latter represents a unique model to decipher the biological basis of SH.

HeCo mice show progenitor anomalies from the early stages of corticogenesis thought to be responsible for the heterotopia phenotype (Bizzotto et al., 2017; Kielar et al., 2014). Some aRGs leave the VZ and divide in aberrant basal positions (Kielar et al., 2014). However, the pathological mechanisms leading to



the detachment of these cells in the *HeCo* VZ remain vastly unexplored.

The primary cilium is a microtubule-based antenna-like structure that serves as platform for signaling pathways. In aRG apical endfeet, this organelle protrudes within the ventricle in order to sense signals from the cerebrospinal fluid. It is formed after mitosis, when the centrosome, composed of two centrioles at the spindle pole, is trafficked toward the apical surface. During this journey, the centrosome associates with *de novo* synthesized membrane or ciliary remnants, which are often carried in vesicle-like structures and will then become the basal body-primary cilium complex (Bernabé-Rubio and Alonso, 2017; Paridaen et al., 2013). Once this complex reaches the plasma membrane, the basal body is docked and the primary cilium is inserted in the apical membrane. Trafficking of proteins from the Golgi apparatus is essential for the assembly of the basal body-primary cilium complex (Bernabé-Rubio and Alonso, 2017; Madhivanan and Aguilar, 2014). Therefore, correct formation of primary cilia depends on diverse subcellular processes that when disrupted could be responsible for the appearance of cilia-related pathologies (Madhivanan and Aguilar, 2014).

Here, we reveal a severe disruption of primary cilia in *Eml1/EML1* mutant conditions, not only in *HeCo* aRGs but also in patient fibroblasts and human induced pluripotent stem cell (iPSC)-derived cortical progenitors. Thus, *Eml1/EML1* has an unexpected role in primary cilia formation. We also uncover a ciliary protein partner of EML1, RRGIP1L, and report the first heterotopia patient showing mutations in this protein. Searching for upstream mechanisms potentially responsible for perturbed primary cilia, converging data pointed toward abnormal Golgi apparatus function in *Eml1/EML1* mutant conditions. We show here signs of abnormal Golgi structure and/or function in *HeCo* aRGs as well as patient fibroblasts and iPSC-derived cortical progenitors. We hence reveal perturbed Golgi apparatus mechanisms likely to be involved in primary cilium formation that most probably contribute to the aRG delamination phenotype.

RESULTS

Perturbation in Early Stages of Corticogenesis

Alterations in the number and distribution of γ -tubulin⁺ and Arl13b⁺ puncta, identifying centrosomes and primary cilia, respectively, were recently observed in the embryonic day 13.5 (E13.5) *HeCo* VZ (Bizzotto et al., 2017). For a view of the ventricular surface only, *en face* imaging was performed in combination with these two markers in wild-type (WT) and *HeCo* brains at the same developmental time point, together with immunostaining for F-actin, in order to delineate apical domains (Figure 1A). Using this approach, we confirmed a decrease of γ -tubulin⁺ and Arl13b⁺ puncta at the *HeCo* ventricular surface (Figures 1B and 1C). We further analyzed the total number of apical domains and quantified centrosome and primary-cilium-containing endfeet in WT and *HeCo* mice. All apical domains as well as centrosome-containing apical endfeet (with or without primary cilia) were decreased in the *HeCo* ventricular surface (Figures 1D–1F), in fitting with aRG delamination

at E13.5 (Kielar et al., 2014). Apical domains not containing centrosome and primary cilia did not differ between *HeCo* and WT mice (Figure 1G).

Given that *Eml1* is expressed in the mouse VZ as early as E12.5 (Bizzotto et al., 2017), WT and *HeCo* cortices were also compared at this time point. First, a 30-min bromodeoxyuridine (BrdU) pulse was performed to analyze the position of cycling progenitor cells in the E12.5 cortical wall. Immunohistochemistry for BrdU and Ki67 confirmed the presence of a proportion of aberrant, superficially localized BrdU⁺Ki67⁺ progenitor cells as previously observed at E13.5 (Figures S1A and S1B; Kielar et al., 2014). At E12.5, *en face* imaging showed no significant change in the number of γ -tubulin⁺ and Arl13b⁺ puncta at the *HeCo* ventricular surface compared to WT, although tendencies for a decrease were observed, possibly indicating an incipient phenotype (Figures S1C–S1E). Apical domain and endfeet numbers were also analyzed, revealing tendencies similar to the E13.5 data (Figures S1F–S1I). A significant decrease in the number of centrosome and primary cilia containing apical endfeet per region of interest (ROI) was observed at E12.5 (Figure S1G). There was a slight but significant increase in the number of apical domains without centrosome and primary cilia at the *HeCo* ventricular surface (Figure 1I).

Analyses of the numbers of aRG endfeet at E12.5 and E13.5 support the hypothesis that some *Eml1* mutant aRGs delaminate from the ventricular surface at the early stages of corticogenesis.

Primary Cilia Formation Is Impaired in *Eml1* Mutant Conditions

We next questioned if, as well as reduced Arl13b puncta, primary cilia structure was abnormal in *HeCo* aRGs. Primary cilia length was first measured from *en face* Arl13b immunodetection, a parameter often studied to investigate defects in their assembly and/or disassembly (Kheradmand Kia et al., 2012). In addition to their decrease in number, primary cilia were found to be shorter at the *HeCo* ventricular surface at both E12.5 and E13.5 (Figures 1H, 1I, S1J, and S1K). Since the *HeCo* ventricular surface seemed more severely affected at E13.5, we focused on this stage to further understand the mechanisms involved.

In order to further examine the *HeCo* primary cilium phenotype, we analyzed their ultrastructure and subcellular localization in WT and *HeCo* brains at E13.5 by electron microscopy (EM) (Figure 2A). In WT aRG endfeet, centrioles are observed in close vicinity to the apical plasma membrane, the mother centriole acting as basal body and thus docking a primary cilium protruding in the ventricle (Figure 2A). In agreement with the *en face* imaging findings, aRG primary cilia measured from EM data were found to be shorter in *HeCo* compared to WT (Figures 2A–2C). In addition, when short cilia could be observed, these structures often lacked a properly formed basal body. Instead, densely packed microtubules were often present in place of centrioles (Figure 2A, white arrow). Furthermore, a significant increase in the number of cilia within vesicle-like structures was also evident in *HeCo* aRGs compared to WT (Figure 2A, black asterisk, and Figure 2D). These were often also mis-oriented basally rather than facing the ventricle (Figure 2A, white asterisk, and Figure 2E).

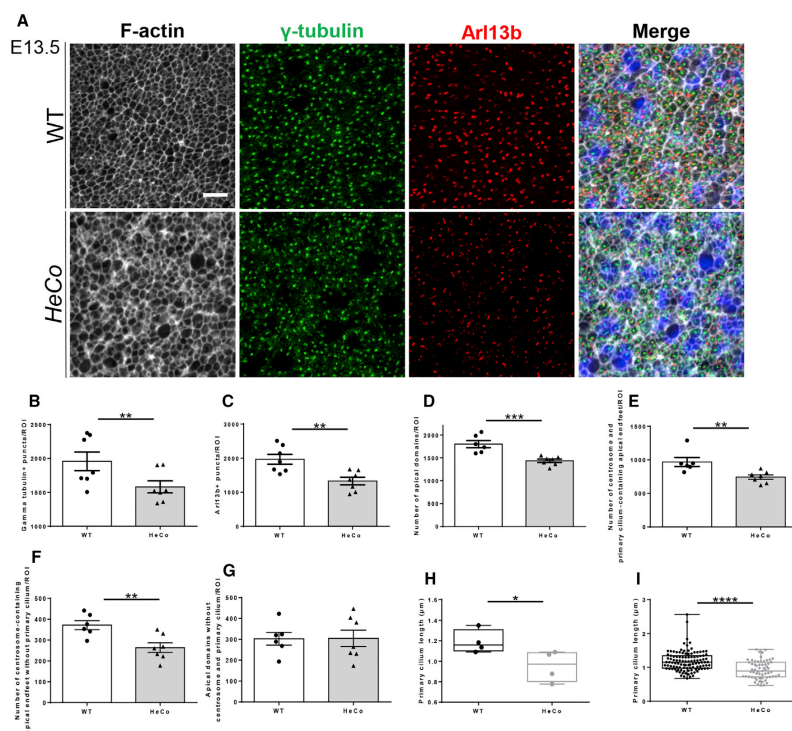


Figure 1. Centrosomes, Primary Cilia, and Apical Endfeet Are Decreased at the *HeCo* Ventricular Surface
 (A) *En face* confocal imaging of the WT and *HeCo* ventricular surface using F-actin (white), anti- γ -tubulin (green), and anti-Arl13b (red) immunostaining.
 (B) Quantification of γ -tubulin⁺ puncta per ROI in WT and *HeCo* mice.
 (C) Quantification of Arl13b⁺ puncta per ROI in WT and *HeCo* mice.
 (D) Quantification of number of apical domains in WT and *HeCo* mice.
 (E) Quantification of centrosome and primary cilium-containing apical endfeet in WT and *HeCo* mice.
 (F) Quantification of centrosome-containing apical endfeet without primary cilium in WT and *HeCo* mice.
 (G) Quantification of apical domains without centrosome and primary cilium in WT and *HeCo* mice. This represents 17% and 20% of the total number of apical domains, respectively.
 (H and I) Quantification of Arl13b⁺ primary cilium length in WT (n = 5 from 3 litters, 110 primary cilia) and *HeCo* (n = 5 from 4 litters, 61 primary cilia). Each point represents an embryo (H) or primary cilium (I).
 Each point in (B)–(G) represents an embryo (WT: n = 7 from 4 litters; *HeCo*: n = 6 from 5 litters). Scale bar, 10 μ m (A). Data are represented as mean \pm SEM and unpaired t test (B–G), and box and whisker plots show the median \pm minimum-maximum range followed by Mann-Whitney test (H and I). ****p < 0.0001, ***p < 0.001, **p < 0.01, and *p < 0.05.
 See also Figure S1.

Thus, a decrease in the number and length of ventricular primary cilia, which are also often found within vesicles inside the cell, strongly suggests defects in their formation in *HeCo* aRGs during the early-to-middle (early-mid) stages of cortical development.

We also searched for potential primary cilia defects in other neuronal progenitor types. Upon Arl13b immunostaining, the E13.5 cortical wall of WT and *HeCo* mice was subdivided

in six equally sized bins. An increased proportion of Arl13b puncta was identified in upper-VZ/subventricular zone (SVZ)-containing bin 4 (with a decrease in the SVZ/intermediate zone [IZ]-containing bin 5) in *HeCo* cortices (Figures S1L and S1M). These preliminary data may indicate that primary cilia are also abnormal in other progenitors populating more basal regions of the developing cortex.

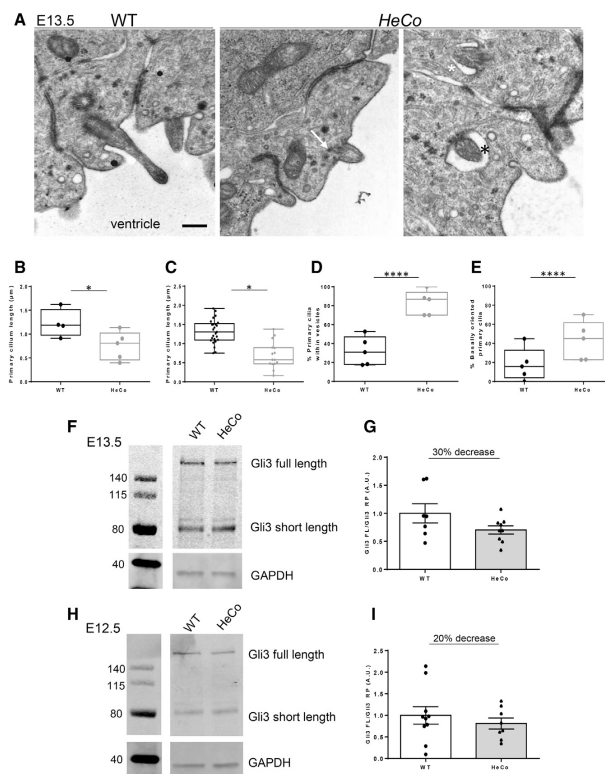


Figure 2. Primary Cilia Formation Is Impaired in *Eml1* Mutant Conditions, although No Changes in Shh Signaling Were Observed

(A) Representative images of EM acquisitions of the apical surface of WT and *HeCo* brains. White arrow shows that the basal body is not properly assembled in *HeCo* aRGs. Instead, densely packed microtubules are observed. The black asterisk indicates apically oriented primary cilium within a vesicle. The white asterisk indicates basally oriented primary cilium within a vesicle. (B and C) Quantification of primary cilium length in WT ($n = 4$ embryos from 3 litters, 25 primary cilia) and *HeCo* ($n = 5$ embryos from 3 litters, 15 primary cilia) VZ. Each point represents an embryo (B) or a primary cilium (C). (D and E) Percentage of primary cilia found within vesicles in WT and *HeCo* VZ (D), and percentage of basally oriented primary cilia in WT and *HeCo* VZ (E). Each point represents an embryo ($n = 5$ per condition from 3 litters; 150–169 cells). Statistical tests were performed considering the frequency across cells analyzed.

(F) Representative western blot of WT and *HeCo* E13.5 cortical lysates immunodetected for Gli3 and GAPDH.

(G) Quantifications from E13.5 western blots, with band intensities normalized to GAPDH (WT: $n = 9$ embryos from 2 litters; *HeCo*: $n = 7$ embryos from 2 litters).

(H) Representative western blot of WT and *HeCo* E12.5 cortical lysates immunodetected for Gli3 and GAPDH.

(I) Quantifications from E12.5 western blots, with band intensities normalized to GAPDH (WT: $n = 10$ embryos from 2 litters; *HeCo*: $n = 8$ embryos from 2 litters).

Scale bar, 0.5 µm (A). Box and whisker plots show the median \pm minimum-maximum range followed by Mann-Whitney test (B and C) or chi-square test (D and E) or mean \pm SEM (G and I). **** $p < 0.0001$ and * $p < 0.05$.

There Are No Major Changes in *HeCo* Cortex Shh Signaling at Early-Mid Corticogenesis

Primary cilia are central for the transduction of Sonic hedgehog (Shh) signaling (Wheway et al., 2018). Conditional knockout mice of ciliary proteins often show changes in Shh signaling in the developing brain impacting the levels and/or processing of its downstream effectors, notably the Gli transcription factors (Besse et al., 2011; Willaredt et al., 2008; Wilson et al., 2012). Gli proteins are found in a short-length (SL) repressor form or in a full-length (FL) activator form upon Shh stimulation. The primary cilium phenotype observed in *HeCo* aRGs prompted us to analyze this pathway. We analyzed the levels of Gli3 in cortical lysates from *HeCo* and WT mice at E12.5 and E13.5 by western blot (Figures 2F–2I). There was a tendency toward a decreased Gli3 full-length:Gli3 short-length ratio in *HeCo* cortices (Figures 2G and 2I) that was stronger at E13.5 than E12.5, the stage at which the severest primary cilia phenotype was observed. Despite these consistent subtle differences, there were no signif-

icant Shh changes observed between *HeCo* and WT E12.5/ E13.5 cortical lysates.

Protein Partners of *Eml1* Help Indicate that *RPGRIP1L* Is a Heterotopia Gene

Eml1 appears to have crucial functions regulating aRG behavior (Kielar et al., 2014; Bizzotto et al., 2017; this study), although the molecular pathways in which it is involved have not yet been clearly linked to aRG phenotypes. Performing a comprehensive analysis of potential *Eml1*-interacting partners identified in a previous screen (Bizzotto et al., 2017), the ciliary protein *Rpgrip1l* was identified. This protein is known to localize to the base of the primary cilium, in the transition zone, and mutations were previously identified in Joubert and Meckel ciliopathy syndromes (Wiegering et al., 2018). To confirm the interaction between *Eml1* and *Rpgrip1l*, Neuro2A cells were co-transfected with FLAG-tagged *EML1* and *c-myc*-tagged *RPGRIP1L* plasmids. 48 h later, antibodies directed at the tag of one of the proteins

(e.g., anti-FLAG; Figure 3A) were incubated with cell lysates to capture the protein of interest. Protein G Sepharose was added to capture the antibody-protein complexes, and after elution, these were then separated on protein gels. Immunodetection of western blots was performed with antibodies directed against the opposing protein tag (e.g., anti *c-myc*). Co-immunoprecipitation (coIP) experiments were performed in both directions, and this confirmed the interaction between EML1 and RPGRIP1L with either anti-FLAG (Figure 3A) or anti-*c-myc* (Figure 3F) antibodies used for the initial precipitation. These results further support that EML1 may play a role in primary-cilium-related protein complexes.

Simultaneously, compound heterozygous variations in *RPGRIP1L* (GenBank: NM_015272.2) were identified in a patient (P700-5) with SH (Figures 3B–3D; Table S1). P700-5 also exhibited agenesis of the corpus callosum and cerebellar dysplasia (Figures 3D4 and 3D5; Table S2). Nucleotide variations in *RPGRIP1L* were confirmed by Sanger sequencing. A c.3706C>T pathogenic variation in exon 24 (R1236C, sorting intolerant from tolerant [SIFT; <https://sift.bii.a-star.edu.sg/>] 0.03, damaging) was transmitted from the father. A c.3562G>A nucleotide change in exon 22 (V1188M, SIFT tolerated) was transmitted from the mother (Figure 3C; Table S1). Since autosomal recessive mutations in *RPGRIP1L* have previously been associated with Joubert and Meckel syndromes (OMIM: 610937), the unusual C-terminal mutations identified here (Figure 3E) may be important for the cortical phenotype observed.

Given the interaction of EML1 and RPGRIP1L and the resemblance of the phenotypes found in patients, we postulated that the interaction between these proteins may be altered in the presence of patient mutations. Both individual RPGRIP1L mutations led to a dramatic loss of interaction with EML1, using either anti-FLAG or anti-*c-myc* (Figures 3F, 3G, S2A, and S2B) for immunoprecipitation. The RPGRIP1L interaction was also tested using an EML1 construct expressing a patient mutation (family P135, mutation T243A; Kielar et al., 2014). Under these conditions, dramatically reduced quantities of FLAG-EML1-T243A were observed in anti-*c-myc* immunoprecipitates (Figure 3G). These data confirm that when either RPGRIP1L or EML1 is mutated, the interaction between the proteins is compromised.

These combined data suggest that convergent primary-cilia-related mechanisms are responsible for the heterotopia in *EML1* and *RPGRIP1L* patients. We then assessed the localization of RPGRIP1L mutant proteins in a human cell line (retinal pigmented epithelial cells [RPE1 cells]). RPE1 cells were transfected with recombinant *c-myc*-RPGRIP1L WT, *c-myc*-RPGRIP1L-R1236C, or *c-myc*-RPGRIP1L-V1188M. While WT RPGRIP1L clustered in perinuclear regions with a puncta-like pattern (white box), as previously shown for this protein (Gerhardt et al., 2015), the same type of staining was not observed when transfecting cells with the mutant constructs (Figure S2C). This suggests an altered subcellular localization of RPGRIP1L expressing heterotopia mutations.

To begin to test the impact of the individual *RPGRIP1L* heterotopia mutations at the early stages of corticogenesis, they were overexpressed in WT mouse brain. *In utero* electroporation at E13 was performed of individual *c-myc*-RPGRIP1L mutant constructs with a pCAG-IRES-GFP (pCAGIG) reporter construct to

identify electroporated cells, as well as an Arl13b-RFP construct targeting the primary cilium. At E14, Pax6⁺GFP⁺ cells were quantified across six equally sized bins spanning the cortical wall, and the percentage of cells in the region encompassing the VZ was assessed (bins 1–3) compared to the SVZ, IZ, and cortical plate [CP; bins 4–6; Figure S2D). Mutant forms of RPGRIP1L, especially the V1188M mutation, led to an apparent shift of Pax6⁺GFP⁺ and Pax6⁺GFP⁻ cells to basal positions in the cortical wall (Figure S2E). In addition, the *c-myc*-RPGRIP1L V1188M construct showed the presence of polarized rosette-like structures composed of primary cilia-containing Pax6⁺ cells in abnormal superficial regions (two out of three embryos; Figure S2F). Internalization of Pax6⁺ cells has previously been associated with primary cilia defects (Higginbotham et al., 2013; Lien et al., 2006).

Primary Cilia Formation Is Impaired in *EML1* and *RPGRIP1L* Patient Fibroblasts

Convergent suggestions for a link between primary cilia and heterotopia led us to assess the growth dynamics of this organelle in human patient fibroblasts. A cell culture approach for analyzing primary cilia assembly and/or disassembly was adopted (Kheradmand Kia et al., 2012). Five different lines of human fibroblasts were cultured from two *EML1*-patients (P3489 and P135; Kielar et al., 2014), the above-described *RPGRIP1L*-heterotopia patient (P700), and two similarly aged controls (control 1 and control 2). We studied primary cilium formation (1) under basal conditions (72 h after plating), when cells are asynchronously dividing; and (2) after serum starvation (SS), which was performed for 48 or 96 h (Figures 4A–4E, S3A, and S3B). SS induces cells to enter quiescence (G0) and thus grow a primary cilium (Figure S3A).

The percentage of cells presenting a primary cilium in the three different conditions was analyzed. Under basal conditions (Figure 4B) and 48 h after SS (Figure S3C), each of the three patient lines showed significantly fewer cells possessing a primary cilium. At 96 h, one of the *EML1* patient lines (P3489) reached levels similar to those of the control lines, while the other patient lines continued to show a significantly decreased proportion of primary-cilium-containing fibroblasts (Figure 4D). Under basal conditions and 48 h after SS, primary cilia length did not seem to be severely compromised compared to control lines (although the P135 and P700 fibroblast lines showed a tendency to have shorter primary cilia; Figures 4C and S3D). However, when performing SS for 96 h, all patient lines showed a significant decrease in the length of primary cilia compared to control conditions (Figure 4E).

These results suggest that *EML1*- and *RPGRIP1L*-mutant cells do not assemble cilia efficiently, in fitting with a role for EML1 and RPGRIP1L in primary cilium formation. Importantly, *RPGRIP1L* patient fibroblasts showed the same dynamics as *EML1* patient fibroblasts, further suggesting that perturbed mechanisms underlying the heterotopia phenotype may converge.

Human Cortical Progenitors with *EML1* Mutations Also Show Primary Cilia Anomalies

We decided to further analyze primary cilia in human cortical progenitor cells *in vitro*. These were differentiated from

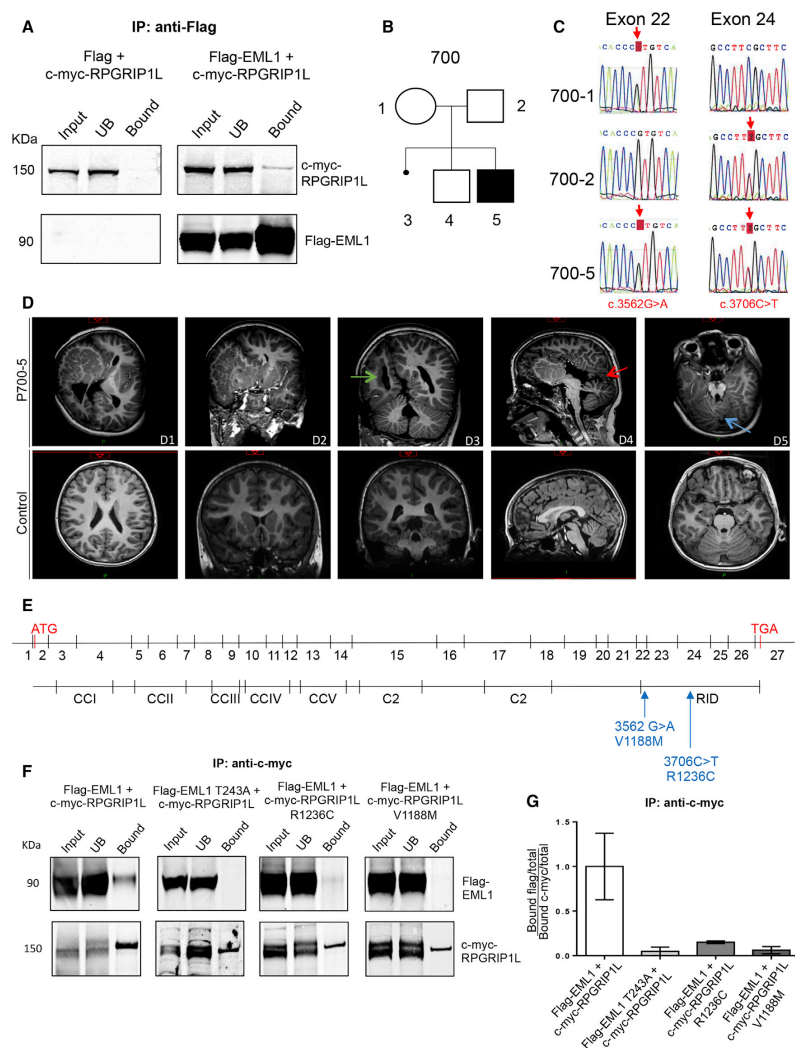


Figure 3. EML1 Interacts with RPGRIP1L, in which Mutations Were Identified in a Heterotopia Patient

(A) Representative western blots showing immunoprecipitation with anti-FLAG when co-transfecting FLAG/FLAG-EML1 with c-myc-RPGRIP1L (3 experiments per condition). The FLAG peptide alone (1 kDa) is a short sequence not recognized under these western blot conditions. Input: cell lysate prior to IP; UB (unbound) corresponds to the fraction of proteins not attaching to the bait (here FLAG-tagged protein).

(B) Pedigree of the family (P700), with one healthy boy, one affected boy, and one miscarriage.

(C) Sanger sequence chromatograms for the parents and affected child of a portion of the *RPGRIP1L* gene. Compound heterozygous mutations were identified in patient 700-5 (red arrows), one inherited from the mother and one from the father. Nucleotides are shown in red (T), black (G), green (A), and blue (C).

(legend continued on next page)

iPSCs from two control individuals and two *EML1*-mutation patients (controls 1.1 and 2.1, P3489, and P135; Figure S3E; Kielar et al., 2014; Gaspard et al., 2008; Shi et al., 2012). EM analyses of control-line-derived cortical cultures revealed the presence of a mother centriole docking a properly arranged primary cilium surrounded by ciliary pockets (Figure 4F). When investigating primary cilia in patient-derived cortical progenitors, we had difficulty identifying these organelles and those primary cilia observed showed abnormalities, including disturbed ciliary-like structures with no proper microtubule arrangement (Figure 4F, P135) or ciliary pockets that appeared distended (Figure 4F, P3489). Thus, the primary cilium also appears perturbed in human patient-derived cortical progenitors, suggesting a conserved role of *Eml1*/*EML1* across evolution.

Subcellular Localization and *EML1*-Interacting Proteins Shed Light on Potential Pathways Involved in the Centrosome-Primary Cilia Phenotype

EML1 has a cell-cycle-dependent localization in mouse neuronal progenitor cells *in vitro* (Kielar et al., 2014). It co-localizes with the microtubule network in interphase Vero cells (Kielar et al., 2014); however, a ciliary localization has not been described for this protein family (Fry et al., 2016). Its localization was hence further explored in aRGs, as well as in ciliated RPE1 cells, using exogenous expression of an *EML1*-tagged plasmid, since there are no known reliable antibodies to detect the endogenous protein. Transfection of YFP-*EML1* in RPE1 cells showed recombinant *EML1* throughout the cytoplasm, including in perinuclear regions, with no obvious association with the primary cilium (Figure S4A). *In utero* electroporation of pCAG-IRES-Tomato (to delineate aRG morphology) and EGFP-*EML1* identified recombinant *EML1* ubiquitously expressed in aRG apical processes (Figure S4B).

To learn more about *EML1*'s cellular role, we screened for additional interacting partners using full-length *EML1*, differing from the previous screen, which used only the N terminus (Bizzotto et al., 2017). Indeed, most mutations fall in the C-terminal β propeller structure (Fry et al., 2016), indicating the potential importance of this domain. Pull-down experiments were performed with purified Strep-tagged full-length *EML1* and E13.5 WT mouse cortex lysates (Figure 5A). Captured proteins were identified by mass spectrometry (MS). Label-free quantitative analyses based on the extracted ion chromatogram (XIC) method revealed a list of 240 proteins enriched in the Strep-tagged *EML1* condition (Table S3). We compared this 240-protein list with the N-terminal interactors identified previously

(Bizzotto et al., 2017). 85 out of 240 proteins commonly interacted with both the *EML1* N-terminus and the full-length protein, confirming the specificity of the new screen (Figure 5B). The remaining proteins may be specific for interactions with the *EML1* C-terminal domain.

To further identify cytoplasmic proteins, the new 240-protein list was further filtered to exclude nuclear proteins (as previously performed in Bizzotto et al., 2017), and a final list of 113 proteins was obtained (Table S3). The expression pattern across the murine developing cortex (E14.5) was examined for genes encoding these proteins using publicly available resources (GenePaint [https://gp3.mpg.de/]; data were available for 71 out of 113 proteins; Figure 5C). 63.4% of the 113 proteins clearly showed expression in the VZ (8.9% showed a CP expression only, and a further 27.7% were of unknown expression).

Cilia-related proteins were identified in both N-terminal and full-length lists (Table S4), revealing a total of 42 potential cilia-related *EML1* interactors. Gene Ontology (GO) analyses for the 113-protein list were performed using the DAVID (Database for Annotation, Visualization and Integrated Discovery) functional annotation tool [https://david.ncifcrf.gov/home.jsp] and STRING (Search Tool for the Retrieval of Interacting Genes/Proteins [https://string-db.org]) publicly available resources (Figure 5D; Tables S4, S5, and S6). Cell-cell adhesion, microtubule and actin-associated proteins, and Golgi-derived protein transport were identified among other categories in DAVID GO analyses (Figure 5D; Tables S4 and S5). STRING analyses revealed similar results, including membrane-bounded organelle, cytoskeleton, and cell junction among the most enriched "cellular component" GO categories (Table S6). Thus, in addition to cilia proteins, several other categories of proteins point to previously uncharacterized roles for *EML1*.

Golgi-Related Protein Partners of *EML1*, Including VCIP135

The prominent apical process localization of recombinant *EML1* in interphase aRGs, as well as the GO categories identified, prompted us to further focus on protein trafficking from the Golgi apparatus, localized in aRG apical processes (Taverna et al., 2016).

Given the importance of cargo trafficking and Golgi-derived protein transport for primary cilium formation, we searched for Golgi-related proteins in the MS lists (Table S4). VCIP135 (also known as VCPIP1) showed high specificity for the *EML1*-bound condition. This protein mediates Golgi apparatus cisternae regrowth after mitosis as well as maintenance of this organelle during interphase. Knockdown of VCIP135 is known

(D) Representative T1-weighted section of brain magnetic resonance imaging (MRI) of P700-5 and control showing a unilateral, extensive, subcortical heterotopia spanning from the frontal lobe (D1) to the parieto-temporal region (D2). In the occipital lobe, the cortical malformation is characterized by right-sided nodular periventricular subependymal heterotopia (D3, green arrow). Note that the overlying cortex is thinner and appears dysplastic (D1–D3). P700-5 presents corpus callosum agenesis (D4, red arrow) and cerebellar dysplasia (D5, blue arrow).

(E) Schematic representation of the *RPGRIP1L* gene (above) and protein domains (below). Blue arrows indicate the position of compound heterozygous mutations found in P700-5.

(F) Representative western blot of immunoprecipitation with anti-c-myc when co-transfecting (WT or mutant) FLAG-*EML1* with (WT or mutant) c-myc-RPGRIP1L (3 experiments per condition).

(G) Quantification of immunoprecipitation experiments comparing the amount of *EML1* bound to RPGRIP1L in WT and mutant conditions. The bound prey protein was normalized to total levels of the protein and immunoprecipitated bait protein. Data are represented as mean \pm SEM. See also Figure S2.

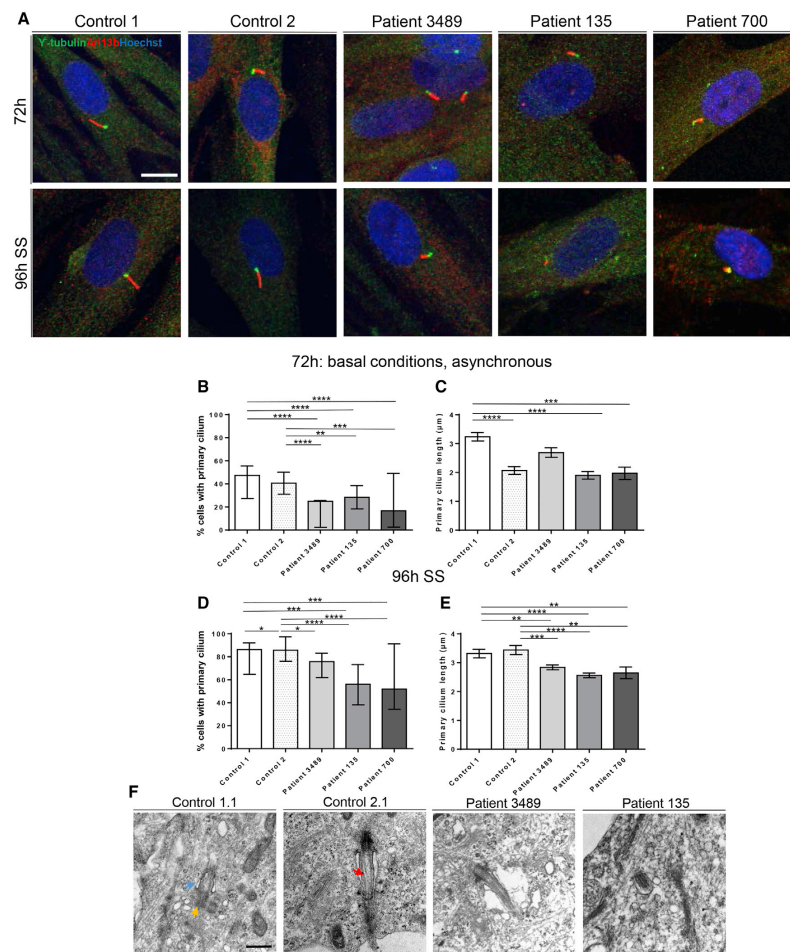


Figure 4. Primary Cilium Formation Is Perturbed in *EML1* and *RPGRIP1L* Patient Fibroblasts and Cortical Progenitors Differentiated from *EML1* Patient-Derived iPSCs

(A) Representative images of immunocytochemistry for γ -tubulin (green) and Arl13b (red) in control (control 1 and 2) and patient fibroblasts (P3489: *EML1* W225R; P135: *EML1* T243A R138X; and P700: *RPGRIP1L* R1236C V1188M) at basal conditions (72 h) and 96 h after serum starvation (SS).
 (B) Percentage of fibroblasts presenting a primary cilium in basal conditions (2–4 experiments per condition).
 (C) Quantifications of primary cilium length in fibroblasts in basal conditions (n = 24–109 primary cilia from 2 to 4 experiments).
 (D) Percentage of fibroblasts presenting a primary cilium at 96 h SS (3–4 experiments per condition).
 (E) Quantifications of primary cilium length in fibroblasts at 96 h SS. n = 64–141 primary cilia from 3 to 4 experiments.
 (F) Representative EM images of human cortical progenitors derived from control and *EML1* mutation patient iPSCs. Yellow arrow, basal body; blue arrow, ciliary pockets; and red arrow, primary cilium.
 Scale bars, 10 μ m (A) and 0.5 μ m (F). Data are represented as median \pm minimum–maximum range and chi-square test (B and D) or mean \pm SEM and one-way ANOVA followed by unpaired t test (C and E). ****p < 0.0001, ***p < 0.001, **p < 0.01, and *p < 0.05.
 See also Figure S3.

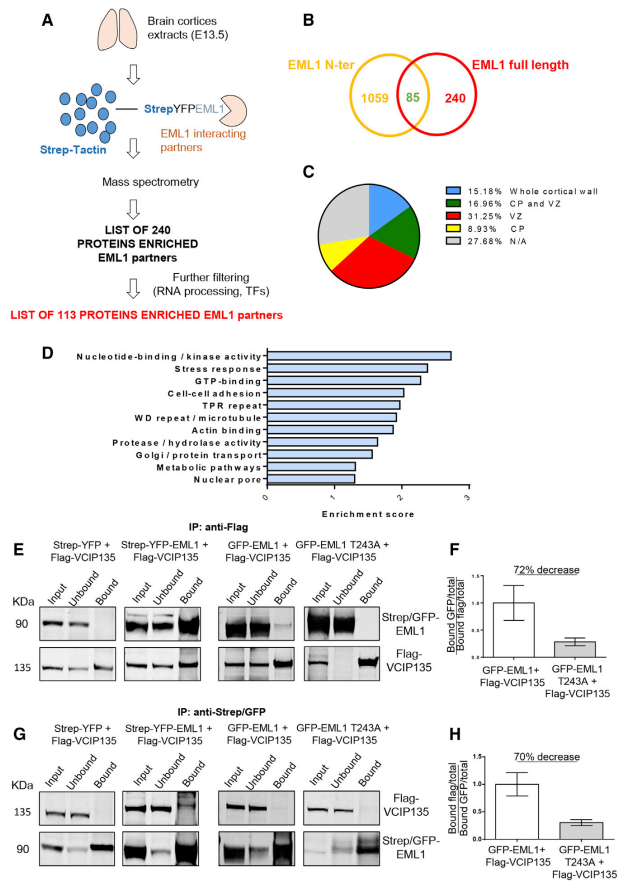


Figure 5. Mass Spectrometry Analyses Reveal Additional EML1-Interacting Partners, among Them the Golgi Protein VCIP135

(A) Schematic of the proteomics workflow. Either Strep-YFP or Strep-YFP-EML1 purified with Strep-Tactin beads was used for pull-down experiments using embryonic cortex lysates. Binding partners were obtained by quantitative label-free MS analyses performed from four replicates.

(B) Diagram indicating number of common proteins identified in full-length and N-terminal (Bizzotto et al., 2017) EML1 MS screens.

(C) Diagram representing expression of EML1-interacting partners in the E14.5 murine cortical wall (GenePaint).

(D) Gene Ontology analyses performed with the publicly available software DAVID for the 113-protein list. Only those categories with an enrichment score >1 are represented.

(E) Representative western blot of immunoprecipitation with anti-FLAG when co-transfecting FLAG-VCIP135 with Strep-YFP, Strep-YFP-EML1, GFP-EML1, and GFP-EML1-T243A (2–3 experiments per condition).

(F) Quantification of immunoprecipitation experiments comparing the amount of EML1 bound to VCIP135 in WT and mutant conditions. The bound prey protein was normalized to total levels of the protein and levels of the bait protein.

(G) Representative western blot of immunoprecipitation with Strep or GFP when co-transfecting Strep-YFP with FLAG-VCIP135, Strep-YFP-EML1 with FLAG-VCIP135, GFP-EML1 with FLAG-VCIP135, and GFP-EML1-T243A with FLAG-VCIP135 (2–3 experiments per condition).

(H) Quantification of immunoprecipitation experiments comparing the amount of VCIP135 bound to EML1 in WT and mutant conditions. The bound prey protein was normalized to total levels of the protein and levels of the bait protein.

Data are represented as mean \pm SEM (F and H). See also Figures S4 and S5.

to lead to Golgi fragmentation (Uchiyama et al., 2002; Zhang et al., 2014; Zhang and Wang, 2015). The interaction of Strep-tagged EML1 with FLAG-tagged VCIP135 was tested by performing coIP experiments in Neuro2A cells. An interaction was confirmed using either anti-FLAG or Strep for the IP (Figures 5E and 5G). We next checked if EML1 mutation perturbed this interaction, performing coIP experiments with GFP-EML1 T243A and FLAG-VCIP135. Using anti-FLAG and anti-GFP, a reduction of the interaction between the two proteins was observed (Figures 5E–5H). Therefore, a patient mutation in the β propeller domain of EML1 disrupts the interaction with VCIP135, suggesting that EML1 may play a role associated with the Golgi apparatus.

hairpin (shmiRNA) against *Vcip135* and a scrambled control shmiRNA (shmiRNA control) were generated. Efficiency was tested (reduction by 40 %) by performing transfections of these constructs in Neuro2A cells, followed by qRT-PCR (Figure S5B). *In utero* electroporation together with a pCAG-IRES-Tomato construct was performed at E13, and brains were analyzed 24 h later (Figure S5A). Tomato⁺ cells were quantified across six equally sized cortical bins. A significant shift of Tomato⁺ cells was observed from bins 1 to 3 toward more basal positions in the *Vcip135* KD condition (Figure S5C). This suggests that Golgi-related proteins, and more specifically the Eml1-interacting protein *Vcip135*, are important for progenitor cell position.

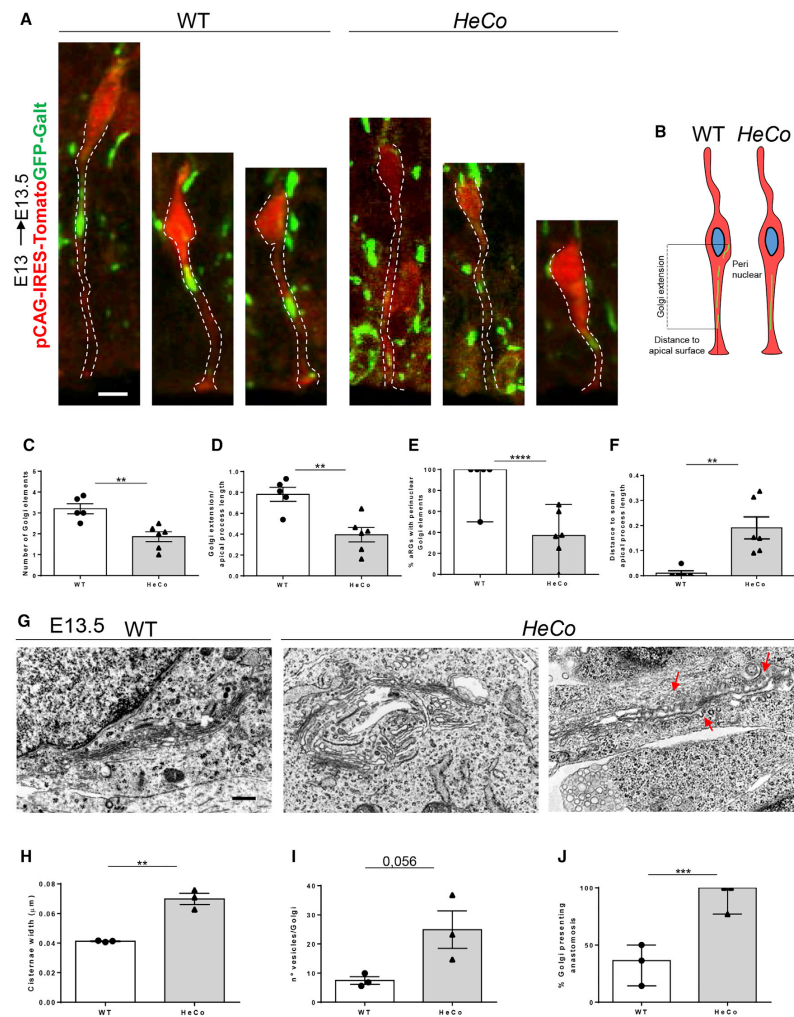


Figure 6. The Golgi Apparatus Is Severely Disrupted in *Em1* Mutant aRGs in Brain Slices

(A) WT and *HeCo* aRGs electroporated with pCAG-IRES-Tomato (cell morphology) and pCAG-Galt-EGFP (Golgi apparatus).

(B) Schema representing the parameters quantified and the Golgi phenotype observed in aRGs.

(C) Quantification of number of Golgi elements.

(D) Quantification of Golgi extension.

(E) Quantification of the percentage of cells containing perinuclear Golgi elements. Statistical tests were performed considering the frequency across cells analyzed.

(F) Quantification of the distance between the basal-most Golgi element to the aRG soma.

(G) Representative EM images of the Golgi apparatus in WT and *HeCo* aRGs at E13.5. Red arrow shows anastomosis.

(legend continued on next page)

The Golgi Apparatus Is Severely Disrupted in *HeCo* Neuronal Progenitors

A Golgi localization for recombinant Eml1 could not be easily identified in Pax6⁺ neuronal progenitors due to the abundant soluble fraction of the protein (Figure S4C). We decided to query this organelle in *HeCo* aRGs. The Golgi apparatus has recently been described to be restricted to aRG apical processes, where it exists as a series of individualized stacks (Taverna et al., 2016), defined here as “Golgi elements.” *In utero* electroporation of a pCAG-IRES-Tomato plasmid, as well as a pCAG-Galt-EGFP plasmid targeting the Golgi apparatus, was performed at E13, and WT and *HeCo* brains were analyzed at E13.5. Golgi position was assessed in WT and *HeCo* aRGs as in Taverna et al. (2016), and the number of perinuclear Golgi elements was also assessed.

Golgi apparatus distribution was strikingly different in *HeCo* compared to WT aRGs at E13.5 (Figures 6A–6F). The number of Golgi elements was significantly reduced, as was the extension of this organelle in the apical process (Figures 6C and 6D). Consistently, there were fewer Golgi elements in perinuclear regions, and these were further away from the soma (Figures 6E and 6F). These data indicate that in the *HeCo* VZ the Golgi apparatus is subdivided in fewer stacks and does not span as far across the apical process of aRGs (depicted in Figure 6B).

In order to further examine the Golgi apparatus phenotype, several parameters were assessed by EM (Figures 6G–6J). Golgi cisternae width was significantly increased in *HeCo* aRGs (Figures 6G and 6H), and there was a tendency for increased vesicles surrounding this organelle (Figure 6I). We also assessed if the Golgi apparatus showed signs of anastomosis, a process characterized by the fusion and aberrant branching of Golgi cisternae. Indeed, there was a significant increase in the anastomosis-presenting Golgi apparatus in *HeCo* compared to WT aRGs (Figure 6G, red arrows, and Figure 6J). These abnormal Golgi features point toward a pathological disruption of this organelle.

The multiple Golgi apparatus phenotypes suggest there may also be functional Golgi alterations in *HeCo* aRGs. An *in vitro* approach was established to assess Golgi-derived trafficking in aRG-like cells in culture. Pax6⁺ progenitor-enriched cell cultures (Sun et al., 2011) were prepared from the dorsal telencephalon of E13.5 WT and *HeCo* embryos (Figure 7A). These cells were transfected with the thermosensitive vesicular stomatitis virus G protein VSVts405-G-EGFP (VSVG-EGFP). This modified protein is stored in the endoplasmic reticulum (ER)-Golgi compartments when cells are incubated at 39.5°C. Upon incubation at 32°C, the protein starts to exit these compartments and is trafficked toward the plasma membrane (Alterio et al., 2015;

Bergmann, 1989). Using this approach combined with immunocytochemistry for the Golgi marker GM130, VSVG-EGFP anterograde trafficking was analyzed 5 and 30 min after incubation at 32°C (Figure 7B). The presence or absence of GFP⁺ puncta outside the Golgi apparatus was assessed at these two time points, and the number of puncta was quantified. As expected, 5 min after incubation at 32°C, most of the VSVG-EGFP protein was found within the Golgi both in WT and *HeCo* cells, with only some sparse GFP⁺ puncta found in the cytoplasm (average of two puncta per cell in both conditions; data not shown; Figures 7B and 7C). However, analyses at 30 min showed fewer *HeCo* cells presenting GFP⁺ puncta outside of the Golgi (17% decrease) (Figures 7B and 7D). This decrease was significant when considering 2 GFP⁺ puncta/cell as the baseline (Figure 7E). *HeCo* cells also showed a lower overall number of GFP⁺ puncta compared to WT cells (Figure 7F). Our data hence converge to suggest that Golgi apparatus structure and its anterograde transport are perturbed in *HeCo* cells, with a reduction in post-Golgi trafficking demonstrated in the VSVG-EGFP assay.

EML1 Patient Fibroblasts and Human Cortical Progenitors Also Show Golgi Anomalies

We queried if the Golgi apparatus was also perturbed in EML1 patient fibroblasts. The Golgi marker TGN46 was assessed in basal conditions (72 h), quantifying the number of Golgi fragments as well as Golgi volume (Figures S5D–S5F). P135 patient cells showed an increased number of Golgi fragments as well as an increased volume, and the P3489 line showed similar tendencies (Figures S5D–S5F).

We also assessed the Golgi apparatus by EM in human cortical progenitors derived from either control or EML1 patient iPSCs (Figure 7G). Control line-derived cortical progenitors exhibited a flat cisternae-containing Golgi apparatus. This was, however, not true for the EML1 patient samples. Here, we observed a significant increase in the percentage of cells presenting vacuolized Golgi (Figure 7G, red asterisk, and Figure 7H). Primary cilia defects were previously found to be associated with anomalies of Golgi-dependent processes (Hua and Ferland, 2018). EML1 mutant Golgi apparatus defects are hence likely to be associated with the severe primary cilium defects identified.

DISCUSSION

Our study unravels an unprecedented role for Eml1/EML1 in primary cilia formation. Through a plethora of approaches, we report severe anomalies in this organelle in Eml1/EML1 mutant conditions and confirm an EML1 ciliary protein partner, RPGRIP1L. We identified a first heterotopia patient presenting

(H) Quantification of cisternae width.

(I) Quantification of the number of vesicles surrounding each Golgi apparatus.

(J) Quantification of the percentage of Golgi apparatus presenting anastomosis.

Each point in (C)–(F) represents an embryo (WT: n = 5 embryos from 3 litters, with 3–6 cells analyzed per embryo; *HeCo*: n = 4 embryos from 2 litters, with 2–11 cells analyzed per embryo). Data in (D) and (F) are normalized by the apical process length to avoid bias due to interkinetic nuclear migration. Each point in (H)–(J) represents an embryo (n = 3 embryos per condition from 3 litters, with 4–12 cells analyzed per embryo). Statistical test performed considering frequency across cells analyzed (J). Scale bars, 10 μm (A) and 0.5 μm (G). Data are represented as mean ± SEM and unpaired t test (C, D, F, H, and I) or median ± minimum-maximum range and Fisher's exact test (E and J). ****p < 0.0001, ***p < 0.001, and **p < 0.01. See also Figure S4.

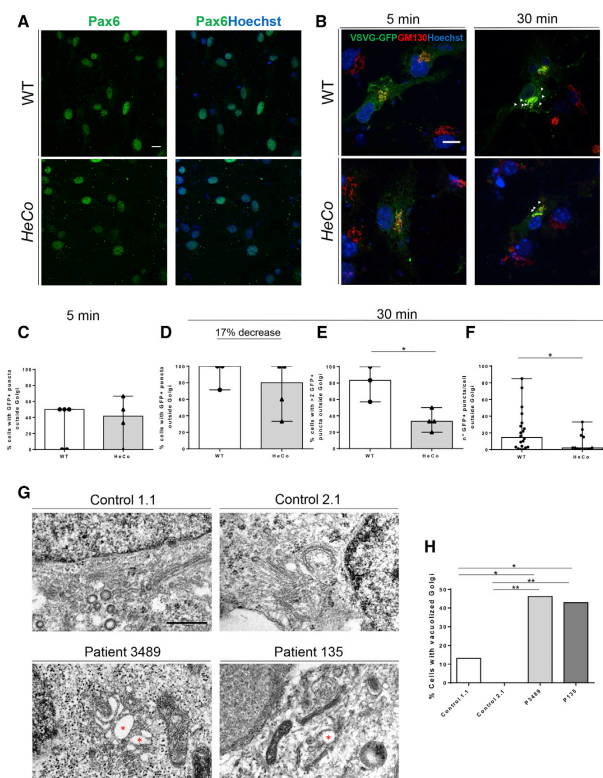


Figure 7. Golgi Anterograde Trafficking Is Perturbed in *Eml1* Mutant Progenitors *In Vitro*, and This Organelle Is Also Disrupted in iPSC-Derived Cortical Progenitors

(A) Pax6 (green) immunostaining in primary cultures of mouse neuronal progenitors from WT and HeCo mice (E13.5).

(B) Neuronal progenitor cells were transfected with VSVG-EGFP and incubated at 39°C. They were then incubated at 32°C and fixed 5 or 30 min later. Immunostaining with GM130 (red) was performed.

(C) Percentage of cells containing GFP⁺ puncta outside the Golgi at 5 min.

(D) Percentage of cells containing GFP⁺ puncta outside the Golgi at 30 min.

(E) Percentage of cells containing >2 GFP⁺ puncta per cell outside the Golgi at 30 min.

(F) Number of GFP⁺ puncta per cell outside the Golgi at 30 min.

(G) Representative EM images of the Golgi apparatus in cortical progenitors derived from control or EML1 patient iPSCs. Red asterisk shows vacuolized Golgi apparatus.

(H) Quantification of the percentage of Golgi apparatuses containing vacuolized Golgi. 20–28 cells were analyzed for each condition.

Cultures in (C)–(F) are from at least 3 embryos from 2 litters (n = 13–19 cells per condition). Each point in (C)–(E) represents an independent experiment. Statistical tests were performed considering the frequency across cells analyzed. Each point in (F) represents a cell. Scale bars, 10 μm (A and B) and 0.5 μm (G). Data are represented as median ± minimum-maximum range with Fisher's exact test (C, D, E, and H) or Mann-Whitney test (F). **p < 0.01, and *p < 0.05. See also Figure S5.

mations can arise (Bizzotto and Francis 2015). Centrosomal proteins are mostly associated with microcephaly (Bizzotto and Francis, 2015; Uzquiano et al., 2018), while defects in primary cilia have

been associated with microcephaly, polymicrogyria, periventricular heterotopia (PV), focal cortical dysplasia, and ciliopathies (Ding et al., 2019; Gabriel et al., 2016; Kheradmand Kia et al., 2012; Park et al., 2018; Sheen et al., 2004). Of interest, certain rare mutations in OFD1, localized in the basal body and involved in primary cilium formation, have been previously associated with SH (Del Giudice et al., 2014). Our study further links the primary cilium to severe heterotopia conditions in mouse and human. Additionally, this is one of the few studies linking abnormal primary cilia to epilepsy (Canning et al., 2018; Park et al., 2018), a condition also suffered by patients with *EML1* mutations.

Although this study focused on aRGs, it is also important to study *Eml1*/*EML1* function and primary cilia in other neocortical progenitors, which may contribute to the pathology. Our preliminary data concerning *Arl13b* distribution throughout the cortical wall in *HeCo* brains suggest potential abnormalities in more basal cortical regions likely to contain intermediate progenitors. We have also shown previously that *EML1* is expressed in the

mutations can arise (Bizzotto and Francis 2015). Centrosomal proteins are mostly associated with microcephaly (Bizzotto and Francis, 2015; Uzquiano et al., 2018), while defects in primary cilia have been associated with microcephaly, polymicrogyria, periventricular heterotopia (PV), focal cortical dysplasia, and ciliopathies (Ding et al., 2019; Gabriel et al., 2016; Kheradmand Kia et al., 2012; Park et al., 2018; Sheen et al., 2004). Of interest, certain rare mutations in OFD1, localized in the basal body and involved in primary cilium formation, have been previously associated with SH (Del Giudice et al., 2014). Our study further links the primary cilium to severe heterotopia conditions in mouse and human. Additionally, this is one of the few studies linking abnormal primary cilia to epilepsy (Canning et al., 2018; Park et al., 2018), a condition also suffered by patients with *EML1* mutations.

Although this study focused on aRGs, it is also important to study *Eml1*/*EML1* function and primary cilia in other neocortical progenitors, which may contribute to the pathology. Our preliminary data concerning *Arl13b* distribution throughout the cortical wall in *HeCo* brains suggest potential abnormalities in more basal cortical regions likely to contain intermediate progenitors. We have also shown previously that *EML1* is expressed in the

SVZ of the gyrencephalic ferret brain (Kielar et al., 2014), and a more recent study confirmed its expression in basal RGs present in this zone in the human developing cortex (Nowakowski et al., 2017). Basal RG progenitors are thought to be crucial for neocortical expansion and gyrification and may be affected in severe cortical malformations (e.g., Bershteyn et al., 2017). It would thus be relevant to study EML1 and cilia function in this cell type.

Related to EML1 location and subcellular function, we did not identify its expression within the primary cilium in interphase cells. We hence investigated the molecular and cellular mechanisms that might be upstream of its insertion in the apical plasma membrane. Searching for additional interactors, we identified an appealing list of candidate partners that may play a role in the phenotype. We focused on the Golgi apparatus, since cargo sorting and trafficking are known to be critical for the correct formation of the centrosome-primary cilium complex (Bernabé-Rubio and Alonso, 2017; Madhivanan and Aguilar, 2014). In addition to VCIP135, other Golgi-related proteins identified by MS were shown to co-localize with this organelle (e.g., CK1 δ); be important for its structure, morphology, and function (e.g., Scyl1, Map4, Camsap3, and Clasp1/2); or mediate cilia-targeted protein transport (e.g., Arf4). It is worth noting that some MS partners also showed ciliary localization and/or functions (e.g., Nup98 and Neurl4), and some were even reported to be localized both in the Golgi and in the centrosome-primary cilium (e.g., CK1 δ , Map4, and Usp9x) and be important for their structure and/or function (e.g., Staufen2, Kifc1, Kif7, and Macf1). Of note, Rpgrip11 appears also to be partially localized outside the cilia (Sang et al., 2011).

An interaction of EML1 with the Golgi protein VCIP135 was confirmed by heterologous expression in Neuro2A cells. The EML1 T243A patient missense mutation perturbs this interaction, as well as the interaction with the ciliary protein RFGRIIP1L. To further confirm that aRG delamination in mutant conditions is related to these reduced interactions, rescue experiments with WT and mutant EML1 protein could be performed.

VSVG data also point toward a cargo sorting and/or trafficking defect in *HeCo Pax6⁺* cells *in vitro*. Furthermore, the Golgi apparatus in *Eml1/EML1* mutant conditions shows an abnormal distribution and structure in mouse aRGs, patient fibroblasts, and human cortical progenitor cells. We hence have convincing cumulative evidence that this organelle normally requires Eml1/EML1 in these cell types. Correct Golgi-derived function is also critical for primary cilium formation (Bernabé-Rubio and Alonso, 2017; Madhivanan and Aguilar, 2014), which leads us to suggest that these Golgi phenotypes may be upstream of the centrosome-primary cilium defect identified in *Eml1/EML1* mutant conditions.

Previous studies have tentatively associated Golgi defects with cortical migration malformations, such as *ARFGEF2* mutations leading to microcephaly and PV (Sheen et al., 2004) and *DYNC1H1* mutations mainly leading to posterior pachygyria, polymicrogyria, and microcephaly (Schiavo et al., 2013). However, experiments reporting Golgi apparatus anomalies in the context of mutations in these two proteins were performed *in vitro* and not directly in neuronal progenitor cells (Fiorillo et al., 2014; Jaarsma and Hoogenraad, 2015; Sheen et al., 2004). Instead, we assessed the Golgi in neuronal progenitor

cells (human and mouse), including in mouse aRGs *in vivo*, and were able to link Golgi anomalies to the pathogenesis of severe SH.

It remains to be elucidated if the Golgi functions altered in *Eml1/EML1* mutant conditions impact exclusively the centrosome-primary cilium pathway. If Golgi-dependent protein transport is more widely perturbed, then it could also affect the delivery of key adherens junction components to the plasma membrane, which is crucial for aRG polarity and behavior (Sheen et al., 2004; Uzquiano et al., 2018). This could loosen cell contacts between aRGs, allowing their delamination and contributing to the ectopic progenitor phenotype. Further experiments are thus required to understand the possible mechanisms related to Golgi-plasma membrane phenotypes in *Eml1/EML1* mutant conditions, as well as in other cortical malformation models.

Several signaling pathways integrated by the primary cilium (i.e., mTOR, Shh, Hippo, and Wnt; Wheway et al., 2018) might be expected to be disrupted in *Eml1/EML1* mutant conditions. For instance, changes in the mTOR signaling pathway have been previously associated with diverse pathological cortical phenotypes (Benova and Jacques, 2019; D'Gama et al., 2017; Foerster et al., 2017; Park et al., 2018). However, we did not find changes in this pathway in the *HeCo* telencephalon during the early-mid corticogenesis (data not shown). We also did not find any major changes in Shh signaling in *HeCo* dorsal telencephalon extracts during the same stages. Nevertheless, other approaches examining these pathways in aRGs specifically would be necessary to completely rule out their implication in the onset of the ectopic progenitor and thus heterotopia phenotype.

Assessing other pathways known to be mediated by the primary cilium could also help shed light on the downstream pathological mechanisms contributing to progenitor phenotypes. Another pathway associated with the primary cilium is the Hippo pathway (Wheway et al., 2018), although the relationship remains relatively unexplored. This pathway is known to regulate tissue homeostasis and hence to regulate cell growth, size, and shape (Ma et al., 2019). Primary cilium defects combined with changes in apical domain and endfeet features, as well as metaphase cell shape (this study; Bizzotto et al., 2017) make this pathway an appealing candidate underlying abnormal VZ dynamics in *Eml1* mutant conditions. Mutations in proteins involved in Hippo signaling have been previously associated with cortical malformations (Cappello et al., 2013; O'Neill et al., 2018). A recent study in the mouse also reported changes in the levels of key Hippo pathway proteins in the VZ of a model for SH, largely phenocopying the *HeCo* mouse phenotype (Liu et al., 2018). Therefore, assessing this pathway in *Eml1* mutant conditions would shed further light on the molecular mechanisms downstream of the primary cilium aRG phenotype.

In this study, we focused on the role of Eml1/EML1 during interphase; however, this protein can play various roles during the cell cycle (Bizzotto et al., 2017). This is consistent with the extra-ciliary role of many proteins important for the centrosome-primary cilium (Hua and Ferland, 2018). Further studying the function of Eml1 and its ciliary protein partners during different stages of the cell cycle will shed further light on their multivalent roles in dividing cortical progenitors. During

interphase, our data are consistent with the fact that fewer Eml1 mutant aRG endfeet form cilia, potentially due to abnormal ciliary protein targeting. Eml1 mutant aRG processes are hence deficient, either through abnormal signaling or via weakened membrane attachments due to abnormal adhesion component trafficking. We propose that these mechanisms contribute to progenitor delamination, initiating a sequence of events leading to heterotopia.

STAR★METHODS

Detailed methods are provided in the online version of this paper and include the following:

- **KEY RESOURCES TABLE**
- **LEAD CONTACT AND MATERIALS AVAILABILITY**
- **EXPERIMENTAL MODEL AND SUBJECT DETAILS**
 - Animals
 - Human Cell Culture
 - Heterotopia Patients with Mutations in EML1
 - Clinical Phenotype of the Patient P700-5
 - Human Fibroblast Cultures
 - Generation of Human iPSCs and Thereof Derived Cortical Progenitors
 - Retina Epithelial Pigmented Cell Culture
 - Mouse Neuronal Progenitor Cell Culture
 - Neuro2A Cell Culture
 - Freestyle 293F Cell Culture
- **METHOD DETAILS**
 - En Face Immunohistochemistry and Imaging
 - Electron Microscopy
 - Exome Sequencing of Heterotopia Patients: Analyses of *RPGRIP1L* Mutations
 - Embryonic Cortex Lysate
 - hTERT RPE-1 Cell Transfection
 - Freestyle 293F Cell Transfection, Protein Purification, and Pull Down for Mass Spectrometry
 - Mass Spectrometry
 - Neuro2A Transfection, Co-immunoprecipitation
 - Western Blot
 - Mouse Progenitor Cell Culture Transfection
 - Immunocytochemistry
 - Shmir Design and RT-qPCR
 - In Utero Electroporation
 - BrdU Injections and Immunohistochemistry
- **QUANTIFICATION AND STATISTICAL ANALYSIS**
 - En Face Imaging
 - Electron Microscopy
 - Immunohistochemistry and Immunocytochemistry Images
 - Immunoprecipitation and Western Blot
 - Statistical Analyses
- **DATA AND CODE AVAILABILITY**

SUPPLEMENTAL INFORMATION

Supplemental Information can be found online at <https://doi.org/10.1016/j.celrep.2019.06.096>.

ACKNOWLEDGMENTS

We thank Dr. M. Nosten-Bertrand for advice with statistical analyses and Dr. M. Stouffer, Dr. S. Bizzotto, Dr. A. Andreu-Cervera, G. Martinez Lorenzana, and A. Muzerelle for experimental help. We thank G. Arras from the LSMP for his assistance in MS data analysis and Dr. A. Houdusse for her advice. We thank Dr. A. Shihavuddin for his help with *en face* imaging data analysis. We are grateful to the following people for kindly gifting us materials and sharing protocols: Dr. C. Delevoye (TGN46 antibody), Dr. B. Goud (VSVG-GFP construct), Dr. A. Baffet (RPE1 cells and neuronal progenitor cell culture), Dr. V. Marthiens (neuronal progenitor cell culture), Dr. X. Zhang (FLAG-VCIP135 construct), Dr. M. Richards and Dr. R. Bayliss (Strep-YFP-EML1 construct), Dr. C. Lebrand (CAG-Tomato vector), Dr. F. Murakami (pCAG-Galt-EGFP construct), Dr. F. Watrin (small hairpin RNA [shmiRNA] empty vector), Dr. H. Lickert (*Arl13b*-RFP construct), and Dr. S. Schneider-Maunoury (*c-myc*-*RPGRIP1L* construct and *Shh* pathway antibodies). We thank the animal experimentation facility and cellular and tissue imaging platforms at the Institut du Fer à Moulin, supported also by the Région Ile de France and the FRC Rotary. We thank Dr. A. Croquelois for original mice, G. Granec (IFM) and the TAAM (CDTA Orleans) for the maintenance of the *HeCo* mouse line. For patient sample provision and sequencing, we thank Mélanie Jennesson Lyve and Jacques Motte (Reims Hospital), Anne-Gaëlle le Moing (Amiens Hospital), the Institut Imagine Biobank, Jamel Chelly (IGBMC, Strasbourg), Robert Olasso, Jean-Baptist Petit and Vincent Meyer (CNRGH, Evry), and Mara Cavallin and Karine Poirier (Institut Imagine, Paris) for their very helpful support, and all families for kindly agreeing to provide samples. A.U., D.M.R., A.H., and F.F. are associated with the BioPsy Labex project and the Ecole des Neurosciences de Paris Ile-de-France (ENP) network. Our salaries and labs were supported by Inserm; Centre National de la Recherche Scientifique (CNRS); Sorbonne University; French Agence National de la Recherche (ANR-13-BSV4-0008-01 and ANR-16-CE16-0011-03 to F.F. and N.B.-B.); Fondation Battencourt Schueller (F.F.); the European Union (EU-HEALTH-2013, DESIRE, number 60253 to F.F. and N.B.-B.); the ERA-Net NEURON JTC 2015 Neurodevelopmental Disorders program affiliated with the ANR (for NEURON8-Full-815-006 STEM-MCD to F.F., N.B., and J.L.); the Fondation Maladies Rares/Phenomin (project IR4995 to F.F.); the European Cooperation in Science and Technology (COST Action CA16118 to G.M.S.M., N.B.-B., and F.F.); and the Hector Foundation II (to J.L.). This project was further supported by the French ANR under the frame of E-Rare-3, the ERA-Net for Research on Rare Diseases (ERARE18-049). A.U. received an ENP PHD grant and a Company of Biologists travel grant and was also funded by the Fondation de France (Prix Valérie Chamillard, selected by the Fondation Française pour la Recherche sur l'Épilepsie). D.L. was supported by Région Ile-de-France (2013-2-EML-02-ICR-1) and Fondation pour la Recherche Médicale (DGE2012125630) grants.

AUTHOR CONTRIBUTIONS

A.U. conceived, designed, and performed experiments, analyzed data, and wrote the manuscript. C.C.-D. performed electron microscope experiments and data analyses. A.J. performed iPSC-derived neuronal progenitor cell cultures under the supervision of J.L. D.M.R. contributed to identification of the mutated gene for the P700 family and performed experiments. A.H. performed biochemistry experiments. F.D. carried out the MS experimental work, and D.L. supervised MS and data analysis. A.B. and J.-F. D. performed exome-sequencing experiments. C.M. contributed to confirmation of *RPGRIP1L* gene mutations under the supervision of N.B.-B. G.M.S.M. provided P3489 fibroblasts and contributed to cilia discussions. F.F. conceived and designed experiments, helped with data interpretation, and wrote the manuscript.

DECLARATION OF INTERESTS

The authors declare no competing interests.

Received: February 21, 2019

Revised: May 31, 2019

Accepted: June 27, 2019

Published: July 30, 2019

REFERENCES

- Aigouy, B., Farhadifar, R., Staple, D.B., Sagner, A., Röper, J.C., Jülicher, F., and Eaton, S. (2010). Cell flow reorients the axis of planar polarity in the wing epithelium of *Drosophila*. *Cell* **142**, 773–786.
- Alterio, J., Masson, J., Diaz, J., Chachlaki, K., Salman, H., Areias, J., Al Awabdh, S., Emerit, M.B., and Darmon, M. (2015). Yif1B is involved in the anterograde traffic pathway and the Golgi architecture. *Traffic* **16**, 978–993.
- Ban, H., Nishishita, N., Fusaki, N., Tabata, T., Saeki, K., Shikamura, M., Takada, N., Inoue, M., Hasegawa, M., Kawamata, S., and Nishikawa, S. (2011). Efficient generation of transgene-free human induced pluripotent stem cells (iPSCs) by temperature-sensitive Sendai virus vectors. *Proc. Natl. Acad. Sci. USA* **108**, 14234–14239.
- Benova, B., and Jacques, T.S. (2019). Genotype-phenotype correlations in focal malformations of cortical development: a pathway to integrated pathological diagnosis in epilepsy surgery. *Brain Pathol.* **29**, 473–484.
- Bergmann, J.E. (1989). Using temperature-sensitive mutants of VSV to study membrane protein biogenesis. *Methods Cell Biol.* **32**, 85–110.
- Bernabé-Rubio, M., and Alonso, M.A. (2017). Routes and machinery of primary cilium biogenesis. *Cell. Mol. Life Sci.* **74**, 4077–4095.
- Bershteyn, M., Nowakowski, T.J., Pollen, A.A., Di Lullo, E., Nene, A., Wynshaw-Boris, A., and Kriegstein, A.R. (2017). Human iPSC-derived cerebral organoids model cellular features of lissencephaly and reveal prolonged mitosis of outer radial glia. *Cell Stem Cell* **20**, 435–449.e434.
- Besse, L., Neti, M., Anselme, I., Gerhardt, C., Rütger, U., Laclef, C., and Schneider-Maunoury, S. (2011). Primary cilia control telencephalic patterning and morphogenesis via Gli3 proteolytic processing. *Development* **138**, 2079–2088.
- Bizzotto, S., and Francis, F. (2015). Morphological and functional aspects of progenitors perturbed in cortical malformations. *Front. Cell. Neurosci.* **9**, 30.
- Bizzotto, S., Uzquiano, A., Dingli, F., Ershov, D., Houllier, A., Arras, G., Richards, M., Loew, D., Minc, N., Croquelois, A., et al. (2017). Emi1 loss impairs apical progenitor spindle length and soma shape in the developing cerebral cortex. *Sci. Rep.* **7**, 17308.
- Bustin, S.A., Benes, V., Garson, J.A., Hellemans, J., Huggett, J., Kubista, M., Mueller, R., Nolan, T., Pfaffl, M.W., Shipley, G.L., et al. (2009). The MIQE guidelines: minimum information for publication of quantitative real-time PCR experiments. *Clin. Chem.* **55**, 611–622.
- Canning, P., Park, K., Gonçalves, J., Li, C., Howard, C.J., Sharpe, T.D., Holt, L.J., Pelletier, L., Bullock, A.N., and Leroux, M.R. (2018). CDKL family kinases have evolved distinct structural features and ciliary function. *Cell Rep.* **22**, 885–894.
- Cappello, S., Gray, M.J., Badouel, C., Lange, S., Einsiedler, M., Srour, M., Chitayat, D., Hamdan, F.F., Jenkins, Z.A., Morgan, T., et al. (2013). Mutations in genes encoding the cadherin receptor-ligand pair DCHS1 and FAT4 disrupt cerebral cortical development. *Nat. Genet.* **45**, 1300–1308.
- Croquelois, A., Giuliani, F., Savary, C., Kielar, M., Amiot, C., Schenk, F., and Welker, E. (2009). Characterization of the HeCo mutant mouse: a new model of subcortical band heterotopia associated with seizures and behavioral deficits. *Cereb. Cortex* **19**, 563–575.
- D’Gama, A.M., Woodworth, M.B., Hossain, A.A., Bizzotto, S., Hatem, N.E., LaCoursiere, C.M., Najm, I., Ying, Z., Yang, E., Barkovich, A.J., et al. (2017). Somatic mutations activating the mTOR pathway in dorsal telencephalic progenitors cause a continuum of cortical dysplasias. *Cell Rep.* **21**, 3754–3766.
- Del Giudice, E., Macca, M., Imperati, F., D’Amico, A., Parent, P., Pasquier, L., Layet, V., Lyonnet, S., Stamboul-Darmency, V., Thauvin-Robinet, C., and Franco, B. (2014). CNS involvement in OFD1 syndrome: a clinical, molecular, and neuroimaging study. *Orphanet J. Rare Dis* **9**, 74.
- Delous, M., Baala, L., Salomon, R., Laclef, C., Vierkotten, J., Tory, K., Golzio, C., Lacooste, T., Besse, L., Ozilou, C., et al. (2007). The ciliary gene RPRG1L is mutated in cerebello-oculo-renal syndrome (Joubert syndrome type B) and Meckel syndrome. *Nat. Genet.* **39**, 875–881.
- Ding, W., Wu, Q., Sun, L., Pan, N.C., and Wang, X. (2019). Cenpj regulates cilia disassembly and neurogenesis in the developing mouse cortex. *J. Neurosci.* **39**, 1994–2010.
- Fiorillo, C., Moro, F., Yi, J., Weil, S., Brisca, G., Astrea, G., Severino, M., Romano, A., Battini, R., Rossi, A., et al. (2014). Novel dynein DYNC1H1 neck and motor domain mutations link distal spinal muscular atrophy and abnormal cortical development. *Hum. Mutat.* **35**, 298–302.
- Foerster, P., Daclin, M., Asm, S., Faucourt, M., Boletta, A., Genovesio, A., and Spassky, N. (2017). mTORC1 signaling and primary cilia are required for brain ventricle morphogenesis. *Development* **144**, 201–210.
- Fry, A.M., O’Regan, L., Montgomery, J., Adib, R., and Bayliss, R. (2016). EML proteins in microtubule regulation and human disease. *Biochem. Soc. Trans.* **44**, 1281–1288.
- Gabriel, E., Wason, A., Ramani, A., Gooi, L.M., Keller, P., Pozniakovskiy, A., Poser, I., Noack, F., Telugu, N.S., Calegari, F., et al. (2016). CPAP promotes timely cilium disassembly to maintain neural progenitor pool. *EMBO J.* **35**, 803–819.
- Gaspard, N., Bouschet, T., Hourez, R., Dimidschstein, J., Naeije, G., van den Ameel, J., Espuny-Camacho, I., Herpoel, A., Passante, L., Schiffmann, S.N., et al. (2008). An intrinsic mechanism of corticogenesis from embryonic stem cells. *Nature* **455**, 351–357.
- Gerhardt, C., Lier, J.M., Burmühl, S., Struchtrup, A., Deutschmann, K., Vetter, M., Leu, T., Reeg, S., Grune, T., and Rütger, U. (2015). The transition zone protein Ppprip11 regulates proteasomal activity at the primary cilium. *J. Cell Biol.* **210**, 115–133.
- Guo, J., Higginbotham, H., Li, J., Nichols, J., Hirt, J., Ghukasyan, V., and Anton, E.S. (2015). Developmental disruptions underlying brain abnormalities in ciliopathies. *Nat. Commun.* **6**, 7857.
- Higginbotham, H., Guo, J., Yokota, Y., Umberger, N.L., Su, C.Y., Li, J., Verma, N., Hirt, J., Ghukasyan, V., Caspar, T., and Anton, E.S. (2013). Arl13b-regulated cilia activities are essential for polarized radial glial scaffold formation. *Nat. Neurosci.* **16**, 1000–1007.
- Hua, K., and Ferland, R.J. (2018). Primary cilia proteins: ciliary and extraciliary sites and functions. *Cell. Mol. Life Sci.* **75**, 1521–1540.
- Iefremova, V., Manikakis, G., Krefft, O., Jabali, A., Weynans, K., Wilkens, R., Marsoner, F., Brändl, B., Müller, F.J., Koch, P., and Ladewig, J. (2017). An organoid-based model of cortical development identifies non-cell-autonomous defects in Wnt signaling contributing to Miller-Dieker syndrome. *Cell Rep.* **19**, 50–59.
- Jaarsma, D., and Hoogenraad, C. (2015). Cytoplasmic dynein and its regulatory proteins in Golgi pathology in nervous system disorders. *Front. Neurosci.* **9**, 397.
- Jung, B., Padula, D., Burtcher, I., Landerer, C., Lutter, D., Theis, F., Messias, A.C., Geerlof, A., Sattler, M., Kremmer, E., et al. (2016). Pitchfork and Gprasp2 target Smoothened to the primary cilium for Hedgehog pathway activation. *PLoS ONE* **11**, e0149477.
- Kheradmand Kia, S., Verbeek, E., Engelen, E., Schot, R., Poot, R.A., de Coo, I.F.M., Lequin, M.H., Poulton, C.J., Pourfarzad, F., Grosveld, F.G., et al. (2012). RTTN mutations link primary cilia function to organization of the human cerebral cortex. *Am. J. Hum. Genet.* **91**, 533–540.
- Kielar, M., Tuy, F.P., Bizzotto, S., Lebrand, C., de Juan Romero, C., Poirier, K., Oegema, R., Mancini, G.M., Bahi-Buisson, N., Olaso, R., et al. (2014). Mutations in Emi1 lead to ectopic progenitors and neuronal heterotopia in mouse and human. *Nat. Neurosci.* **17**, 923–933.
- Kimura, T., and Murakami, F. (2014). Evidence that dendritic mitochondria negatively regulate dendritic branching in pyramidal neurons in the neocortex. *J. Neurosci.* **34**, 6938–6951.
- Lamprecht, M.R., Sabatini, D.M., and Carpenter, A.E. (2007). CellProfiler: free, versatile software for automated biological image analysis. *Biotechniques* **42**, 71–75.
- Li, A., Saito, M., Chuang, J.Z., Tseng, Y.Y., Dedesma, C., Tomizawa, K., Kaitzuka, T., and Sung, C.H. (2011). Ciliary transition zone activation of





- phosphorylated Tctex-1 controls ciliary resorption, S-phase entry and fate of neural progenitors. *Nat. Cell Biol.* 13, 402–411.
- Lien, W.H., Klezovitch, O., Fernandez, T.E., Delrow, J., and Vasioukhin, V. (2006). alpha-catenin controls cerebral cortical size by regulating the hedgehog signaling pathway. *Science* 311, 1609–1612.
- Liu, W.A., Chen, S., Li, Z., Lee, C.H., Mirzaa, G., Dobyns, W.B., Ross, M.E., Zhang, J., and Shi, S.H. (2018). PARD3 dysfunction in conjunction with dynamic HIPPO signaling drives cortical enlargement with massive heterotopia. *Genes Dev.* 32, 763–780.
- Ma, S., Meng, Z., Chen, R., and Guan, K. (2019). The Hippo pathway: biology and pathophysiology. *Annu. Rev. Biochem.* 88, 7.2–7.28.
- Madhivanan, K., and Aguilar, R.C. (2014). Cilopathies: the trafficking connection. *Traffic* 15, 1031–1056.
- Marthiens, V., Kazanis, I., Moss, L., Long, K., and Ffrench-Constant, C. (2010). Adhesion molecules in the stem cell niche—more than just staying in shape? *J. Cell Sci.* 123, 1613–1622.
- Mellacheruvu, D., Wright, Z., Couzens, A.L., Lambert, J.P., St-Denis, N.A., Li, T., Miteva, Y.V., Hauri, S., Sardiu, M.E., Low, T.Y., et al. (2013). The CRAPome: a contaminant repository for affinity purification-mass spectrometry data. *Nat. Methods* 10, 730–736.
- Nowakowski, T.J., Bhaduri, A., Pollen, A.A., Alvarado, B., Mostajo-Radji, M.A., Di Lullo, E., Haussler, M., Sandoval-Espinosa, C., Liu, S.J., Velmeshev, D., et al. (2017). Spatiotemporal gene expression trajectories reveal developmental hierarchies of the human cortex. *Science* 358, 1318–1323.
- O'Neill, A.C., Kyrousi, C., Einsiedler, M., Burtscher, I., Drukker, M., Markie, D.M., Kirk, E.P., Gotz, M., Robertson, S.P., and Cappello, S. (2018). Mob2 insufficiency disrupts neuronal migration in the developing cortex. *Front. Cell. Neurosci.* 12, 57.
- Palade, G.E. (1952). A study of fixation for electron microscopy. *J. Exp. Med.* 95, 285–298.
- Palmer, T.D., Willhoite, A.R., and Gage, F.H. (2000). Vascular niche for adult hippocampal neurogenesis. *J. Comp. Neurol.* 425, 479–494.
- Paridaen, J.T., Wilsch-Bräuninger, M., and Huttner, W.B. (2013). Asymmetric inheritance of centrosome-associated primary cilium membrane directs cilio-genesis after cell division. *Cell* 155, 333–344.
- Park, S.M., Lim, J.S., Ramakrishna, S., Kim, S.H., Kim, W.K., Lee, J., Kang, H.C., Reiter, J.F., Kim, D.S., Kim, H.H., and Lee, J.H. (2018). Brain somatic mutations in MTOR disrupt neuronal cilio-genesis, leading to focal cortical dyslamination. *Neuron* 99, 83–97.e7.
- Perez-Riverol, Y., Csordas, A., Bai, J., Bernal-Llinares, M., Hewapathirana, S., Kundu, D.J., Inuganti, A., Griss, J., Mayer, G., Eisenacher, M., et al. (2019). The PRIDE database and related tools and resources in 2019: improving support for quantification data. *Nucleic Acids Res.* 47 (D1), D442–D450.
- Poulet, P., Carpentier, S., and Barillot, E. (2007). myProMS, a web server for management and validation of mass spectrometry-based proteomic data. *Proteomics* 7, 2553–2556.
- Richards, M.W., Law, E.W., Rennalls, L.P., Busacca, S., O'Regan, L., Fry, A.M., Fennell, D.A., and Bayliss, R. (2014). Crystal structure of EML1 reveals the basis for Hsp90 dependence of oncogenic EML4-ALK by disruption of an atypical β -propeller domain. *Proc. Natl. Acad. Sci. USA* 111, 5195–5200.
- Sang, L., Miller, J.J., Corbit, K.C., Giles, R.H., Brauer, M.J., Otto, E.A., Baye, L.M., Wen, X., Scales, S.J., Kwong, M., et al. (2011). Mapping the NPHP-JBTS-MKS protein network reveals cilio-pathology disease genes and pathways. *Cell* 145, 513–528.
- Schiavo, G., Greensmith, L., Hafezparast, M., and Fisher, E.M. (2013). Cytoplasmic dynein heavy chain: the servant of many masters. *Trends Neurosci.* 36, 641–651.
- Shaheen, R., Sebai, M.A., Patel, N., Ewida, N., Kurdi, W., Altweijri, I., Sogaty, S., Almadawi, E., Seidahmed, M.Z., Alnemri, A., et al. (2017). The genetic landscape of familial congenital hydrocephalus. *Ann. Neurol.* 81, 890–897.
- Sheen, V.L., Ganesh, V.S., Topcu, M., Sebire, G., Bodell, A., Hill, R.S., Grant, P.E., Shugart, Y.Y., Imitola, J., Khoury, S.J., et al. (2004). Mutations in ARFGEF2 implicate vesicle trafficking in neural progenitor proliferation and migration in the human cerebral cortex. *Nat. Genet.* 36, 69–76.
- Shi, Y., Kirwan, P., Smith, J., Robinson, H.P., and Livesey, F.J. (2012). Human cerebral cortex development from pluripotent stem cells to functional excitatory synapses. *Nat. Neurosci.* 15, 477–486, S1.
- Sun, T., Wang, X.J., Xie, S.S., Zhang, D.L., Wang, X.P., Li, B.Q., Ma, W., and Xin, H. (2011). A comparison of proliferative capacity and passing potential between neural stem and progenitor cells in adherent and neurosphere cultures. *Int. J. Dev. Neurosci.* 29, 723–731.
- Taverna, E., Mora-Bermúdez, F., Strzyz, P.J., Florio, M., Icha, J., Häffner, C., Norden, C., Wilsch-Bräuninger, M., and Huttner, W.B. (2016). Non-canonical features of the Golgi apparatus in bipolar epithelial neural stem cells. *Sci. Rep.* 6, 21206.
- Uchiyama, K., Jokitalo, E., Kano, F., Murata, M., Zhang, X., Canas, B., Newman, R., Rabouille, C., Pappin, D., Freemont, P., and Kondo, H. (2002). VCIP135, a novel essential factor for p97/p47-mediated membrane fusion, is required for Golgi and ER assembly in vivo. *J. Cell Biol.* 159, 855–866.
- Uzquiano, A., Gladwyn-Ng, I., Nguyen, L., Reiner, O., Gotz, M., Matsuzaki, F., and Francis, F. (2018). Cortical progenitor biology: key features mediating proliferation versus differentiation. *J. Neurochem.* 146, 500–525.
- Valot, B., Langella, O., Nano, E., and Zivy, M. (2011). MassChroQ: a versatile tool for mass spectrometry quantification. *Proteomics* 11, 3572–3577.
- Wang, L., Hou, S., and Han, Y.G. (2016). Hedgehog signaling promotes basal progenitor expansion and the growth and folding of the neocortex. *Nat. Neurosci.* 19, 888–896.
- Wheway, G., Nazlamova, L., and Hancock, J.T. (2018). Signaling through the primary cilium. *Front. Cell Dev. Biol.* 6, 8.
- Wiegand, A., Rütter, U., and Gerhardt, C. (2018). The ciliary protein Rpgrip11 in development and disease. *Dev. Biol.* 442, 60–68.
- Willaredt, M.A., Hasenpusch-Theil, K., Gardner, H.A., Kitanovic, I., Hirschfeld-Warneken, V.C., Gojak, C.P., Gorgas, K., Bradford, C.L., Spatz, J., Wöfl, S., et al. (2008). A crucial role for primary cilia in cortical morphogenesis. *J. Neurosci.* 28, 12887–12900.
- Wilson, S.L., Wilson, J.P., Wang, C., Wang, B., and McConnell, S.K. (2012). Primary cilia and Gli3 activity regulate cerebral cortical size. *Dev. Neurobiol.* 72, 1196–1212.
- Zhang, X., and Wang, Y. (2015). Cell cycle regulation of VCIP135 deubiquitinase activity and function in p97/p47-mediated Golgi reassembly. *Mol. Biol. Cell* 26, 2242–2251.
- Zhang, X., Zhang, H., and Wang, Y. (2014). Phosphorylation regulates VCIP135 function in Golgi membrane fusion during the cell cycle. *J. Cell Sci.* 127, 172–181.

6.4 Publication IV

Human cerebral organoids reveal progenitor pathology in EML1-linked cortical malformation

Jabali A, Hoffrichter A, Uzquiano A, Marsoner F, Wilkens R, Siekmann M, Bohl B, Rossetti A C, Horschitz S, Koch P, Francis F, Ladewig J. EMBO Rep. 2022 Mar 15:e54027. DOI: 10.15252/embr.202154027

Human cerebral organoids reveal progenitor pathology in EML1-linked cortical malformation

Ammar Jabali^{1,2,3,4}, Anne Hoffrichter^{1,2,3} , Ana Uzquiano^{5,6,7}, Fabio Marsoner^{1,2,3}, Ruven Wilkens^{1,2,3}, Marco Siekmann^{1,2,3}, Bettina Bohl^{1,2,3} , Andrea C Rossetti^{1,2,3}, Sandra Horschitz^{1,2,3}, Philipp Koch^{1,2,3}, Fiona Francis^{5,6,7}  & Julia Ladewig^{1,2,3,4,*} 

Abstract

Malformations of human cortical development (MCD) can cause severe disabilities. The lack of human-specific models hampers our understanding of the molecular underpinnings of the intricate processes leading to MCD. Here, we use cerebral organoids derived from patients and genome edited-induced pluripotent stem cells to address pathophysiological changes associated with a complex MCD caused by mutations in the echinoderm microtubule-associated protein-like 1 (*EML1*) gene. *EML1*-deficient organoids display ectopic neural rosettes at the basal side of the ventricular zone areas and clusters of heterotopic neurons. Single-cell RNA sequencing shows an upregulation of basal radial glial (RG) markers and human-specific extracellular matrix components in the ectopic cell population. Gene ontology and molecular analyses suggest that ectopic progenitor cells originate from perturbed apical RG cell behavior and yes-associated protein 1 (YAP1)-triggered expansion. Our data highlight a progenitor origin of *EML1* mutation-induced MCD and provide new mechanistic insight into the human disease pathology.

Keywords *EML1*; malformation of human cortical development; cerebral organoids; perturbed progenitor cells; YAP1 signaling

Subject Categories Molecular Biology of Disease; Neuroscience

DOI 10.15252/embr.202154027 | Received 20 September 2021 | Revised 11 February 2022 | Accepted 17 February 2022

EMBO Reports (2022) e54027

Introduction

Human cortical expansion and lamination relies on the intrinsic organization and behavior of RG cells and precise neuronal migration (Lui *et al.*, 2011). Disruption of these processes can cause MCD including microcephaly (small brain), megalencephaly (large brain),

lissencephaly (loss of gyrification), polymicrogyria (numerous small gyrifications), and heterotopia (abnormally positioned neurons) (Klingler *et al.*, 2021). These abnormalities can coexist in complex forms. For example, individuals carrying a mutation in the *EML1* gene (coding for a microtubule-associated protein (Richards *et al.*, 2015)) exhibit megalencephaly with a polymicrogyria-like cortex above a ribbon-like subcortical heterotopia (ri-SH) in the region of the former outer subventricular zone (SVZ), resembling a second inner cortex (Kielar *et al.*, 2014; Oegema *et al.*, 2019). Patients can also exhibit hydrocephalus (Shaheen *et al.*, 2017). *EML1*-patients suffer from severe developmental delay, often drug-resistant epilepsy, visual impairment, and intellectual disabilities (Kielar *et al.*, 2014; Shaheen *et al.*, 2017; Oegema *et al.*, 2019). *Eml1* mouse models show ectopic proliferating cells in the developing cortical wall, perturbed apical RG cell behavior, and aberrant primary cilia (Kielar *et al.*, 2014; Bizzotto *et al.*, 2017; Uzquiano *et al.*, 2019). Although they exhibit heterotopia, they fall short of recapitulating the complete spectrum of phenotypes observed in humans such as a polymicrogyria-like cortex or megalencephaly (Kielar *et al.*, 2014; Collins *et al.*, 2019), highlighting differences in disease manifestation between humans and non-human model organisms. Here, we explore the function of *EML1* during cortical development using human-induced pluripotent stem (iPS) cells and thereof derived cortical cultures.

Results and Discussion

EML1-deficient cerebral organoids exhibit subcortical heterotopia-like phenotypes

To dissect the molecular role of *EML1* underlying human cortical development and associated disorders, we reprogrammed fibroblasts from two independent previously characterized patients harboring mutations in the *EML1* gene (for more details see Material and Methods and (Kielar *et al.*, 2014)) into iPS cells (two clones

1 Medical Faculty Mannheim, Central Institute of Mental Health, Heidelberg University, Mannheim, Germany

2 Hector Institute for Translational Brain Research, Mannheim, Germany

3 German Cancer Research Center, Heidelberg, Germany

4 Institute of Reconstructive Neurobiology, School of Medicine & University Hospital Bonn, University of Bonn, Bonn, Germany

5 INSERM U 1270, Paris, France

6 Sorbonne Université, UMR-S 1270, Paris, France

7 Institut du Fer à Moulin, Paris, France

*Corresponding author. Tel: +49621 1703 6091; E-mail: julia.ladewig@zi-mannheim.de

each; characterization of iPSC cells is illustrated in Fig EV1A and B). *EML1* patient-specific mutations (patient 1, compound heterozygous, R138X, T243A; patient 2, homozygous, and W225R) were confirmed by sequencing (Fig EV1C and D). To decipher the specific role of *EML1* in an isogenic system, we also generated heterozygous *EML1*-knockout (*EML1*-heKO) iPSC cells from two independent controls by applying CRISPR-Cas9 genome editing. Of note: homozygous *EML1*-KO clones were prone to die and could not be further cultured. *EML1*-heKO lines were validated by genotyping (Fig EV1E). Reduced expression of *EML1* was confirmed for both *EML1*-heKO lines (Fig EV1F). We then differentiated iPSC cells into cortical progenitors (Shi et al, 2012) and forebrain organoids (Iefremova et al, 2017; Krefft et al, 2018). To investigate whether certain *EML1* mutation-induced phenotypic changes are recapitulated within cerebral organoids, we first analyzed patient- and control-derived organoids at day 33 ± 2, the time point at which cerebral organoids have developed ventricular zone (VZ)-, SVZ-, and cortical plate (CP)-like areas as well as cells reminiscent of basal (b)RG (Iefremova et al, 2017). Immunocytochemical analyses revealed that control organoids consist of stratified structures including VZ and CP areas (Fig 1A). In strong contrast, *EML1* patient-derived organoids exhibited massive amounts of ectopically localized cells accumulating at the basal side of the VZ areas, in part organized into neural rosettes with accumulation of adherent junction markers such as N-cadherin (NCAD) in their centers (Fig 1B). In addition, β-III-tubulin-positive neurons were organized in two bands, an upper diffuse band located above the ectopic cells and a lower band located in between the VZ area and the ectopic cell population (Fig 1A). To assess the phenotypic changes in all *EML1*-deficient conditions (*EML1*-patient 1, *EML1*-patient 2, *EML1*-heKO 1, and *EML1*-heKO 2), we performed immunohistochemistry and quantified the percent of VZ areas with ectopically localized neural rosettes and the percent of heterotopic or disorganized cortical areas in control and *EML1*-deficient organoids. We confirm a significant increase in neural rosettes and heterotopic clusters of MAPT-positive neurons in all *EML1*-deficient organoids compared to controls (Fig 1C–E, day 20 ± 2).

Perturbed cell intrinsic properties of *EML1*-deficient apical radial glial cells

To understand the origin of the perturbed ectopic cell population in the *EML1*-deficient organoids, we examined RG cell behavior in

more detail in *EML1*-deficient and control organoids at early developmental time points (day 20 ± 2). *EML1*-deficient *in vivo* and *in vitro* models show changes in microtubule-associated processes including mitotic spindle length, cell shape, and primary cilia (Bizzotto et al, 2017; Uzquiano et al, 2019). It was suggested that the changes in spindle length and cell morphology might cause increased mechanical stress in the VZ and by that indirectly encourage RG cell delamination (Bizzotto et al, 2017). To test whether a non-cell autonomous mechanism leads to the accumulation of ectopic progenitor cells in *EML1*-deficient organoids, we generated hybrid organoids composed of EGFP-*EML1*-heKO or EGFP-control iPSC cells mixed with isogenic control iPSC cells before organoid generation. When investigating the hybrid organoids at day 20 ± 2, we found a significant increase in the number of EGFP-positive *EML1*-heKO cells at the basal side of VZ areas compared to the controls (Fig 2A and B). These data hint toward cell intrinsic mechanisms leading to the ectopic progenitor cells in *EML1*-deficient organoids. It has been shown that changes in the mitotic spindle and primary cilia can directly impact division mode and RG cell delamination (LaMonica et al, 2013; Mora-Bermúdez et al, 2014; Bizzotto et al, 2017). We first tested whether the division mode is perturbed in *EML1*-impaired conditions. To that end we visualized mitotic cells (Figs 2C and EV2A) and quantified the plane of cell divisions. While in control organoids the majority of cells exhibit a vertical plane of cell division, we found a significant decrease in vertical division modes in all *EML1*-impaired conditions. In parallel, *EML1*-impaired organoids exhibit an increase in oblique and horizontal division angles (Fig 2D, day 20 ± 2). Of note, both oblique and horizontal plane of cell divisions at the VZ surface were described to favor cell delamination (LaMonica et al, 2013). We next investigated the primary cilium and found a significant decrease in the length of the primary cilium in all *EML1*-deficient-derived cortical progenitor cells upon ARL13B immunostaining (Figs 2E and EV2B) and confirmed perturbed ultrastructure of patient and *EML1*-heKO-derived primary cilia by electron microscopy (Fig 2F, (Uzquiano et al, 2019)). To investigate whether *EML1*'s microtubule function causes the observed defects in primary cilia, we stabilized microtubules in control and *EML1*-deficient cultures using EpothiloneD (Zhang et al, 2012) (EpoD). Immunoblot analyses confirmed a significant increase in stabilized (acetylated) tubulin upon EpoD treatment in all *EML1*-deficient samples (Fig EV2C and D). When investigating the primary cilia in control- and *EML1*-deficient

Figure 1. Deficiency of *EML1* causes ectopic neural rosettes and neuronal heterotopia in cerebral organoids.

- A Day 33 ± 2 control- and *EML1* patient-derived cerebral organoids stained for β-III-tubulin and DAPI. VZ and CP areas are marked by white brackets, ectopic neural rosettes by red bracket, and heterotopic neurons by red arrows.
- B Day 33 ± 2 control- and *EML1* patient-derived cerebral organoid stained for the adherens junction marker N-cadherin (NCAD) expressed at the VZ surface and within the ectopic neural rosettes.
- C Day 20 ± 2 cerebral organoids derived from controls, patients, and *EML1*-heKOs stained for the neuronal marker MAPT and the adherens junction marker NCAD, counterstained with DAPI. Ectopic neural rosettes and neuronal heterotopia are highlighted with dotted yellow lines.
- D Quantification of VZ areas with ectopic neural rosettes (three batches, three organoids analyzed per batch, significance based on Kruskal–Wallis test, $P = 0.0001$, Dunn's *post hoc* test for multiple comparisons performed to define statistical differences between genotypes, and single data points presented are colored by batch).
- E Quantification of heterotopic, disorganized, or organized cortical areas (three batches, three organoids per batch, significance based on Kruskal–Wallis test, $P = 0.0001$ for "organized" and "heterotopic"; no significant difference for "disorganized," Dunn's *post hoc* test performed for multiple comparisons to define statistical differences between genotypes).
- Data information: * marks statistical significance in relation to Control 1, # in relation to Control 2. P -values: ***/### < 0.001. VZ, ventricular zone; CP, cortical plate. Data in graphs are represented as means ± SD. Scale bars: (A) 100 μm; (B) 100 μm, enlarged 25 μm; and (C) 50 μm. Source data are available online for this figure.

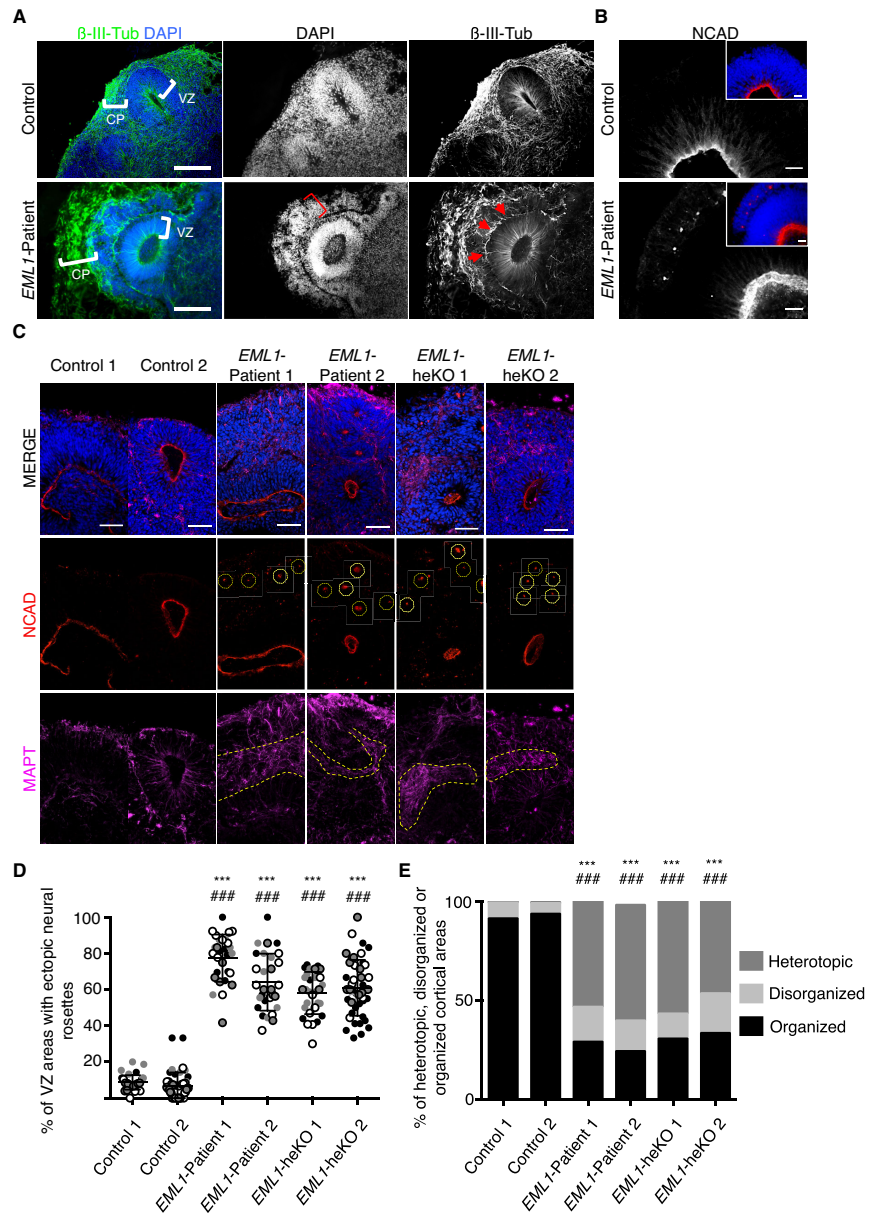


Figure 3.

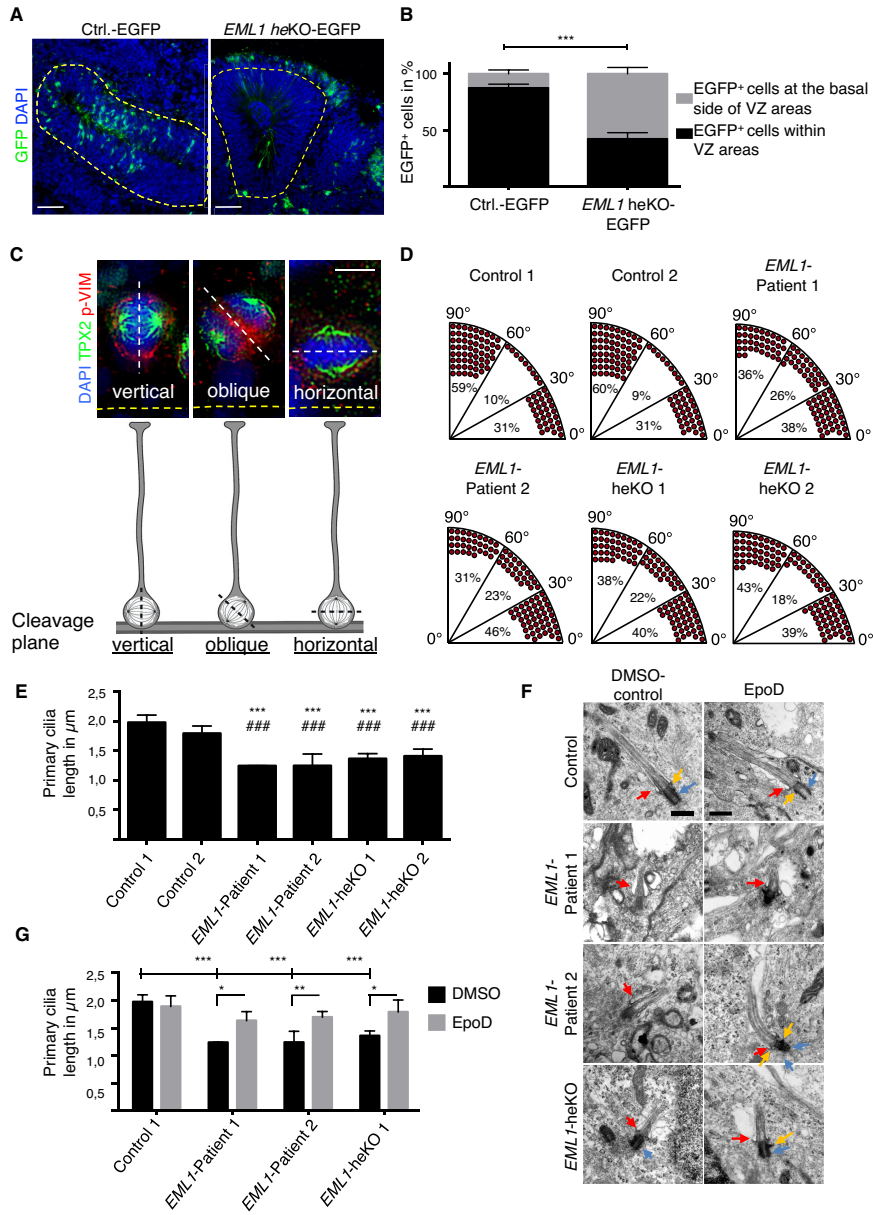


Figure 2.

Figure 2. Ectopic progenitor cells originate from apical RG with perturbed cell intrinsic behavior.

- A Hybrid organoids generated from controls mixed with control-EGFP⁺ or *EML1*-heKO-EGFP⁺ cells (day 20 ± 2). Yellow dotted lines indicate VZ areas.
- B Quantification of control-EGFP⁺ or *EML1*-heKO-EGFP⁺ cells within or at the basal side of VZ areas (three batches, three organoids each, significance based on Mann–Whitney test, ****P* = 0.0001 for “EGFP⁺” cells at the basal side of VZ areas”).
- C Representative images and scheme of cleavage plan orientation. Upper panel: cells immunostained for p-Vim (red) and TPX2 (green), counterstained with DAPI, white dotted line indicates cleavage plane orientation, and yellow dotted line VZ surface.
- D Quantification of horizontal, vertical, and oblique plane of cell divisions in control and *EML1*-deficient organoids (day 20 ± 2; three batches and three organoids each).
- E Quantification of primary cilia length in control and *EML1*-deficient cortical progenitors (* marks statistical significance in relation to Control 1, # in relation to Control 2, three biological replicates, four areas per sample, significance based on Kruskal–Wallis test and Dunn’s *post hoc* test, *****P* = 0.0001).
- F Electron microscopy of primary cilia derived from control or *EML1*-deficient cortical progenitors in DMSO control or following EpohiloneD (EpoD) exposure (blue arrow: basal body, yellow arrow: appendages, and red arrow: ciliary pockets).
- G Quantification of primary cilia length in control and *EML1*-deficient cortical progenitors with/without EpoD exposure. Three biological replicates, four areas per sample, significance based on two-way ANOVA, and Sidak’s multiple comparisons *post hoc* test, *P* = 0.0213.
- Data information: Data in graphs are represented as means ± SD. Scheme in C was designed using biorender.com. Scale bars: (A) 50 μm; (C) 5 μm; and (F) 0.5 μm. Source data are available online for this figure.

cultures upon EpoD treatment, we found a clearly improved primary cilia structure and a significant rescue of the primary cilia length in *EML1*-deficient EpoD-treated conditions compared to DMSO controls (Figs 2F and G, and EV2B). Our data confirm that *EML1*-deficiency leads to perturbed spindle orientation and primary cilia, which might directly impact aRG cell division mode and delamination resulting in ectopic progenitor cell localization.

Single-cell RNA sequencing (scRNAseq) and immunohistochemical analyses identify a perturbed progenitor cell population in *EML1*-deficient organoids

To further investigate the cellular identity of the ectopically located cells in *EML1*-deficient cerebral organoids, we performed scRNAseq on *EML1*-heKO 1 and respective isogenic control organoids (pooled dissected areas from nine organoids each, three independent batches, and day 33 ± 2; schematic overview Fig EV3A). We identified different cell populations including RG cells (RG1), RG cells transitioning to bRG cells (RG to bRG), RG cells transitioning to neurons (RG2), intermediate progenitors (IP), and young neurons (YN) based on known marker genes (Pollen *et al*, 2015; Liu *et al*, 2017; Nowakowski *et al*, 2017; Velasco *et al*, 2019; Fan *et al*, 2020) (Figs 3A and EV3B). In control organoids we detected expression of *EML1* in progenitor cells (Fig EV3C), an expression pattern

consistent with that found during early mouse and human brain development (Kielar *et al*, 2014; Nowakowski *et al*, 2017; Loo *et al*, 2019). We also observed the presence of a recently described mesenchymal-like cell cluster (MLC) (Eze *et al*, 2021) (Figs 3A and EV3B). As the function and role of these cells in cortical development is unclear, we excluded them from further analyses. When comparing the cell type composition between *EML1*-heKO and isogenic control-derived organoids, we found a clear decrease of 22.5% in RG1 cells and a striking increase of 23.4% in the abundance of RG to bRG cells in the *EML1*-heKO condition, while only minor variations in the other cell clusters were observed (Fig 3B). We further investigated molecular characteristics of the *EML1*-heKO-derived RG to bRG cluster compared to control. Here, we found a set of differentially expressed genes in the *EML1*-heKO. When further investigating these genes, we identified a clear upregulation of ECM and bRG markers (Pollen *et al*, 2015; Liu *et al*, 2017) in *EML1*-heKO-derived samples (Fig EV3D). The ECM genes *COL1A2*, *COL3A1*, and *LUM*, which are associated with human cerebral cortex expansion and folding (Fietz *et al*, 2012; Long *et al*, 2018), were found among the significantly upregulated genes in the *EML1*-heKO (Figs 3C and EV3D). Notably, a decrease in the expression of ECM genes including *COL1A2* was connected to reduced brain convolutions as found in lissencephaly (Karzbrun *et al*, 2018). It is tempting to speculate that an increase in these ECM genes in the *EML1*-heKO might play a role in the development of the

Figure 3. ScRNA-seq reveals cellular identity of ectopic cells in *EML1*-heKO cerebral organoids.

- A scRNA-seq of 2,335 control and 3,358 *EML1*-heKO cells (three pooled independent batches and three organoids each). Cells shown in UMAP plot and colored by annotated cell type.
- B Comparison of cell type composition between control and *EML1*-heKO. Numbers indicate percentage of total cells belonging to the respective cell type.
- C Normalized expression values of *COL1A2*, *COL3A1*, *LUM*, and *MEIS2* per cell type (three pooled batches and three organoids each).
- D Gene ontology (GO) term analysis of RG to bRG cells in control and *EML1*-heKO shows percentage of counts belonging to the set of genes associated with the respective GO term (three pooled batches and three organoids each).
- E Control- and *EML1*-heKO-derived cerebral organoid stained for *COL1A2* and *MEIS2*. VZ areas are encircled, and squares indicate areas enlarged in F.
- F Control- and *EML1*-heKO-derived cerebral organoid stained for *COL1A2*, *MEIS2*, and *MAP2*.
- G Representative images showing EGFP control and EGFP-*EML1*-heKO hybrid cerebral organoid stained for EGFP, *FAM107A*, and *NCAD*. Yellow dotted lines indicate morphology of EGFP⁺ cells (4 independent batches each, 3 organoids per batch, at least 30 ectopic rosettes in total).
- Data information: RG1: radial glia1, RG to bRG: radial glia to basal radial glia, RG2: radial glia to young neurons, IP, intermediate progenitors; YN, young neurons; MLC, mesenchymal-like cells. (C and D) Asterisks indicate Bonferroni corrected *P*-values. Wilcoxon rank sum test: ***< 0.001, *< 0.05, ns, not significant. Scale bars: (E) 50 μm; (F) 10 μm; and (G) 50 μm, enlarged 10 μm. Source data are available online for this figure.

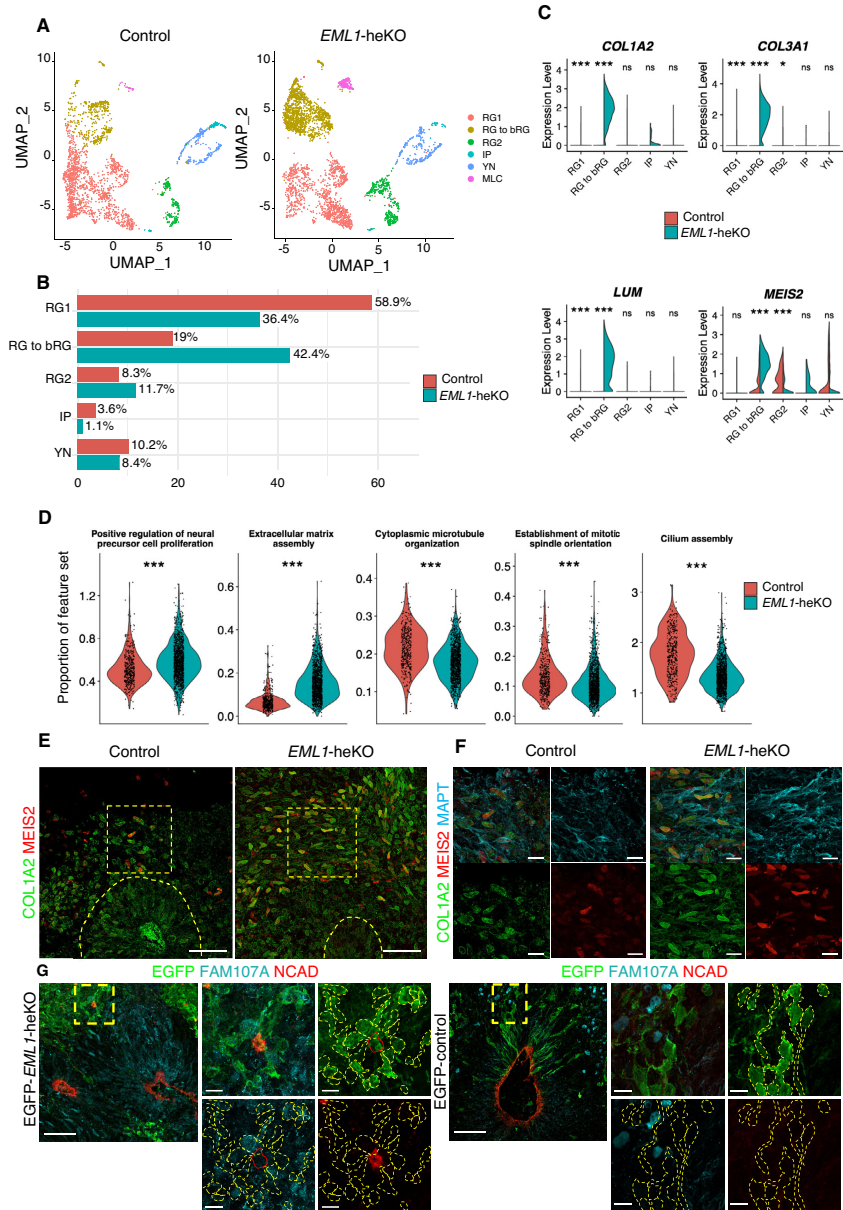


Figure 3.

polymicrogyria-like cortex and megalencephaly observed in patient MRIs (Oegema et al, 2019). We also found that the proneurogenic gene *MEIS2* was significantly enriched in this cluster in the *EML1*-heKO (Fig 3C). GO term analyses reveal significant alterations in positive regulation of neural precursor cell proliferation, ECM assembly, cytoplasmic microtubule organization, establishment of mitotic spindle orientation, and cilium assembly in the *EML1*-heKO RG to bRG cell cluster compared to control (Fig 3D). When performing immunocytochemical analyses on *EML1*-heKO and isogenic control organoids (day 33 ± 2) we found in the control a few COL1A2 and MEIS2⁺ cells in the CP area, some of which co-stain for MAPT, whereas *EML1*-heKO samples exhibit a broader co-expression of COL1A2 and MEIS2 with hardly any overlap with MAPT within the ectopic cell population (Figs 3E and F, and EV3E and F, day 33 ± 2). To further delineate the nature of the ectopic progenitor cells, we applied our hybrid organoids. This system allows to decipher the morphology of the cells within the ectopic rosettes as well as their marker expression. When investigating EGFP-*EML1*-heKO hybrid organoids at day 30 ± 2, we found EGFP⁺ cells organized into ectopic rosettes, which were marked by accumulation of NCAD in their centers (Fig 3G). The EGFP⁺ cells found around the NCAD centers exhibit different morphologies. Most of the cells do not show a RG-like elongated organization with an apical and/or basal process but rather perturbed morphologies (Fig 3G). Some of the ectopic cells stain positive for the bRG marker FAM107A (Fig 3G). Individual EGFP/FAM107A double-positive ectopic cells contact the centers of the rosettes suggesting an apical domain enriched in NCAD, very unusual for bRG cells during normal brain development (Fig 3G, (Martínez-Martínez et al, 2016)). In control hybrids, the majority of the EGFP⁺ cells found at a basal location in the VZ areas exhibited a radial morphology with an apical and/or basal process. Taken together, our data suggest that the ectopic progenitors in the *EML1*-heKO are composed of a perturbed progenitor population, which does not exist as such in control organoids or is very rare and is most likely

not reflecting a cell population present during normal human brain development.

Deregulated YAP signaling in *EML1*-deficient organoids drives ectopic cell expansion

To further dissect progenitor cell behavior that may be responsible for the large numbers of ectopic localized progenitor cells, we examined cell proliferation (day 20 ± 2). We found a significant increase in mitotic cells (labeled with p-VIM) located at the basal side of the VZ areas in all *EML1*-deficient organoids compared to the controls (Figs 4A and EV4A). No clear change in cell mitosis at the VZ surface was observed between the different conditions (Fig EV4B). We also found that the basally located mitotic cells in the *EML1*-deficient organoids exhibit an increase in cell cycle re-entry (quantified by BrdU⁺ KI67⁺ cells) compared to the control (Figs 4B and EV4C). In addition, GO-term analyses confirmed an enhanced positive regulation of cell proliferation in the RG to bRG cell cluster (Fig 3D). The distinct increase in mitotic cell behavior outside the VZ areas raises the intriguing question about the underlying mechanisms. Recent data from mice suggest that premature cortical progenitor delamination, ectopic rosette formation, periventricular neuronal heterotopia, and megalencephaly might result from deregulation of the Hippo signaling pathway (Cappello et al, 2013; Liu et al, 2018; O'Neill et al, 2018; Saito et al, 2018; Najas et al, 2020)—a conserved signaling pathway that controls cell proliferation and tissue development (Camargo et al, 2007; Zhao et al, 2011). To assess whether YAP1, a major downstream effector of the Hippo pathway (Sahu & Mondal, 2021), is altered in *EML1*-deficient cerebral organoids, we investigated *YAP1* expression in our scRNAseq data. We found a significant upregulation of *YAP1* in the *EML1*-KO RG to bRG cell cluster compared to control (Figs 4C and EV4D). We further analyzed expression of the YAP1 interaction partner TEAD2 (Mukhtar et al, 2020) and downstream target genes *CCND3* and *CYR61* and found that they exhibit significantly increased expression

Figure 4. YAP signaling drives ectopic progenitor cell expansion in *EML1*-deficient organoids.

- A Quantification of mitotic cells located at the basal side of VZ areas in control and *EML1*-deficient conditions (three batches and three organoids analyzed per batch).
- B Quantification of BrdU⁺ KI67⁺ cells located at the basal side of VZ areas in control and *EML1*-deficient conditions (three batches and three organoids analyzed per batch).
- C Normalized expression of *YAP1*, *TEAD2*, *CCND3*, and *CYR61* in RG to bRG cells. Separate violins show expression in control and *EML1*-heKO. Asterisks indicate Bonferroni corrected *P*-values. Percentages indicate amount of cells in each group expressing the respective gene (three pooled batches and three organoids each).
- D, E Immunofluorescence staining for (D) p-VIM and YAP1 or (E) Pax6 and YAP1 in control- and *EML1*-heKO-derived organoids (day 20 ± 2, squares indicate areas enlarged in adjacent part of the panel, respectively).
- F Quantification of basally located p-Vim⁺ cells with nuclear YAP1 signal per VZ area in control- and *EML1*-heKO-derived organoids (three batches and three organoids analyzed per batch).
- G Quantification of PAX6⁺ cells with nuclear YAP1 signal per VZ area in control- and *EML1*-heKO-derived organoids (three batches and three organoids analyzed per batch).
- H Immunofluorescence staining for p-Vim in *EML1*-heKO- and control-derived organoids in DMSO-, Verteporfin-, or Fluvastatin-treated conditions, counterstained with DAPI. Dotted line indicates VZ areas.
- I Quantification of p-VIM⁺ cells located at the basal side of VZ areas in control- or *EML1*-heKO-derived organoids under DMSO-, Verteporfin-, or Fluvastatin-treated condition (three batches and three organoids analyzed per batch).
- J Quantification of ectopic neural rosettes per VZ area in *EML1*-heKO-derived organoids in DMSO-, Verteporfin-, or Fluvastatin-treated conditions (three batches and three organoids analyzed per batch).

Data information: Data in graphs are represented as means ± SD. Significance based on Kruskal–Wallis test (A–B, F, G, J), or two-way ANOVA (on log₁₀ normalized data) (I) or Wilcoxon rank sum test (C). Dunn's *post hoc* (A, F–G, J) or Tukey *post hoc* (I) test for multiple comparisons was performed to define statistical differences between genotypes. *P*-values: *** < 0.001, ** < 0.01, * < 0.05. Scale bars: (D and E) 50 μm, enlarged 10 μm; (H) 50 μm. Source data are available online for this figure.

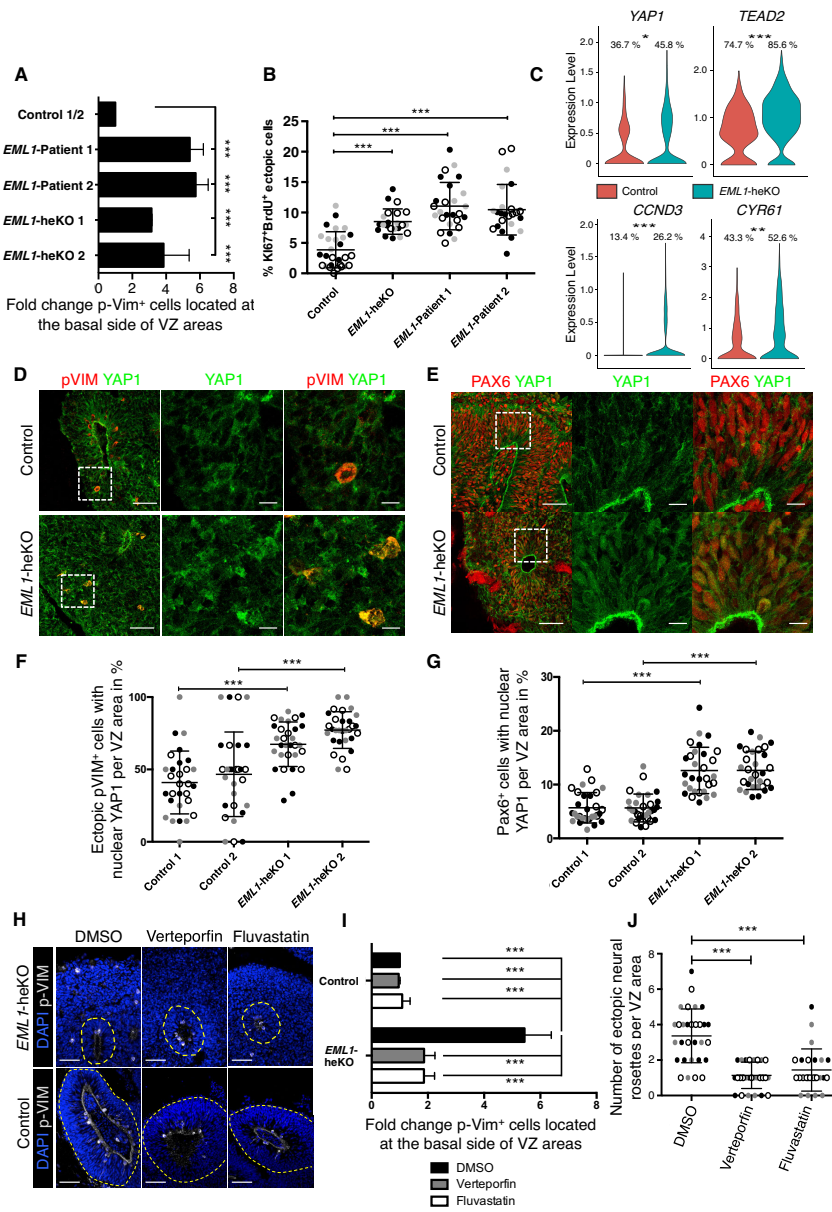


Figure 4.

levels in the RG to bRG cluster of the *EML1*-KO (Figs 4C and EV4D). To further test whether YAP1 signaling is indeed associated with the massive expansion of the ectopic progenitor cells, we stained control and *EML1*-heKO sections with an antibody against YAP1 and p-VIM (day 20 ± 2). Here, we found significantly more basally located p-VIM-positive cells exhibiting nuclear YAP1, suggesting active YAP1, in *EML1*-heKO-derived organoids compared to the isogenic control (Fig 4D and F). We also observed a significant increase in nuclear YAP1 in PAX6⁺ cells within the VZ areas in the *EML1*-heKO compared to controls (Fig 4E and G). Of note, most of the nuclear YAP1 PAX6 co-expressing cells were located in distal positions to the VZ surface (Fig 4E). To further determine the functional role of YAP1 in driving defective RG cell behavior and cortical malformation, we pharmacologically inhibited YAP1 function using Verteporfin (Kostic et al, 2019) or its nuclear translocation using Fluvastatin (Oku et al, 2015). Decrease in nuclear YAP1 upon Fluvastatin treatment was confirmed by immunohistochemistry (Fig EV4E). When assessing progenitor cell proliferation, we found a significant decrease in mitotic cells at the basal side of the VZ areas in Verteporfin- and Fluvastatin-treated *EML1*-heKO organoids. No difference in ab-ventricular cell mitosis could be observed in control organoids upon Verteporfin or Fluvastatin treatment (Fig 4H and I). In addition, pharmacological inhibition of YAP1 significantly reduced the numbers of ectopic neural rosettes in *EML1*-heKO organoids (Figs 4J and EV4F). YAP1 was reported to contribute to the evolutionary expansion of the neocortex by promoting bRG cell proliferation (Kostic et al, 2019). It is tempting to speculate that YAP1 is activated in the ectopic progenitor cells due to their basal location in the tissue, by that representing an indirect effect of *EML1* deficiency. Of note, additional signaling pathways might be impacted by *EML1* deficiency and it would be interesting to further investigate them in the future.

Concluding remarks

Using a human *in vitro* model, we identified for the first time that deficiency in *EML1* leads to the formation of ectopic neural rosettes and occurrence of perturbed progenitor cells, which show increased ECM production and YAP1-mediated expansion. In addition, we confirmed a role of *EML1* in primary cilia formation and progenitor cell proliferation. Although this study shows the formation of ectopic cells (heterotopia) and allowed us to decipher new underlying pathomechanisms in *EML1*-deficient cerebral organoids, which were not yet identified in *Eml1*-mouse models, the developmental stage of the model used does not fully enable us to investigate the entire scope of MCD in humans caused by *EML1* impairment. For instance, the direct correlation between perturbed *EML1*-derived progenitor cells and the observed polymicrogyria-like cortex and megalencephaly in *EML1* patients needs to be further investigated. It is also of note that the organoid system is prone to heterogeneity and even though we could reproduce major findings in two *EML1* patient-derived and two *EML1*-heKO lines, key experiments should be repeated in additional iPSC lines to ensure full reproducibility. Nevertheless, our human *in vitro* approach allowed insight into so far not described pathological features and pathomechanisms of early stages of heterotopia formation.

Material and Methods

Generation of human iPSC cells

Skin fibroblasts were obtained from the Coriell Biorepository (Control 1, 2-year-old female, catalog ID GM00969), from a healthy donor (Control 2, 44-year-old healthy female derived with given informed consent within the collaborative research center project SFB636 B7 (ID number B7_028#4)) and from two patients harboring mutations in the *EML1* gene (Patient 1, P135, 14 years male; Patient 2, 3489, newborn (8 days) male), both with given informed consent and obtained according to the guidelines of the local institutional review boards (IRBs APHP-Délégation Interrégionale à la Recherche Clinique, Paris and Erasmus Medical Center, Rotterdam). Research on human cells was approved by the French Ministry of Health (L.1243.3, DC-2015-2559). Patient 1 carries a compound heterozygous *EML1* mutation. An A c.481C>T nucleotide mutation in exon 5, changing an arginine residue (Arg138) to a stop codon, and a c.796A>G mutation in exon 8, changing a threonine into an alanine residue, leading to an impaired association of EML1 with microtubules. Patient 2 carries a c.673T>C mutation—W225R, in which a hydrophobic nonpolar residue changed to highly basic hydrophilic residue—this residue can be found deep in the beta propeller structure where the HELP domain is present (Kielar et al, 2014; Richards et al, 2014). Fibroblasts were reprogrammed by non-integrative delivery of OCT4, SOX2, KLF4, and c-MYC using Sendai virus (SeV) vectors (CytoTune-iPS 2.1 Sendai Reprogramming Kit, Thermo Fisher (Ban et al, 2011); Ethics Committee II of Heidelberg University approval no. 2009-350N-MA for hiPSC generation). Pluripotent stem cells were validated as described in Iefremova et al (2017). iPSCs were cultured as colonies in Essential 8 (E8) medium on Geltrex-coated (GT, Thermo Fisher Scientific) cell culture plates with daily medium change. Cells were passaged using EDTA (Thermo Fisher Scientific) and seeded in a 1:3 to 1:10 ratio. Following passaging, medium was supplemented with 5 μM Y-27632 (Cell Guidance Systems) to promote cell survival. All human iPSC cell lines were regularly checked and confirmed negative for mycoplasma. Reagents and resources used in this study can be seen in Table 1.

Generation and validation of *EML1*-heKO lines

EML1-heKO lines were generated using CRISPR/Cas9 and homology-directed repair (HDR) (Santa Cruz). Successful site-specific double-strand break followed by integration of the HDR sequence leads to the disruption of the *EML1* gene and the integration of a puromycin selection cassette. In brief, 1 million iPSC cells derived from either control 1 or control 2 were transfected with three different gRNAs (1 μg in total) directed against early exons of the *EML1* gene (Exons 2 and 5) alongside the respective HDR plasmids using the NucleofectorTM2b (Lonza) and the Cell Line Nucleofector[®] Kit V (Lonza) according to the manufacturer's protocol. Following nucleofection, cells were plated on GT-coated cell culture plates in E8 medium supplemented with 5 μM Y-27632. Puromycin (1 μg/ml, Merck Milipore) selection was initiated 48 h following transfection. Clones were manually picked 7–12 days following nucleofection into GT-coated 48-well cell culture plates. Integration of the HDR cassette was validated on genomic DNA by PCR. PCR primers were designed to recognize the *EML1* wild-type allele

Table 1. Reagents and resources used in this study.

Reagent or Resource	Vendor	Identifier
A83-01	Biomol	Cay9001799
B27-Supplement	Thermo Fisher Scientific	17504044
BCA Protein Assay Kit	Thermo Fisher Scientific	23225
Blasticidin S Hydrochlorid	Carl Roth	CP14.2
Boric acid	Thermo Fisher Scientific	B0394
BrdU	BD-Bioscience	550891
BSA	Sigma Aldrich	A3294
cAMP	Sigma Aldrich	D0627
Chromium Single Cell 3' Library & Gel Bead Kit v2	10xGenomics	PN-120267
DAPI	Biologend	422801
DMEM/F12	Thermo Fisher Scientific	11320074
DMEM/F-12 with Glutamin and HEPES	Thermo Fisher Scientific	11330-057
DNase	Sigma Aldrich	AMPD1-1KT
PBS	Sigma Aldrich	D8537
EDTA	Thermo Fisher Scientific	15575020
EML1 CRISPR/Cas9 KO Plasmid (h)	Santa Cruz	sc-406445
EML1 HDR Plasmid (h)	Santa Cruz	sc-406445-HDR
EpothiloneD	Abcam	ab143616
Epoxy resin	PolyScience	EPON218
Extractme Genomic DNA Kit	7Bioscience	EM13
Fetal Bovine Serum (FBS)	Thermo Fisher Scientific	10270106
FGF-2 (154)	Cell Guidance Systems	GFH146
Fluvastatin	Sigma Aldrich	SML0038
Geltrex, hESC-Qualified	Thermo Fisher Scientific	A1413302
Glucose	Carl Roth	HN06.2
GlutaMAX	Thermo Fisher Scientific	35050038
Glutaraldehyde	Sigma Aldrich	G5882
HCL	Thermo Fisher Scientific	15538334
Heparin	Sigma Aldrich	H3149
Insulin	Sigma Aldrich	91077C
iScript cDNA synthesis kit	Bio-Rad	1708890
KnockOut Serum Replacement (KOSR)	Thermo Fisher Scientific	10828028
LAAP	Sigma Aldrich	A8960
L-cysteine	Sigma Aldrich	168149
LDN-193189	Cell Guidance Systems	SM23
Mowiol 4-88	Carl Roth	0713.1

Table 1 (continued)

Reagent or Resource	Vendor	Identifier
N2-Supplement	Thermo Fisher Scientific	17502048
Natriumselenit	Sigma Aldrich	S5261
NEAA	Thermo Fisher Scientific	11140035
Papain	Sigma Aldrich	P3125
Paraformaldehyd (PFA)	Sigma Aldrich	P6148
Penicillin/Streptomycin	Thermo Fisher Scientific	15140122
peqGOLD TriFast	VWR	30-2010
Pierce™ Protease Inhibitor	Thermo Fisher Scientific	A32955
Pluronic F-127	Sigma Aldrich	P2443
Puromycin	Merck Millipore	540222
SDS	Carl Roth	CN30.1
Sendai Reprogramming Kit (CytoTune-iPS 2.1)	Thermo Fisher Scientific	A16517
Taq Polymerase	Biozym	331610
TGFβ1	Cell Guidance Systems	GFH39
Transferrin	Sigma Aldrich	T3705
Triton X-100	Merck Millipore	108603
TrypLE Express	Thermo Fisher Scientific	12605-028
Verteporfin	Sigma Aldrich	SML0534
XAV939	Cell Guidance Systems	SM38
Y-27632	Cell Guidance Systems	SM02

or the integration of the puromycin cassette. Of note: only heterozygous *EML1*-(he)KO iPSC clones could be expanded, stored, and further differentiated into cerebral organoids.

Generation of cerebral organoids

Cerebral organoids were generated as described with slight adaptations (Jefremova *et al.*, 2017; Krefft *et al.*, 2018). In brief, U-bottom 96-well plates were coated with 5% Pluronic F-127 (Sigma Aldrich) in phosphate buffered saline (PBS) for 15 min to create low attachment wells. iPSC cell colonies were dissociated using TrypLE Express (Thermo Fisher Scientific) and 6,000 cells were plated per low attachment well in 150 µl E8 medium supplemented with 50 µM Y-27632. Medium was changed every other day. At day 5, medium was changed to neural induction medium (Table 2). Medium was changed every other day. On days 9–11, when translucent neural ectoderm was visible, organoids were embedded in a 3:2 ratio of GT to neural induction medium and further cultured in Pluronic F-127-coated 6 cm dishes in neural differentiation medium (Table 3) under continuous agitation at 70 rpm on an orbital shaker (Infors Celltron HD) with a medium change every 3 to 4 days. When indicated, organoids were exposed to 100 nM Verteporfin (Sigma

Table 2. Neural induction medium.

Component	Final conc.
DMEM/F12	93.3%
N2 supplement	0.5% (v/v)
B27 supplement	1%
cAMP	300 ng/ml
LDN-193189	0.2 mM
A83-01	0.5 mM
XAV939	2 μ M
GlutaMAX	1% (v/v)
NEAA	1% (v/v)
D-Glucose	4.44 mM
Heparin	10 μ g/ml
KOSR	2% (v/v)
Penicillin/Streptomycin	1% (v/v)

Table 3. Neural differentiation medium.

Component	Final conc.
DMEM/F12	93.3%
N2 supplement	0.5% (v/v)
B27 supplement	1%
cAMP	300 ng/ml
GlutaMAX	1% (v/v)
NEAA	1% (v/v)
D-Glucose	4.44 mM
Insulin	2.5 μ g/ml
KOSR	2% (v/v)
Penicillin/Streptomycin	1% (v/v)

Aldrich) or 300 nM Fluvastatin (Sigma Aldrich) for 96 h from day 16 onwards with daily medium changes.

Generation of hybrid organoids

EGFP-labeled iPS cells (*EML1*-heKO and isogenic control) were generated using a lentiviral construct expressing EGFP under the PGK promoter as well as a blasticidin resistance cassette (pLentiPGK-EGFP-SV40-blasticidin (Koch *et al.*, 2006)). Forty-eight hours post-transfection, iPS cells were cultured for at least 2 weeks using E8 medium supplemented with 10 μ g/ml blasticidin (Carl Roth). Homogeneous EGFP expression was validated by visual monitoring using epifluorescence microscopy. Hybrid organoids were generated by mixing either control-EGFP- or *EML1*-heKO-EGFP-derived iPS cells with control iPS cells in a 1:1,000 ratio before organoid generation.

BrdU labeling of cerebral organoids

For 5-bromo-2'-deoxyuridine (BrdU) labeling, day 30 \pm 2 cerebral organoids were incubated for 2 h in medium containing 10 μ M BrdU (BD Bioscience). After 2 h of incubation, cerebral organoids

were washed three times with fresh medium and transferred into a new 6 cm culture dish. Following 24 h, cultivation time cerebral organoids were fixed and further processed for immunohistochemistry.

Generation of iPS cell-derived cortical progenitors

Differentiation of iPS cells into cortical progenitors was performed as described with slight adaptations (Shi *et al.*, 2012; Iefremova *et al.*, 2017; Uzquiano *et al.*, 2019). In brief, iPS cell colonies cultured in E8 medium were dissociated using TrypLE (Thermo Fisher Scientific) and seeded as single cells onto GT-coated cell culture plates in E8 medium supplemented with 5 μ M Y-27632. Once the cell culture reached 98% confluence, neural induction was initiated by changing the culture medium to neural induction medium containing DMEM/F12 (Thermo Fisher Scientific), 0.5% N2 supplement, 1% B27 supplement, (Thermo Fisher Scientific), cAMP (300 ng/ml, Sigma Aldrich), LDN-193189 (0.2 mM, Cell Guidance Systems), A83-01 (0.5 mM, Biomol), XAV939 (2 μ M, Cell Guidance Systems), 1% GlutaMAX (Thermo Fisher Scientific), 1% NEAA (Thermo Fisher Scientific), and 4.44 mM Glucose (Carl Roth). Cells were maintained in this medium for 8–11 days, collected by dissociation with TrypLE and replated in neural differentiation media containing DMEM/F12, 0.5% N2 supplement, 1% B27 supplement, and cAMP (300 ng/ml) on GT-coated cell culture plates. Cells were split in a 1:2 ratio when cultures reached 100% confluence using TrypLE. Electron microscopy analyses were performed on cortical progenitors passaged twice. When indicated, 0.5 nM EpothiloneD (EpoD, abcam) was added to the medium for 72 h with one medium change after 48 h before cells were fixed and analyzed or harvested for Western blot analysis.

Electron microscopy of neural progenitor cells

Samples were processed and imaged as previously described in Uzquiano *et al.* (2019). Briefly, cells were fixed for 1 h in phosphate buffer (PB), 0.1 M buffer containing 4% paraformaldehyde (PFA, Sigma Aldrich), and 2.5% glutaraldehyde (Sigma Aldrich) at 4°C. Following fixation, cells were postfixed in 2% osmium tetroxide diluted in 0.2 M Palade buffer. After osmication, cells were dehydrated in a series of ethanol baths and flat embedded in epoxy resin (EPON 812, Polysciences). After resin polymerization, small pieces were dissected from flat-embedded cultures, mounted in plastic stubs and sectioned. Ultrathin sections (70 nm) were stained with uranyl acetate and lead citrate. Sections were examined in a Philips CM100 electron microscope. Digital images were obtained with a CCD camera (Gatan Orius).

Immunofluorescence and specific antibody information

Cells were washed twice with PBS, fixed for 10 min with 4% PFA, and washed again twice with PBS and used either directly for immunostaining or stored at 4°C. Organoids were fixed, embedded, and cryo-sectioned into 20 μ m sections as described previously (Iefremova *et al.*, 2017; Krefft *et al.*, 2018). For detection of the pluripotency-associated markers, TRA-1-60, TRA-1-81, and SSEA-3 samples were incubated with primary antibodies at room temperature for 4 h, washed three times, incubated with secondary antibody for 45 min, counterstained with DAPI (Biolegend), and mounted with Mowiol 4-88 mounting solution (Carl Roth). For detection of BrdU and Ki67,

slices were permeabilized using 0.5% Triton X-100 in PBS for 30 min, washed with PBS, treated with 2 N HCl (Thermo Fisher Scientific) for 10 min, and washed twice with PBS. Then, slices were treated with 0.1 M boric acid (Thermo Fisher Scientific) for 10 min and washed three times with PBS. Slices were then blocked with 10% fetal bovine serum and 0.1% Triton X-100 in PBS for 1 h at room temperature and subsequently stained overnight in blocking solution at 4°C with antibodies against BrdU and Ki67. On the next day, slices were washed three times with PBS and secondary antibodies were applied in blocking solution for 1 h at room temperature, counterstained with DAPI, and mounted with Mowiol. For all other antibodies, cells or organoid sections were blocked and permeabilized in 10% fetal bovine serum (Thermo Fisher Scientific) in PBS with 0.3% Triton X-100 for 1 h at room temperature (RT), incubated with primary antibodies for 16 h at 4°C, washed three times with PBS, incubated with secondary antibodies for 1 h, counterstained with DAPI, and mounted with Mowiol. Images were acquired with either the confocal microscope Leica TCS SP5II or the fluorescence microscope Leica DM6 B microscope and processed using the software Leica Application Suite AF, Leica Application Suite X, as well as ImageJ.

Primary and secondary antibodies and dilutions used in this study can be seen in Tables 4 and 5. Software and algorithms used for analysis can be seen in Table 6.

Immunoblot and specific antibody information

Cells were washed twice with ice-cold PBS, scraped off into PBS, and collected via centrifugation. Cell pellets were lysed in RIPA buffer (150 mM NaCl, 0.2% SDS (Carl Roth), 0.2% Triton X-100 (Merck Millipore), 25 mM EDTA, 50 mM Tris-HCl, pH 7.4) containing Pierce™ protease inhibitor (Thermo Fisher Scientific) and Pierce™ phosphatase inhibitor (Thermo Fisher Scientific) for 1 h on ice. Genomic DNA was sheared by sonication. Subsequently, cell debris was precipitated by centrifugation at 16,000 rcf for 15 min at 4°C. Protein concentration of cleared cell lysates was determined using the BCA protein assay kit (Thermo Fisher Scientific). For immunoblotting, 25 µg of protein was boiled in 6× SDS sample buffer for 5 min at 95°C. Lysates were resolved on 10% gels and transferred onto 0.2 µm nitrocellulose membranes by semi-dry blotting. Nitrocellulose membranes were blocked in 5% BSA in TBST for 1 h at RT and subsequently incubated overnight with primary antibody in blocking solution at 4°C. The next day, membranes were washed three times with TBST, incubated with IR-dye-conjugated secondary antibodies (DyLight™, Cell Signaling Technology) diluted 1:15,000 in TBST for 1 h at room temperature. Subsequently, membranes were washed three times before visualization of target proteins using an Odyssey IR imaging system (LI-COR Biosciences). Primary antibodies and concentrations were as follows: Acetylated α -tubulin (AC-TUB) (Cell Signaling Technology, 1:1,000) and β -Actin (Cell Signaling Technology, 1:15,000). Of note: due to the lack of a reliable EML1 antibody, we were not able to include data on EML1 protein levels.

Single-cell RNA sequencing experiments

Organoids at day 33 \pm 2 were microdissected to enrich for cortical areas. The dissected tissue was dissociated by incubating in papain (Sigma Aldrich) solution containing papain buffer (1 mM L-cysteine and 0.5 mM EDTA in Earle's balanced salt solution), 20 units

Table 4. Antibodies used in this study.

Reagent or Resource	Vendor	Identifier
Antibodies IF		
AFP	Hölzel	Cat# 12177-MM27
ARL13B	Antibodies Incorporated	Cat# 75-287, RRID: AB_2341543
Anti-BrdU	BD-Biosciences	Cat# 347580, RRID: AB_10015219
COL1A2	Abcam	Cat# ab96723, RRID: AB_10679394
FAM107A	Sigma Aldrich	HPA055888
Anti-GFP	Aves Labs	Cat# GFP-1020, RRID: AB_10000240
Ki67	Cell Signaling	Cat# 9129 RRID: AB_2687446
MAPT	Synaptic Systems	Cat# 314 004, RRID: AB_1547385
MEIS2	Sigma Aldrich	Cat# WH0004212M1, RRID: AB_1842419
N-cadherin	BD-Bioscience	Cat# 610921, RRID: AB_398236
PAX6	Biologend	Cat# 901301, RRID: AB_2565003
p-Vimentin	MBL	Cat# D076-3, RRID: AB_592963
SMA	abcam	Cat# ab5694, RRID: AB_2223021
TPX2	Novus Biologicals	Cat# NBS00-179, RRID: AB_10002747
TRA-1-60	Merck Millipore	Cat# MAB4360, RRID: AB_2119183
TRA-1-81	Merck Millipore	Cat# MAB4381, RRID: AB_177638
TUBB3	Biologend	Cat# 802001, RRID: AB_2564645
SSEA3	abcam	Cat# ab16286, RRID: AB_882700
YAP1	Cell Signaling	Cat# 14074, RRID: AB_2650491
Alexa Fluor 568 -Goat anti-mouse IgG (H + L)	Thermo Fisher Scientific	Cat# A-11004, RRID: AB_2534072
Alexa Fluor 488 -Goat anti-Rabbit IgG (H + L)	Thermo Fisher Scientific	Cat# A-11008, RRID: AB_143165
Alexa Fluor 555 -Goat anti-Rabbit IgG (H + L)	Thermo Fisher Scientific	Cat# A-21428, RRID: AB_2535849
Alexa Fluor 647 -Goat anti-Guinea Pig IgG (H + L)	Thermo Fisher Scientific	Cat# A-21450, RRID: AB_2735091
Alexa Fluor 488 -Goat anti-Chicken IgY (H + L)	Thermo Fisher Scientific	Cat# A-11039, RRID: AB_2534096
Antibodies immunoblot:		
Acetylated α -tubulin (AC-TUB)	Cell Signaling Technology	5335, RRID: AB_10544694
β -Actin	Cell Signaling Technology	3700, RRID: AB_2242334

Table 4 (continued)

Reagent or Resource	Vendor	Identifier
Anti-mouse IgG (H + L) (DyLight 680 Conjugate)	Cell Signaling Technology	5470, RRID: AB_10696895
Anti-rabbit IgG (H + L) (DyLight 800 4X PEG Conjugate)	Cell Signaling Technology	5151, RRID: AB_10697505

papain, and 10 µg/ml of DNase (Sigma Aldrich) for 20 min at 37°C. Following incubation, excessive papain solution was removed, 3 ml organoid differentiation medium was added, and samples were mechanically dissociated using wide-bore 1,000 µl pipette tips coated with 1% bovine serum albumin (BSA) in PBS. The cell suspension was centrifuged at 400 g for 4 min at 4°C. The supernatant was removed, the cell pellet was resuspended in 1 ml ice-cold PBS + 0.04% BSA, and filtered through a 30 µm cell strainer. Counting and viability were assessed using Trypan blue staining (Countess automatic cell counter, Thermo Fisher Scientific). Single cell library preparation was performed using the 10x Genomics Chromium platform according to the 10x Genomics Chromium Single Cell 3' Library & Gel Bead Kit v2 chemistry user guide (10x Genomics).

The prepared cDNA libraries were processed by the High Throughput Sequencing Unit of the Genomics & Proteomics Core Facility of the German Cancer Research Center (DKFZ). The libraries were sequenced on two lanes on the Illumina HiSeq 4K platform with a protocol specific for 10x scRNA libraries (paired-end 26 + 74).

Fastq files were parsed to cellranger (10x Genomics) count in order to generate a count matrix. FastQC was used for general sequencing quality control (Andrews, 2015). If not stated otherwise, data analysis was performed using the Seurat (v3.2.2) package in R (Stuart et al, 2019). Count matrix was filtered with following parameters: Any feature that was expressed in less than three cells was removed from the analysis. For the control sample, any cell with < 2,000 expressed features, more than 10% mitochondrial genes expressed, or less than 5,000 total UMI counts was removed from further analysis. For the *EML1*-heKO sample, any cell with < 1,500 expressed features, more than 10% mitochondrial genes expressed, or < 3,000 total UMI counts was removed from further analysis. The data were normalized using sctransform. Dimensional reduction was performed using UMAP with dims = 1:30. Shared nearest-neighbor graph was constructed with dims = 1:30. Clusters were generated with resolution = 0.4. Cells were defined by interpreting expression of known marker genes. One group of cells that was defined as

Table 5. Primary antibodies and dilutions.

Antibodies	Vendor	Cat. No.	Raised against	Dilution
Primary antibodies				
AFP	Hözel	Cat# 12177-MM27	mouse	1:300
ARL13B	Antibodies Incorporated	Cat# 75-287	mouse	1:100
Anti-BrdU	BD-Biosciences	Cat# 347580	mouse	1:50
COL1A2	Abcam	Cat# ab96723	rabbit	1:300
FAM107A	Sigma Aldrich	Cat# HPA055888	rabbit	1:400
Anti-GFP	Aves Labs	Cat# GFP-1020	chicken	1:500
Ki67	Cell Signaling	Cat# 9129	rabbit	1:500
MAPT	Synaptic Systems	Cat# 314 004	guinea pig	1:1,000
MEIS2	Sigma	Cat# WH0004212M1	mouse	1:200
N-cadherin	BD-Bioscience	Cat# 610921	mouse	1:500
PAX6	Biologend	Cat# 901301	rabbit	1:500
p-Vimentin	MBL	Cat# D076-3	mouse	1:1,000
SMA	abcam	Cat# ab5694	rabbit	1:300
TPX2	Novus Biologicals	Cat# NB500-179	rabbit	1:500
TRA-1-60	Merck Millipore	Cat# MAB4360	mouse	1:300
TRA-1-81	Merck Millipore	Cat# MAB4381	mouse	1:300
TUBB3	Biologend	Cat# 802001	rabbit	1:1,000
SSEA3	abcam	Cat# ab16286	rat	1:500
YAP1	Cell Signaling	Cat# 14074	rabbit	1:300
Secondary antibodies				
Alexa Fluor 568-Goat anti-mouse IgG (H + L)	Thermo Fisher Scientific	Cat# A-11004	goat anti-mouse	1:1,000
Alexa Fluor 488-Goat anti-Rabbit IgG (H + L)	Thermo Fisher Scientific	Cat# A-11008	goat anti-rabbit	1:1,000
Alexa Fluor 555-Goat anti-Rabbit IgG (H + L)	Thermo Fisher Scientific	Cat# A-21428	goat anti-rabbit	1:1,000
Alexa Fluor 647-Goat anti-Guinea Pig IgG (H + L)	Thermo Fisher Scientific	Cat# A-21450	goat anti-guinea	1:1,000
Alexa Fluor 488-Goat anti-Chicken IgY (H + L)	Thermo Fisher Scientific	Cat# A-11039	goat anti-chicken	1:1,000

Table 6. Software and algorithms used in this study.

Software and Algorithms	Source	Identifier
Cell Ranger v 3.0.1	10x Genomics	https://support.10xgenomics.com/single-cell-gene-expression/software/downloads/latest
Fiji software (ImageJ 1.52i)	Wayne Rasband, NIH, USA	Fiji, RRID:SCR_002285
ggplot2	Hadley (2016)	RRID:SCR_014601
Prism 6	GraphPad Prism version 6.0d	GraphPad Prism, RRID:SCR_002798
Seurat v3.0.0	Stuart et al (2019)	https://github.com/satijalab/seurat/releases/tag/v3.0.0
SPSS	https://www.ibm.com/	IBM SPSS statistics 25
R	R Core	https://www.r-project.org/

mesenchymal-like cells was removed for further analysis. Violin plots were generated with Seurat (Stuart et al, 2019) and ggplot2 (Hadley, 2016) and show normalized expression values. For GO violin plots, the genes that are collected in a GO term were retrieved from org.Hs.eg.db (org.Hs.eg.db: Genome wide annotation for Human. R package version 3.12.0.). For each GO term of interest, the expression per cell was calculated as proportion of feature set. For detailed information about the data analysis pipeline in R, refer to https://github.com/ahoffrichter/Jabali_et_al_2021_scrNAseq_analysis. Software and algorithms used for analysis can be seen in Table 6.

PCR analysis

Genomic DNA (for patient mutations and *EML1*-heKO validation) was isolated using the Extractme genomic DNA kit (7Bioscience) according to the manufacturers protocol. Triplicate total mRNA samples were isolated using peqGOLD TriFast (VWR) following the

supplier's instructions. One microgram total mRNA was used for reverse transcription with the iScript cDNA synthesis kit (BioRad) following the manufacturer's protocol. Semi-quantitative PCR reactions were run in at least triplicates using Taq Polymerase (Biozym). PCR conditions and cycle numbers were adjusted to each primer pair for specific DNA amplification on cDNA obtained from commercially available human fetal (single donor, female, 19 weeks of gestation). For quantitative RT-PCR (qRT-PCR), PCR products were assessed by dissociation curve and gel electrophoresis. Data were normalized to 18S rRNA levels. Primers used to validate *EML1*-patient-specific mutations and the *EML1*-heKO as well as *EML1* expression can be seen in Table 7.

Quantitative assessment of 2D and 3D cell cultures

Ectopic neural rosettes were quantified based on NCAD staining and localization in the organoid structure. More precisely, accumulation of NCAD at the basal side of VZ areas was defined as ectopic neural rosettes and quantified per VZ area using the cell counter tool in ImageJ. The percent of VZ areas with ectopic neural rosettes was then calculated for the different conditions. *Organization of neurons* was investigated per cortical area (composed of a VZ and CP area) based on MAPT staining and localization. If the majority of MAPT-positive neurons were found within the CP area, we called them organized. In case MAPT-positive neurons distributed in the CP as well as in the VZ area, we defined that as disorganized. Criteria for heterotopia were met in case clusters or bands of MAPT-positive cells found between the VZ area and the CP region. The percent of heterotopic, disorganized, or organized cortical areas was then calculated for the different conditions. The number and localization of EGFP-positive cells within hybrid organoids were investigated by defining VZ and CP areas and quantifying the EGFP-positive cells in the respective areas using the cell counter tool in ImageJ. *Mitotic planes* were quantified at the VZ surface by analyzing 20- μ m-thick tenner serial sections stained for p-vimentin (to identify dividing cells) and TPX2 (a spindle assembly factor which plays a role in inducing microtubule assembly and growth during M phase used to visualize the plane of dividing

Table 7. Primers used in this study.

Primer	Forward	Reverse	Source
P135 Mut. Exon 5 (T_A 45°C)	GACGTTCTATGTATATATT	TGTTTGATTAGTCCTATAAA	IDT
P135 Mut. Exon 8 (T_A 60°C)	CTGCATGCCCTTTGGGG	TGACCGTGTCTGCTAATGC	IDT
3489 Mut. (T_A 60°C)	GCTGGGCACTGAGGTATCTT	ACCACAGCTATTTTCGTTTCAGGA	IDT
Validation of <i>EML1</i>-heKO:	T_A 60°C for all primer combinations:		
Before Cas. gRNA 1	AGGGAAGAATGATGTACAATGAGA		IDT
In Cas. gRNA 1		AAAAAGCCGGAGCCAGTACA	IDT
Before Cas. gRNA 2/3	CCTGTTAGCATTTGTCCACG		IDT
In Cas. gRNA 2/3		GGAGCGATCGCAGATCCTTG	IDT
<i>EML1</i> WT behind Cas. gRNA 1		TCACTCAAACGCCACCTTT	IDT
<i>EML1</i> WT behind Cas. gRNA 2/3		TTCTTTTCCACTGGAAGACC	IDT
<i>EML1</i> expression:	T_A 60°C for both pairs:		
<i>EML1</i> -qPCR	GGGTCTATGGGTACAGGGGT	ACTGCTAGGCACTTCACGTC	IDT
18s-qPCR	TTCTTTGGACCGCCGAAG	GCCGCATCGCCGTCGG	IDT

cells). The angle of the spindle of apical radial glia cells in relation to the prospective ventricular surface was investigated using the ImageJ angle tool. *Cell proliferation* at the VZ surface or basal to the VZ areas was quantified based on the distribution of p-Vim-positive cells in the respective localization using the cell counter tool in ImageJ. *BrdU⁺ KI67⁺ cells* at the basal side of the VZ areas were quantified using ImageJ plugin Cell Counter. *PAX6-positive cells displaying nuclear YAP1* were quantified per VZ area following immunohistochemistry. More specifically, the total amount of PAX6-positive cells within a VZ area was determined and divided by the amount of PAX6-positive cells displaying a nuclear YAP1 signal within this area. All quantitative assessments were performed on at least three different organoids derived from at least three independent batches. The *length of the primary cilia* was investigated in cortical progenitors following ARL13B immunostaining using the length measurement tool in ImageJ on three biological replicates. Images for all quantitative assessments were acquired using the confocal microscope Leica TCS SP5II or the fluorescence microscope Leica DM6 B microscope. In order to make the different batches analyzed distinguishable from one another, different shapes and color codes were utilized in the graphs displayed in this study. VZ areas or organoids analyzed from one batch for example are represented by black dots, grey dots, white dots with black border, or grey dots with black border.

Statistical analysis

All quantitative data were generated based on biological triplicates and tested for normal distribution using the D'Agostino & Pearson omnibus normality test. If criteria for normal distribution were met, statistical significance was tested using parametric testing in the form of one-way ANOVA or two-way ANOVA tests followed by *post hoc* testing (Sidak's multiple-comparison test or Tukey's multiple-comparison test) based on the experimental design ($*P < 0.05$, $**P < 0.01$, and $***P < 0.001$). If criteria for normal distribution were not met, non-parametric testing in the form of a two-tailed Mann–Whitney- or Kruskal–Wallis test followed by *post hoc* testing (Dunn's multiple-comparison test) was conducted. All deviations from means are depicted as mean with SD or SEM. All analyses were performed with the help of R statistical software package, IBM SPSS statistics 25, and GraphPad Prism 6. Gene expression was compared between control and *EML1*-heKO cells within cell type using the Wilcoxon rank sum test. Values show Bonferroni-corrected *P*-values ($*P < 0.05$, $**P < 0.01$, and $***P < 0.001$). Comparison of proportion of GO feature sets was performed using the Wilcoxon rank sum test ($*P < 0.05$, $**P < 0.01$, and $***P < 0.001$). Software and algorithms used for analysis can be seen in Table 6.

Generation of schemes

Synopsis image as well as schemes in Figs 2C and EV3A were created using biorender.com.

Data availability

The sc-RNA-seq data will be deposited in NCBI's Gene Expression Omnibus and will be accessible through a GEO Series accession number. For detailed information about the data analysis pipeline in

R and the scRNAseq datasets generated and / or analyzed during the current study, refer to the GitHub repository https://github.com/ahoffrichter/Jabali_et_al_2021_scRNAseq_analysis. Any additional information required to reanalyze the data reported in this study is available from the lead contact upon request.

Expanded View for this article is available online.

Acknowledgements

We thank Nadia Bahi-Buisson, Grazia Mancini, and Anne-Gaëlle Le Moing for their contributions of patient samples, and Carmen Cifuentes-Diaz for her contribution to EM studies. The work was supported by the ERA-NET NEURON, JTC 2015 Neurodevelopmental Disorders, STEM-MCD (to JL), the German research foundation (DFG), Project LA 2933/2-1 (to JL), the French ANR, under the frame of E-Rare-3, the ERA-Net for Research on Rare Diseases (E-RARE18-049, to FF), the French Foundation for Medical Research for a team FRM grant (Equipe FRM to FF), and the generous financial support by the Hector Stiftung II (to PK and JL). Open Access funding enabled and organized by Projekt DEAL.

Author contributions

Ammar Jabali: Data curation; Validation; Investigation; Visualization; Methodology; Writing – original draft; Writing—review & editing. **Anne Hoffrichter:** Data curation; Software; Formal analysis; Investigation; Visualization. **Ana Uzquiano:** Investigation; Methodology. **Fabio Marsoner:** Investigation. **Ruven Wilkens:** Investigation; Visualization; Methodology. **Marco Siekmann:** Validation; Methodology. **Bettina Bohl:** Investigation; Visualization; Methodology. **Andrea, Carlo Rossetti:** Validation. **Sandra Horschitz:** Methodology. **Philipp Koch:** Resources; Funding acquisition; Validation; Writing—original draft; Writing—review & editing. **Fiona Francis:** Resources; Writing—original draft; Writing—review & editing. **Julia Ladewig:** Conceptualization; Resources; Supervision; Funding acquisition; Validation; Investigation; Visualization; Writing—original draft; Writing – review & editing.

In addition to the CRediT author contributions listed above, the contributions in detail are:

JL conceived and designed the research project; AJ, AU, PK, FF, and JL designed experiments; AJ, AU, FM RW, and MS performed experiments and collected data; AJ, AH, AU, BB, ACR, FF, PK, and JL analyzed data; and AJ and SH reprogrammed *EML1* patient samples. FF communicated with clinicians for patient sample collection. FF and PK were involved in ongoing critical discussion. JL and AJ wrote the manuscript with critical help from FF, AU, and PK. All authors provided ongoing critical review of experiments, results, and commented on the manuscript.

Disclosure and competing interest statement

The authors declare that they have no conflict of interest.

References

- Andrews S (2015) FastQC: A Quality Control Tool for High Throughput Sequence Data [Online]. "FastQC," <http://www.bioinformatics.babraham.ac.uk/projects/fastqc/> <https://qubeshub.org/resources/fastqc>
- Ban H, Nishishita N, Fusaki N, Tabata T, Saeki K, Shikamura M, Takada N, Inoue M, Hasegawa M, Kawamata S et al (2011) Efficient generation of transgene-free human induced pluripotent stem cells (iPSCs) by temperature-sensitive Sendai virus vectors. *Proc Natl Acad Sci U S A* 108 (34): 14234–14239

- Bizzotto S, Uzquiano A, Dingli F, Ershov D, Houllier A, Arras G, Richards M, Loew D, Minc N, Croqueolois A et al (2017) Eml1 loss impairs apical progenitor spindle length and soma shape in the developing cerebral cortex. *Sci Rep* 7(1): 17308
- Camargo FD, Gokhale S, Johnnidis JB, Fu D, Bell CW, Jaenisch R, Brummelkamp TR (2007) YAP1 increases organ size and expands undifferentiated progenitor cells. *Curr Biol* 17(23): 2054–2060
- Cappello S, Gray MJ, Badouel C, Lange S, Einsiedler M, Srour M, Chitayat D, Hamdan FF, Jenkins ZA, Morgan T et al (2013) Mutations in genes encoding the cadherin receptor-ligand pair DCHS1 and FAT4 disrupt cerebral cortical development. *Nat Genet* 45(11): 1300–1308
- Collins SC, Uzquiano A, Selloum M, Wendling O, Gaborit M, Osipenko M, Birling MC, Yalcin B, Francis F (2019) The neuroanatomy of Eml1 knockout mice, a model of subcortical heterotopia. *J Anat* 235(3): 637–650
- Eze UC, Bhaduri A, Haeussler M, Nowakowski TJ, Kriegstein AR (2021) Single-cell atlas of early human brain development highlights heterogeneity of human neuroepithelial cells and early radial glia. *Nat Neurosci* 24(4): 584–594
- Fan X, Fu Y, Zhou X, Sun L, Yang M, Wang M, Chen R, Wu Q, Yong J, Dong J et al (2020) Single-cell transcriptome analysis reveals cell lineage specification in temporal-spatial patterns in human cortical development. *Sci Adv* 6(34): eaaz2978
- Fietz SA, Lachmann R, Brandl H, Kircher M, Samusik N, Schroder R, Lakshmanaperumal N, Henry I, Vogt J, Riehn A et al (2012) Transcriptomes of germinal zones of human and mouse fetal neocortex suggest a role of extracellular matrix in progenitor self-renewal. *Proc Natl Acad Sci U S A* 109(29): 11836–11841
- Hadley W (2016) *Ggplot2*, New York, NY: Springer Science+Business Media LLC
- Iefremova V, Manikakis G, Krefft O, Jabali A, Weynans K, Wilkens R, Marsoner F, Brändl B, Müller F-, Koch P et al (2017) An organoid-based model of cortical development identifies non-cell-autonomous defects in Wnt signaling contributing to Miller-Dieker Syndrome. *Cell Rep* 19(1): 50–59
- Karzbrun E, Kshirsagar A, Cohen SR, Hanna JH, Reiner O (2018) Human brain organoids on a chip reveal the physics of folding. *Nat Phys* 14(5): 515–522
- Kielar M, Tuy FPD, Bizzotto S, Lebrand C, de Juan Romero C, Poirier K, Oegema R, Mancini GM, Bahi-Buisson N, Olaso R et al (2014) Mutations in Eml1 lead to ectopic progenitors and neuronal heterotopia in mouse and human. *Nat Neurosci* 17(7): 923–933
- Klingler E, Francis F, Jabaudon D, Cappello S (2021) Mapping the molecular and cellular complexity of cortical malformations. *Science* 371(6527): eaba4517
- Koch P, Siemen H, Biegler A, Itskovitz-Eldor J, Brüstle O (2006) Transduction of human embryonic stem cells by ecotropic retroviral vectors. *Nucleic Acids Res* 34(18): e120
- Kostic M, Paridaen JTM, Long KR, Kalebic N, Langen B, Grübling N, Wimberger P, Kawasaki H, Namba T, Huttner WB (2019) YAP activity is necessary and sufficient for basal progenitor abundance and proliferation in the developing neocortex. *Cell Rep* 27(4): 1103–1118.e6
- Krefft O, Jabali A, Iefremova V, Koch P, Ladewig J (2018) Generation of standardized and reproducible forebrain-type cerebral organoids from human induced pluripotent stem cells. *J Vis Exp* (131): 56768
- LaMonica BE, Lui JH, Hansen DV, Kriegstein AR (2013) Mitotic spindle orientation predicts outer radial glial cell generation in human neocortex. *Nat Commun* 4: 1665
- Liu J, Liu W, Yang LU, Wu Q, Zhang H, Fang AL, Li L, Xu X, Sun LE, Zhang J et al (2017) The primate-specific gene TMEM14B marks outer radial glia cells and promotes cortical expansion and folding. *Cell Stem Cell* 21(5): 635–649.e8
- Liu WA, Chen S, Li Z, Lee CH, Mirzaa G, Dobyns WB, Ross ME, Zhang J, Shi SH (2018) PARD3 dysfunction in conjunction with dynamic HIPPO signaling drives cortical enlargement with massive heterotopia. *Genes Dev* 32(11–12): 763–780
- Long KR, Newland B, Florio M, Kalebic N, Langen B, Kolterer A, Wimberger P, Huttner WB (2018) Extracellular matrix components HAPLN1, lumican, and collagen I cause hyaluronic acid-dependent folding of the developing human neocortex. *Neuron* 99(4): 702–719.e6
- Loo L, Simon JM, Xing L, McCoy ES, Niehaus JK, Guo J, Anton ES, Zylka MJ (2019) Single-cell transcriptomic analysis of mouse neocortical development. *Nat Commun* 10(1): 134
- Lui JH, Hansen DV, Kriegstein AR (2011) Development and evolution of the human neocortex. *Cell* 146(1): 18–36
- Martínez-Martínez M, De Juan Romero C, Fernández V, Cárdenas A, Götz M, Borrell V (2016) A restricted period for formation of outer subventricular zone defined by Cdh1 and Trnp1 levels. *Nat Commun* 7: 11812
- Mora-Bermúdez F, Matsuzaki F, Huttner WB (2014) Specific polar subpopulations of astral microtubules control spindle orientation and symmetric neural stem cell division. *eLife* 3: e02875
- Mukhtar T, Breda J, Grison A, Karimaddini Z, Grobecker P, Iber D, Beisel C, van Nimwegen E, Taylor V (2020) Tead transcription factors differentially regulate cortical development. *Sci Rep* 10(1): 4625
- Najas S, Pijuan I, Esteve-Codina A, Usieto S, Martínez JD, Zwijnen A, Arbonés ML, Martí E, Le Dréau G (2020) A SMAD1/5-YAP signalling module drives radial glia self-amplification and growth of the developing cerebral cortex. *Development* 147(13): dev187005
- Nowakowski TJ, Bhaduri A, Pollen AA, Alvarado B, Mostajo-Radji MA, Di Lullo E, Haeussler M, Sandoval-Espinosa C, Liu SJ, Velmeshev D et al (2017) Spatiotemporal gene expression trajectories reveal developmental hierarchies of the human cortex. *Science* 358(6368): 1318–1323
- Oegema R, McGillivray G, Leventer R, Le Moing AG, Bahi-Buisson N, Barnicoat A, Mandelstam S, Francis D, Francis F, Mancini GMS et al (2019) EML1-associated brain overgrowth syndrome with ribbon-like heterotopia. *Am J Med Genet C Semin Med Genet* 181(4): 627–637
- Oku Y, Nishiya N, Shito T, Yamamoto R, Yamamoto Y, Oyama C, Uehara Y (2015) Small molecules inhibiting the nuclear localization of YAP/TAZ for chemotherapeutics and chemosensitizers against breast cancers. *FEBS Open Bio* 5: 542–549
- O'Neill AC, Kyrousi C, Einsiedler M, Burtcher I, Drukker M, Markie DM, Kirk EP, Götz M, Robertson SP, Cappello S (2018) Mob2 insufficiency disrupts neuronal migration in the developing cortex. *Front Cell Neurosci* 12: 57
- Pollen A, Nowakowski T, Chen J, Retallack H, Sandoval-Espinosa C, Nicholas C, Shuga J, Liu S, Oldham M, Diaz A et al (2015) Molecular identity of human outer radial glia during cortical development. *Cell* 163(1): 55–67
- Richards MW, Law EW, Rennalls LP, Busacca S, O'Regan L, Fry AM, Fennell DA, Bayliss R (2014) Crystal structure of EML1 reveals the basis for Hsp90 dependence of oncogenic EML4-ALK by disruption of an atypical β -propeller domain. *Proc Natl Acad Sci U S A* 111(14): 5195–5200
- Richards MW, O'Regan L, Roth D, Montgomery JM, Straube A, Fry AM, Bayliss R (2015) Microtubule association of EML proteins and the EML4-ALK variant 3 oncoprotein require an N-terminal trimerization domain. *Biochem J* 467(3): 529–536
- Sahu MR, Mondal AC (2021) Neuronal Hippo signaling: from development to diseases. *Dev Neurobiol* 81(2): 92–109

- Saito K, Kawasoe R, Sasaki H, Kawaguchi A, Miyata T (2018) Neural progenitor cells undergoing Yap/Tead-mediated enhanced self-renewal form heterotopias more easily in the diencephalon than in the telencephalon. *Neurochem Res* 43(1): 180–189
- Shaheen R, Sebai MA, Patel N, Ewida N, Kurdi W, Altweijri I, Sogaty S, Almadawi E, Seidahmed MZ, Alnemri A et al (2017) The genetic landscape of familial congenital hydrocephalus. *Ann Neurol* 81(6): 890–897
- Shi Y, Kirwan P, Smith J, Robinson HP, Livesey FJ (2012) Human cerebral cortex development from pluripotent stem cells to functional excitatory synapses. *Nat Neurosci* 15(3): pp. 477–86, S1
- Stuart T, Butler A, Hoffman P, Hafemeister C, Papalexi E, Mauck WM, Hao Y, Stoeckius M, Smibert P, Satija R (2019) Comprehensive integration of single-cell data. *Cell* 177(7): 1888–1902.e21
- Uzquiano A, Cifuentes-Diaz C, Jabali A, Romero DM, Houllier A, Dingli F, Maillard C, Boland A, Deleuze JF, Loew D et al (2019) Mutations in the heterotopia gene Eml1/EML1 severely disrupt the formation of primary cilia. *Cell Rep* 28(6): 1596–1611.e10
- Velasco S, Kedaigle AJ, Simmons SK, Nash A, Rocha M, Quadrato G, Paulsen B, Nguyen L, Adiconis X, Regev A et al (2019) Individual brain organoids reproducibly form cell diversity of the human cerebral cortex. *Nature* 570(7762): 523–527
- Zhang B, Carroll J, Trojanowski JQ, Yao Y, Iba M, Potuzak JS, Hogan A-M L, Xie SX, Ballatore C, Smith AB et al (2012) The microtubule-stabilizing agent, epothilone D, reduces axonal dysfunction, neurotoxicity, cognitive deficits, and Alzheimer-like pathology in an interventional study with aged tau transgenic mice. *J Neurosci* 32(11): 3601–3611
- Zhao B, Tumaneng K, Guan KL (2011) The Hippo pathway in organ size control, tissue regeneration and stem cell self-renewal. *Nat Cell Biol* 13(8): 877–883



License: This is an open access article under the terms of the Creative Commons Attribution-NonCommercial-NoDerivs 4.0 License, which permits use and distribution in any medium, provided the original work is properly cited, the use is non-commercial and no modifications or adaptations are made.

7. Eidesstattliche Erklärung

Die vorliegende Dissertation wurde unter der Leitung von Frau Dr. Julia Ladewig angefertigt.

Hiermit versichere ich, dass diese Dissertation von mir persönlich, selbstständig und ohne unzulässige Hilfe Dritter sowie ohne die Benutzung anderer als der angegebenen Quellen angefertigt wurde. Die Daten, die im Rahmen einer Kooperation gewonnen wurden, sind ausnahmslos gekennzeichnet. Die aus externen Quellen direkt oder indirekt übernommenen Daten, Abbildungen und Konzepte sind unter Angabe der jeweiligen Quelle gekennzeichnet.

Die vorliegende Arbeit wurde an keiner anderen Hochschule als Dissertation eingereicht. Ich habe früher noch keinen Promotionsversuch unternommen.

Bonn, 08.05.23
(Datum)

A. Jabali
(Ammar Alexander Jabali)

8. Danksagung

Dr. Julia Ladewig möchte ich zunächst für die Themenstellung und für die Möglichkeit danken, meine Promotion in ihrer Gruppe und am Hector Institut für Translationale Hirnforschung durchführen zu können. Im Besonderen danke ich für das entgegengebrachte Vertrauen, die Freiheit dieses Projekt nach eigenen Vorstellungen zu gestalten und die fachliche Betreuung, sowie die Möglichkeit bereits zu einem frühen Zeitpunkt mit anderen Wissenschaftlern zu kollaborieren und meine Arbeit einem wissenschaftlichen Publikum präsentieren zu können.

Bei Professor Dr. Philipp Koch möchte ich mich nicht nur für die Begutachtung dieser Arbeit bedanken, sondern für konstruktive Diskussionen und die Unterstützung darin wissenschaftliche Ideen und Projekte zu entwickeln und zu verfolgen.

Professor Dr. Michael Pankratz möchte ich für die Begutachtung dieser Arbeit danken.

Prof. Dr. Günther Weindl und Prof. Dr. Hubert Schorle danke ich dafür, dass sie sich bereiterklärt haben mein Prüfungskomitee zu vervollständigen.

Allen aktuellen und ehemaligen Mitarbeitern der Arbeitsgruppen Ladewig und Koch, sowie Fiona Francis und Ana Uzquiano danke ich für eine hervorragende Zusammenarbeit, für eine angenehme Arbeitsatmosphäre und für inspirierende Gespräche.

Besonders möchte ich Bettina, Annasara, Anne, Ruven, Marco, Andrea, Isa und Helene für tatkräftige und mentale Unterstützung in und außerhalb des Labors von Herzen danken.

Nicht zuletzt danke ich all denjenigen die mir nahestehen und die ich liebe für diese außerordentliche Geduld und das Vertrauen, das mir während dieser Jahre entgegengebracht worden ist und diese Arbeit ermöglicht haben.